

**A STUDY ON THE FORMATION AND EVOLUTION OF
TROPICAL CYCLONE OVER BAY OF BENGAL
USING WEATHER RESEARCH & FORECASTING
(WRF) MODEL**

BY

MD. NAZRUL ISLAM

ROLL NO: 0855551
SESSION: JULY'2008



*A THESIS SUBMITTED TO THE DEPARTMENT OF PHYSICS,
KHULNA UNIVERSITY OF ENGINEERING & TECHNOLOGY
IN PARTIAL FULFILLMENT OF THE REQUIREMENT FOR THE
DEGREE OF MASTER OF PHILOSOPHY*



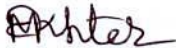
DEPARTMENT OF PHYSICS
KHULNA UNIVERSITY OF ENGINEERING & TECHNOLOGY
KHULNA-9203, BANGLADESH
NOVEMBER, 2013

DEDICATED
TO
MY PARENTS, TEACHERS, WIFE AND KIDS

DECLARATION

This to certify that the thesis work entitled as “Study on the formation and evolution of Tropical cyclone over Bay of Bengal using Weather Research & Forecasting (WRF) model” has been carried out in partial fulfillment of the requirement for M. Phil. degree in the Department of Physics, Khulna University of Engineering & Technology, Khulna-9203, Bangladesh. The above research work or any part of this work has not been submitted to anywhere for the award of any degree or diploma. No other person’s work has been used without due acknowledgement.

Supervisor



Dr. Md. Abdullah Elias Akhter

Candidate



Md. Nazrul Islam

ACKNOWLEDGEMENT

I have had a lot of help with this thesis work from many individuals in various selfless Ways. I take this opportunity here to express my gratitude.

With my great manner it is great pleasure for me to express my deepest sense of gratitude, indebtedness and honour to my respected supervisors Dr. Md. Abdullah Elias Akhter, Professor & Head, Department of Physics, Khulna University of Engineering & Technology, Khulna for suggesting me the problem and for his able guidance, encouragement and constant consultation throughout the course of the research work without which it would not be possible on my part to complete the work.

It is a matter of great pleasure for me to record the deepest sense of gratitude to Professor Dr. Shibendra Shekher Sikder, Department of Physics, Khulna University of Engineering & Technology, Khulna, who has given me a strong support in various ways during the entire period of my study in this department.

I am indebted also to Professor Dr. Md. Mahbub Alam, and Professor, Dr. Jolly Sultana, Department of Physics, KUET for their invaluable suggestions and inspiration during my study in this department.

I gratefully acknowledge Mr. Md. Kamrul Hasan Reza, Assistant Professor and Mr. Sujit Kumar Shil, Lecturer, Department of Physics, KUET for their cooperation regarding writing the thesis.

I convey my sincere thanks to Professor Dr. Md. Abdus Satter, honorable Vice-Chancellor Jessore Science and Technology University who extended his helping hands and gave me potential administrative supports and constant encouragements during this research work.

My thanks are for my colleagues Engg. Md. Ahasun Habib, Dr. Md. Zafirul Islam, Mr. Md. Fisol Habib, Mr. Md. Kabir Hossain, Mr. Md. Abdur Rahaman, Tipu Sultan for their inspiration when I was doing my research works.

My personal thankful greetings are to my good friends and well wishers for their help and cooperation. I am highly grateful to my parents, brothers, sisters and nearest relatives for their inspiration, encouragement and support to carry out this M.Phil thesis work.

My thanks are due to research staff of SMRC and Bangladesh Meteorological Department (BMD) for providing necessary data with other necessary help.

I am very much grateful to my father, mother, father in law and mother in law for their support during the period when I was doing research and there are numerous people who could not be mentioned individually but their interesting discussions have prompted much thought on various aspects, I would also like to thank them.

I would like to extend my special thanks to my wife Mrs. Tania Sultana, for keeping me free from most of the family dealings during the work and also for continuous cooperation, encouragement and tremendous help which she kindly extended for me throughout the progress of my study.

I also wish to thank the authority of Khulna University of Engineering & Technology (KUET), for providing me with the necessary permission and financial assistance for conducting this thesis work.

All thanks and gratitude is due to Almighty Allah whose blessings are always with me.

**KHULNA UNIVERSITY OF ENGINEERING & TECHNOLOGY
DEPARTMENT OF PHYSICS**

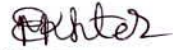
Approval

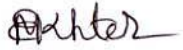
This is to certify that the thesis work submitted by *Md. Nazrul Islam* " *Study of the Formation and Evolution of Tropical Cyclone over Bay of Bengal Using Weather Research & Forecasting (WRF) Model*" has been accepted by the board of examiners for the partial fulfillment of the requirements for the degree of *Master of Philosophy* in the Department of *Physics*, Khulna University of Engineering & Technology, Khulna, Bangladesh in November 29, 2013.


Board of Examiners

Sl. No. Name, Designation & Address

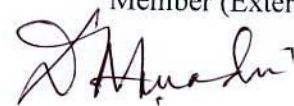
1. Prof. Dr. Md. Abdullah Elias Akhter
Department of Physics
Khulna University of Engineering & Technology
2. Head
Department of Physics
Khulna University of Engineering & Technology
Khulna 9203
3. Prof. Dr. Shibendra Shekher Sikder
Department of Physics
Khulna University of Engineering & Technology
Khulna 9203
4. Prof. Dr. Jolly Sultana
Department of Physics
Khulna University of Engineering & Technology
Khulna 9203
5. Prof. Dr. D. A. Quadir
(CSO (Rtd), SPARSO)
Department of Physics
Uttara University
Dhaka -1000


.....
Chairman & Supervisor


.....
Member


.....
Member 29/11/13


.....
Member 29/11/13

.....
Member (External)


Contents

	Page No
Acknowledgement	i
Contents	iii
List of Tables	v
List of Figures	vi
Abbreviations	xv
Abstract	xvii
Chapter I Introduction:	1
1.1 General introduction	2
1.2 Adjoining land masses and geophysical location of Bay of Bengal	7
1.3 Objectives and scope of the research work	9
1.4 Socio-economic benefit of the research work	9
1.5 Outline of the research work	10
CHAPTER II Literature Review: Description of Tropical cyclones and Weather Research Forecasting (WRF) mode	11
2.1 Tropical cyclone	12
2.1.1 Definition, classification and expression of Tropical cyclone	12
2.1.2 Life cycle, structure and configuration of tropical cyclone	18
2.1.3 Observation of movement and forecasting of Tropical cyclone	26
2.1.4 Earlier studies and chronological improvement of Prediction model.	31
2.2 The Weather Research and Forecasting (WRF) model	38
2.2.1 Definition of WRF model	38
2.2.2 Advanced Research of ARW model	40
2.2.3 Initial conditions	48

2.2.4	Nesting options	53
2.2.5	physics options	57
2.2.6	Land-surface model	59
CHAPTER III	Methodology:	64
3.1	Preface	65
3.2	Model arrangement for the Bay of Bengal	66
3.3	Model initialization	68
3.4	Life history of selected tropical cyclones	68
3.4.1:	Very severe cyclonic storm Nargis	68
3.4.2:	Very severe cyclonic storm Thane	69
3.4.3:	Cyclonic storm Mahasen	69
CHAPTER IV	Results and Discussion:	71
4.1	Analysis of model results and discussion	72
4.1.1	Prediction of formation	72
4.2	Evolution of tropical cyclones	82
4.2.1	Evolution of minimum sea level pressure (MSLP)	82
4.2.2	Evolution of pressure drop(Δp)	101
4.2.3	Evolution of maximum wind speed (MWS)	104
4.2.4	Evolution of relative vorticity (ξ)	113
4.2.5	Evolution of radius of maximum wind (RMW)	131
4.2.6	Relations among different parameters of tropical cyclone derived from model results.	133
4.2.7	Evolution of tracks (movement) of tropical cyclones	140
CHAPTER V	Conclusions:	147
	References	152
	Appendices	168

LIST OF TABLES

Table No	Description	Page No
1.1	Deaths associated with noteworthy tropical cyclone disasters in the world.	5
2.1	Local name of tropical cyclone in different basin.	13
2.2	Saffir-Simpson Hurricane Scale with examples	15
2.3	Classification of tropical cyclones in North Indian Ocean (Bay of Bengal and Arabian Sea), Maximum Sustain Surface Wind Speed	16
2.4	Classification of low pressure systems (cyclonic disturbances) presently in use countries around the Bay of Bengal for national purposes.	16
2.5	The list of North Indian Ocean cyclone names.	17
2.6	Seasonal lengths and time of maximum occurrence of Tropical Cyclones.	25
2.7	Country wise landfall frequency of the tropical cyclones of the Bay of Bengal for the period 1877-2003.	28
2.8	'T' Classification of cyclonic disturbances and corresponding wind speed and pressure drop, [62].	30
3.1	The tropical cyclone selected for the present modeling study.	66
3.2	Selected parameterization schemes of different physics options.	67
4.1	Minimum sea level pressure (MSLP) of selected tropical cyclone at the stage of highest intensity.	84
4.2	Maximum pressure drop of selected tropical cyclone	102
4.3	Maximum Wind Speed (MWS) of selected tropical cyclone at the stage of highest intensity	105
4.4	Maximum relative vorticity (ξ) at 850 hpa of selected tropical cyclone	114
4.5	Radius of maximum wind (RMW) of selected tropical cyclone	132
4.6	The model simulated different parameters of selected tropical cyclones at the stage of highest intensity.	135

LIST OF FIGURES

Figure No	Description	Page No
1.1	SST distribution over the areas with tropical cyclogenesis.	3
1.2	Movement and landfall of a few tracks of tropical cyclones of the Bay of Bengal and Arabian Sea	4
1.3	Bay of Bengal Map.	8
2.1	Visible satellite image of 1991 Bangladesh Cyclone at 0623 UTC on 29 April.	13
2.2	Satellite image showing the structure of the tropical cyclone.	19
2.3	Radar image showing the structure of mature hurricane.	19
2.4	Model vertical profile of a mature typical tropical cyclone. The central portion is the eye and eye wall.	20
2.5	Wind speed record of Waglan Island during the direct hit of Typhoon York over Hong Kong on 16 September 1999. Notice the dramatic fall and rise in wind strength during the passage of the eye of York.	21
2.6	Regions where tropical cyclones form and the typical paths they take.	24
2.7	The WRF System components.	40
2.8	ARW η coordinate.	44
2.9	Horizontal and vertical grids of the ARW.	47
2.10	Schematic showing the data flow and program components in WPS, and how WPS feeds initial data to the ARW. Letters in the rectangular boxes indicate program names. GEOGRID: defines the model domain and creates static files of terrestrial data. UNGRIB: decodes GriB data. METGRID: interpolates meteorological data to the model domain.	49
2.11	Specified and relaxation zones for a grid with a single specified row and column, and four rows and columns for the relaxation zone. These are typical values used for a specified lateral boundary condition for a real-data case.	53
2.12	1-way and 2-way nesting options in the ARW	54

2.13	Arakawa-C grid staggering for a portion of a parent domain and an imbedded nest domain with a 3:1 grid size ratio. The solid lines denote coarse grid cell boundaries, and the dashed lines are the boundaries for each fine grid cell. The horizontal components of velocity (“U” and “V”) are defined along the normal cell face and the thermodynamic variables (θ) are defined at the center of the grid cell (each square). The bold typeface variables along the interface between the coarse and the fine grid define the locations where the specified lateral boundaries for the nest are in effect.	55
3.1	Model domain with 24km×24km horizontal resolution	67
4.1 (a-d)	Figure 4.1 (a-d): Observed SLP of Nargis (used 0000 UTC of 24 April 2008 as model initial field) (a) 06 hrs simulated SLP of Nargis at 0600 UTC of 24 April (b) 66 hrs simulated SLP of Nargis at 1800 UTC of 26 April (c) 114 hrs simulated SLP of Nargis at 1800 UTC of 28 April (d) 138 hrs simulated SLP of Nargis at 1800 UTC of 29 April.	74
4.2 (e-h)	Figure 4.2 (e-h): Observed SLP of Nargis (used 0000 UTC of 24 April 2008, as model initial field) (e) 162 hrs simulated SLP of Nargis at 1800 UTC of 30 April (f) 186 hrs simulated SLP of Nargis at 1800 UTC of 01 May (g) 210 hrs simulated SLP of Nargis at 1800 UTC of 02 May (h) 216 hrs simulated SLP of Nargis at 0000 UTC of 03 May.	75
4.3 (a-d)	Observed SLP of Thane (a) 0 hrs simulated SLP at 0000 UTC of 23 Dec. 2011 (used as model initial field) (b) 24 hrs simulated SLP of Thane at 0000 UTC of 24 Dec. (c) 72 hrs simulated SLP of Thane at 0000 UTC of 25 Dec. (d) 90 hrs simulated SLP of Thane 1800 UTC of 26 December.	77
4.4 (e-h)	Observed SLP of Thane (used at 0000 UTC of 23 Dec. 2011, as model initial field) (e) 138 hrs simulated SLP of Thane at 1800 UTC of 28 Dec. (f) 162 hrs simulated SLP of Thane at 1800 UTC of 29 Dec. (g) 186 hrs simulated SLP of Thane at 1800 UTC of 30 Dec. (h) 190 hrs simulated	78

SLP of Thane at 0000 UTC of 31 December.

- 4.5 (a-d) Observed SLP of Mahasen (a) at 0600 UTC of 08 May, 2013 (used 0000 UTC as model initial field) (b) 66 hrs simulated SLP of Thane at 1800 UTC of 10 May (c) 72 hrs simulated SLP of Mahasen at 0000 UTC of 11 May (d) 96 hrs simulated SLP of Mahasen 0000 UTC of 12 May. 80
- 4.6 (e-h) Observed SLP of Mahasen (used at 0000 UTC of 08 May 2013, as model initial field) (e) 126 hrs simulated SLP of Mahasen at 0600 UTC of 13, May (f) 162 hrs simulated SLP of Mahasen at 1800 UTC of 14, May (g) 186 hrs simulated SLP of Mahasen at 1800 UTC of 15, May (h) 192 hrs simulated SLP of Mahasen at 0000 UTC of 16, May. 81
- 4.7 (a,b,c) Evolution of model simulated and observed MSLP with time of selected cyclones (a) Nargis (2008), (b) Thane (2011) and (c) Mahasen. 85
- 4.8 (a-d) Model simulated SLP (hPa) of cyclone Nargis (2008) at different stages: (a) at 0000UTC of 26 April (used as initial field) (b) at 0600UTC of 26 April (c) at 1800UTC of 28 April (d) at 1800UTC of 01 May. 86
- 4.9 (a-d) Model simulated SLP (hpa) of cyclone Nargis (2008) at different stages: (a) at 0000UTC of 27 April (used as initial field) (b) at 1800UTC of 27 April (c) at 1800UTC of 28 April (d) at 1800UTC of 01 May.. 87
- 4.10 (a-d) Model simulated SLP (hpa) of cyclone Nargis (2008) at different stages: (a) at 0000UTC of 28 April (used as initial field) (b) at 1800UTC of 28 April (c) at 1800UTC of 30 April (d) at 0000UTC of 03 May. 88
- 4.11 (a-d) Model simulated SLP (hpa) of cyclone Nargis (2008) at different stages: (a) at 0000UTC of 29 April (used as initial field) (b) at 1800UTC of 29 April (c) at 1800UTC of 30 April (d) at 1800UTC of 01 May. 89
- 4.12 (a-d) Model simulated SLP (hpa) of cyclone Nargis (2008) at different stages: (a) at 0000UTC of 30 April (used as initial field) (b) at 1800UTC of 30 April (c) at 1800UTC of 02 May (d) at 0000UTC of 03 May. 90

4.13 (a-d)	Model simulated SLP (hpa) of cyclone Nargis (2008) at different stages: (a) at 0000UTC of 01 May (used as initial field) (b) at 1800UTC of 02 May (c) at 0000UTC of 03 May (d) at 0600UTC of 03 May	91
4.14 (a-d)	Model simulated SLP (hpa) of cyclone Thane (2011) at different stages: (a) at 0000UTC of 26 Dec. (used as initial field) (b) at 0600UTC of 26 Dec. (c) at 1800UTC of 27 Dec. (d) at 0000UTC of 31 December	92
4.15 (a-d)	Model simulated SLP (hpa) of cyclone Thane (2011) at different stages: (a) at 0000UTC of 27 Dec. (used as initial field) (b) at 1800UTC of 29 Dec. (c) at 0000UTC of 30 Dec. (d) at 0000UTC of 31 December.	93
4.16 (a-d)	Model simulated SLP (hpa) of cyclone Thane (2011) at different stages: (a) at 0000UTC of 28 Dec. (used as initial field) (b) at 1800UTC of 29 Dec. (c) at 0000UTC of 30 Dec. (d) at 0000UTC of 31 December.	94
4.17 (a-b)	Model simulated SLP (hpa) of cyclone Thane (2011) at different stages (used at 0000UTC of 29 Dec. as initial field): (e) at 0600UTC of 29 Dec. (f) at 0000UTC of 30 Dec. (g) at 0000UTC of 30 Dec. (h) at 0000UTC of 31 Dec.	95
4.18 (a-d)	Model simulated SLP (hpa) of cyclone Mahasen (2013) at different stages: (a) at 0000UTC of 12 May (used as initial field) (b) at 1200UTC of 12 May (c) at 1200UTC of 15 May (d) at 0000UTC of 16 May.	96
4.19 (a-d)	Model simulated SLP (hPa) of cyclone Mahasen (2013) at different stages: (a) at 0000UTC of 13 May (used as initial field) (b) at 1200UTC of 14 May (c) at 1800UTC of 15 May (d) at 0000UTC of 16 May.	97
4.20 (a-d)	Model simulated SLP (hpa) of cyclone Mahasen (2013) at different stages: (a) at 0000UTC of 14 May (used as initial field) (b) at 1200UTC of 14 May (c) at 1800UTC of 15 May (d) at 0000UTC of 16 May.	98
4.21 (a-d)	Model simulated SLP (hpa) of cyclone Mahasen (2013) at different stages: (a) at 0000UTC of 15 May (used as initial field) (b) at 0600UTC of 15 May (c) at 1800UTC of 15 May (d) at 1800UTC of 16 May.	99
4.22 (a-d)	Model simulated SLP (hpa) of cyclone Mahasen (2013) at different stages (used at 0000UTC of 16 May as initial field): (a) at 0000UTC of 16 May (b) at 0600UTC of 15 May (c) at 1800UTC of 15 May (d) at 0600UTC of 16 May.	100

4.23 (a, b, c)	Evolution of model simulated and observed pressure drop with time of selected Cyclones (a) Nargis, (b) Thane (2011) (c) Mahasen (2013).	103
4.24 (a, b, c)	Evolution of model simulated, estimated from model pressure drope and observed MWS with time of selected cyclones (a) Nargis, (b) Thane (2011) and Mahasen (2013)	106
4.25 (a-d)	Model simulated surface wind (speed in m/s) of cyclone Nargis (2008) at different stages: (a) at 0000UTC of 26 April (used as initial field) (b) at 0600UTC of 26 April (c) at 0000UTC of 28 April (d) at 1800UTC of 01 May.	107
4.26 (e-h)	Model simulated surface wind (speed in m/s) of cyclone Nargis (2008) at different stages (used at 0000UTC of 26 April as initial field): (e) at 0000UTC of 29 April (f) at 0000UTC of 30 April (g) at 0000UTC of 01 May (h) at 0000UTC of 02 May	108
4.27 (a-d)	Model simulated surface wind (speed in m/s) of cyclone Thane (2011) at different stages: (a) at 0000UTC of 26 December (used as initial field) (b) at 0600UTC of 26 December (c) at 0000UTC of 28 December (d) at 0000UTC of 30 December.	109
4.28 (e-h)	Model simulated surface wind (speed in m/s) of cyclone Thane (2011) at different stages (used at 0000UTC of 26 December as initial field): (e) at 0000UTC of 29 December (f) at 0060UTC of 29 December (g) at 0000UTC of 30 December (h) at 0000UTC of 31 Decembe	110
4.29 (a-d)	Model simulated surface wind (speed in m/s) of cyclone Mahasen (2013) at different stages: (a) at 1200UTC of 12 May (used as initial field) (b) at 1800UTC of 12 May (c) at 0000UTC of 13 May (d) at 0000UTC of 16 May.	111
4.30 (e-h)	Model simulated surface wind (speed in m/s) of cyclone Mahasen (2013) at different stages (used at 0000UTC of 12 May as initial field): (e) at 0000UTC of 14 May (f) at 0060UTC of 15 May (g) at 0012UTC of 15 May (h) at 0000UTC of 16 May.	112
4.31 (a, b, c)	Evolution of vorticity at 850 hpa with forecasting houre of selected cyclones (a) Nargis(2008) (b) Thane (2011) and (c) Mahasen (2013)	115

- 4.32 (a-d) Model simulated 850 hpa relative vorticity ($\times 10^{-5} \text{s}^{-1}$) of cyclone Nargis 116
(2008) at different stages: (a) at 0000UTC of 26 April (used as initial field) (b) at 0600UTC of 26 April (c) at 0600UTC of 30 April (d) at 0000UTC of 02 May.
- 4.33 (a-d) Model simulated 850 hpa relative vorticity ($\times 10^{-5} \text{s}^{-1}$) of cyclone Nargis 117
(2008) at different stages: (a) at 0000UTC of 27 April (used as initial field) (b) at 1800UTC of 29 April (c) at 1200UTC of 30 April (d) at 1200UTC of 02 May.
- 4.34 (a-d) Model simulated 850 hpa relative vorticity ($\times 10^{-5} \text{s}^{-1}$) of cyclone Nargis 118
(2008) at different stages: (a) at 0000UTC of 28 April (used as initial field) (b) at 0600UTC of 29 April (c) at 0600UTC of 30 April (d) at 0600UTC of 02 May.
- 4.35 (a-d) Model simulated 850 hpa relative vorticity ($\times 10^{-5} \text{s}^{-1}$) of cyclone Nargis 119
(2008) at different stages: (a) at 0000UTC of 29 April (used as initial field) (b) at 1800UTC of 29 April (c) at 1800UTC of 30 April (d) at 1200UTC of 02 May.
- 4.36 (a-d) Model simulated 850 hpa relative vorticity ($\times 10^{-5} \text{s}^{-1}$) of cyclone Nargis 120
(2008) at different stages: (a) at 0000UTC of 30 April (used as initial field) (b) at 0600UTC of 30 April (c) at 1800UTC of 01 May (d) at 1800UTC of 02 May.
- 4.37 (a-d) Model simulated 850 hpa relative vorticity ($\times 10^{-5} \text{s}^{-1}$) of cyclone Nargis 121
(2008) at different stages (used at 0000UTC of 26 April as initial field): (e) at 0000UTC of 01 May (f) at 0000UTC of 02 May.(g) at 1200UTC of 02 May (h) at 1800UTC of 02 May.
- 4.38 (a-d) Model simulated 850 hpa relative vorticity ($\times 10^{-5} \text{s}^{-1}$) of cyclone Thane (2011) 122
at different stages: (a) at 0000UTC of 26 Dec. (used as initial field) (b) at 0600UTC of 26 Dec. (c) at 1800UTC of 26 Dec. (d) at 1800UTC of 30 Dec.
- 4.39 (a-d) Model simulated 850 hpa relative vorticity ($\times 10^{-5} \text{s}^{-1}$) of cyclone Thane (2011) 123
at different stages: (a) at 0000UTC of 27 Dec. (used as initial field) (b) at 0600UTC of 27 Dec. (c) at 1800UTC of 29 Dec. (d) at 0000UTC of 31 Dec.

4.40 (a-d)	Model simulated 850 hpa relative vorticity ($\times 10^{-5} \text{s}^{-1}$) of cyclone Thane (2011) at different stages: (a) at 0000UTC of 28 Dec. (used as initial field) (b) at 1800UTC of 28 Dec. (c) at 1200UTC of 29 Dec. (d) at 1800UTC of 30 Dec.	124
4.41 (a-d)	Model simulated 850 hpa relative vorticity ($\times 10^{-5} \text{s}^{-1}$) of cyclone Thane (2011) at different stages: (a) at 0000UTC of 29 Dec. (used as initial field) (b) at 0600UTC of 29 Dec. (c) at 0000UTC of 30Dec. (d) at 0000UTC of 31 Dec.	125
4.42 (a-d)	Model simulated 850 hpa relative vorticity ($\times 10^{-5} \text{s}^{-1}$) of cyclone Mahasen (2013) at different stages: (a) at 0000UTC of 12 May (used as initial field) (b) at 0600UTC of 12 May (c) at 0600UTC of 13 May (d) at 1800UTC of 15 May.	126
4.43 (a-d)	Model simulated 850 hpa relative vorticity ($\times 10^{-5} \text{s}^{-1}$) of cyclone Mahasen (2013) at different stages: (a) at 0000UTC of 13 May (used as initial field) (b) at 0600UTC of 13 May (c) at 1200UTC of 15 May (d) at 0000UTC of 16 May.	127
4.44 (a-d)	Model simulated 850 hpa relative vorticity ($\times 10^{-5} \text{s}^{-1}$) of cyclone Mahasen (2013) at different stages: (a) at 0000UTC of 14 May (used as initial field) (b) at 0600UTC of 14 May (c) at 0600UTC of 15 May (d) at 0000UTC of 16 May.	128
4.45 (a-d)	Model simulated 850 hpa relative vorticity ($\times 10^{-5} \text{s}^{-1}$) of cyclone Mahasen (2013) at different stages: (a) at 0000UTC of 15 May (used as initial field) (b) at 1200UTC of 12 May (c) at 1800UTC of 15 May (d) at 0000UTC of 16 May.	129
4.46 (a-d)	Model simulated 850 hpa relative vorticity ($\times 10^{-5} \text{s}^{-1}$) of cyclone Mahasen (2013) at different stages: (a) at 0000UTC of 16 May (used as initial field) (b) at 1200UTC of 12 May (c) at 0600UTC of 13 May (d) at 1800UTC of 15 May.	130
4.47 (a, b, c)	Evolution of model simulated RMW of selected cyclones (a) Naggis (2008), (b) Thane (2011) and (c) Mahasen	133

- 4.48 Relationship of simulated maximum wind speed (MWS) i.e., V_{\max} and simulated(a) central pressure drop (Δp), (b) square root of pressure drop ($\sqrt{\Delta p}$), (c) 850 hpa vorticity and (d) radius of maximum wind (RMW) of selected tropical cyclone Nargis (2008) at the stage of highest intensity. 136
- 4.49 Relationship of simulated maximum wind speed (MWS) i.e., V_{\max} and simulated(a) central pressure drop (Δp), (b) square root of pressure drop ($\sqrt{\Delta p}$), (c) 850 hpa. vorticity and (d) radius of maximum wind (RMW) of selected tropical cyclone Thane (2011) at the stage of highest intensity 137
- 4.50 Relationship of simulated maximum wind speed (MWS) i.e., V_{\max} and simulated(a) central pressure drop (Δp), (b) square root of pressure drop ($\sqrt{\Delta p}$), (c) 850 hpa. vorticity and (d) radius of maximum wind (RMW) of selected tropical cyclone Mahasen(2013) at the stage of highest intensity. 138
- 4.51(a, b, c, d, e, f) Model simulated and observed track of very severe cyclonic storm Nargis (2008) (a) 24 hrs forecast beginning 0000UTC of 26 April, (b) 48 hrs forecast beginning 0000UTC of 27 April, (c) 72 hrs forecast beginning 0000UTC of 28 April, (d) 96 hrs forecast beginning 0000UTC of 29 April, (e) 120 hrs forecast beginning 0000UTC of 30 April, (f) 120 hrs forecast beginning 0000UTC of 01 May. 141
- 4.52 (a, b, c, d) Model simulated and observed track of very severe cyclonic storm Thane (2011) (a) 24 hrs forecast beginning 0000UTC of 26 December, (b) 48 hrs forecast beginning 0000UTC of 27 December, (c) 72 hrs forecast beginning 0000UTC of 28 December, (d) 96 hrs forecast beginning 0000UTC of 29 December. 142
- 4.53 (a, b, c, d, e) Model simulated and observed track of cyclonic storm Mahasen (2013) (a) 24 hrs forecast beginning 0000UTC of 12 May, (b) 48 hrs forecast beginning 0000UTC of 13 May, (c) 72 hrs forecast beginning 0000UTC of 14 May, (d) 96 hrs forecast beginning 0000UTC of 15 May, (e) 120 hrs forecast beginning 0000UTC of 16 May. 143

4.54 Comparison of mean position error in track forecasting against the range 146
of the forecasting hours (Note: CME means combined mean error in
track forecasts of three selected cyclones, VSCS mean very severe
cyclonic storm, CS mean cyclonic storm).

ABBREVIATIONS

AFWA	Air Force Weather Agency
API	Application Program Interface
ARPS	Advanced Regional Prediction System
ARW	Advanced Research WRF
BUFR	Binary Universal Form for the Representation of Meteorological Data
CAPE	Convectively Available Potential Energy
CAPS	Center for the Analysis and Prediction of Storms
CGM	Conjugate Gradient Method
COAMPS	Coupled Ocean / Atmosphere Mesoscale Prediction System
COMET	Cooperative Program for Operational Meteorology, Education, and Training
DFI	Digital Filtering Initialization
DTC	Developmental Tested Center
ECMWF	The European Centre for Medium-Range Weather Forecasts
EOF	Empirical Orthogonal Function
ESMF	Earth System Modeling Framework
FAA	Federal Aviation Administration
FGAT	First Guess at Appropriate Time
FSL	Forecast System Laboratory
GFDL	Geophysical Fluid Dynamics Laboratory
GFS	Global Forecast System
GRIB	Gridded Binary
KMA	Korean Meteorological Administration
LSM	Land Surface Model
MKS	Meter Kilogram Second
MM5	Pennsylvania State / NCAR Mesoscale Model Version 5
MMM	Mesoscale and Microscale Meteorology Division
MRF	Medium Range Forecast Model
NAM	North American Mesoscale Model
NCAR	National Center for Atmospheric Research



NCEP	National Centers for Environmental Prediction
NFS	Non-hydrostatic Forecast System (Central Weather Bureau of Taiwan)
NMM	Nonhydrostatic Mesoscale Model
NOAA	National Oceanographic and Atmospheric Administration
NRL	Navy Research Laboratory
NWP	Numerical Weather Prediction
OSU	Oregon State University
PBL	Planetary Boundary Layer
PPM	Piecewise Parabolic Method
QNM	Quasi Newton Method
RHS	Right Hand Side
RRTM	Rapid Radiative Transfer Model
RUC	Rapid Update Cycle
SI (WRF)	Standard Initialization
TKE	Turbulent Kinetic Energy
UCAR	University Corporation for Atmospheric Research
YSU	Yonsei University (Korea)
VAR	Variational Assimilation
WRF	Weather Research and Forecasting Model

ABSTRACT

In the tropics the tropical cyclone is one of the most disastrous atmospheric phenomena of the tropics, which forms over the warm oceans and ravage life and property especially over the coastal belt due to extremely strong winds and associated storm surges at the time of landfall. The Bay of Bengal is highly vulnerable to tropical cyclogenesis. To save the life and minimize the damages it is necessary to make advance warning and prediction of tropical cyclone quite ahead of time. Therefore a study has been conducted to investigate the formation, evolution, structure, track and landfall of tropical cyclones using Advanced Research WRF (ARW) model. The study has been performed for three land falling tropical cyclones of different intensities formed in the Bay of Bengal and had their landfall to the coast of Bangladesh, Myanmar and east coast of India. These are very severe cyclonic storm Nargis (2008), very severe cyclonic storm Thane (2011) and cyclonic storm Mahasen (2013). The model has been set for the Bay of Bengal basin at 9 km horizontal resolution with Kain-Fritsch (KF) cumulus parameterization, WRF-single moment (WSM) 3-class microphysics and Yonsei University PBL schemes. The GFS resolution has been used as initial field and lateral boundary conditions.

The present study shows that the ARW model is capable of forecasting the formation of the first low pressure system 24 hrs ahead from its actual genesis without incorporation of any artificial vortex and is capable to forecast the formation of the first depression. The model successfully simulates the realistic evolution process and more or less realistic intensification of tropical cyclones. For some cases the model under estimated the intensity of the cyclonic system. The model results indicate that the longer range prediction provides better intensity forecast. The model generates a realistic structure of the tropical cyclones with high spatial details. This has been possible due to the higher spatial resolution of the regional model. One of the outstanding findings of the study is that the model has successfully predicted the tracks, recurvature and time of landfall of the selected tropical cyclones with high accuracy even in the 96 hrs prediction. Therefore the model has high potential to predict the formation, evolution, intensity, track and landfall of the tropical cyclones of the Bay of Bengal.

Chapter-I
Introduction

1.1 General Introduction

The tropical cyclones (TC) are perhaps the most devastating of natural disasters of the tropics because of the loss of human life they cause and the large economic losses they induce ([1]; [2]; [3]; [4]; [5]). A single storm in Bangladesh in 1970 killed nearly half a million people ([6]; [7]). Vulnerability to tropical cyclones is becoming more pronounced because the fastest population growth is in tropical coastal regions. Understanding tropical cyclone genesis, development and associated characteristic features has been a challenging subject in meteorology over the last several decades. In recent years, attempts to associate tropical cyclone trends with climate change resulting from greenhouse warming has led to additional attention being paid to tropical cyclone prediction ([8]; [9]; [10]).

A tropical cyclone (TC) is the generic term for a non-frontal warm core synoptic scale low-pressure system originating over tropical or sub-tropical waters with organized convection and definite cyclonic surface wind circulation- counter clockwise in the Northern Hemisphere and clockwise in the Southern Hemisphere [11]. It is a low-pressure system with maximum sustainable winds over 62 km/hr, which can go up to around 300 km/hr. A mature tropical cyclone has a horizontal dimension of around 500-1500 km and extends through the depth of the troposphere, about 15 km ([12]; [6]). The well developed system vertically extends up to 100 hPa level with several towers of cumulus clouds organized in a number of spiral bands. The mature cyclone often has a clear region around its center with diameter of about 5-50 km, which is called the eye of the cyclone and is characterized by descending motion. Away from the center the system has strong upward motion due to large-scale convergence of moist air within the boundary layer. The convective clouds are formed due to adiabatic ascent of this highly moist air and enormous energy in the form of latent heat is released through condensation of water vapor. This condensation heat allows the pre-existing atmospheric lows to develop into the tropical cyclones provided all other conditions are favorable. The tropical cyclones are formed in the tropical warm ocean with sea surface temperature (SST) higher than 26.5°C and with latitudes higher than 5°N in an atmosphere with low vertical wind shear ([11]; [7]). Such a high surface temperature is necessary to produce a steep lapse rate for maintaining the vertical circulation in a cyclone [7]. Figure 1.1 shows SST distribution over the areas with tropical cyclogenesis.

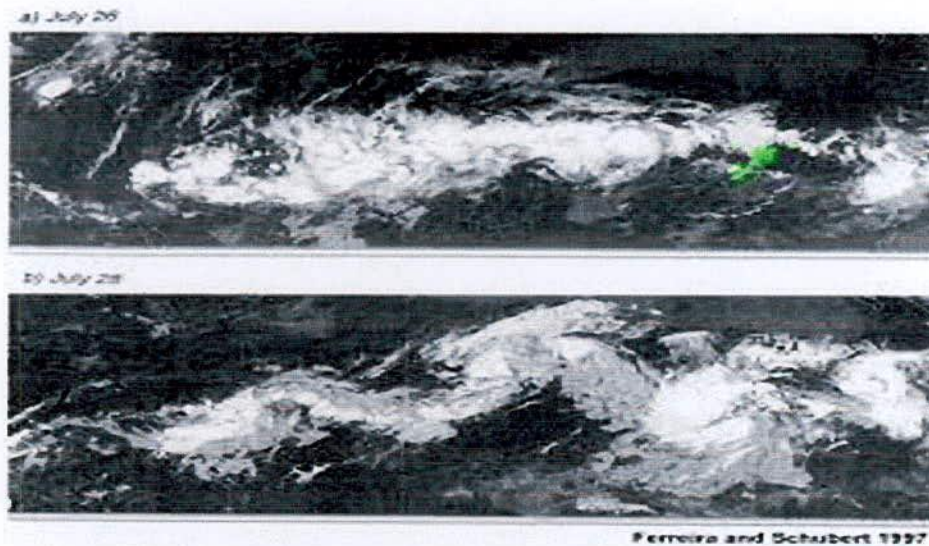


Figure 1.1 shows SST distribution over the areas with tropical cyclogenesis.

Tropical cyclones are heat engine that convert the heat energy of the tropical ocean into winds and waves [14]. They can produce extremely strong winds, tornadoes, torrential rain, high waves, and storm surges. The heavy rains and storm surges can produce extensive flooding. Tropical cyclones on the open sea cause large waves, heavy rain, and high winds, disrupting international shipping and, at times, causing shipwrecks. However, the most devastating effects of a tropical cyclone occur when they cross coastlines, making landfall. Strong winds can damage or destroy vehicles, buildings, bridges, and other outside objects, turning loose debris into deadly flying projectiles. The storm surge is responsible for major damages due to a tropical cyclone. The strong wind of the tropical cyclone exerts frictional force on the water surface which is proportional to the square of the wind speed. This frictional force causes high gravity waves with heights of up to 10-12 meters. These waves cause water to flow inland and lash everything in its path. The ultimate effect is the heavy loss of lives, properties and damages to ecosystem and environment.

The tropical cyclones being formed in the Bay of Bengal frequently hit the coastal regions of Bangladesh, India, Myanmar and, to a lesser extent, Sri Lanka (Figure 1.2) and thereby cause damages to lives and properties. The Bay of Bengal basin is highly vulnerable to strong tropical cyclogenesis because it generally maintains a temperature between $(28-30)^{\circ}\text{C}$ during the tropical cyclone seasons [15]. The distribution of the average temperature of the Bay of Bengal also

indicate that the Bay of Bengal SST is sufficiently warm and has high potential for tropical cyclogenesis due to the existence of sufficiently large energy pool in its deep boundary layer [16]. The above authors have also shown that the depth of 26° C isotherm (D26) varies from (70-100)m during the cyclone seasons and lies over the central and southern Bay. Besides, high values of Cyclone Heat Potential (CHP > 16 kcal/cm²) has been found over the regions of the Bay of Bengal with high frequency of tropical cyclone formation. The CHP is the integral heat content within the layer between the surface and the depth of D26. The high SST and the deep warm layer with large CHP have caused this Bay to become a breeding ground of the tropical cyclones. The shallow waters of Bay of Bengal, the low flat coastal terrain, and the funneling shape of the coastline lead to devastating losses of lives and property due to the surge from a storm of even moderate intensity [17]. The great Bakergong cyclone of 1876 ceased 200,000 lives, which is tremendous in respect to the total population of the country at that time, occurred with 12 m height storm surge, the world's highest recorded storm surge, in this basin ([18]; [19])

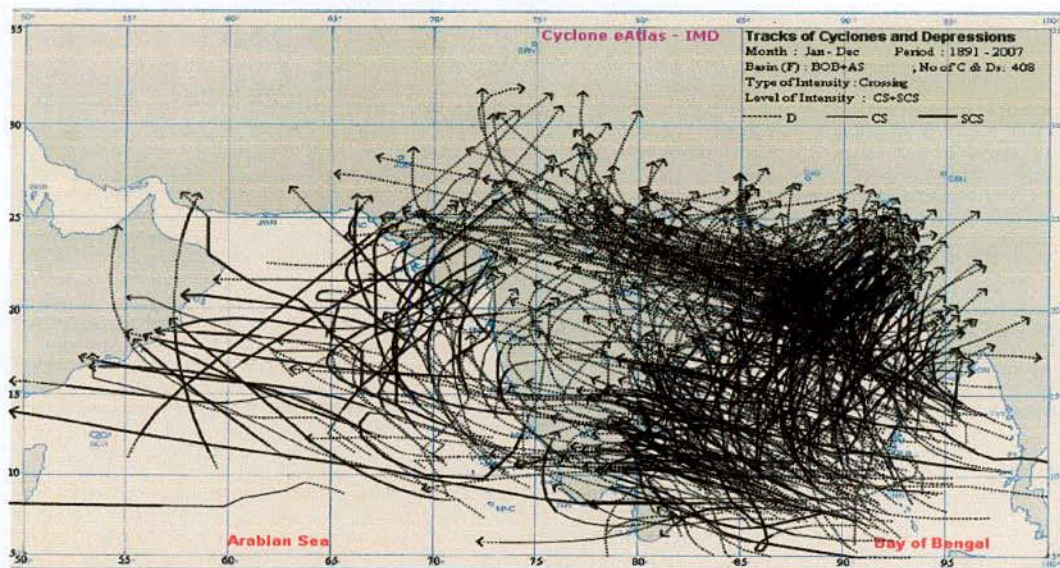


Figure 1.2 Movement and landfall of a few tracks of tropical cyclones of the Bay of Bengal and Arabian Sea [20].

Table 1.1 Deaths associated with noteworthy tropical cyclone disasters in the world ([21]; [22]; [23]; [7])

Year	Location	Deaths
1970	Bangladesh	500,000
1737	India	300,000
1888	China	300,000
1923	Japan	250,000
1876	Bangladesh	200,000
1897	Bangladesh	175,000
1991	Bangladesh	140,000
2008 (Nargis)	Myanmar	130,000
1833	India	50,000
1854	India	50,000
1864	India	50,000
1822	Bangladesh	40,000
1912	Bangladesh	40,000
1919	Bangladesh	40,000
1942	India	40,000
1780	Antilles	22,000
1779	India	20,000
1839	India	20,000
1989	India	20,000
1965	Bangladesh	19,279
1999	India	15,000
1965	Bangladesh	12,000
1963	Bangladesh	11,520
1961	Bangladesh	11,466
1985	Bangladesh	11,069
1937	Hong Kong	11,000
1971	India	10,000
1977	India	10,000
1906	Hong Kong	10,000
1941	Bangladesh	7,500
1963	Cuba-Haiti	7,196
1900	Texas	6,000
1990	USA	6,000
1988	Bangladesh	5,708
1960	Bangladesh	5,149
1895	India	5,000
1960	Japan	5,000
1973	India	5,000
2007	Bangladesh	3,300
2011	India	48

On an average 80 tropical cyclones with wind speed equal to or greater than 62 km/hr (35 knots) form in the world ocean of which 5.5% occurs in the Bay of Bengal which are most deadly ([17]; [24]). It would seem that Bay of Bengal basin is not a high-risk cyclone-prone area. The situation,

however, is otherwise. Mortality associated with the tropical cyclones in the North Indian Ocean is considerably high mainly due to poor socio-economic conditions of the bordering countries (May be seen from Table 1.1). Damages to the life and property depend also on near-shore bathymetry and coastal topography of the northern Bay in addition. In the past out of 10 recorded cases of very heavy loss of life (ranging from about 40,000 to well over 200,000) in the world due to tropical cyclones, 8 cases were in the Bay of Bengal and the Arabian Sea (5 in Bangladesh and 3 in India) (WMO, [19]). Considering the world's tropical cyclones with death tolls in excess of 5,000 during the year 1584-1991, [22] reported that about 53% of the world deaths from these cyclones took place in Bangladesh and about 23% in India, for a combined total of 76% in these 2 countries. In the past, a deadliest severe tropical cyclone has swept the low-lying areas of Bangladesh and adjacent west-Bengal of India, killing more than 500,000 people in November 1970 [7]. The super cyclone of 29 April 1991 that attained the wind speed of 259 km/hr (140 knots) (JTWC, [25]) and hit the coast of Bangladesh along the Meghna estuary had produced the maximum storm surge height of around 8 m and caused 140,000 lives ([21]; [24]; [7]). The tropical cyclone of 29 October 1999 hit the coast of Orissa with wind speed of 260 km/hr and produced heavy rainfall causing flood. The storm surges of more than 8 m height were associated with this super cyclone. About 15,000 lives were lost. over a million were rendered homeless and existing infrastructures were damaged ([21]; [24]). Nargis, very severe cyclonic storm equivalent to category 4 of Saffir-Simpson scale, is one of the deadliest tropical cyclones developed in the Bay of Bengal which hit low-lying delta of Irrawaddy in Myanmar in May 2008 killing more than 84,000 people [26]. A very severe cyclonic storm in the recent history equivalent to category 1 of Saffir-Simpson scale developed over the Bay of Bengal on December, 2011 killing more than 48 people, with a wind speed of 120-140 kmph. It crossed north Tamil Nadu and Puducherry Coast between Puducherry and Cuddalore. A cyclonic Storm, Mahasen crossed Bangladesh coast near lat. 22.8°N and long. 91.4°E, about 30 km south of Feni around 1330 hrs IST of 16th May 2013 with a sustained maximum wind speed of about 85-95 kmph. It weakened into a well marked low pressure area over Nagaland in the early morning and moved away towards Myanmar as a low pressure area in the morning of 17th. The above facts amply illustrate the importance of an efficient cyclone warning service in this region. Though there are several studies on the structure and movement of these tropical cyclones in this region, accurate and reliable forecast of landfall with sufficient lead time are still not achieved. Accurate prediction of landfall and intensity of tropical cyclone is of paramount importance in taking proactive mitigation measures for reducing damages to life and property in the vulnerable region. The present study has been performed using Numerical Weather Prediction (NWP)

modelling techniques. The formation and evolution for two tropical cyclonic events of different intensities viz. severe cyclonic storm with a core hurricane wind Nargis (2008) and very severe cyclonic storm Thane (2011) in the Bay of Bengal have been investigated using the Advanced Research WRF (ARW) Model at grid spacing of 24 km. Here WRF stands for Weather Research and Forecasting. WRF is a new generation mesoscale numerical weather forecasting community model, which has the potential to simulate meteorological phenomena ranging from meters to thousands of kilometers. The WRF model is a fully compressible and nonhydrostatic model (with a runtime hydrostatic option). Its vertical coordinate is a terrain-following hydrostatic pressure coordinate. Advance Research WRF (ARW), developed by the Mesoscale and Microscale Meteorological (MMM) Division of National Centre for Atmospheric Research (NCAR) of USA, is a dynamic solver (Skamarock et al., 2008 [27]), which is compatible with the WRF system to simulate broad spectrum of meteorological phenomena. Final Reanalysis (FNL) data (1°x1° resolution) generated by National Centre for Environment Prediction (NCEP) have been used as model initial fields for this study.

1.2 Adjoining land masses and Geophysical location of the Bay of Bengal

The Bay of Bengal, the largest bay of the world, forms the northeastern part of the Indian Ocean. Bay of Bengal is located between latitudes 3°N to 24°N and longitudes 69°E to 98°E. It resembles a triangle in shape, and is bounded in the west by the east coasts of Sri Lanka and India, on the north by the deltaic region of the Ganges-Brahmaputra-Meghna River systems with great Himalayan Mountain Ranges and Tibetan plateau to further north, and on the east by the Myanmar peninsula extended up to the Andaman-Nicobar ridges. The southern boundary of the Bay is approximately along the line drawn from Dondra Head in the south of Sri Lanka to the north tip of Sumatra ([28]; [29]). The Bay occupies an area of about 2,173,000 sq km. The average depth is 2,600m with a maximum depth of 5,258m ([30];[28]). Bangladesh is situated at the head of the Bay of Bengal. The head in the bay are very numerous, including the Andaman, Nicobar and Mergui groups. A number of large rivers — Padma (Ganges), Meghna, Jamuna (Brahmaputra), Irrawaddy, Krishna and Cauvery and their distributaries — flow into the Bay of Bengal. Among the important ports are Cuddalore, Chennai, Kakinada, Tuticorin, Machilipatnam, Paradip, Kolkata, Mongla, Chittagong and Yangon. Cox's Bazar, one of the longest stretches of beaches in the world, is situated on head of the Bay of Bengal.

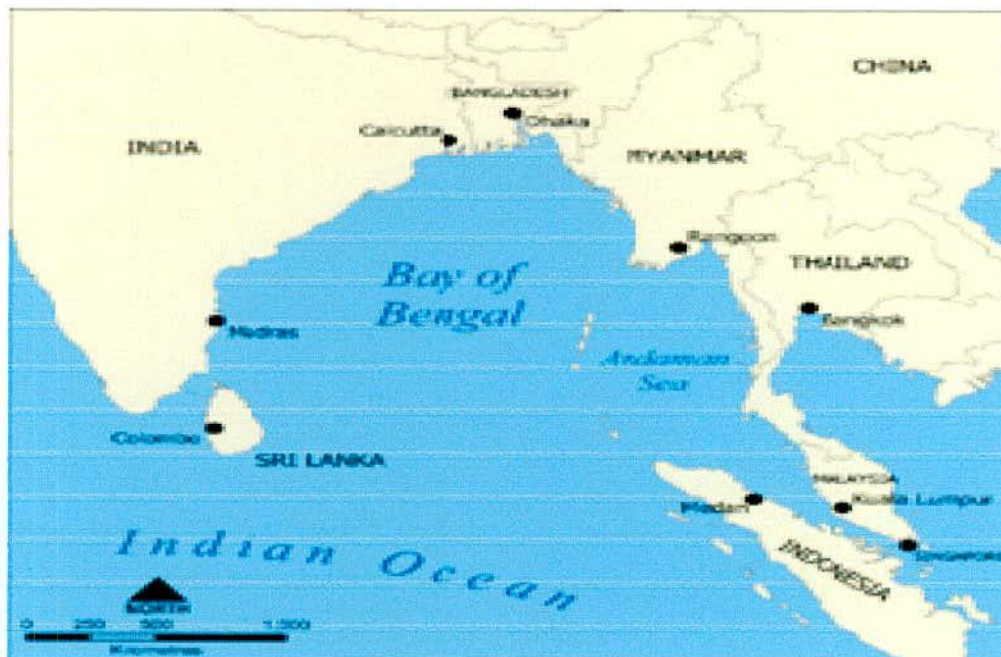


Figure 1.3 Bay of Bengal Map.

The mean annual temperature of the surface water of Bay of Bengal is about 28°C. The maximum temperature is observed in May (30°C) and the minimum (25°C) in January-February. But the annual variation in temperature is not great, about 2°C in the south and 5°C in the north [29]. Bay of Bengal has the semi-diurnal type of tides, i.e. two high and two low tides during period of 24 hours and 52 minutes. The highest tide is seen where the influence of bottom relief and the configuration of the coast are prominent, i.e. in shallow water and in the Bay and Estuary. The average height of tidal waves at the coast of Sri Lanka is 0.7m and in the deltaic coast of the Ganges it is 4.71m. In the Bay of Bengal tidal currents specially develop in the mouths of the rivers, like the Hooghly and the Meghna ([29]). Due to the influence of water density and wind the seasonal changes of the sea level in the Bay are remarkable and one of the highest in the world. The range at Khidirpur is 166cm, Kolkata 130 cm and at Chittagong 118cm [29]. But towards the southwestern coast at Madras and Vishakhapatnam the range is small compared to the northern and northeastern coasts of the Bay. The lowest variation of sea level at the southeastern coast of India is due to its geographical location at the edge of a comparatively deep sea. Weather conditions are often brutal in the Bay of Bengal as the area is ravished by heavy monsoon rains. Destructive cyclones are common in the months of April-May and October-

1.3 Objectives and Scope of the Research Work

The present study has been conducted with the following objectives:

- To investigate the applicability of ARW model which is a new generation model of Numerical Weather Prediction (NWP) family.
- To setup the model and its various optional parameters which suit most for the study of Bay of Bengal cyclones
- To investigate the physics and dynamics related to formation and evolution of the tropical cyclones.
- To investigate the horizontal structure of the tropical cyclones at its mature state.

1.4 Socio-Economic Benefit of the Research Work

The loss of life, property and human suffering caused by tropical cyclones in coastal areas in various parts of the globe are well known. The major damages are caused by storm surges associated with tropical cyclones. The tropical cyclones are extremely disastrous for the Bay of Bengal region particularly for estuarine coast of Bangladesh mainly due to the shallow topography of the coast and funnel shape of the coastline providing suitable condition for generating high storm surges.

The tropical cyclones can neither be destroyed nor be prevented, but the damages can be minimized by proper management practices which include preparedness, rescue operation and rehabilitation. For taking proper measures for preparedness and rescue operation the advance warning and prediction of tropical cyclone quite ahead of time is highly important. For prediction of tropical cyclone it is necessary to understand the physical mechanism of its formation, evolution and structure.

There is no way to study the tropical systems through meteorological observations alone as the oceanic areas of the world severely lack in meteorological networks. Only the operational satellite observations provide information on the physical presence of the weather systems via cloud pictures on now-casting basis. The three dimensional detail structures of tropical cyclones are not yet fully retrievable from the satellite observing system. However, the Numerical Weather Prediction (NWP) models are used to obtain short and medium range prediction of weather including tropical cyclones. The initial data used in these models are obtained through assimilation of data from all sources of observations. The models produce the predictions of three dimensional- fields of meteorological elements.

weather including tropical cyclones. The initial data used in these models are obtained through assimilation of data from all sources of observations. The models produce the predictions of three dimensional- fields of meteorological elements.

In addition to the prediction of tropical cyclones using NWP models it is possible to carry out studies for gaining in-depth knowledge and understanding on the formation, evolution and structure characteristics. Better understanding of the tropical cyclones will guide to develop more sophisticated and realistic NWP models for the Bay of Bengal.

The results of the present study will provide improved knowledge on the physics and dynamics of tropical cyclones of Bay of Bengal. Thus the improved prediction from NWP models will provide advance information for cyclone preparedness and rescue operations which can save valuable lives and properties. In this way the present study has immense social values and economic importance. Besides, the knowledge gained through this research will create new avenues for further studies for improving the NWP models useful for Bay of Bengal region.

1.5 Layout of the research work

The thesis has been constructed with the following layout: Abstract, which summarizes the contents of the dissertation which reflects the gist of the research work performed for this dissertation. Chapter I contains general introduction. It describes the geophysical settings of Bay of Bengal and adjacent land masses, objectives and scope of the study and explains how the research results will be of social and economic benefit. Chapter II contains an overview of tropical cyclones which describes the current state of knowledge about the tropical cyclonic system based on literature review also contains a description of Advance Research WRF (ARW) model used in the present study. Chapter III contains the methodology of this study. Chapter IV contains the results and discussions of the study. It deals with model setup, model initialization and analysis and discussion on the formation, evolution and tracks movement of selected tropical cyclones of Bay of Bengal based on model results. In Chapter V, the conclusion of the research findings have been brought in with a few recommendations for future research in his subject.

Chapter-II: Literature Preview

**Description of tropical cyclone and Weather Research Forecasting
(WRF) model**

2.0 Tropical Cyclone

Various item of tropical cyclone are discuss in the following sections

2.1 Definition, classification and naming of Tropical Cyclone:

2.1.1 Definition of Tropical cyclone

A tropical cyclone is a rotational low pressure system in tropics when the central pressure falls by 5 to 6 hpa from the surrounding and maximum sustained wind speed reaches 34 knots (about 62 km/hr). In meteorology, a cyclone (or a vortex) is an area of low atmospheric pressure characterized by inward spiraling winds that rotate counter clockwise in the northern hemisphere and clockwise in the southern hemisphere of the Earth [31]. The word cyclone was first introduced by Captain Hanry Piddington in 1845 which have been derived from the Greek word *kyklos*, meaning "coils of a snake". Other meteorologists of the world immediately accepted the term and it is still current today. Satellite pictures of cyclones show that the nomenclature is very appropriate. Since the generic term 'cyclone' covers a wide variety of meteorological phenomena, such as tropical cyclones, extra-tropical cyclones, and tornadoes, meteorologists rarely use it without additional qualification. Cyclones occurring in the tropical regions are called tropical cyclones and those occurring elsewhere are called extra-tropical cyclones [12]. A tropical cyclone is the generic term for a non-frontal synoptic scale low-pressure system originating over tropical or sub-tropical waters with organized convection and definite cyclonic surface wind circulation [11]. The tropical cyclone is an atmospheric system fueled by the heat released when moist air rises and the water vapor in it condenses [32]. Tropical cyclone is warm core (relatively warmer than the environment at the same pressure level) system while the extra-tropical cyclones and polar lows are cold core frontal systems [11].

Tropical cyclones are heat engine that convert the heat energy of the tropical ocean into winds and waves [14]. They can produce extremely strong winds, tornadoes, torrential rain, high waves, and storm surges. The heavy rains and storm surges can produce extensive flooding in the coastal zone. The energy in an average hurricane may be equivalent to more than 10,000 atomic bombs of the size of the Nagasaki bomb [33]. Although their effects on human populations can be

devastating, tropical cyclones also can have beneficial effects by relieving drought conditions. They carry heat away from the tropics and play an important role in the mechanism of the global atmospheric circulation that maintains equilibrium in the Earth troposphere.

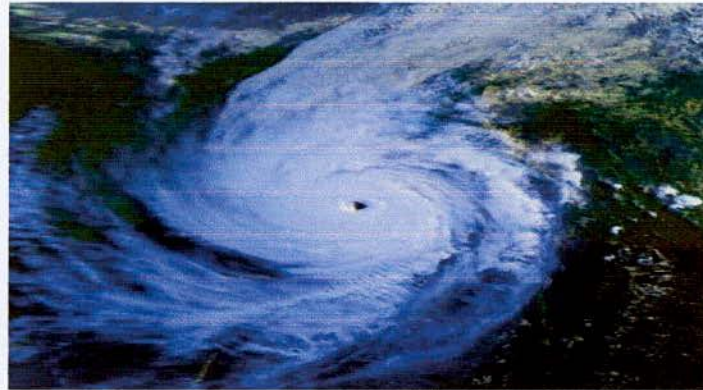


Figure 2.1 Visible satellite image of 1991 Bangladesh Cyclone at 0623 UTC on 29 April (Wikipedia, 2007 [34]).

Depending on their location and strength, there are various terms by which tropical cyclones are known, such as hurricane, typhoon, tropical storm, cyclonic storm and tropical depression. Table 2.1 shows the local name of tropical cyclone in different basin.

Table 2.1 Local name of tropical cyclones in different basin [12].

Area	Local Name
North Indian Ocean (Bay of Bengal and Arabian sea)	Tropical Cyclone
North Atlantic Ocean	Hurricane
Northwest Pacific Ocean	Typhoon
Australia	Willy-willies
Northeast Pacific Ocean	Papagallos
Philippine	Baguios
Madagascar	Trovadoes

2.1.2 Classifications of Tropical Cyclone

Tropical cyclones are classified in accordance with the World Meteorological Organization's recommendation by their maximum sustained wind speeds near the centre. They are classified into three main groups, based on intensity: tropical depressions, tropical storms, and a third group

of more intense storms, whose name depends on the region. For example, if a tropical storm in the Northwestern Pacific reaches hurricane'- strength winds on the Beaufort scale, it is referred to as a typhoon; if a tropical storm passes the same benchmark in the North-East Pacific Ocean, or in the Atlantic, it is called hurricane and in the Southwest Pacific Ocean and Southeast Indian Ocean, it is called 'severe tropical cyclone and in the North Indian Ocean, it is called severe cyclonic storm ([24]; [11]; [6] [35]). A tropical depression is an organized system of clouds and thunderstorms with a defined surface circulation and maximum sustained winds of less than 17 m/s (33 knots, 38 mph, or 62 km/hr). It has no eye and does not typically have the organization or the spiral shape of more powerful storms. However, it is already a low-pressure system, hence the name depression [24]. A tropical storm or tropical cyclone is an organized system of strong thunderstorms with a defined surface circulation and maximum sustained winds between 17 and 32 m/s (34-63) knots, 39-73 mph, or 62-117 km/hr). At this point, the distinctive cyclonic shape starts to develop, although an eye is not usually present [24]. A hurricane or typhoon or severe tropical cyclone is a system with sustained winds of at least 33 m/s (64 knots, 74 mph, or 118 km/hr). A cyclone of this intensity tends to develop an eye, an area of relative calm (and lowest atmospheric pressure) at the center of circulation. The eye is often visible in satellite images as a small, circular, cloud-free spot. Maximum sustained winds in the strongest tropical cyclones have been estimated at about 85 m/s (165 knots, 190 mph, 305 km/hr) [24].

A widely used Hurricane scale is the Saffir- Simpson scale (Table 2.2). The Saffir Simpson Hurricane Scale is a rating based on the hurricane's present intensity. This is used to give an estimate of the potential property damage and flooding expected along the coast from a hurricane landfall. Wind speed is the determining factor in the scale, as storm surge values are highly dependent on the slope of the continental shelf and the shape of the coastline, in the landfall region. Note that all winds are using the U.S. 1-minute average. This scale is generally used for identifying the intensity of hurricanes in Atlantic and Eastern Pacific Oceans.

Table 2.2 Saffir-Simpson Hurricane Scale (NOAA, 2009[35]) with examples

Category	Speed	Damage	Storm Surge	Effect
Very severe cyclonic storm Nargis (2008) was a Category 4 hurricane while moving over the Myanmar coast,[26].	Extreme Hurricane	More extensive curtainwall failures with some complete roof structure failures on small residences. Trees, Shrubs and all signs are blown down. Complete destruction of mobile homes. Extensive damage to doors and windows.	Generally (13-18)ft (4m-5.5m) above normal	Low-lying escape routes may be cut by rising water 3-5 hours before Arrivale of the hurricane center. Major damage to lower floors of structures near the shore. Terrain lower than 10 ft. Above sea level may be flooded requiring massive evacuation of residential areas as far inland as 6 miles (10 km)
Very severe cyclonic storm Thane (2011) of maximum winds 139 km/hr, crossed Coast on 31 st December 2011 was category 1 Hurricane [37].	64-82 knots 119-153 km/hr Minimal Hurricane	No real damage to building structure. Damage primarily to unanchored mobile homes, shrubbery, and trees. Some damage to poorly constructed sings.	Generally (4-5) ft (1.2m-1.5m) above normal	Low-lying coastal roads inundated, minor pier damage, some small craft in exposed anchorage torn from moorings.
Cyclonic storm Mahasen (2013) of maximum winds 95km/hr, crossed Coast on 17 th May 2013 was category 1 Hurricane.	39-44 knots 75-85 km/hr Minimal Hurricane	No real damage to building structure. Damage primarily to unanchored mobile homes, shrubbery, and trees. Some damage to poorly constructed sings.	Generally (3-5) ft (1.0m-1.5m) above normal	Low-lying coastal roads inundated, minor pier damage, some small craft in exposed anchorage torn from moorings

Each basin uses a separate system of terminology. The following classification (Table 2.3) is used for tropical cyclones developed in the North Indian Ocean by the Regional Specialized Meteorological Centre (RSMC) in Indian Meteorological Department (IMD). Table 2.4 shows the existing classifications of low pressure systems (cyclonic disturbances) in the countries around the Bay of Bengal which is used for national purposes.

Table 2.3 Classification of tropical cyclones in North Indian Ocean (Bay of Bengal and Arabian Sea), Maximum Sustain Surface Wind Speed by [19]).

Sl no	Types of Disturbances	mph	knots	Km/hr
1	Low (L)	>19	>17	>31
2	Depression (D)	19-31	17-27	31-51
3	Deep depression (DD)	32-38	28-33	52-61
4	Cyclonic Storm (CS)	39-54	34-47	62-88
5	Severe Cyclonic Storm (SCS)	55-73	48-63	89-118
6	Very Severe Cyclonic Storm (VSCS)	74-137	64-119	119-221
7	Super Cyclonic Storm (SuCS)	≥138	≥120	≥222

Table 2.4 Classification of low pressure systems (cyclonic disturbances) presently in uses countries around the Bay of Bengal for national purposes [19].

Country	Type of Disturbance	Corresponding Wind Speed
Bangladesh	1. Low Pressure area (L) 2. Well marked low 3. Depressoin (D) 4. Deep depression (DD) 5. Cyclonic Strom (CS) 6. Severe Cyclonic Strom (SCS) 7. Very Severe Cyclonic Strom (VSCS) 8. Super Cyclonic Storm (SuCS)	>17 knots (>31 km/hr) 17-21 knots (31-40 km/hr) 22-27 knots (41-51 km/hr) 28-33 knots (52-61 km/hr) 34-47 knots (62-88 km/hr) 48-63 knots (89-117 km/hr) 64-119 knots (118-221 km/hr) ≥120 knots (222 km/hr or above)
India	1. Low Pressure area (L) 2. Depressoin (D) 3. Deep depression (DD) 4. Cyclonic Strom (CS) 5. Severe Cyclonic Strom (SCS) 6. Very Severe Cyclonic Strom (VSCS) 7. Super Cyclonic Storm (SuCS)	>17 knots (>31 km/hr) >17 knots (>31 km/hr) 17-27 knots 28-33 knots 34-47 knots 48-63 knots 64-119 knots ≥120 knots
Myanmar	1. Low (L) 2. Depressoin (D) 3. Cyclonic Strom (CS) 4. Severe Cyclonic Strom (SCS)	>17 knots (>31 km/hr) 17-33 knots 34-63 knots 34-47 knots ≥64 knots
Sri Lanka	1. Low Pressure area (L) 2. Depressoin (D) 3. Deep depression (DD) 4. Cyclonic Strom (CS) 5. Severe Cyclonic Strom (SCS) 6. Very Severe Cyclonic Strom (VSCS) 7. Super Cyclonic Storm (SuCS)	>17 knots (>31 km/hr) 17-27 knots 28-33 knots 34-47 knots 48-63 knots 64-119 knots ≥120 knots

2.1.3 Naming of Tropical Cyclones

Presently, most tropical cyclones are given a name using one of several lists of tropical cyclone names. Storms reaching tropical storm strength were initially given names to eliminate confusion when there are multiple systems in any individual basin at the same time, which assists in warning people of the coming storm. In most cases, a tropical cyclone retains its name throughout its life; however, under special circumstances, tropical cyclones may be renamed while active. These names are taken from lists that vary from region to region and are usually drafted a few years ahead of time. The lists are decided on, depending on the regions, either by committees of the World Meteorological Organization or by national weather offices involved in the forecasting of the storms. Each year, the names of particularly destructive storms (if there are any) are retired and newnames are chosen to take their place. Table 2.5 shows the list of North Indian Ocean cyclone names.

The Importance for naming tropical cyclones is:

- It would help identify each individual tropical cyclone.
- It helps the public to become fully aware of its development.
- Local and international media become focused to the tropical cyclone.
- It does not confuse the public when there is more than one tropical cyclone in the same area.
- The name of the tropical cyclone is well remembered by millions of people as it is unforgettable event whose name will long be remembered. Warnings reach a much wider audience very rapidly.



Table 2.5: The list of North Indian Ocean cyclone names,([19];[35])

Contributed by	List 1	List 2	List 3	List 4
Bangladesh	Onil	Ogni	Nisha	Giri
India	Agni	Akash	Bijli	Jal
Maldives	Hibaru	Gonu	Aila	Keila
Myanmar	Pyarr	Yemyin	Phyan	Thane
Oman	Baaz	Sidr	Ward	Mujan
Pakistan	Fanoos	Nargis	Laila	Nilam
Sri Lanka	Mala	Abe	Bandu	Mahasen
Thailand	Mukda	Khai-Muk	Phet	Phailin
Bangladesh	Helen	Chapala	Ockhi	Fani
India	Lehar	Megh	Sagar	Vayu
Maldives	Madi	Vaali	Baazu	Hikaa
Myanmar	Na-nauk	Kyant	Daye	Kyarr
Oman	Hudhud	Nada	Luban	Maha
Pakistan	Nilofar	Vardah	Titli	Bulbul
Sri Lanka	Priya	Sama	Das	Soba
Thailand	Komen	Mora	Phethai	Amphan

2.2 Life cycle, Structure and Configuration of Tropical Cyclone

2.2.1 The life cycle of tropical cyclone

The complete life cycle of a tropical cyclone usually spans about 9 days but may be only 2 or 3 days or more than 20 days. The life time of tropical cyclone is different for different areas. The average life time of tropical cyclones is 3-5 days in the Bay of Bengal, 7 days in the Pacific Ocean and 9 days in the Atlantic Ocean [12]. The life cycle of a tropical cyclone may be divided into four stages: Formative - The formation of a tropical cyclone is dependent upon a number of favourable environmental conditions which are frequently present in the Inter Tropical Convergence Zone. These include a warm ocean surface (at least 26.5°C) and several physical parameters contributing to a deeply humid and unstable atmosphere. The formation process begins in an area of low pressure coinciding with vigorous convective cloud in the tropics between about 5° and 22° latitude. Usually the cloud cluster drifts slowly towards the west as the convection increases and winds begin spiralling in towards the system centre:

- Immature - As the tropical low becomes further organized and the surface winds reach gale force it is then declared a tropical cyclone according to international convention. Satellite and radar observations of the system show the distinctive spiral banding pattern.
- Mature - If the ocean and atmosphere environment continues to be favourable the cyclone may continue to intensify as it moves poleward. The cloud system becomes more circular in shape and develops a distinct eye. This is the severe cyclone stage where the cyclone is most dangerous. Approximately half of the cyclones that form progress to full maturity.
- Decaying - the power of the cyclone decreases when it moves over land or poleward over colder waters. In this decaying stage the winds often decrease rapidly and the cyclone eye and cloud patterns disappear.

2.2.2 Structure of Tropical cyclone

Structurally, a tropical cyclone is a large, rotating system of clouds, wind, and thunderstorms around an area of low atmospheric pressure near the Earth's surface having horizontal dimensions of around 500-1500 km (Ali, 1999a[12]). Tropical cyclones vertically extend up to upper troposphere. For a well developed system it may extend up to tropopause. The system is characterized by a calm region at the centre with diameter of around 5 to 50 km, which is known

as the eye of the cyclone (Ali, 1999a[12]). In some cases this diameter may be double. The eye is more or less circular in shape. Around eye is the core region of the tropical cyclones which has very strong wind and is characterized by dense cloud overcast which is known as Central Dense Overcast (CDO). The CDO extends over a region of approximately 100-200 km radius from the centre depending on. The overall size of the system. Away from the CDO is the outer periphery of the tropical clone. In the satellite pictures, the cloud distributions in the outer periphery are found to be banding features.

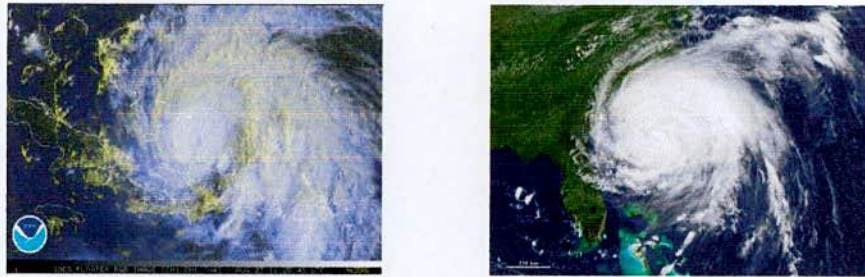


Figure 2.2 Satellite image showing the structure of the tropical cyclone [38].

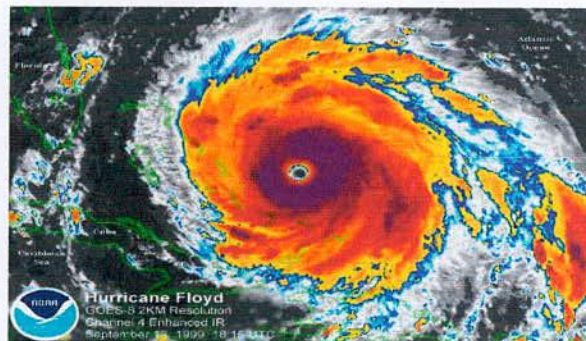
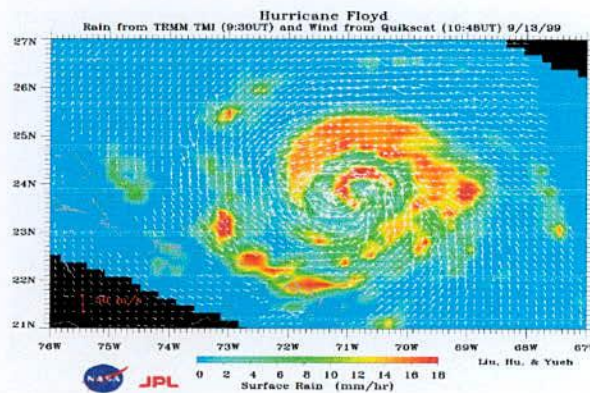


Figure 2.3 Radar image showing the structure of mature hurricane [35].

The overall circulation feature of the tropical cyclone is shown in Figures 2.3-2.5. The area of broken clouds at the center is its eye. Notice that the clouds align themselves into spiraling bands (called spiral rain bands) that swirl in toward the storm's center, where they wrap themselves around the eye. Here rain bands are bands of showers and thunderstorms. Adjacent to the eye, an area about 16—80 km wide, is the eye wall, a ring of intense thunderstorms that whirl around the storm's center and extend upward to almost 15 km above sea level [38]. Within the eye wall, we find the heaviest precipitation and the strongest winds which may be seen from Figure 2.6. The study [39] shows that the rainfall has a logarithmic relation with the cloud temperature of the tropical cyclones.

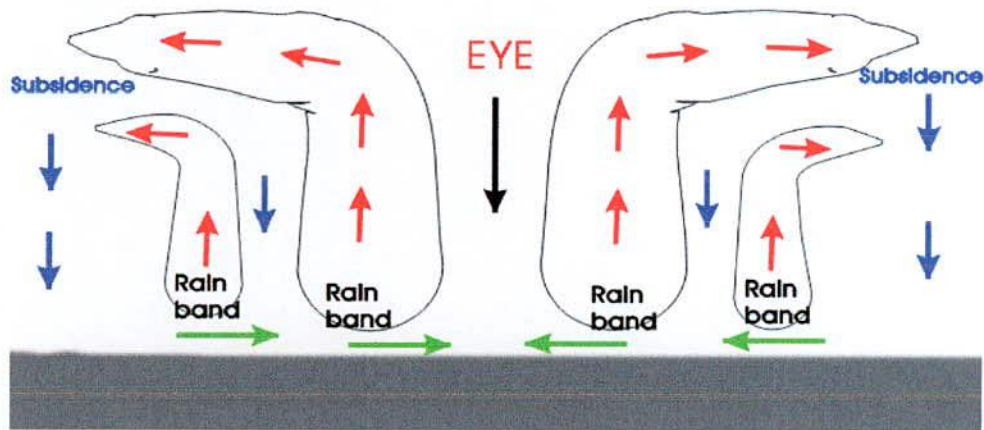


Figure 2.4 Model vertical profile of a mature typical tropical cyclone. The central portion is the eye and eye wall [13].

Tropical cyclones are driven by the release of large amounts of latent heat of condensation as moist air is carried upwards and its water vapor condenses. This heat is distributed vertically around the center of the storm. It is to be mentioned that thermodynamically the tropical cyclone has a warm core with maximum heating in the mid-upper troposphere. At the lower level in the boundary layer it has a cold core [11]. A tropical cyclone is a closed circulation with inflow at low levels, uplift in the wall cloud, diffluence aloft and subsidence in the surroundings (Figure 2.5). The system works like a karnot engine ([14]; [40]; [41]). The energy generated in the cycle is consumed by friction, mainly along the sea surface. The thermodynamic efficiency of this cycle (ϵ) is calculated simply as $\epsilon = (T_w - T_c)/T_w$. So the warmer the sea-surface (T_w) and the colder the tropopause (T_c), the more efficient the tropical cyclone will be. Assuming a typical SST of 300 K and a tropopause temperature of 200 K, you find that the typical tropical storm

efficiency is 1/3. In terms of pressure distributions, the centre of the cyclone has lowest pressure and the pressure drop of the cyclone determines the intensity or maximum wind speed of the system. According to Fletcher (1955)[42], the maximum wind speed, $V = 17 \sqrt[3]{(p_o - p_c)}$ where p_o is the outer pressure and p_c is the central pressure in hPa and V_{max} in knots. But this formula is not found unique for all the basins. A formula, $V_{max} = 13.6 \sqrt[3]{(p_o - p_c)}$, similar to Fletcher's has been proposed by Nessa and Choudhury (1981)[43] for Bay of Bengal cyclones.



Figure 2.5 Wind speed record of Waglan Island during the direct hit of Typhoon York over Hong Kong on 16 September 1999. Notice the dramatic fall and rise in wind strength during the passage of the eye of York [44].

2.2.3 Cyclogenesis

Tropical cyclogenesis is the technical term describing the development and strengthening of a tropical cyclone in the atmosphere. The mechanisms through which tropical cyclogenesis occurs are distinctly different from those through which mid-latitude cyclogenesis occurs. Tropical cyclogenesis involves the development of a warm-core cyclone, due to significant convection in a favorable atmospheric environment. Each year approximately 80-90 tropical cyclones reaching tropical storm intensity occur around the globe ([45]; [1]; [46]) with about two thirds of this reaching hurricane intensity. Understanding tropical cyclone genesis, development and associated characteristic features has been a challenging subject in meteorology over the several decades.

2.2.4 Formation of Tropical Cyclone

The formation of tropical cyclones is the topic of extensive ongoing research and is still not fully understood. The development of tropical cyclones begins with a low-pressure zone that draws in a poorly organized cluster of thunderstorms with weak surface winds; this is a tropical disturbance [14]. The feedback mechanism in the development of a tropical cyclone was described by Holland ([40]; [41]). The six steps of these mechanisms are given below:

(i). A cluster of thunderstorms (in or near the ITCZ, over warm water) heats the middle and upper troposphere, by latent heat release. This heating only occurs when the air parcel, rising from the surface, is warmer than the environment, in other words when it is buoyant. And this only happens when the environmental lapse rate at some levels exceeds the moist adiabatic lapse rate, i.e. when the atmosphere is conditionally unstable.

(ii). This heating explains the development of a weak surface low, by hydrostatic balance.

(iii). This centre of low pressure at sea level triggers winds, which converge into the low and, if the cluster is at least 5° of latitude from the equator, the winds are deflected by the Coriolis force sufficiently to cause cyclonic rotation.

(iv). The surface winds promote evaporation and heat transfer from the ocean surface into the marine boundary layer. This link is essential. Normal thunderstorms are short-lived, because thunderstorms cool the boundary-layer air. According to Dalton's equation, the evaporation rate is linearly proportional to the wind speed. It may be even more sensitive, because strong winds produce ocean spray, much of which evaporates.

(v). The convergence of wind, plus the increased water vapour content, produces moisture convergence over the low.

(vi). This convergence fuels the cloud cluster, so that more rain falls, and more latent heat is released in the troposphere (stage 1). This heating deepens the surface low (stage 2). Consequently stages 3 - 6 are repeated on a larger scale, over and over again. A tropical depression is born, which may further intensify into a tropical cyclone. The stronger the surface winds, the more effective the heat transfer from the ocean.

To undergo these steps to form a hurricane, several environmental conditions must first be in place ([47], [48], [45], [49]; [11]):

- Warm ocean waters (of at least 26.5°C) throughout about the upper 50 m of the tropical ocean must be present. The heat in these warm waters is necessary to fuel the tropical cyclone by supplying enough evaporating moisture.
- The atmosphere must cool fast enough with height, such that it is potentially unstable to moist convection. It is the thunderstorm activity which allows the heat stored in the ocean waters to be liberated for tropical cyclone development.
- The mid.-troposphere (5 km) must contain enough moisture to sustain the thunderstorms. Dry mid levels are not conducive to the continuing development of widespread thunderstorm activity.
- The disturbance must occur at a minimum distance of at least 500 km (at least 5° poleward) from the equator. For tropical cyclonic storms to occur there is a requirement that the Coriolis force must be present because the Coriolis force initiates and maintains tropical cyclone rotation.
- There must be low values (less than about 10 m/s) of vertical wind shear between the surface and the upper troposphere. Large values of vertical wind shear disrupt the incipient tropical cyclone by removing the rising moist air too quickly, preventing the development of the tropical cyclone. Or, if a tropical cyclone has already formed, large vertical shear can weaken or destroy it by interfering with the organization around the cyclone center.
- There must be a pre-existing near-surface disturbance that shows convergence of moist air and is beginning to rotate. Tropical cyclones cannot be generated spontaneously. They require a weakly organized system that begins to spin and has low level inflow of moist air.

The above feedback loop does not work over cold waters. It does not work over land, because the latent heat feedback does not work, instead, there is a negative feedback: stronger winds imply frictional retardation. And even when all conditions are right, tropical cyclones are relatively rare: most cloud clusters do not develop into tropical storms, and most tropical storms do not grow into tropical cyclones (or hurricanes). There is another negative feedback: convective motion stabilizes the atmosphere, and only a continued influx of warm, moist air at low levels can sustain the convection. Moreover, tropical cyclones extract a lot of heat from the ocean, and some slow-moving cyclones have dissipated because the heat transfer and wind-driven upwelling lowered the SST below 26.5°C ([40];[41]).

2.2.5 Formation Areas

The favorable locations for tropical cyclone genesis are in or just pole-ward of the Inter Tropical Convergence Zone (ITCZ) or a monsoon trough which is a worldwide band of thunderstorm

activity along the tropical belt [47]. The ITCZ is generally located near the monsoon shear line between low-level equatorial westerlies and easterly trades. The disturbances embedded in the easterly trade wind flow are also conducive to the formation of tropical cyclones [46].

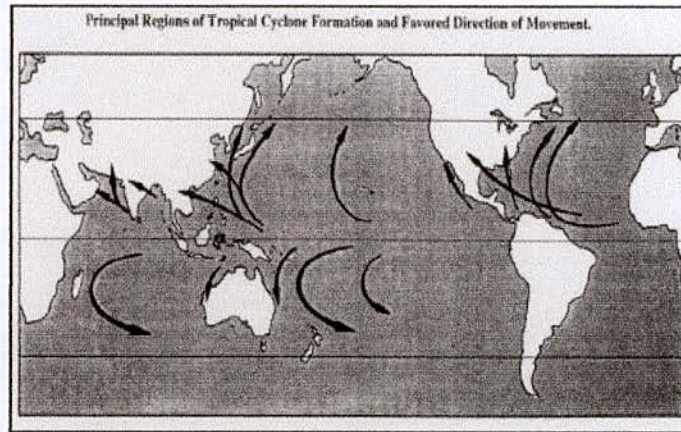


Figure 2.6 Regions where tropical cyclones form and the typical paths they take [35].

Tropical cyclones form where sea temperatures are high, exceeding 26°C ([49]; [1 1]). They originate on the eastern side of oceans, but move west, intensifying as they move. Most of these systems form between 5° and 20° of the equator (in fact, about two-thirds of all tropical cyclones form between 10° and 20° of the equator) except for the Southeast Pacific and the South Atlantic Oceans, where environmental conditions are not favourable ([33]; [38]). Because the Coriolis effect initiates and maintains tropical cyclone rotation, Tropical cyclones rarely form or move within about 5° of the equator, where the Coriolis effect is weakest ([35]; [33]). However, it is reported that tropical cyclones were formed within this boundary as did Typhoon Vamei in 2001 and Cyclone Agni in 2004. There are seven tropical cyclone basins (Figure 2.7) where storms occur on a regular basis[35]:

- (i). Atlantic basin, Including the North Atlantic Ocean, the Gulf of Mexico, and the Caribbean Sea
- (ii). Northeast Pacific basin, from Mexico to about the dateline
- (iii). Northwest Pacific basin, from the dateline to Asia including the South China Sea
- (iv). North Indian basin, including the Bay of Bengal and the Arabian Sea
- (v). Southwest Indian basin, from Africa to about 100°E
- (vi). Southeast Indian/Australian basin (100°E to 142°E)
- (vii). Australian/Southwest Pacific basin (142°E to about 120°W)

2.2.6 Times of Occurrence

Tropical cyclones occur at particular times. Worldwide, tropical cyclone activity peaks in Late summer and early fall ([33]; [11]). This is associated with the period of maximum sea surface temperature (SST), although other factors, such as the seasonal variation of the monsoon trough location, are also important ([46]; [17]). On a worldwide scale, May is the least active month, while September is the most active. However, each particular basin has its own seasonal patterns. In the North Atlantic, the hurricane season is from 1 June to 30 November. The storm season in the North Atlantic becomes highly active during August-September-October, with a maximum frequency of occurrence in September [50]. The Northeast Pacific has a broader period of activity, beginning in late May or early June and going until late October or early November with a peak in storminess in late August/early September. More tropical cyclones form in the tropical Northwest Pacific than anywhere else in the world. More than 25 tropical storms develop each year, and about 18 become typhoons. These typhoons are the largest and most intense tropical cyclones in the world. The Northwest Pacific sees tropical cyclones year-round, with a minimum in February and a peak in late August/early September. In the Australian region, the tropical cyclone season typically extends from November to May with maximum cyclone activity in January and February ([51], [52]; [53]; [54]). In the Southwest Indian basin cyclone season starts from late October/early November, reaching a double peak in activity-one in mid-January and one in mid-February to early March, and then ends in May. In the North Indian basin, storms are most common from April to June and October to December, with double peak of activity in May and November.

Table 2.6 Seasonal lengths and time of maximum occurrence of Tropical Cyclones,[24].

Basin	Season	Peak Time	% of Global Total
North Atlantic	June to November	September	11%
Northeast Pacific	May to November	Late August/early September	20%
Northwest Pacific	April to December	Late August/early September	31%
Southeast Indian/Australia	November to May	January and February	8%
Australian/Southwest Pacific	November to May	January and February	11%
Southwest Indian	Late October to May	Mid-January and mid-February	12%
North Indian	April to June and October to December	to early March May and November	7%

2.3 Movement observation and Forecasting of Tropical Cyclone

2.3.1 Movement of Tropical Cyclone

Cyclones have two motions: one is wind speed called intensity of cyclone and another is translational speed of the cyclone. The path of motion is referred to as a tropical cyclone's track. The translational speed or movement of cyclone is different for different cyclones. A cyclone also does not move with same speed through its whole trajectory. The movement speed of cyclones in the Northwest Pacific Ocean and western side of the North Atlantic

Ocean is maximum and it is least in the North Indian Ocean (Arabian Sea and Bay of Bengal). The translational speed of a mature tropical cyclone in Bay of Bengal is about 8-10 knots [12]. Once formed, tropical cyclones tend to move westward and pole-ward (Figure 2.7). If they do not dissipate over land or cold water, they usually recurve pole-ward and eastward, often moving into middle and high latitudes before finally dissipating or transforming to extra-tropical cyclones which, unlike their tropical cousins, derive their energy from the potential energy stored in the pole-to-equator temperature gradient [6]. The motions and tracks of tropical cyclones are controlled by different factors. Some are discussed below:

- **Steering winds:** It has been found that the tropical cyclone movement is steered by the upper tropospheric wind overlying the system. This is called the steering wind.
- **Coriolis effect:** The Coriolis force adds additional vorticity to the cyclonic system and turns the east-west moving systems towards north in the northern hemisphere and towards south in the southern hemisphere.
- **Interaction with the mid-latitude westerlies:** When the tropical cyclone moving poleward comes under the mid-latitude westerlies, it takes turn towards the east.

2.3.2 Storm Surges

The storm surges are the large water waves generated due to the frictional stress of the strong wind on water surface and large pressure drop at the centre of the cyclone. In many major tropical cyclone disasters, storm surge is frequently a key factor. As the cyclone approaches the coastal area, strong on-shore winds can cause a rise of several meters in sea level by water current and waves; the result is water crossing the coast and flooding large areas of the interior. The storm surge height also depends on the track of the cyclones and point of landfall. The factors that combine to cause a storm surge are partly meteorological and partly hydrographic, including the state and nature of the tide, the topography of the sea bed in the vicinity of the coast and the configuration of the coast line. Countries most vulnerable to storm surges are those that

experience the more severe tropical cyclones and have low-lying land along the closed and/or semi-enclosed bays facing the ocean. Such countries include Bangladesh, China, India, Japan, Mexico and the United States and, in the southern hemisphere, Australia. Storm surges also pose the threat disaster in temperate zones, particularly in the North Sea where the strong winds of an intense depression may blow towards an exposed coastline. The North Sea is surrounded by land to the west, south and east. It has been the scene of storm surges that have caused heavy loss of life and extensive damage in the countries whose coastline have been affected. These countries have therefore established elaborate protective measures such as complex systems of dikes, flood gates, canals, reservoirs, etc. and warning systems for storm surge. Based on the details of peak storm surge, the entire coast line of India and Bangladesh has been divided into four zones: very high risk prone (surge height greater than 5 m), high risk prone (surge height between 3 m to 5 m), moderate risk prone (surge height between 1.5 m and 3m), and minimal risk prone (surge height less than 1.5 m). Coastal areas of Bangladesh, North Orissa and West Bengal are the most vulnerable zones to storm surges of height greater than 5 m and so also is the Krishna estuary in Andhra Pradesh. South Orissa, North Coastal Andhra Pradesh and South Tamil Nadu are the areas, where surge height between 3 m to 5 m was recorded.

2.3.3 Notable tropical cyclones

Following are some notable tropical cyclone in different perspective: The 1970 Bhola cyclone is the deadliest tropical cyclone on record, killing over 500,000 people after striking the densely populated Ganges Delta region of Bangladesh on 12 December, 1970 ([7]; [56]). Its powerful storm surge was responsible for the high death toll. Hurricane Katrina, hit Louisiana and Mississippi of United States in August 2005, is estimated as the costliest tropical cyclone Worldwide causing \$81.2 billion in property damage (2005 USD) [57]. The most intense storm on record was Typhoon Tip in the northwestern Pacific Ocean in 1979, which reached a minimum pressure of 870 hPa and maximum sustained wind speeds of 305 km/hr [58]. Tip, however, does not solely hold the record for fastest sustained winds in a cyclone. Typhoon Keith in the Pacific and if Hurricanes Camille and Allen in the North Atlantic currently share this record with Tip. Camille was the only storm to actually strike land while at that intensity, making it, with 305 km/hr sustained winds and 335 km/hr gusts, the strongest tropical cyclone on record at landfall. In addition to being the most intense tropical cyclone on record, Tip was the largest cyclone on record, with tropical storm-force winds 2,170 km in diameter. The smallest storm on record, Cyclone Tracy, was roughly 100 km wide before striking Darwin, Australia in 1974. Hurricane John is the longest-lasting tropical cyclone on record, lasting 31 days in 1994. Prior to

the advent of satellite imagery in 1961, however, many tropical cyclones were underestimated in their durations; John is the second longest-tracked tropical cyclone in the Northern Hemisphere on record, behind Typhoon Ophelia of 1960 which had a path of 12500 km.

2.3.4 Vulnerability of the Bay of Bengal region due to Tropical Cyclones

The Bay of Bengal basin is highly vulnerable to tropical cyclogenesis because it generally maintains a temperature between 28-30°C during the tropical cyclone seasons [15]. The distribution of the average temperature of the Bay of Bengal also indicate that the Bay of Bengal SST is sufficiently warm and has high potential for tropical cyclogenesis due to the existence of sufficiently large energy pool in its deep boundary layer [16]. The shallow waters of Bay of Bengal, the low flat coastal terrain, and the funneling shape of the coastline lead to devastating losses of lives and property due to the surge from a storm of even moderate intensity [17]. The greatest single event that killed 500,000 people, in the recent past (1970), occurred in this basin [7]. On an average 80 tropical cyclones with wind speed equal to or greater than 35 knots (62 km/hr) form in the world ocean of which 5.5% occurs in the Bay of Bengal which are most deadly ([7]; [24]; [22]). The vulnerability of the coastal zone of Bay of Bengal due to tropical cyclones during the period 1877-2003 has been studied by the present author [59]. In this period 532 tropical cyclones were formed in the Bay of Bengal of which 218 attained the intensity of severe cyclonic Storms (SCS) which have the maximum sustainable wind speed above 88 km/hour and the remaining 314 stayed in the stage of Cyclonic Storms (CS) having the maximum sustainable wind speed of 62-88 km/hour. The study shows that 58.8% of the tropical cyclones formed in the Bay of Bengal hit the east coast of India, while Bangladesh, Myanmar and Sri Lanka are hit by 16.2%, 10.9% and 3.4% (Table 2.7). Though Bangladesh has lower number of tropical cyclones in respect of landfall, but the storm surge heights are higher in the Bangladesh coast. A country wise breakup of the landfall of cyclone shows that Bangladesh gets about 1% of the world's total cyclones ([60], [22]), however the most deadly cyclones in the world ravage Bangladesh.

Table 2.7: Country wise landfall frequency of the tropical cyclones of the Bay of Bengal for the period 1877-2003 [59].

Type of disturbance	Bangladesh	India	Myanmar	Sri Lanka	Dissipated in the sea	Total
CS	39(7.3)	195(36.7)	26(4.9)	11(2.1)	43(8.1)	314(59.1)
SCS	47(8.8)	118(22.2)	32(6.0)	7(1.3)	14(2.6)	218(40.9)
CS+SCS	86(16.1)	313(58.9)	58(10.0)	18(3.4)	57(10.7)	532(100)

*The values in the parenthesis are landfall frequency as percent of total frequency.

2.3.5 Observation

The observation of tropical cyclone is very important for forecasting. But intense tropical cyclones pose a particular observation challenge since they are formed in the deep sea where there is no much of surface and upper air meteorological observations except some scanty observations in the islands and commercial ships and a few number of floating buoys. Thus the measurements through the satellite sensors are the main data source for observation and monitoring of the tropical cyclones. It is however possible to take in-situ measurements, in real-time, by sending specially equipped reconnaissance flights into the cyclone. In the Atlantic basin, these flights are regularly flown by United States government hurricane hunters [11]. The reconnaissance aircraft was introduced in 1944. The aircraft used are WC-130 Hercules and WP-3D Orions, both four-engine turboprop cargo aircraft. These aircraft fly directly into the cyclone and take direct and remote-sensing measurements. The aircraft launch GPS (Global Positioning System) dropsondes inside the cyclone. These sondes measure temperature, humidity, pressure, and especially winds between flight level and the ocean's surface. A new era in hurricane observation began when a remotely piloted Aerosonde, a small drone aircraft, was flown through Tropical Storm Ophelia as it passed Virginia's Eastern shore during the 2005 hurricane season. This demonstrated a new way to probe the storms at low altitudes that human pilots seldom dare. Tropical cyclones far from land are tracked by weather satellites capturing visible and -infrared images from space, usually at half-hour to quarter-hour intervals. As a storm approaches land, it can be observed by land-based Doppler radar. Radar plays a crucial role around landfall because it shows a storm's location and intensity minute by minute. Recently, academic researchers have begun to deploy mobile weather stations fortified to withstand hurricane-force winds. Satellite data, although extremely useful, are not a complete substitute for reconnaissance aircraft observations because of the difficulties involved in translating radiances into required parameters. Nevertheless, satellite observations are widely used in monitoring tropical cyclone activities in regions where no reconnaissance is yet available. Satellite measurements provide cloud images, vertical sounding, cloud vector wind, surface wind measurements through radar scatterometer, etc. The interpretation techniques of satellite imagery for estimation of maximum sustainable wind speed and central pressure drop have been developed (Dvorak, 1984[61]) and further modified for north Indian Ocean, which is shown in Table 2.8 [62].

Table 2.8: ‘T’ Classification of cyclonic disturbances and corresponding wind speed and pressure drop, [62].

T-Number CI-Number	Synoptic Classification of disturbance	Wind speed in knots	Wind speed in km/hr	Pressure drop in hPa
T1.0	L			
T1.5	D	25	46.3	
T2.0	DD	30	55.6	4.5
T2.5	CS	35	64.9	6.1
T3.0		45	83.4	10.0
T3.5	SCS	55	101.9	15.0
T4.0	VSCS	65	120.5	20.9
T4.5		77	142.7	29.4
T5.0		90	166.8	40.2
T5.5		102	189.0	51.6
T6.0		115	213.1	56.6
T6.5	SuCS	127	235.4	80.0
T7.0		140	259.5	97.2
T7.5		155	287.3	119.1
T8.0		170	315.1	143.3

2.3.6 Forecasting

Tropical cyclone forecasting is the science and art of forecasting where a tropical cyclone’s center, and its effects, is expected to be at some point in the future. There are several elements to tropical cyclone forecasting: track forecasting, intensity forecasting, rainfall forecasting, storm surge, and tornado forecasting. Components of a modern weather forecasting system include: data collection, data assimilation and numerical weather prediction, model output post-processing and forecast presentation to end-user. Today’s forecasters use a system called numerical weather prediction (NWP) model to forecast the weather. Numerical weather prediction models are computer simulations of the atmosphere. They take the analysis as the starting point and evolve the state of the atmosphere forward in time using understanding of physics and fluid dynamics. Commonly, the set of equations used is known as the primitive equations. These equations are nonlinear and are impossible to solve exactly. Therefore, numerical methods are used to obtain

approximate solutions. The horizontal domain of a model is either global, covering the entire Earth, or regional, covering only part of the Earth. Regional models also are known as limited-area models. Different models use different solution methods. Global models often use spectral methods for the horizontal dimensions and finite difference methods for the vertical dimension; while regional models usually use finite difference methods in all three dimensions. Regional models also can use finer grids to explicitly resolve smaller-scale meteorological phenomena, since they do not have to solve equations for the whole globe. Models are initialized using observed data from radiosondes, weather satellites, and other instruments. The irregularly-spaced observations are processed by data assimilation and objective analysis methods, which perform quality control and obtain values at locations by the model's mathematical algorithms (usually an evenly-spaced grid). The data are then used in the model as the starting point for a forecast. The primitive equations are initialized from the assimilated data and rates of change are determined. The rates of change are used to predict the state of the atmosphere a short time into the future. The equations are then applied to this new atmospheric state to find new rates of change, and these new rates of change are used to predict the atmosphere at a yet further time into the future. This time stepping procedure is continually repeated until the solution reaches the desired forecast time. The size of the time step generally depends upon the distance between the points on the computational grid. Time steps for global climate models may be of the order of tens of minutes, while time steps for regional models may be a few seconds to a few minutes. The raw output of models is modified by post-processing software before being presented. The final stage in the forecasting process is presentation of the forecasts to end-user.

2.4 Earlier studies and Chronological improvement of Prediction Models

2.4.1 Earlier studies of Tropical Cyclone

Aerology in the hurricane warning service [63] developed a procedure for identifying tropical disturbances and the progress of their development by following the movement of 24 hr pressure change patterns. In the 1940s, [64] described the wave system that generally embraces and supports the well-developed min disturbances and identified a number of necessary conditions for the development of the wave circulation into a cyclone. In the 1950s, [65] successfully answered a number of questions concerning energy sources and the transformations required for developing and maintaining the cyclone. In the 1960s, the weather satellite supplied for the first time a means of continuously monitoring the movement and development of tropical disturbances and for accumulating a meaningful climatology of them [66]. In the 1960s and

1970s, computer models ([67]; [68]; [69]) provided some additional insight to the problem; but the results were difficult to interpret because, firstly, these models almost invariably produced a full hurricane from every disturbance, and secondly, problems were encountered in parameterizing the unique contribution of cumulus clouds, in the releasing and redistributing energy, which is vital to the support of the hurricane wind system. In the late 1970s, W. M. Gray and his collaborator used many years of data from aircraft flights through hurricanes to derive a different physical basis for the pressure falls that lead to hurricane development [45]. Despite these milestones and other achievements, up to 1980, there remains more scientific agreement or uncertainty concerning the details of the dominant physical processes responsible for hurricane development. However, ([11], [47],[48], [45], [49]) the following conditions for cyclone formation — i) large values of low level relative vorticity, ii) Coriolis parameter (at least a few degrees poleward of the equator), iii) weak vertical wind of horizontal winds, iv) high SSTs exceeding 26°C and a deep thermocline, v) instability through an atmospheric layer and vi) large values of humidity in the middle troposphere. Although the above six parameters are not sufficient conditions for cyclogenesis, ([48], [49]) argued that tropical cyclone formation will be most frequent, in the regions and seasons when the product of the six genesis parameters is a maximum. Gray defined the product of (i), (ii) and (iii) as the dynamic potential for cyclone development, and the product of (iv), (v) and (vi) may be taken as the thermodynamic potential. He derived the seasonal genesis parameter (SGP) from these six parameters [48]; [70] discussed the life cycle, surface structure, upper air structure and many other properties of a tropical cyclone. He also discussed some theories of its formation. Some other theories also evolved afterwards viz. Conditional Instability of Second Kind (CISK) ([71,72]),[73]; [74]; [75]) and Wind-Induced Surface Heat Exchange (WISHE) ([76]. [77]; [78]; [79]; [1] also has discussed various features of tropical cyclones. He also discussed some physical processes related to the tropical cyclone. In ([47]; [48]) produced a global map of genesis points for all tropical cyclones over the 20-year period 1952-1971. Preferred regions of tropical cyclone formation include the western Atlantic, eastern Pacific, western North Pacific, North Indian Ocean, South Indian Ocean and Australian/Southwest Pacific. Most of the cyclones (87%) formed between 20°N and 20°S. About two thirds of all tropical cyclones form in the Northern Hemisphere, and the number of tropical cyclones occurring in the Eastern Hemisphere is about twice that in the Western Hemisphere. These differences are partially due to the absence of tropical cyclones in the South Atlantic and the eastern South Pacific during the 20-year period study. Also identified regions of cyclone formation) [63], which was a little bit different

and has compiled available records of events occurred in the Bay of Bengal and Arabian Sea [21]. The events occurred in the Bay of Bengal basin statistically and found the bimodal occurrences in this basin. Analyzing the crossings of the tropical cyclones through different coastal boundaries of the Bay of Bengal in different seasons ([81];[80]), discussed the vulnerability of different coasts in different seasons. The intensity is a vital factor of the tropical cyclone. In terms of the sustained wind speed the intensity of tropical cyclones are categorized [42] has given a very simple formula [$v_{\max}=17\sqrt{(p_0-p)}$] in terms of the pressure drop to estimate the wind speed in knots. But that formula is not found unique for all the basins. [82] have done a preliminary investigation on estimation of maximum sustained wind associated with Bay of Bengal cyclones. A formula similar to Fletcher's formula [$v_{\max}= 13.6 \sqrt{(p_0-p)}$] has been proposed [43] for Bay of Bengal cyclones which developed a model to predict the maximum surge height associated with cyclones affecting Bangladesh [83]. The maximum sustained wind and central pressure drop are generally determined from the interpretation of satellite data using Dvorak techniques. This techniques were used [84] for May 1997 cyclone to study evolution and intensity, variation in terms of T-number and related physical parameters. [85], on using the methods of image, suggested that the track of the Bay of Bengal cyclone would follow the equation of a rose petal [86]. Showed that the tracks of Bay of Bengal cyclones follow cubic curves. However, these models do not serve the purpose fully for predicting the tropical cyclone intensity. Cyclone track prediction techniques are categorized in two categories — 1) Subjective and 2) objective. Synoptic, Satellite, RADAR and Persistence methods fall in the subjective category whereas statistical and dynamical methods fall in the objective category [87] have classified different methods of cyclone track predictions. They also have given a list, with references, of some of the important works carried out on different aspects [88] have reviewed some past and present developments in cyclone track prediction problem by dynamical models. He also discussed several approaches developed by various groups for generating synthetic vortex (bogusing), an important aspect to represent the initial field for cyclone prediction by dynamical models. It has developed a scheme [89] for generation of synthetic observations based on empirical structure of tropical cyclones and their assimilation in the objective analysis for preparing initial fields for running forecast model. They also carried out experiments to determine the importance of initial humidity field on forecast model performance and found that it has crucial importance in the accuracy of track prediction by the forecast model. For their experimentation purpose they used a semi-implicit semi-Lagrangian, multi-layer primitive equation model, casting sigma coordinate system in vertical and staggered Arakawa C-grid in the horizontal. The details of the model they have used can be found in [90]. A bogusing procedure based on merging of an idealized vortex

with initial analysis was implemented [91] in a quasi-Lagrangian limited area model (QLM), earlier used as a hurricane prediction model in the National Centre for Environmental Predictions (NCEP), National Meteorological Centre (NMC), Washington. This model was later adopted in India Meteorological Department (IMD). Mathur and Ruess [92] conducted several case studies of hurricane track prediction with QLM in NMC Washington and demonstrated good skill of the model. Prasad and Rao [93] have reported results of a study on cyclone track prediction by the same model in a few cases in the Bay of Bengal and Arabian Sea. Several studies have been conducted for studying various aspects of cyclones using high resolution Pennsylvania State University (PSU)/National Centre for Atmospheric Research (NCAR) non-hydrostatic meso-scale model (MM-5) ([94]; [95]) have evaluated the performance of fourteen different models in simulating Typhoon Flo-1990 under model inter-comparison project (COMPARE III). The performance of all the models was tested for different sets of initial conditions generated by different data assimilation and vortex initialization schemes. It was shown by the authors that the horizontal resolution enhanced from 50 km through 20 km down to 10 km grid had a large impact on the intensity prediction. However, the differences leading to different intensity predictions among models were not identified. Besides above, in the recent decades there are a lot of studies on tropical cyclone forecasting and structure simulation. SPARRSO used a model called Typhoon Analysis (TYAN) which was found to predict the track and landfall with high accuracy. As [7], the model predicted exact landfall of the 29 April 1991 super cyclone two days in advance.

Also used this mode [18] for Bay of Bengal basin and he suggested that this model may be used for tropical cyclone prediction for the Bay of Bengal on an operational basis. It [99] made a multiscale numerical study of Hurricane Andrew-1992 with PSU/NCAR meoscale (MM5) model with triple nested grid with 6 km horizontal resolution. Davis and Bosart [100] utilized MM5 model to simulate genesis of hurricane Diana-1984 and documented that physics play an important role during transformation from marginal storm to hurricane intensity. Barun [101] employed MM5 model to simulate asymmetrical structure of eye and eyewall of BOB-1991 hurricane. They reported that model is able to predict intensity of the storm up to 48 hrs and underestimate between 48 hrs and 72 hrs. He further emphasized that delayed landfall could be due to overestimation of the intensity of the system. Yang and Ching [105] studied sensitivity of different parameterization schemes using MM5 by applying to Typhoon Toraji-2001. It revealed that Grell convection scheme and Goddard Graupel cloud microphysics scheme give better track whereas warm rain scheme gives lowest central surface pressure and Medium Resolution Forecast (MRF) planetary boundary layer gives the intensity and track in agreement with the

observations. Prasad [107] made cyclone prediction experiments with a Quasi-Lagrangian Model (QLM) for 9 cyclonic storms developing during the four year period 1997-2000. Rao and Prasad [108] made further evaluation of the Quasi-Lagrangian Model (QLM) for cyclone track prediction in the North Indian Ocean. In [109] made advance forecasting of cyclone track over north Indian Ocean by using Global Circulation Model (GCM). Prasad and Rao [110] made simulation studies on cyclone track prediction by Quasi-Lagrangian Model (QLM) in some historical and recent cases in the Bay of Bengal using Global reanalysis and forecast Grid Point datasets. Parameterization of convection, boundary layer and explicit moisture processes. In [112] studied warm ocean anomaly, air sea fluxes, and the rapid intensification of tropical cyclone Nargis-2008. Debsarma [113] performed a study on simulation of cyclone Thane-2011 by using WRF-ARW Model and Numerical Storm Surge model.

2.4.2 Development of Prediction Models

It is worthwhile to discuss some historical events of prediction models. Before the advent of dynamic prediction models, hurricane movement was regarded conceptually as the response of a vortex to a steering current [114]. Most forecast decision making was centered around the identification of the steering level and the reasoning about changes that could modify the steering and future track of the system (this process is still pursued diagnostically by forecasters to test the credibility of model results). In the 1940s, [115] used the wind direction and speed at the top of the hurricane as an index to the movement of the vortex. Riehl [116] proposed one of the earliest models to provide objective predictions of movement of a cyclone. He considered that the best available index to steering the hurricane is the geostrophic flow of the environment at the level of nondivergence (4-6 km). He computed zonal and meridional components of geostrophic wind from 500 hPa analysis. These data were used as inputs to a regression based upon historic storm cases to obtain the westward and northward components of displacement for the ensuing 24 hrs period. During the late 1950s and early 1960s, the search for methods less sensitive to subjective analysis led to the use of statistical screening procedures to select predictors from surface charts and thus more powerful models came forward for use at the National Hurricane Center, USA ([117]; [118]). These models were primarily responsible for a significant increase in forecast skills at the National Hurricane Center in the 1960s. The impact of research on hurricane structure and energy processes was felt mainly in the heuristic reasoning applied by forecasters to test the credibility and acceptance of machine-guidance products, including track predictions from various models. In late 1970s, [119]; [120]) have proposed statistical models applicable for the

Bay of Bengal basin. For Indian seas, [121] developed a scheme of prediction of tropical cyclones based on climatology and persistence. In 1980s, three classes of models for predicting hurricane movement were in use: 1) kinematic analog models, 2) dynamic analog models and 3) pure dynamical models. First draws upon the climatology of hurricane tracks and of persistence of movement to produce a most-probable displacement of the centre. The output is a function of initial position, past movement, and calendar time of occurrence. The computation does not take into account the environment or its influences on the hurricane. The second extracts from historical cases the dynamical properties of the near or the large-scale environment that correlate with some aspect of hurricane movement. These are combined in a multiple regression statement as analogs to the migration of vortex. The third class, not concern with history, combines basic principles of fluid motion, the thermodynamics of an ideal gas and the application of conservation relationships to predict the behavior and displacement of the hurricane vortex. The first two classes suffer from incomplete hurricane climatology, especially with regard to the cases with critical changes in movement and strength. Dynamical models encounter at least three kinds of problems. The first is that of initialization - the description of the initial state of the atmosphere when computation begins, especially the description of processes in the vigorous inner core of the vortex. The second is the fact that higher (spatial) resolution is needed to describe what is going on in the inner core than is needed for the large-scale environment. Third, an adequate simulation of the heating generated by cumulus convection has not been adequately resolved.

Dynamic Analogs. The first completely objective procedure for predicting hurricane movement, using machine analyses of current weather data, was developed for use at National Hurricane Center in 1964 and known as NHC-64. This model and its updated successor, NHC-67, employ predictors obtained from analyses of circulation at 1000, 700 and 500 hPa over large synoptic scale domain. The predictors are based upon statistical screening of data from historical hurricane cases. The method computes latitudinal and meridional components of motion and then generates storm positions for successive 12 hrs intervals up to 72 hrs in advance. This method provides more conservative estimates of the poleward component of motion than do other models. For this reason, it has been adapted for use in the Western Pacific Ocean by Japan and the People's Republic of China. In the late 1960s, a statistically constrained dynamical model is developed that returned to the concept of steering level [122]). This method makes machine analyses at standard pressure surfaces (850, 700, 500 and 300 hPa) and then filters out the perturbations with scale sizes of hundreds of kilometers, including the hurricane vortex,

which is reduced to a point entity. This point moved in accordance with the initial large scale geostrophic flow for 72 to 96 hrs. Changes in the large-scale flow and the bias imposed by the geostrophic assumptions are adjusted by subtracting the observed vector error after 12 hrs of movement from the computed position for subsequent 12 hrs intervals. Statistical Analogs. In 1967, an analog model was developed, known as HURRAN (Hurricane Analogy), [123]. The only current information required by this model is the position, direction, and speed of movement of the system for the preceding 12 hrs. Drawing upon a 100-year record of hurricane stored on tape, the model computes the most probable track for a 72 hrs period based on the movement of historic hurricanes that had occurred at the same time of the year and whose positions and movement vectors were similar to the present case. The output is a probabilistic statement of track positions at 12 hrs intervals up to 72 hrs ahead. For each position, a probability ellipse is defined within which the storm centre has a 50% probability of residing at that time period. The principal shortcoming of HURRAN and other analog methods is limited usefulness during highly anomalous movements, since too few analogs are available for computing track positions on such occasions. This handicap was alleviated when an auxiliary method known as CLIPER (CLImatology and PERsistence) was developed [124]. This method draws its predictors solely from climatology and persistence (of past motion), as its name indicates. The output, similar to that HURRAN, is a probabilistic statement, including a family of probability ellipses. In combination, HURRAN and CLIPER provide more reliable prediction of zonal movement than did the alternative prediction methods, while NHC-67 provided more reliable predictions of meridional movement. The NHC-72 model combined HURRAN, CLIPER and NHC-67 in to a single procedure that accounts for an astonishing amount of the variance in both zonal and meridional components of movement. The NHC-73 model, developed by Neumann and Lawrence [125], incorporates predictors from prognostic charts of the 500 hPa circulation. The first dynamical model to be successfully applied operationally was developed at the Massachusetts Institute of Technology (MIT) by Sanders and Burpee [126]. This barotropic model, known as SANBAR, computes pressure-weighted mean winds for the layer 1000 to 100 hPa, from which stream functions are generated and used as inputs to the prediction model. A grid resolution of 165 km over a geographically fixed domain is used. In the initialization process, the vortex is replaced with an ideal vortex modified to provide initial steering that is consistent with the observed motion of the system. The first primitive equation (three-dimensional) model was developed by Rosenthal and Anthes in 1969 [127]). They demonstrated that, while axisymmetric hurricane models are adequate for studying many aspects of hurricane dynamics, a number of significant structural features, including the spiral rainbands, cannot be simulated

without accounting for asymmetries in circulation. Many research groups and agencies have developed their own global general circulation models as well as local/limited area models. Some of the better known numerical models are:

2.4.2.1 Global Models

- GFS Global Forecast System (previously AVN) - developed by NOAA
- NOGAPS - developed by the US Navy to compare with the GFS
- GEM Global Environmental Multiscale - developed by the Meteorological Service of Canada (MSC)
- ECMWF - a model run by the European Centre for Medium-Range Weather Forecasts
- UKMO developed by the UK Met Office
- GME developed by the German Weather Service, DWD
- FSU GSM Florida State University Global Spectral Model

2.4.2.2 Regional Models

- WRF The Weather Research and Forecasting Model was developed cooperatively by NCEP and the meteorological research community. WRF has several configurations, including
- WRF-NMM The WRF Nonhydrostatic Mesoscale Model is the primary short-term weather forecast model for the U.S.
- ARW Advanced Research WRF developed primarily at the U.S. National Center for Atmospheric Research (NCAR)
- AHW Advance Hurricane WRF
- MM5 the Fifth Generation Penn State/NCAR Mesoscale Model
- QLM Quasi-Lagrangian Limited Area Model
- FSUNRSM Florida State University Nested Regional Spectral Model
- NAM North American Mesoscale Model
- HIRLAM High Resolution Limited Area Model
- GEM-LAM Global Environmental Multiscale Limited Area Model, the high resolution (2.5 km) GEM by the Meteorological Service of Canada (MSC)
- ALADIN The high-resolution limited-area hydrostatic and non-hydrostatic model developed and operated by several European and North African countries under the leadership of Meteo-France.

2.5 The Weather Research and Forecasting (WRF) Model

Description of the Weather Research and Forecasting model is given below

2.5.1 Definition of (WRF) Model

The Weather Research and Forecasting (WRF) model is a numerical weather prediction (NWP) and atmospheric simulation system designed for both research and operational applications. WRF is supported as a common tool for the university/research and operational communities to promote closer ties between them and to address the needs of both. The development of WRF has been a multi-agency effort to build a next-generation mesoscale forecast model and data assimilation system to advance the understanding and prediction of mesoscale weather and accelerate the transfer of research advances into operations. The WRF effort has been a collaborative one among the National Center for Atmospheric Research's (NCAR) Mesoscale and Microscale Meteorology (MMM) Division, the National Oceanic and Atmospheric Administration's (NOAA) National Centers for Environmental Prediction (NCEP) and Earth System Research Laboratory (ESRL), the Department of Defense's Air Force Weather Agency (AFWA) and Naval Research Laboratory (NRL), the Center for Analysis and Prediction of Storms (CAPS) at the University of Oklahoma, and the Federal Aviation Administration (FAA), with the participation of university scientists. WRF reflects flexible, state-of-the-art, portable code that is efficient in computing environments ranging from massively-parallel supercomputers to laptops. Its modular, single-source code can be configured for both research and operational applications. Its spectrum of physics and dynamics options reflects the experience and input of the broad scientific community. Its WRF-Var variational data assimilation system can ingest a host of observation types in pursuit of optimal initial conditions, while its WRF-Chem model provides a capability for air chemistry modeling. WRF is maintained and supported as a community model to facilitate wide use internationally, for research, operations, and teaching. It is suitable for a broad span of applications across scales ranging from large-eddy to global simulations. Such applications include real-time NWP, data assimilation development and studies, parameterized-physics research, regional climate simulations, air quality modeling, atmosphere-ocean coupling, and idealized simulations. As of this writing, the number of registered WRF users exceeds 6000, and WRF is in operational and research use around the world. The principal components of the WRF system are depicted in

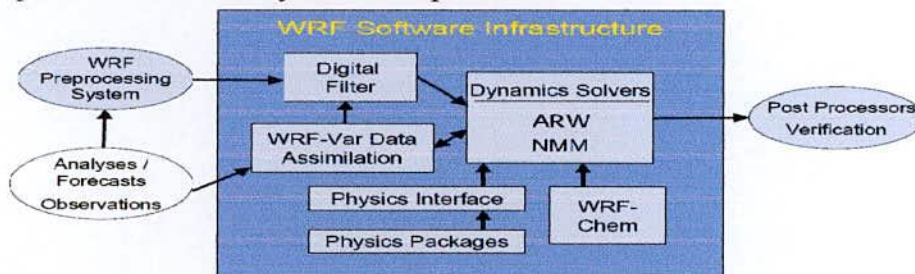


Figure 2.7: The WRF System components.

Framework (WSF) provides the infrastructure that accommodates the dynamics solvers, physics packages that interface with the solvers, programs for initialization, WRF-Var, and WRF-Chem. There are two dynamics solvers in the WSF: the Advanced Research WRF (ARW) solver (originally NMM (Nonhydrostatic Mesoscale Model) solver developed at NCEP. Community support for the former is provided by the MMM Division of NCAR and that for the latter is provided by the Developmental Testbed Center (DTC).

2.5 Advanced Research of ARW Model

The Advance Research WRF (ARW) is the ARW dynamics solver together with other components of the WRF system compatible with that solver and used in producing a simulation. Thus, it is a subset of the WRF modeling system that, in addition to the ARW solver, encompasses physics schemes, numerics/dynamics options, initialization routines, and a data assimilation package (WRF-Var).

The ARW solver shares the WSF with the NMM solver and all other WRF components within the framework. Physics packages are largely shared by both the ARW and NMM solvers, although specific compatibility varies with the schemes considered. The association of a component of the WRF system with the ARW subset does not preclude it from being a component of WRF configurations involving the NMM solver. The following section highlights the major features of the ARW, Version 3, and reflects elements of WRF Version 3, which was first released in April 2008.

2.5.1 Major Features of the ARW System, Version 3 (ARW Solver):

- *Equations:* Fully compressible, Euler nonhydrostatic with a run-time hydrostatic option available. Conservative for scalar variables.
- *Prognostic Variables:* Velocity components u and v in Cartesian coordinate, vertical velocity w , perturbation potential temperature, perturbation geopotential, and perturbation surface pressure of dry air. Optionally, turbulent kinetic energy and any number of scalars such as water vapor mixing ratio, rain/snow mixing ratio, cloud water/ice mixing ratio, and chemical species and tracers.
- *Vertical Coordinate:* Terrain-following, dry hydrostatic-pressure, with vertical grid stretching permitted. Top of the model is a constant pressure surface.

- *Horizontal Grid*: Arakawa C-grid staggering.
- *Time Integration*: Time-split integration using a 2nd- or 3rd-order Runge-Kutta scheme with smaller time step for acoustic and gravity-wave modes. Variable time step capability.
- *Spatial Discretization*: 2nd- to 6th-order advection options in horizontal and vertical.
- *Turbulent Mixing and Model Filters*: Sub-grid scale turbulence formulation in both coordinates and physical space. Divergence damping, external-mode filtering, vertically implicit acoustic step off-centering. Explicit filter option.
- *Initial Conditions*: Three dimensional for real-data, and one-, two- and three-dimensional for idealized data. Digital filtering initialization (DFI) capability available (real-data cases).
- *Lateral Boundary Conditions*: Periodic, open, symmetric, and specified options available.
- *Top Boundary Conditions*: Gravity wave absorbing (diffusion, Rayleigh damping, or implicit Rayleigh damping for vertical velocity). Constant pressure level at top boundary along a material surface. Rigid lid option.
- *Bottom Boundary Conditions*: Physical or free-slip.
- *Earth's Rotation*: Full Coriolis terms included.
- *Mapping to Sphere*: Four map projections are supported for real-data simulation: polar stereographic, Lambert conformal, Mercator, and latitude-longitude (allowing rotated pole). Curvature terms included.
- *Nesting*: One-way interactive, two-way interactive and moving nests. Multiple levels and integer ratios.
- *Nudging*: Grid (analysis) and observation nudging capabilities available.
- *Global Grid*: Global simulation capability using polar Fourier filter and periodic east-west conditions.

2.5.2 Physics:

- *Microphysics*: Schemes ranging from simplified physics suitable for idealized studies to sophisticated mixed-phase physics suitable for process studies and NWP.
- *Cumulus parameterizations*: Adjustment and mass-flux schemes for mesoscale modeling.
- *Surface physics*: Multi-layer land surface models ranging from a simple thermal model to full vegetation and soil moisture models, including snow cover and sea ice.
- *Planetary boundary layer physics*: Turbulent kinetic energy prediction or non-local K schemes.
- *Atmospheric radiation physics*: Longwave and shortwave schemes with multiple spectral

bands and a simple shortwave scheme suitable for climate and weather applications. Cloud effects and surface fluxes are included.

2.5.3 WRF-Var System

- WRF-Var merged into WRF software framework.
- Incremental formulation of the model-space cost function.
- Quasi-Newton or conjugate gradient minimization algorithms.
- Analysis increments on unstaggered Arakawa-A grid.
- Representation of the horizontal component of background error B via recursive filters (regional) or power spectra (global). The vertical component is applied through projection onto climatologically-averaged eigenvectors of vertical error. Horizontal/vertical errors are non-separable (horizontal scales vary with vertical eigenvector).
- Background cost function (J_b) preconditioning via a control variable transform U defined as $B = UU^T$.
- Flexible choice of background error model and control variables.
- Climatological background error covariances estimated via either the NMC-method of averaged forecast differences or suitably averaged ensemble perturbations.
- Unified 3D-Var (4D-Var under development), global and regional, multi-model capability.

2.5.3 WRF-Chem

- Online (or “inline”) model, in which the model is consistent with all conservative transport done by the meteorology model.
- Dry deposition, coupled with the soil/vegetation scheme.
- Aqueous phase chemistry coupled to some of the microphysics and aerosol schemes.
- Three choices for biogenic emissions: No biogenic emissions; online calculation of biogenic emissions; online modification of user specified biogenic emissions (e.g., EPA Biogenic Emissions Inventory System (BEIS)).
- Two choices for anthropogenic emissions: No anthropogenic emissions and user-specified anthropogenic emissions.
- Two choices for gas-phase chemical reaction calculations: RADM2 chemical mechanism and CBM-Z mechanism.
- Several choices for gas-phase chemical reaction calculations through the use of the Kinetic Pre-Processor (KPP).

- Three choices for photolysis schemes: Madronich scheme coupled with hydrometeors, aerosols, and convective parameterizations; Fast-J Photolysis scheme coupled with hydrometeors, aerosols, and convective parameterizations; FTUV scheme coupled with hydrometeors, aerosols, and convective parameterizations.
- Choices for aerosol schemes: The Modal Aerosol Dynamics Model for Europe (MADE/SORGAM); Model for Simulating Aerosol Interactions and Chemistry (MOSAIC); and The GOCART aerosol model (experimental).
- A tracer transport option in which the chemical mechanism, deposition, etc., has been turned off.

2.5.5 WRF Software Framework

- Highly modular, single-source code for maintainability.
- Two-level domain decomposition for parallel and shared-memory generality.
- Portable across a range of available computing platforms.
- Support for multiple dynamics solvers and physics modules.
- Separation of scientific codes from parallelization and other architecture-specific issues.
- Input/Output Application Program Interface (API) enabling various external packages to be installed with WRF, thus allowing WRF to easily support various data formats.
- Efficient execution on a range of computing platforms (distributed and shared memory, vector and scalar types). Support for accelerators (e.g., GPUs).
- Use of Earth System Modeling Framework (ESMF) and interoperable as an ESMF component.
- Model coupling API enabling WRF to be coupled with other models such as ocean, and land models using ESMF, MCT, or MCEL.

2.5.6 Governing Equations

The ARW dynamics solver integrates the compressible, nonhydrostatic Euler equations. The equations are cast in flux form using variables that have conservation properties, following the philosophy of Ooyama [131]. The equations are formulated using a terrain-following mass vertical coordinate [132]. The model equations are in the following sections.

Vertical Coordinate and Variables

The ARW equations are formulated using a terrain-following hydrostatic-pressure vertical coordinate denoted by η and defined as

$$\eta = (p_h - p_{ht})/\mu \quad \text{where } \mu = p_{hs} - p_{ht}. \quad 2.1$$

p_h is the hydrostatic component of the pressure, and p_{hs} and p_{ht} refer to values along the surface and top boundaries, respectively. The coordinate definition (2.1), proposed by [132], is the traditional σ coordinate used in many hydrostatic atmospheric models. η varies from a value of 1 at the surface to 0 at the upper boundary of the model domain (Fig. 2.8). This vertical coordinate is also called a mass vertical coordinate. Since $\mu(x, y)$ represents the mass per unit area within the column in the model domain at (x, y) , the appropriate flux form variables are

$$V = \mu \mathbf{v} = (U, V, W), \quad \Omega = \mu \dot{\eta}, \quad \Theta = \mu \theta. \quad (2.2a)$$

$\mathbf{v} = (u, v, w)$ are the covariant velocities in the two horizontal and vertical directions, respectively, while $\omega = \dot{\eta}$ is the contravariant 'vertical' velocity, θ is the potential temperature. Also appearing in the governing equations of the ARW are the non-conserved variables $\phi = gz$ (the geopotential), p (pressure), and $\alpha = 1/\rho$ (the inverse density).

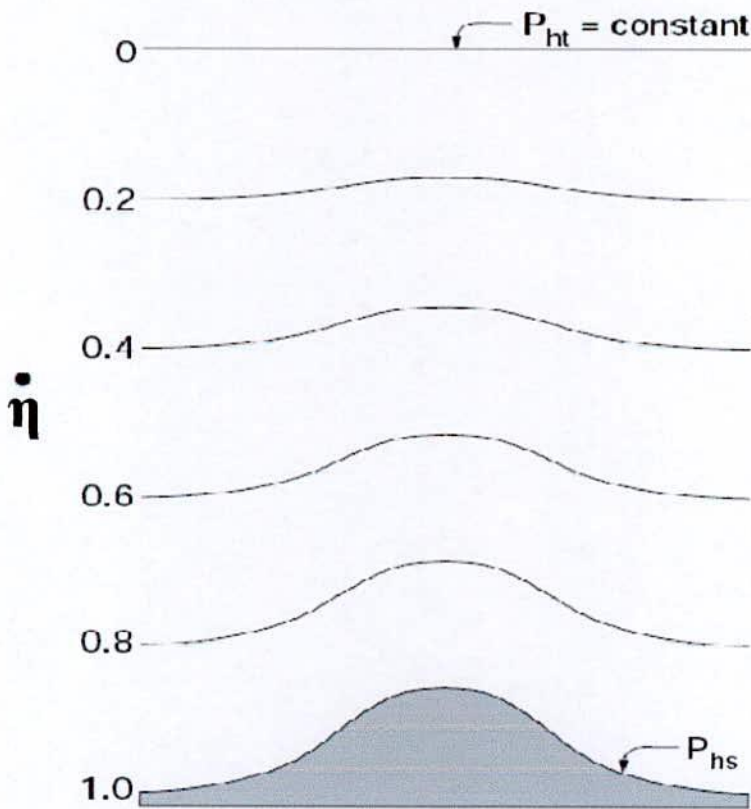


Figure 2.8: ARW η coordinate [27].

2.5.7 Flux-Form Euler Equations

Using the variables defined above, the flux-form Euler equations can be written as

$$\partial_t U + (\nabla \cdot \mathbf{V}u) - \partial_x(p\partial_\eta\phi) + \partial_\eta(p\partial_x\phi) = F_U \quad (2.2)$$

$$\partial_t V + (\nabla \cdot \mathbf{V}v) - \partial_y(p\partial_\eta\phi) + \partial_\eta(p\partial_y\phi) = F_V \quad (2.3)$$

$$\partial_t W + (\nabla \cdot \mathbf{V}w) - g(\partial_\eta p - \mu) = F_W \quad (2.4)$$

$$\partial_t \Theta + (\nabla \cdot \mathbf{V}\theta) = F_\Theta \quad (2.5)$$

$$\partial_t \mu + (\nabla \cdot \mathbf{V}) = 0 \quad (2.6)$$

$$\partial_t \phi + \mu^{-1}[(\nabla \cdot \mathbf{V}\phi) - gW] = 0 \quad (2.7)$$

along with the diagnostic relation for the inverse density

$$\partial_\eta \phi = -\alpha\mu, \quad (2.8)$$

and the equation of state

$$p = p_0(R_d\theta/p_0\alpha)^\gamma \quad (2.9)$$

In (2.2) – (2.9), the subscripts x , y and η denote differentiation,

$$\nabla \cdot \mathbf{V}a = \partial_x(Ua) + \partial_y(Va) + (\partial_\eta \Omega a),$$

and

$$\nabla \cdot \mathbf{V}a = U\partial_x a + V\partial_y a + \Omega\partial_\eta a,$$

where a represents a generic variable. $\gamma = c_p/c_v = 1.4$ is the ratio of the heat capacities for dry air, R_d is the gas constant for dry air, and p_0 is a reference pressure (typically 10^5 Pascals). The right-hand-side (RHS) terms F_U , F_V , F_W , and F_Θ represent forcing terms arising from model physics, turbulent mixing, spherical projections, and the earth's rotation.

2.5.8 Temporal Discretization

The ARW solver uses a time-split integration scheme. Generally speaking, slow or low-frequency (meteorologically significant) modes are integrated using a third-order Runge-Kutta (RK3) time integration scheme, while the high-frequency acoustic modes are integrated over smaller time steps to maintain numerical stability. The horizontally propagating acoustic modes (including the external mode present in the mass-coordinate equations using a constant-pressure upper boundary condition) and gravity waves are integrated using a forward-backward time integration scheme, and vertically propagating acoustic modes and buoyancy oscillations are integrated using a vertically implicit scheme (using the acoustic time step). The time-split integration for the

flux-form equations is described and analyzed in [134].

2.5.9 Runge-Kutta Time Integration Scheme

The RK3 scheme, described in [135], integrates a set of ordinary differential equations using a predictor-corrector formulation. Defining the prognostic variables in the ARW solver as $\Theta = (U, V, W, \theta, \varphi', \mu', Q_m)$ and the model equations as $\Theta_t = R(\Theta)$, the RK3 integration takes the form of 3 steps to advance a solution $\Phi(t)$ to $\Phi(t+\Delta t)$:

$$\Phi' = \Phi + \frac{\Delta t}{3} R(\Phi) \quad (2.10)$$

$$\Phi'' = \Phi' + \frac{\Delta t}{2} R(\Phi') \quad (2.11)$$

$$\Phi^{t+\Delta t} = \Phi' + \Delta t R(\Phi'') \quad (2.12)$$

where Δt is the time step for the low-frequency modes (the model time step). In (2.10) – (2.12), superscripts denote time levels. This scheme is not a true Runge-Kutta scheme because, while it is third-order accurate for linear equations, it is only second-order accurate for nonlinear equations.

2.5.10 Spatial Discretization

The spatial discretization in the ARW solver uses a C grid staggering for the variables. That is, normal velocities are staggered one-half grid length from the thermodynamic variables. The variable indices, (i, j, k) indicate variable locations with $(x, y, \eta) = (i\Delta x, j\Delta y, k\Delta \eta)$. The points where θ is located as *mass* points, and likewise locations where u , v , and w are defined as *u* points, *v* points, and *w* points, respectively. Variables q_m are defined at the mass points. The diagnostic variables used in the model, the pressure p and inverse density α , are computed at mass points. The grid lengths Δx and Δy are constants in the model formulation; changes in the physical grid lengths associated with the various projections to the sphere are accounted for using the map factors. The vertical grid length $\Delta \eta$ is not a fixed constant; it is specified in the initialization. The user is free to specify the η values of the model levels subject to the constraint that $\eta = 1$ at the surface, $\eta = 0$ at the model top, and η decreases monotonically between the surface and model top. Using these grid and variable definitions, we can define the spatial discretization for the ARW solver.

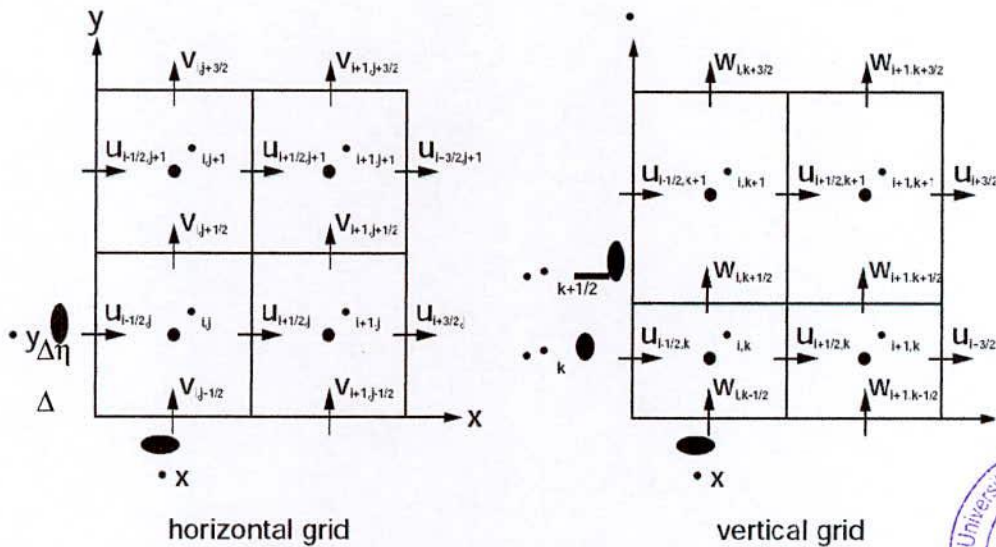


Figure 2.9: Horizontal and vertical grids of the ARW [27]

There are two time steps that a user must specify when running the ARW: the model time step (the time step used by the RK3 scheme and the acoustic time step (used in the acoustic sub-steps of the time-split integration procedure. Both are limited by Courant numbers. In the following sections we describe how to choose time steps for applications.

2.5.11 Map Projection Considerations

For ARW configurations using the Lambert conformal, polarstereographic, or Mercator projections, the timestep constraints is determined by the smallest physical horizontal grid spacing,

i.e. $\min(\Delta x/mx, \Delta y/my)$. For global applications, the grid distance used to determine the timestep should be $\Delta x/mx$ evaluated at the computational latitude at which the polar filters are activated

2.5.12 Turbulent Mixing and Model Filters

A number of formulations for turbulent mixing and filtering are available in the ARW solver. Some of these filters are used for numerical reasons. For example, divergence damping is used to filter acoustic modes from the solution and polar filtering is used to reduce the timestep restriction arising from the converging gridlines of the latitude-longitude grid. Other filters are meant to represent sub-grid turbulence processes that cannot be resolved on the chosen grid.

These filters remove energy from the solution and are formulated in part on turbulence theory and observations, or represent energy sink terms in some approximation to the Euler equation. The details of turbulent mixing and filtering are described [27].

2.6 Initial Conditions

The ARW may be run with user-defined initial conditions for idealized simulations, or it may be run using interpolated data from either an external analysis or forecast for real-data cases.

WRF Preprocessor System, referred to as WPS) that converts the large-scale GriB data into a format suitable for ingest by the ARW's real-data processor.

The programs that generate the specific initial conditions for the selected idealized or realdata case function similarly. They provide the ARW with:

- input data that is on the correct horizontal and vertical staggering;
- hydrostatically balanced reference state and perturbation fields; and
- metadata specifying such information as the date, grid physical characteristics, and projection details.

2.6.1 Use of the WRF Preprocessing System by the ARW

The WPS is a set of programs that takes terrestrial and meteorological data (typically in GriBformat) and transforms them for input to the ARW pre-processor program for real-data cases WPS system. The first step for the WPS is to define a physical grid (including the projection type, location on the globe, number of grid points, nest locations, and grid distances) and to interpolate static fields to the prescribed domain. Independent of the domain configuration, an external analysis or forecast is processed by the WPS GriB decoder, which diagnoses required fields and reformats the GriB data into an internal binary format. With a specified domain, WPS horizontally interpolates the meteorological data onto the projected domain(s). The output data from WPS supplies

a complete 3-dimensional snapshot of the atmosphere on the selected model grid's horizontal staggering at the selected time slices, which is sent to the ARW pre-processor program for real-data cases.

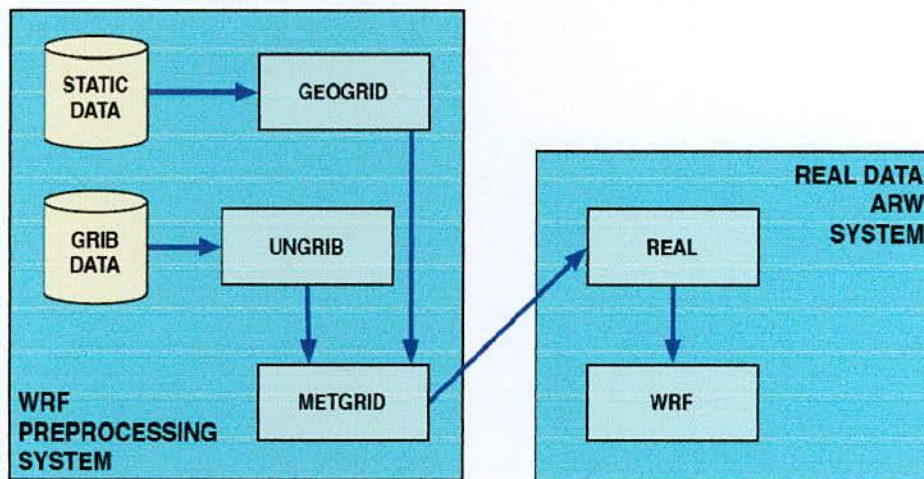


Figure 2.10 Schematic showing the data flow and program components in WPS, and how WPS feeds initial data to the ARW. Letters in the rectangular boxes indicate program names. GEOGRID: defines the model domain and creates static files of terrestrial data. UNGRIB: decodes GriB data. METGRID: interpolates meteorological data to the model domain [27].

The input to the ARW real-data processor from WPS contains 3-dimensional fields (including the surface) of temperature (K), relative humidity (and the horizontal components of momentum (m/s, already rotated to the model projection)). The 2-dimensional static terrestrial fields include: albedo, Coriolis parameters, terrain elevation, vegetation/land-use type, land/water mask, map scale factors, map rotation angle, soil texture category, vegetation greenness fraction, Annual mean temperature, and latitude/longitude. The 2-dimensional time-dependent fields from the external model, after processing by WPS, include: surface pressure and sea-level pressure (Pa), layers of soil temperature (K) and soil moisture (kg/kg, either total moisture, or binned into total and liquid content), snow depth (m), skin temperature (K), sea surface temperature (K), and a sea ice flag.

2.6.2 Reference State

Identical to the idealized initializations, there is a partitioning of some of the meteorological data into reference and perturbation fields. For real-data cases, the reference state is defined by terrain elevation and three constants:

- p_0 (105 Pa) reference sea level pressure;
- T_0 (usually 270 to 300 K) reference sea level temperature; and
- A (50 K) temperature difference between the pressure levels of p_0 and p_0/e .

2.6.3 Vertical Interpolation and Extrapolation

The ARW real-data preprocessor vertically interpolates using functions of dry pressure. The input data from WPS contains both a total pressure and a moisture field (typically relative humidity). Starting at the top each column of input pressure data, the integrated moisture is subtracted from the pressure field step-wise down to the surface. Then, by removing the pressure at the model lid, the total dry surface pressure p_{sd} diagnosed from WPS defines the model total dry column pressure

$$\mu_d^- \mu_d^+ \mu_d^- p_{sd} - p_{dht}. \quad (2.13)$$

With the ARW vertical coordinate η , the model lid p_{dht} , and the column dry pressure known at each (i, j, k) location, the 3-dimensional arrays are interpolated. In the free atmosphere up to the model lid, the vertical calculations are always interpolations. However, near the model surface, it is possible to have an inconsistency between the input surfaces

pressure (based largely on the input surface elevation) and the ARW surface pressure (possibly with a much higher resolution topography). These inconsistencies may lead to an extrapolation. The default behavior for extrapolating the horizontal winds and the relative humidity below

the known surface is to keep the values constant, with zero vertical gradient. For the potential temperature, by default a -6.5 K/km lapse rate for the temperature is applied. The vertical interpolation of the geopotential field is optional and is handled separately. Since a known lower boundary condition exists (the geopotential is defined as zero at the pressure at sea-level), no extrapolation is required.

2.6.4 Masking of Surface Fields

Some of the meteorological and static fields are “masked”. A masked field is one in which the values are typically defined only over water (e.g., sea surface temperature) or defined only over land (e.g., soil temperature). The need to match all of the masked fields consistently to each other requires additional steps for the real-data cases due to the masked data’s presumed use in various physics packages in the soil, at the surface, and in the boundary layer. If the land/water mask for a location is flagged as a water point, then the vegetation and soil categories must also recognize the location as the special water flag for each of their respective categorical indices. Similarly, if the land/water mask is flagged as a land point, the vegetation and soil categories must be

assigned to one of the available land indices. The values for the soil temperature and soil moisture come from WPS on the native levels originally defined for those variables by an external model. WPS does no vertical interpolation for the soil data. While it is typical to try to match the ARW soil scheme with the incoming data, that is not a requirement. Pre-processor *real* will vertically interpolate (linear in depth below the ground) from the incoming levels to the requested soil layers to be used within the model. 5.3 Digital Filtering Initialization

Version 3 of the ARW provides a digital filtering initialization (DFI) to remove noise, which results from imbalances between mass and wind fields, from the model initial state. DFI is applied to the output of the *real* preprocessor before the model simulation begins. If data assimilation is performed using WRF-Var, DFI is applied to the analysis produced by the WRFVar system, rather than the output of program *real*. Under the assumption that any noise is of higher frequency than meteorologically significant modes, DFI attempts to remove this noise by filtering all oscillations above a specified cutoff frequency. Accordingly, the filters in the ARW DFI are low-pass digital filters, which are applied to time series of model fields; the *initialized* model state is the output of the filter at some prescribed time, e.g., the analysis time. Time series of model states are generated through combinations of adiabatic, backward integration and diabatic, forward integration in the model, with the choice of DFI scheme determining the specific combination of integrations. Three DFI schemes — digital filter launch (DFL;[136], diabatic DFI (DDFI;[137], and twice DFI (TDFI;[136]) — are available.

2.6.5 Lateral Boundary Conditions

Several lateral boundary condition options exist for the ARW that are suitable for idealized flows, and a specified lateral boundary condition for real-data simulations is available. These choices are handled via a run-time option in the Fortran namelist file. For nesting, all fine domains use the nest time-dependent lateral boundary condition where the outer row and column of the fine grid is specified from the parent domain. The remaining lateral boundary options are exclusively for use by the most coarse/parent domain.

2.6.6 Periodic Lateral Boundary Conditions

Periodic lateral boundary conditions in the ARW can be specified as periodic in x (west-east), y (south-north), or doubly periodic in (x, y) . The periodic boundary conditions constrain the solutions to be periodic; that is, a generic model state variable ψ will follow the relation

$$\psi(x + nLx, y + mLy) = \psi(x, y)$$

for all integer (n, m) . The periodicity lengths (Lx, Ly) are

$[(\text{dimension of the domain in } x) - 1]\Delta x$ and $[(\text{dimension of the domain in } y) - 1]\Delta y$.

Open lateral boundary conditions, also referred to as gravity-wave radiating boundary conditions, can be specified for the west, east, north, or south boundary, or any combination thereof. The gravity wave radiation conditions follow the approach of ([138]; [139]). Symmetry lateral boundary conditions can be specified for the west, east, north, or south boundary, or any combination thereof. The symmetry boundaries are located on the normal-velocity planes at the lateral edges of the grids. The normal velocities are zero at these boundaries, and on either side of the boundary the normal velocity satisfies the relation

$$U_{\perp}(xb - x) = -U_{\perp}(xb + x),$$

Where xb is the location of the symmetry boundary. All other variables satisfy the relation

$$\psi(xb - x) = \psi(xb + x).$$

2.6.7 Specified Lateral Boundary Conditions

Primarily for real-data cases, the specified boundary condition is also referred to as a relaxation, or nudging, boundary condition. There are two uses of the specified boundaries in the ARW: for the outer-most coarse grid or for the time-dependent boundaries supplied to a nested grid. The specified lateral boundary conditions for the nest are automatically selected for all of the fine grids, even if the coarse grid is using combinations of the symmetry, periodic, or open options. If the specified lateral boundary condition is selected for the coarse grid, then all four grid sides (west, east, north, and south) use specified lateral conditions. However, in tropical channel mode, where the domain wraps completely around the equator, it is possible to combine specified boundary conditions with periodic conditions in the x direction. Note that care is needed in setting the domain up such that the points exactly match longitude at the east and west boundaries when periodic conditions are used in real-data cases. Also note that a Mercator projection is needed to make this possible.

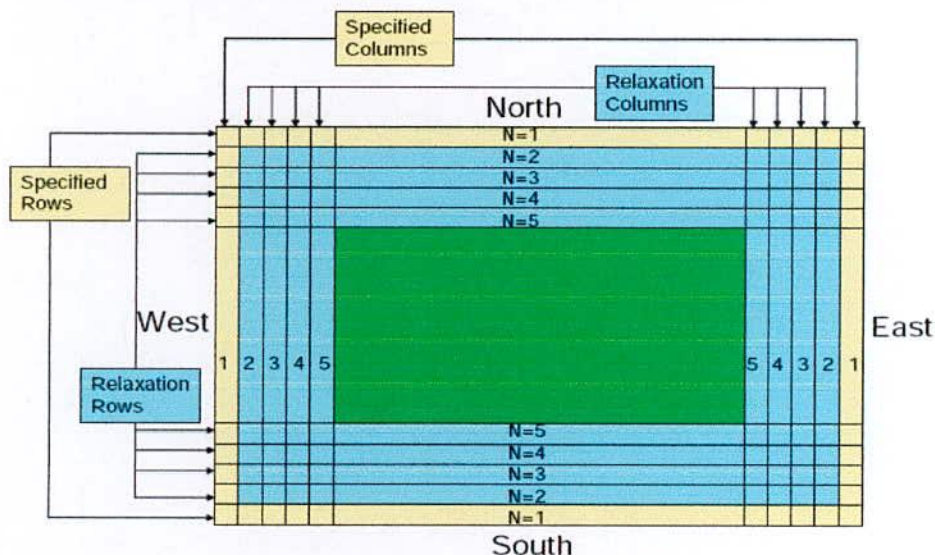


Figure 2.11 Specified and relaxation zones for a grid with a single specified row and column & four rows and columns for the relaxation zone. These are typical values used for a specified lateral boundary condition for a real-data case, [27].

Along the outer edge of the most coarse grid is entirely specified by temporal interpolation using data from an external model). The second region of the lateral boundary for the coarse grid is the relaxation zone. The relaxation zone is where the model is nudged or relaxed towards the large-scale forecast. The size of the relaxation zone is a run-time option.

2.7 Nesting options

The ARW supports horizontal nesting that allows resolution to be focused over a region of interest by introducing an additional grid (or grids) into the simulation. In the current implementation, In the current

Implementation, only horizontal refinement is available: there is no vertical nesting option. The nested grids are rectangular and are aligned with the parent (coarser) grid within which they are nested. Additionally, the nested grids allow any integer spatial ($\Delta x_{coarse}/\Delta x_{fine}$) and temporal refinements of the parent grid (the spatial and temporal refinements are usually, but not necessarily the same). This nesting implementation is in many ways similar to the implementations in other mesoscale and cloudscape models (e.g. MM5, ARPS, COAMPS). The major improvement in the ARW's nesting infrastructure compared with techniques used in other models is the ability to compute nested simulations efficiently on parallel distributed-memory computer systems, which includes support for moving nested grids. The WRF Software

Framework, described in [41], makes these advances possible. In this chapter we describe the various nesting options available in the ARW and the numerical coupling between the grids.

2.7.1 1-Way and 2-Way Grid Nesting

Nested grid simulations can be produced using either 1-way nesting or 2-way nesting as outlined in Fig. 2.12. The 1-way and 2-way nesting options refer to how a coarse grid and the fine grid interact. In both the 1-way and 2-way simulation modes, the fine grid boundary conditions (i.e., the lateral boundaries) are interpolated from the coarse grid forecast. In a 1-way nest, this is the only information exchange between the grids (from the coarse grid to the fine grid). Hence, the name *1-way nesting*. In the 2-way nest integration, the fine grid solution replaces the coarse grid solution for coarse grid points that lie inside the fine grid. This information exchange between the grids is now in both directions (coarse-to-fine for the fine-grid lateral boundary computation and fine-to-coarse during the feedback at each coarse-grid time step). Hence, the name *2-way nesting*. The 1-way nest set-up may be run in one of two different methods. One option is to produce the nested simulation as two separate ARW simulations as described in the leftmost box in Fig 2.12. In this mode, the coarse grid is integrated first and the coarse grid forecast is completed. Output from the coarse grid integration is then processed to provide boundary conditions for the nested run (usually at a much lower temporal frequency than the coarse grid time step), and this is followed by the complete time integration of fine (nested) grid. Hence, this 1-way option is equivalent to running two separate simulations with a processing step in between.

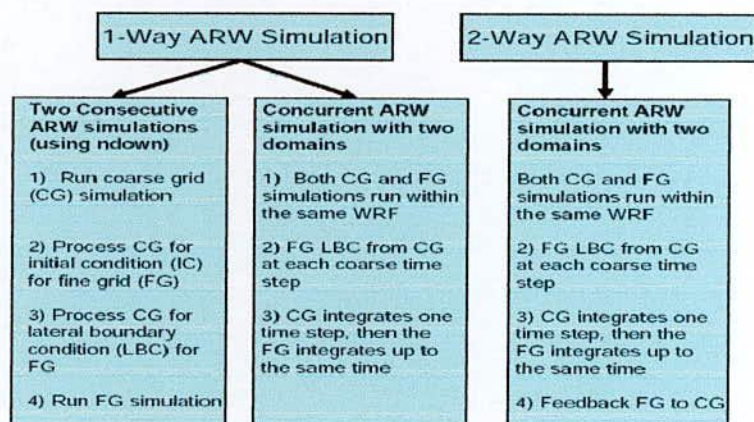


Figure 2.12: 1-way and 2-way nesting options in the ARW

Also with separate grid simulations, an intermediate re-analysis (such as via 3D-Var) can be included. The second 1-way option (lockstep with no feedback), depicted in the middle box in

Fig. 2.12, is run as a traditional simulation with two (or more) grids integrating concurrently, except with the feedback runtime option shut off. This option provides lateral boundary conditions to the fine grid at each coarse grid time step, which is an advantage of the concurrent 1-way method (no feedback).

2.7.2 Staggering and Feedback

The ARW uses an Arakawa-C grid staggering. As shown in Fig. 2.13, the u and v components of horizontal velocity are normal to the respective faces of the grid cell, and the mass/thermodynamic/scalar/chemistry variables are located in the center of the cell. The variable staggering has an additional column of u in the x-direction and an additional row of v in the y-direction because the normal velocity points define the grid boundaries. The horizontal momentum components reflect an average across each cell-face, while each mass/thermodynamic/scalar/chemistry variable is the representative mean value throughout the cell. Feedback is handled to preserve these mean values: the mass/thermodynamic/scalar/chemistry fields are fed back with an average from within the entire coarse grid point (Fig. 2.13), and the horizontal momentum variables are averaged along their respective normal coarse grid cell faces. The horizontal interpolation (to instantiate a grid and to provide time-dependent lateral boundaries) does not conserve mass. The feedback mechanism, for most of the unmasked fields,

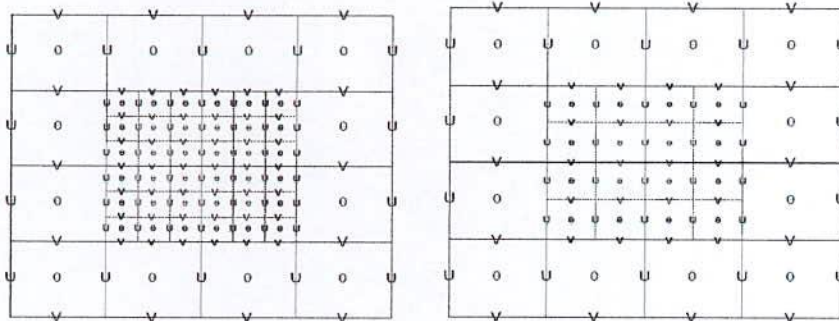


Figure 2.13: Arakawa-C grid staggering for a portion of a parent domain and an imbedded nest domain with a 3:1 grid size ratio. The solid lines denote coarse grid cell boundaries, and the dashed lines are the boundaries for each fine grid cell. The horizontal components of velocity (“U” and “V”) are defined along the normal cell face, and the thermodynamic variables (θ) are defined at the center of the grid cell (each square). The bold typeface variables along the interface between the coarse and the fine grid define the locations where the specified lateral boundaries for the nest are in effect [27]

uses cell averages (for mass/thermodynamic/scalar/chemistry quantities) and cell-face averages for the horizontal momentum fields. The staggering defines the way that the fine grid is situated on top of the coarse grid. For all odd ratios there is a coincident point for each variable: a location that has the coarse grid and the fine grid at the same physical point. The location of this point depends on the variable. In each of the coarse-grid cells with an odd ratio, the middle fine-grid cell is the coincident point with the coarse grid for all of the mass-staggered fields (Fig. 2.13). For the horizontal momentum variables the normal velocity has coincident points along the grid boundaries for odd ratios.

For fields that are averaged back to the coarse grid in the feedback, the mean of the nine mass/thermodynamic/scalar/chemistry (for example, due to the 3:1 grid-distance ratio in the example shown in (Fig. 2.13) fine grid points is fed back to the coarse grid. These fields include most 3-dimensional and 2-dimensional arrays. For the horizontal momentum fields averaged back to the coarse grid in the feedback, the mean of three (for example, due to the 3:1 grid-distance ratio in the example shown in (Fig. 2.13) fine grid points is fed back to the coarse grid from along the coincident cell face. The fields that are masked due to the land/sea category are fed back directly from the coincident points for odd ratios. Masked fields include soil temperature and sea ice. It does not make sense to average neighboring locations of soil temperature on the fine grid if the coarse grid point being feedback to is a water value. Similarly, averaging several sea ice values on the fine grid does not make sense if some of the neighboring points included in the mean are fine grid land points. Only masked fields use the feedback method where a single point from the fine grid is assigned to the coarse grid.

A difference between the odd and even grid-distance ratios is in the feedback from the fine grid to the coarse grid. No coincident points exist for the single point feedback mechanisms for even grid distance ratios (such as used for the land/sea masked 2D fields). For a 2:1 even grid distance ratio, Figure 2.13 shows that each coarse grid point has four fine grid cells that are equally close, and therefore four equally eligible grid points for use as the single fine-grid point that feeds back to the coarse grid. The single-point feedback is arbitrarily chosen as the south-west corner of the four neighboring points. This arbitrary assignment to masked fields implies that even grid distance ratios are more suited for idealized simulations where masked fields are less important.

2.8 Physics Options

2.8.1 Model Physics

This section outlines the physics options available in the ARW. The WRF physics options fall into several categories, each contains several choices. The physics categories are (1) microphysics, (2) Cumulus parameterization, (3) planetary boundary layer (PBL), (4) land-surface model, and (5) radiation. The physics section is insulated from the rest of the dynamics solver by the use of physics drivers. These are between solver-dependent routines: a pre-physics preparation and post physics modifications of the tendencies. The physics preparation involves filling arrays with Physics required variables that include the temperature, pressure, heights, layer thicknesses, and other state variables in MKS units at half-level grid points and on full levels. The velocities are also de-staggered so that the physics part is independent of the dynamical solver's velocity staggering. Physics packages compute tendencies for the velocity components (un-staggered), potential temperature, and moisture fields. The solver-dependent post-physics step will restagger these tendencies as necessary, couple tendencies with coordinate metrics, and convert to variables or units appropriate to the dynamics solver. In the first Runge-Kutta step, prior to the acoustic tendencies are computed for radiation, surface, PBL, and cumulus physics. These tendencies are then held fixed through the Runge-Kutta steps. Microphysics is computed after the last Runge-Kutta step in order to maintain proper saturation conditions at the end of the time-step. The initialization of the physics is called prior to the first model step. This initialization may include reading in data files for physics tables or calculating look-up tables of functions. Each physics module includes an initialization routine for this purpose. Often physics packages will have many of their own constants that should also be included in their own module, while common physical constants are passed in from the physics drivers.

2.8.2 Microphysics

Microphysics includes explicitly resolved water vapor, cloud, and precipitation processes. The model is general enough to accommodate any number of mass mixing-ratio variables, and other quantities such as number concentrations. Four-dimensional arrays with three spatial indices and one species index are used to carry such scalars. Memory, i.e., the size of the fourth dimension in these arrays, is allocated depending on the needs of the scheme chosen, and advection of the species also applies to all those required by the microphysics option. In the current version of the ARW, microphysics is carried out at the end of the time-step as an adjustment process, and so

does not provide tendencies. The rationale for this is that condensation adjustment should be at the end of the time-step to guarantee that the final saturation balance is accurate for the updated temperature and moisture. However, it is also important to have the latent heating forcing for potential temperature during the dynamical sub-steps, and this is done by saving the microphysical heating as an approximation for the next time-step. Currently, the sedimentation process is accounted for inside the individual microphysics modules, and, to prevent instability in the calculation of the vertical flux of precipitation, a smaller time step is allowed. The saturation adjustment is also included inside the microphysics. In the future, however, it might be separated into an individual subroutine to enable the remaining microphysics to be called less frequently than the model's advection step for efficiency. Following are the outline of different schemes of microphysics options available in the current version of ARW.

Kessler scheme: This scheme is a simple warm cloud scheme that includes water vapor, cloud water, and rain. The microphysical processes included are: the production, fall, and evaporation of rain; the accretion and autoconversion of cloud water; and the production of cloud water from condensation, [142]

WRF Single-Moment 3-class (WSM3) scheme: A simple efficient scheme with ice and snow processes suitable for mesoscale grid size, [145]

WRF Single-Moment 5-class (WSM5) scheme: A slightly more sophisticated version that allows for mixed-phase processes and super-cooled water, ([145]; [146])

WRF Single-Moment 6-class (WSM6) scheme: A scheme with ice, snow and graupel processes suitable for high-resolution simulation ([143]; [145]; [148]).

Thompson scheme: A new scheme with ice, snow and graupel processes suitable for high-resolution simulation ([149]; [150]).

Morrison 2-Moment scheme: Double-moment ice, snow, rain and graupel for cloud-resolving simulations [151].

2.8.3 Cumulus parameterization

These schemes are responsible for the sub-grid-scale effects of convective and/or shallow clouds. The schemes are intended to represent vertical fluxes due to unresolved updrafts and downdrafts and compensating motion outside the clouds. They operate only on individual columns where the scheme is triggered and provide vertical heating and moistening profiles. Some schemes additionally provide cloud and precipitation field tendencies in the column, and future schemes may provide momentum tendencies due to convective transport of momentum. The schemes all

provide the convective component of surface rainfall. Cumulus parameterizations are theoretically only valid for coarser grid sizes, (e.g., greater than 10km), where they are necessary to properly release latent heat on a realistic time scale

in the convective columns. While the assumptions about the convective eddies being entirely sub-grid-scale break down for finer grid sizes, sometimes these schemes have been found to be helpful in triggering convection in 5–10 km grid applications.

Kain-Fritsch scheme: Deep and shallow convection sub-grid scheme using a mass flux approach with downdrafts and convectively Available Potential Energy (CAPE) removal time scale, ([152]; [153]; [154]).

Betts-Miller-Janjic scheme: Operational Eta-scheme, Column moist adjustment scheme relaxing towards a well-mixed profile, ([155]; [156]).

Grell-Devenyi ensemble scheme: Multi-closure, multi-parameter, ensemble method with typically 144 sub-grid members, [157].

Grell-3d cumulus scheme: Scheme for higher resolution domains allowing for subsidence in neighboring columns.

2.8.4 Surface Layer

The surface layer schemes calculate friction velocities and exchange coefficients that enable the calculation of surface heat and moisture fluxes by the land-surface models and surface stress in the planetary boundary layer scheme. Over water surfaces, the surface fluxes and surface diagnostic fields are computed in the surface layer scheme itself. The schemes provide no tendencies, only the stability-dependent information about the surface layer for the land-surface and PBL schemes. Currently, each surface layer option is tied to particular boundary-layer options, but in the future more interchangeability and options may become available. Note that some boundary layer schemes (YSU and MRF) require the thickness of the surface layer in the model to be representative of the actual surface layer (e.g. 50-100 meters).

Similarity theory (MM5): This scheme uses stability functions to compute surface exchange coefficients for heat, moisture, and momentum [158].

2.9 Land-Surface Model

The land-surface models (LSMs) use atmospheric information from the surface layer scheme, radiative forcing from the radiation scheme, and precipitation forcing from the microphysics and convective schemes, together with internal information on the land's state variables and

Land-surface properties, to provide heat and moisture flux over land points and sea-ice points. These fluxes provide a lower boundary condition for the vertical transport done in the PBL schemes (or the vertical diffusion scheme in the case where a PBL scheme is not run, such as in large-eddy mode). [Note that large-eddy mode with interactive surface fluxes is not yet available in the ARW, but is planned for the near future.] The land-surface models have various degrees of sophistication in dealing with thermal and moisture fluxes in multiple layers of the soil and also may handle vegetation, root, and canopy effects and surface snow-cover prediction. The landsurface model provides no tendencies, but does update the land's state variables which include the ground (skin) temperature, soil temperature profile, soil moisture profile, snow cover, and possibly canopy properties. There is no horizontal interaction between neighboring points in the LSM, so it can be regarded as a one-dimensional column model for each WRF land grid-point, and many LSMs can be run in a stand-alone mode.

The different land-surface schemes options of ARW are discussed below.

Noah Land Surface Model (LSM) : Unified NCEP/NCAR/AFWA scheme with soil temperature and moisture in four layers, fractional snow cover and frozen soil physics, [163].

Rapid Update Cycle (RUC) Model LSM:RUC operational scheme with soil temperature and moisture in six layers, multi-layer snow and frozen soil physics, ([164]; [165]).

4.10.3 Pleim-XiuLand Surface Model (LSM): Two-layer scheme with vegetation and sub-grid tiling, ([166]; [167]).

2.9.1 Specified Lower Boundary Conditions

For long simulation periods, in excess of about a week, as in applications such as regional climate, ARW has a capability to specify lower boundary conditions on non-prognostic fields as a function of time. Foremost among these is the specification of the sea-surface temperature during the simulation. The Noah, RUC and PX LSMs also need to consider variations in vegetation fraction and albedo with season, so monthly datasets are interpolated to also be read in with the lower boundary file. Sea-ice cover variation can also be specified by this method in Version 3. The lower boundary conditions are simply read in typically at the same frequency as the lateral boundary conditions, and the fields are updated with new current values at each read.

2.9.2 Planetary Boundary Layer

The planetary boundary layer (PBL) is responsible for vertical sub-grid-scale fluxes due to eddy transports in the whole atmospheric column, not just the boundary layer. Thus, when a PBL scheme is activated, explicit vertical diffusion is de-activated with the assumption that the PBL

scheme will handle this process. The most appropriate horizontal diffusion choices are those based on horizontal deformation or constant Kh values where horizontal and vertical mixing are treated independently. The surface fluxes are provided by the surface layer and land-surface schemes. The PBL schemes determine the flux profiles within the well-mixed boundary layer and the stable layer, and thus provide atmospheric tendencies of temperature, moisture (including clouds), and horizontal momentum in the entire atmospheric column. Most PBL schemes consider dry mixing, but can also include saturation effects in the vertical stability that determines the mixing. The schemes are one-dimensional, and assume that there is a clear scale separation between sub-grid eddies and resolved eddies. This assumption will become less clear at grid sizes below a few hundred meters, where boundary layer eddies may start to be resolved, and in these situations the scheme should be replaced by a fully three-dimensional local sub-grid turbulence scheme such as the TKE diffusion scheme.

PBL Schemes options of this model are outlined below;

MediumRange Forecast Model (MRF): Older version of YSU with implicit treatment of entrainment layer as part of non-local-K mixed layer,[169].

YonseiUniversity (YSU): The Yonsei University PBL is the next generation of the MKF PBL,[16].

Mellor-Yamada-Janjic (MYJ): One-dimensional prognostic turbulent kinetic energy scheme with local vertical mixing,[170].

Asymmetrical Convective Model version 2 (ACM2) PBL: Asymmetric Convective Model with non-local upward mixing and local downward mixing,[171].

2.9.3 Atmospheric Radiation

The radiation schemes provide atmospheric heating due to radiative flux divergence and surface downward longwave and shortwave radiation for the ground heat budget. Longwave radiation includes infrared or thermal radiation absorbed and emitted by gases and surfaces. Upward longwave radiative flux from the ground is determined by the surface emissivity that in turn depends upon land-use type, as well as the ground (skin) temperature. Shortwave radiation includes visible and surrounding wavelengths that make up the solar spectrum. Hence, the only source is the Sun, but processes include absorption, reflection, and scattering in the atmosphere and at surfaces. For shortwave radiation, the upward flux is the reflection due to surface albedo. Within the atmosphere the radiation responds to model-predicted cloud and water vapor distributions, as well as specified carbon dioxide, ozone, and (optionally) traces gas

concentrations. All the radiation schemes in WRF currently are column (one-dimensional) schemes, so each column is treated independently, and the fluxes correspond to those in infinite horizontally uniform planes, which is a good approximation if the vertical thickness of the model layers is much less than the horizontal grid length. This assumption would become less accurate at high horizontal resolution.

2.9.4 Longwave radiation (RRTM)

Rapid Radiative Transfer Model (RRTM), which is taken from MM5, is based on [172] and is a spectral-band scheme using the correlated- k method. It uses pre-set tables to accurately represent longwave processes due to water vapor, ozone, and trace gases (if present), as well as accounting for cloud optical depth.

Eta Geophysical Fluid Dynamics Laboratory (GFDL): This long wave radiation scheme is from GFDL. An older multi-band scheme with carbon dioxide, ozone and microphysics effects.

CAM3 Scheme: A spectral-band scheme used in the NCAR Community Atmosphere Model (CAM 3.0) for climate simulations, [173].

2.9.5 Shortwave radiation

Geophysical Fluid Dynamics Laboratory (GFDL): This shortwave radiation is a GFDL version of the parameterization [176]. Two-stream multi-band scheme with ozone from climatology and cloud effects.

MM5 (Dudhia): This scheme [174] is taken from MM5. It has a simple downward integration of solar flux, accounting for clear-air scattering, water vapor absorption. It used in high-resolution simulation, sloping and shadowing effects may be considered.

Goddard Scheme: It has a total of 11 spectral bands and considers diffuse and direct solar radiation components in a two-stream approach that accounts for scattered and reflected components, [175].

CAM3 Scheme: A spectral-band scheme used in the NCAR Community Atmosphere Model (CAM 3.0) for climate simulations, [173].

Post-processing utilities: There are a number of visualization tools available to display WRF-ARW model data. Model data in netCDF (Network Common Data Form) format can essentially be displayed using any tool capable of displaying this data format.

Currently the following post-processing utilities are supported:

*NCL: The NCAR Command Language (NCL) is a free interpreted language designed specifically for scientific data processing and visualization. NCL has robust file input and output. It can read in netCDF, HDF4, HDF4-EOS, GrIB (Gridded Binary), binary and ASC-2 data. The graphics are world class and highly customizable.

*RIP4: RIP (which stands for Read/Interpolate/Plot) is a Fortran program that invokes NCAR Graphics routines for the purpose of visualizing output from gridded meteorological data sets, primary from mesoscale numerical models. RIP4 can currently only read data in netCDF format.

*ARWpost (converter to GrADS and Vis5D): The ARWpost package reads in WRF-ARW model data and creates output in either GrADS or Vis5D format. The converter can read in WPS geogrid and metgrid data, and WRF-ARW input and output files. It can read data in netCDF and GRIBI format.

*WPP: It can read data in netCDF and binary format.

*VAPOR: VAPOR is the Visualization and Analysis Platform for Ocean, Atmosphere, and Solar Researchers. VAPOR was developed at NCAR to provide interactive visualization and analysis of numerically simulated fluid dynamics.

For the present study, ARW post and GrADS (Grid Analysis and Display System) visualization tools are used as post-processing utilities to display WRF-ARW model data.

Chapter-III

Methodology

3.1 Preface

The tropical cyclones (TC) are regarded as the most destructive meteorological phenomenon, which ravage life and property especially over the coastal belt due to extremely strong winds and associated storm surges at the time of landfall. It has been evident that mortality associated with tropical cyclones is considerably high especially in the Bay of Bengal region mainly due to poor socio-economic conditions of bordering countries. In the recent year fairly intense tropical cyclones developed in the Bay of Bengal. In the present study investigation has been conducted on the formation and evolution of tropical cyclones of Bay of Bengal. The (WRF) is a new generation mesoscale numerical weather forecasting community model which has the potential to simulate meteorological phenomena ranging from meters to thousands of kilometers. ARW is a dynamic solver [27], which is compatible with the WRF system to simulate broad spectrum of meteorological phenomena. ARW is developed by the Mesoscale and Microscale Meteorological (MMM) Division of National Centre for Atmospheric Research (NCAR) of USA. It integrates the compressible, non-hydrostatics Euler equation, which are cast in flux form [31] with terrain-following mass vertical coordinates [32]. In the present study three land falling tropical cyclonic storm with different intensities which formed in the Bay of Bengal have been selected. The selected cyclones are, Very Severe Cyclonic Storm Nargis (2008), Very Severe cyclonic Storm Thane (2011) and cyclonic storm Mahasen (2013), (Table 3.1). Nargis has been the most devastating very severe tropical cyclone in 2008. It was a category 4 tropical cyclone according to Saffir-Simpson Hurricane scale. More than 84,000 people died as it hit low-lying areas of Irrawaddy delta of Myanmar on 2 May 2008 [26]. Thane has been the very severe tropical cyclone in 2011. It was a category 1 tropical cyclone according to Saffir-Simpson Hurricane scale. It developed over the Bay of Bengal and crossed north Tamil Nadu and Puducherry Coast between Puducherry and Cuddalore within 0630-0730 hrs IST 03rd December, 2011 with a wind speed of 120-140 kmph. Cyclonic storm Mahasen formed over southeast Bay of Bengal at 1430 IST of 10th May 2013 near latitude 5.0° N and longitude 92.0° E. and moved away towards Myanmar as a low pressure area in the morning of 17th May.

Table 3.1 The tropical cyclone selected for the present modeling study.

SI no	Name of the cyclone	Formation date as depression	Land fall date with position	Type of disturbance	Maximum Wind Speed	Human casualties
01	Nargis (2008)	27 April at 0300 UTC	2 May 08; Near Labutta of Irrawaddy delta, Myanmar	VSCS	90 kts at 0600 UTC of 02 May	Affected population-11 millions House damaged-745764 Deaths human-84000 Death of household animal-155248 above Area covered by salty sea water-72798acres National sector loss-3.37 trillion hect.
02	Thane (2011)	25 December at 1200 UTC	30December ,2011 Tamil Nadu & Puducherry Coast beteen Cuddalore and Puducherry.	VSCS	75 kts at 0600 UTC of 29Decembe r near 12.0°N/82.0°E	Affected population-6000 House damaged-167925 Deaths human-48 Death of household animal-60481 above Area covered by salty sea water-85652acres National sector loss-37407 hect.
03	Mahasen (2013)	10 May at 0900 UTC	16 th May; Mizoram and Manipur and towards Myanmar at 17 th May.	CS	85-95 Kmph at 0600 UTC of 16 th May 2013 near 22.8°N/91.4°E.	Affected population-6000 House damaged-167925 Death of household animal-60481 above Area covered by salty sea water-85652acres National sector loss-37407 hect.

The model simulated results have been presented in the graphical and tabular forms. Grid Analysis and Display System (GrADS) and WinSurfer software have been employed for visualization of model outputs. Finally the model outputs have been compared with Joint Typhoon Warning Center (JTWC) best track data [25], to demonstrate the performance of the modeling exercise. The discussions of the results are provided with necessary physical interpretation.

3.2 Model setup for the Bay of Bengal

3.2.1 Domain selection

To simulate above selected tropical cyclones a domain of dimension (3.0-24.0)°N and (69.0-98.0)°E was selected to cover the Bay of Bengal basin at 9 km horizontal resolution with 27

vertical η levels. Figure 3.1 shows the horizontal domain of the model. The model domain consists of 127×127 grid points. Mercator map projection has been used.



Figure 3.1: Model domain with $24\text{km} \times 24\text{km}$ horizontal resolution

3.2.2 Model physics

In the present modeling exercise Kain-Fritsch (KF) cumulus parameterization scheme and WRF-single moment (WSM) 3-class microphysics scheme (simple ice and snow scheme) have been chosen for simulating all the events. Surface layer was treated using Monin-Obukhov scheme with Carlson-Bolan viscous sub-layer option and boundary layer has been treated with Yonsei University scheme. Noah 4-layer Land Surface Model (LSM) has been utilized with the above combination. Long and short wave radiations have been treated with Rapid Radiative Transfer Model (RRTM) and Dudhia schemes, respectively. Time step of integration was set to 120 seconds for maintaining the computational stability as the model uses 3rd order Runge-Kutta time integration scheme. Table 3.2 summarizes the selected parameterization schemes.

Table 3.2: Selected parameterization schemes of different physics options

physics option	Selected Parameterization schemes
Microphysics	WRF-single moment 3-class (WSM3)
Cumulus parameterizations	Kain-Fritsch(KF) cumulus parameterization
Surface layer physics	monin-Obukhov with Carlson-Bolan viscous sub-layer option
Land surface model	Noah 4-layer Land Surface Model (LSM)
planetary boundary layer physics	Yonsei University scheme
Long wave radiation physics	Rapid Radiative Transfer model (RRTM)

.3.3 Model Initialization

ARW model was run for 24, 48, 72, 96 120,144 hrs to study the formation and evolution of selected three tropical cyclones developed over the Bay of Bengal. National Centre for Environment Prediction (NCEP), Final Reanalysis (FNL) data ($1^{\circ}\times 1^{\circ}$ resolution) was utilized as initial and lateral boundary conditions (LBCs) which is updated at six hourly interval. The model was initialized with 0000, 0600, 1200 and 1800 UTC initial field of corresponding date.

3.4 Life History of Selected Tropical Cyclones

Observations of the selected cyclones such as formation, maximum sustained wind speed, minimum sea level pressure, Vorticity, Radius of maximum wind, etc. are discussed in the following sub sections. This section is mainly based on Joint Typhoon Warning Center (JTWC) best track data [25].

3.4.1 Very Severy Cyclonic Storm Nargis (2008)

Very severe cyclonic Storm Nargis (JTWC: 01B, RSMC Designation: BOBO1) was a strong tropical cyclone that caused the worst natural disaster in the recorded history of Myanmar. The cyclone made landfall in the country on 02 May, 2008, causing catastrophic destruction and at least 84,000 fatalities. In the last week of April 2008, an area of deep convection persisted near a low-level circulation in the Bay of Bengal at about 1150 km east-southeast of Chennai, India. With good outflow and low wind shear, the system slowly organized as its circulation consolidated. Nargis was originated in the south-east Bay of Bengal on 26 April, 2008 as a well marked low. It moved north-west direction and turned into a deep depression on 27 April, 2008. It further intensified and turned into a cyclonic storm on 28 April. The cyclonic storm remained stationary near $13^{\circ}\text{N}/85.3^{\circ}\text{E}$ for a few hours and abruptly changed its direction and started to move towards north-east direction (Figure 5.4). The cyclone further intensified into a very severe cyclonic storm with winds of around 139Km/hr (75 knots) on 29 April, 2008 at 0000 UTC while the cyclone center was at $13.3^{\circ}\text{N}/85.6^{\circ}\text{E}$. Subsequently, the cyclone became disorganized and weakened due to subsidence and drier air as a result, deep convection near the center markedly decreased. On 30 April 2008 the system was weakened to severe cyclonic storm status with maximum sustain at 0600 UTC centered at $14.7^{\circ}\text{N}/87^{\circ}\text{E}$. On 1May 2008, after turning eastward cyclone Nargis rapidly intensifying due to greatly improved outflow in association with an

approaching upper-level trough. Strengthening continued as it developed a well-defined eye with a diameter of 19km, and early on 2May 2008 the JTWC estimated that the cyclone reached the peak winds of 213 km/hr (115 knots) as it approached the coast of Myanmar, making it a Category 4 storm. Around 1200 UTC on 2May 2008, cyclone Nargis made landfall near Irrawaddy delta of Myanmar at peak strength as a very severe cyclonic storm with MSLP of 937 hpa. After landfall it was weakened and traveled farther inland as a tropical storm and tropical depression.

3.4.2 Very Severy Cyclonic Storm Thane (2011)

In association with an active ITCZ, a cyclonic circulation formed over southeast Bay of Bengal on 23rd December 2011. It was associated with scattered convective cloud cluster over the region. Gradually the convective clusters deepened and came closer to each other and a low pressure area formed over the southeast Bay of Bengal on 24th morning with T1.0. It became well marked over the same region in the evening of 24th December 2011. Considering the environmental features, the seasurface temperature (SST) was about (27-28)^o Cover southeast Bay of Bengal, Andaman Sea and adjoining southeast and central Bay of Bengal. It was relatively less towards Tamil Nadu and Sri Lanka coast becoming (26-27)^oC. The ocean thermal energy was about 50-80 KJ/cm over southeast Bay of Bengal and neighborhood. However, it was about 50 KJ/cm near Tamil Nadu and north Sri Lanka coast. The Madden Julian Oscillation (MJO) Index lay over phase 5 witch is favorable for cyclogenesis over the Bay of Bengal. The upper tropospheric ridge at 200 hPa level ran along 10^oN and provided required poleward outflow for intensification of the system. As a result, the lower level convergence and upper level divergence were favorable for intensification. The vertical wind shear of horizontal wind was moderate (15-20 knots) around the low pressure area. It increased towards coast of Sri Lanka and Tamilnadu becoming moderate to high (20-30 knots). Due to all above favorable features, the well marked low pressure area concentrated into a depression and lay centered at 1200 UTC of 25th December 2011 near lat 8.5^oN and long. 88.5^oE. The intensity of the system was T1.5 as per Dvorak's technique. The lowest cloud top temperature was -77^oC. Associated intense to very intense convection lay over the Bay of Bengal, south of lat.15.5^oN and east of long. 82.0^oE. The poleward outflow was distinctly visible in satellite imageries. The maximum sustained surface wind was about 25 knots and the estimated central pressure was about 1000 hPa.

3.4.3 Cyclonic Storm Mahasen (2013)

A depression formed over southeast Bay of Bengal at 1430 hrs IST of 10th May 2013 near latitude 5.0°N and longitude 92.0°E. It moved northwestwards and intensified into a deep depression in the evening of the same day. Continuing its northwestward movement, it **further** intensified into a cyclonic storm, Mahasen in the morning of 11th May 2013. Under the influence of the anticyclonic circulation lying to the east, the cyclonic storm changed its direction of movement initially from northwesterly to northerly and then to north-northeasterly on 13th and 14th May respectively. On 15th May, it further came under the influence of the mid-latitude westerly trough running roughly along 77°E, which further helped in enhancing the north-northeastward movement of the cyclonic storm significantly increased, becoming about 40-50 kmph. The cyclonic storm crossed Bangladesh coast near lat. 22.8°N and long. 91.4°E, about 30km south of Feni around 1330 hrs IST of 16th May 2013 with a sustained maximum surface wind speed of about 85-95 kmph. After the landfall, it continued to move north-northeastwards and weakened gradually due to interaction with land surface. It weakened into a deep depression over Mizoram in the evening and into a depression over Manipur around mid-night of 16th. It further weakened into a well marked low pressure area over Nagaland in the early morning and moved away towards Myanmar as a low pressure area in the morning of 17th May

Chapter-IV

**A STUDY ON THE FORMATION AND EVOLUTION OF
TROPICAL CYCLONE OVER BAY OF BENGAL USING
WEATHER RESEARCH & FORECASTING (WRF) MODEL.**

4.0 Analysis of Model Results and Discussion

ARW model was run for 24, 48, 72, 96, 120, 144 hrs to simulate formation and evolution of tropical cyclones Nargis (2008), run for 24, 48, 72, 96 hrs for that of tropical cyclone Thane (2011) and run for 24, 48, 72, 96, 120 hrs for that of cyclone Mahasen (2013), in the Bay of Bengal. The model was initialized with 0000, 0600, 1200 and 1800 UTC initial and boundary field from GFS resolution data. The model results are presented in the graphical forms and compared with the JTWC best track data to demonstrate the performance of the modeling exercise. The modeling results are discussed in the following sections with necessary physical interpretations.

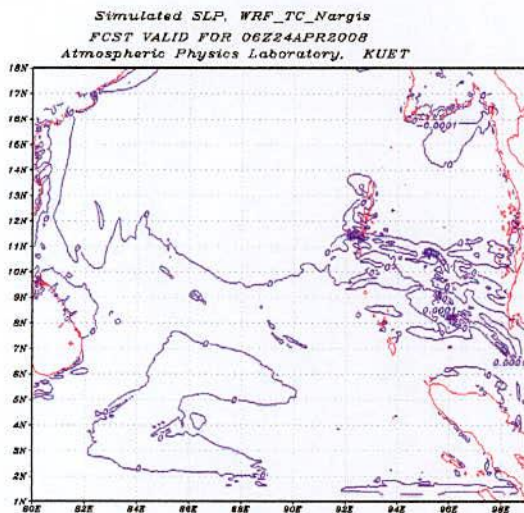
4.1 Prediction of Formation

To study the formation of selected tropical cyclones the prediction experiments were performed up to 96 hrs using the initial field before the formation of the system. The predictions have been updated every 6 hrs using the corresponding initial field of respective dates until the model could produce the low pressure system. Such experiments were performed to test if the model was capable of capturing the formation process of the cyclonic system. It may be noted that the modeling experiments were performed for the Bay of Bengal cyclones ([18]; [98]; [102]; [104]; [106]; [107]; [108]; [109]; [110]; [111]) in the recent years. In the above studies the models were initialized with well marked low or depression. Some authors have superimposed artificial vortex using bogussing technique based on satellite information in the initial field so that the models were able to predict further intensification and movement of the systems. This is the first time as per our knowledge that an attempt has been made to simulate the tropical cyclonic disturbance with initial field 48 hrs before the first formation or detection of the low. But the modeling results show that the model was able to produce the first detected system with initial field before 30-36 hrs. The details of the results are discussed below.

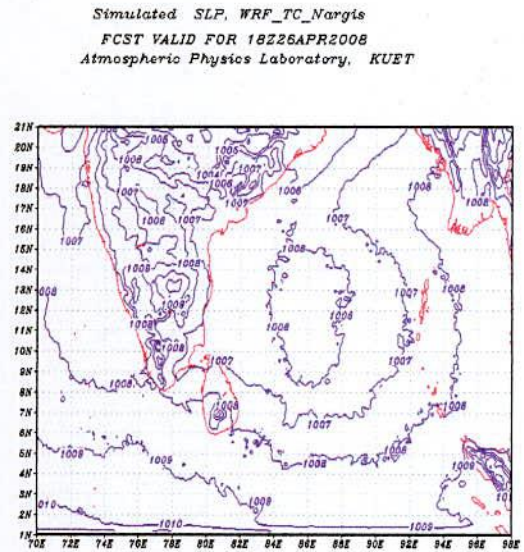
4.1.1 Very Severy Cyclonic Storm Nargis (2008)

As cyclone Nargis originated in the south-east Bay of Bengal on 26 April as a well marked low, the prediction was performed with initial field of 0000 UTC of 24 April 2008 to catch the formation of the system. The model generated a low pressure system at 1800 UTC of 26 April 2008 with MSLP of about 1005 hPa. Figure 4.1(b). The centre of the predicted system was centered at $12^{\circ}\text{N}/86.1^{\circ}\text{E}$ whereas the center of the first observed system was at $11^{\circ}\text{N}/88^{\circ}\text{E}$. According to the model results, the low pressure system moved to the north-west direction and it turned into well-marked low at pressure drop of 2 hPa. figure 4.1(b). The distribution of SLP of this system within next 66 hrs at 1800 UTC of 26 April 2008 the system further intensified into depression according to the model simulation figure 4.1(c,d) and moved to the north-west direction. The figure shows that the system has MSLP of 1000 hPa. The centre of the predicted system was found at $11.7^{\circ}\text{N}/87.2^{\circ}\text{E}$. Similarly next 1800 UTC of 28 April, 29 April, 30 April, 01 May, 02 May and 0000 UTC of 03 May 2008 are shown in figure [4.1(a-d) to 4.2 (e-h)]. The system further intensified into depression according to the model simulation figure 4.2(e-h) and moved to the north-west direction. The figure shows that the system has MSLP of 994 hPa, 970 hPa, 950 hPa, 965 hPa, 998 hPa respectively. The centre of the predicted system was found at $14.1^{\circ}\text{N}/88.2^{\circ}\text{E}$, $17^{\circ}\text{N}/89.5^{\circ}\text{E}$, $17.1^{\circ}\text{N}/92.3^{\circ}\text{E}$, $17.2^{\circ}\text{N}/95.1^{\circ}\text{E}$, $19.6^{\circ}\text{N}/95.5^{\circ}\text{E}$. But the centre of the observed system at $11.5^{\circ}\text{N}/87.2^{\circ}\text{E}$ which is close to the predicted centre. Therefore it is noted that in this case, like the case of the model was capable of predicting of the first formation of the low pressure system 36 hrs in advance which intensifies in to depression during the next 24 hrs of run. That is, the ARW model is able to forecast the formation of depression 72 hrs in advance.



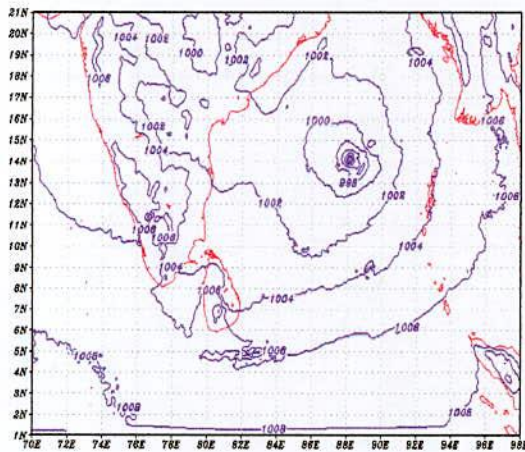


a



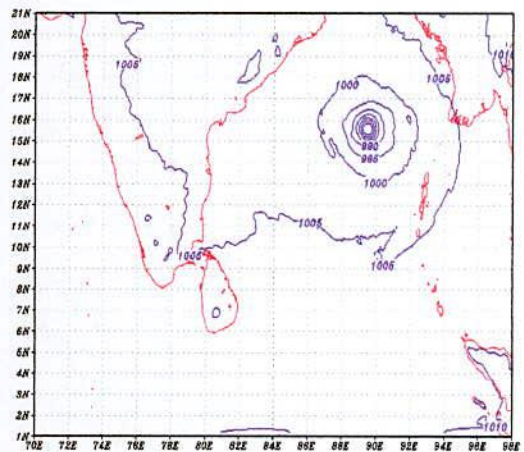
b

Simulated SLP, WRF_TC_Nargis
FCST VALID FOR 18Z28APR2008
Atmospheric Physics Laboratory, KUET



c

Simulated SLP, WRF_TC_Nargis
FCST VALID FOR 18Z29APR2008
Atmospheric Physics Laboratory, KUET

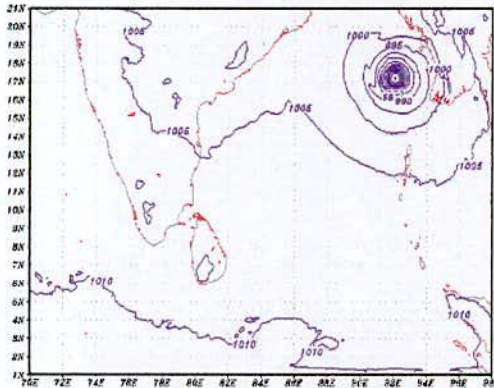


d

Figure 4.1 (a-d): Observed SLP of Nargis (used 0000 UTC of 24 April 2008 as model initial field)

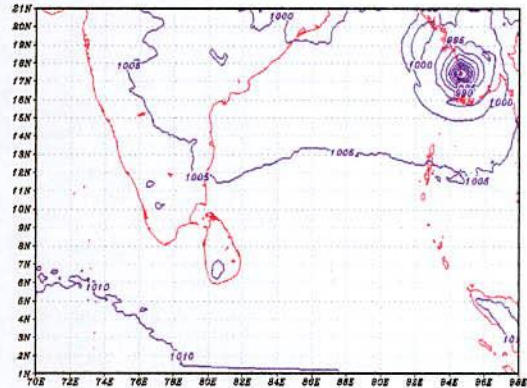
- (a) 06 hrs simulated SLP of Nargis at 0600 UTC of 24 April
- (b) 66 hrs simulated SLP of Nargis at 1800 UTC of 26 April
- (c) 114 hrs simulated SLP of Nargis at 1800 UTC of 28 April
- (d) 138 hrs simulated SLP of Nargis at 1800 UTC of 29 April.

Simulated SLP, WRF_TC_Nargis
 FCST VALID FOR 18Z30APR2008
 Atmospheric Physics Laboratory, KUET



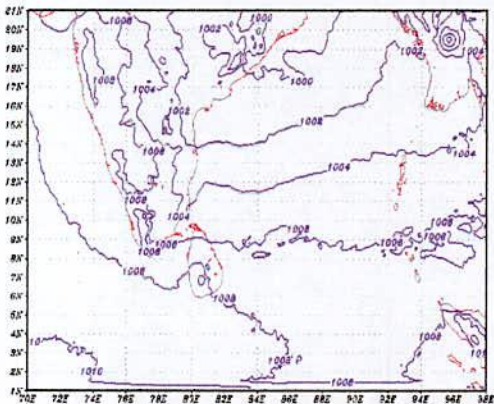
e

Simulated SLP, WRF_TC_Nargis
 FCST VALID FOR 18Z01MAY2008
 Atmospheric Physics Laboratory, KUET



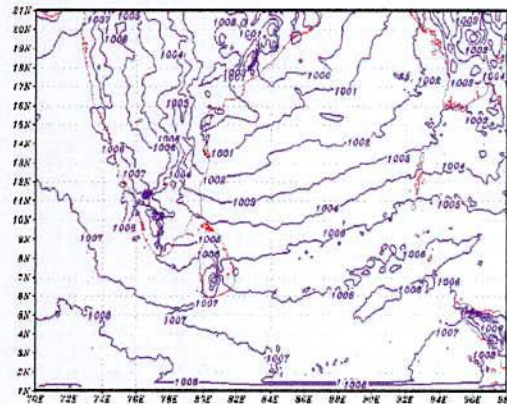
f

Simulated SLP, WRF_TC_Nargis
 FCST VALID FOR 18Z02MAY2008
 Atmospheric Physics Laboratory, KUET



g

Simulated SLP, WRF_TC_Nargis
 FCST VALID FOR 00Z03MAY2008
 Atmospheric Physics Laboratory, KUET



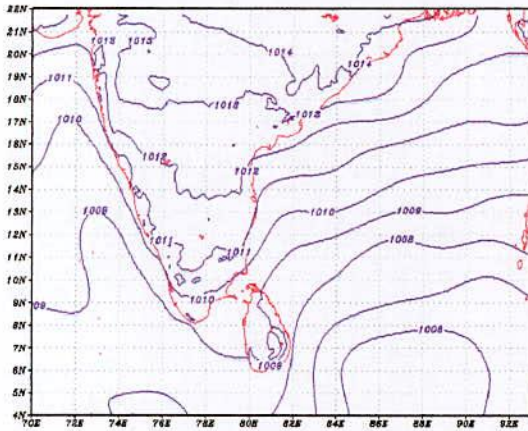
h

Figure 4.2 (e-h): Observed SLP of Nargis (used 0000 UTC of 24 April 2008, as model initial field) (e) 162 hrs simulated SLP of Nargis at 1800 UTC of 30 April (f) 186 hrs simulated SLP of Nargis at 1800 UTC of 01 May (g) 210 hrs simulated SLP of Nargis at 1800 UTC of 02 May (h) 216 hrs simulated SLP of Nargis at 0000 UTC of 03 May.

4.1.2 Very Severe Cyclonic Storm Thane (2011)

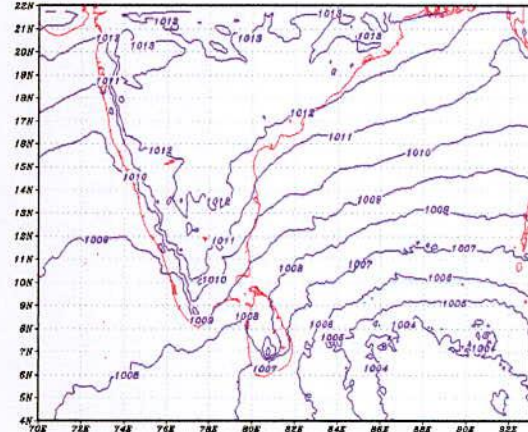
A very severe cyclonic storm Thane crossed Tamil Nadu coast on 30th December morning causing to life and property in north coastal areas of Tamil Nadu and Puducherry. About 48 people died due to this cyclone. In association with the favorable conditions the depression moved initially northwestwards and further intensified into a deep depression at 1800 UTC of 26th December and centered near lat.10.4°N and long.87.5°E but the centre of the observed system at lat. 9.5°N and long.87.5°E. The prediction was performed with initial field of 0000 UTC of 23 December 2011 to catch the formation of the system figure 4.3(a). Continuing its north-northwestwards movement, the deep depression intensified into a cyclonic storm Thane (2011) at 1800 UTC of 26th December 2011 near lat. 11.0°N and long. 87.5°E, but model simulated lat. 11.5°N and long. 87°E, figure 4.3(b) shows that the system has MSLP of 993 hPa. It then moved west-northwestwards and intensified into severe cyclonic storm over southwest and adjoining southeast Bay of Bengal at 1800 UTC of 27th December near lat. 13.2°N and long. 85.6°E. figure 4.3(c) shows that the system has MSLP of 990 hPa. at 0000 UTC of 25th December near lat. 12.5°N and long. 85.0°E but model simulated at 1800 UTC lat. 13.8°N and long. 83.8°E, and figure 4.3(d) shows that the system has MSLP of 990 hPa. about 500km east-southeast of Chennai. It further moved westwards, intensified into a very severe cyclonic storm at 1800 UTC of 26th December near lat.12.5°N and long. 84.5°E, about 450km east-southeast of Chennai. The very severe cyclonic storm 'Thane' then moved west-southwestwards and lay centred at 0300 UTC of 29th December 2011 near lat.12.0°N and long.82.5°E, but model simulated at 1800 UTC lat. 13.6°N and long. 81.2°E, and figure 4.4(e-h) shows that the system has MSLP of 998 hPa. about 270km east of Puducherry. It continued to move west-southwestwards and crossed north Tamil Nadu & Puducherry coast, close to the south of Cuddalore (near lat.11.6°N) between 0100 and 0200 UTC of 30thDecember, 2011. It crossed as a very severe cyclonic storm with an estimated wind speed of 120-140 kmph and estimated central pressure of 969 hPa. Figure (g). After the landfall, the system moved westwards and weakened into a severe cyclonic storm at 0300 UTC of 30thDecember, 2011 over north coastal Tamil Nadu. It further weakened into a deep depression at 0600 UTC near lat. 11.6°N and long. 79.0°E and into a depression at 1200 UTC of 30th December near Salem (Tamil Nadu). The depression moved further westwards and weakened into a well marked low pressure area over north Kerala and neighborhood at 0000 UTC of 31st December 2011, Figure (h). It then emerged into Arabian Sea and lay as a low pressure area over southeast Arabian Sea at 1200 UTC of 31stDecember 2011. It became less marked on 1stJanuary 2012.

Simulated SLP, WRF_TC_Thane
 DAY FCST VALID FOR 00Z23DEC2011
 Atmospheric Physics Laboratory, KUET



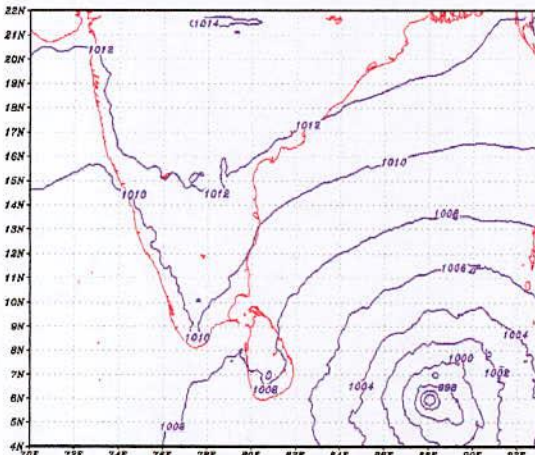
a

Simulated SLP, WRF_TC_Thane
 DAY FCST VALID FOR 00Z24DEC2011
 Atmospheric Physics Laboratory, KUET



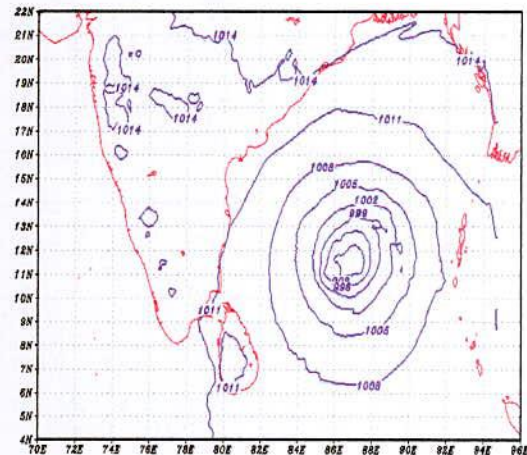
b

Simulated SLP, WRF_TC_Thane
 DAY FCST VALID FOR 00Z25DEC2011
 Atmospheric Physics Laboratory, KUET



c

Simulated Sea Level Pressure, WRF_TC_Thane
 DAY FCST VALID FOR 18Z26DEC2011
 Atmospheric Physics Laboratory, KUET

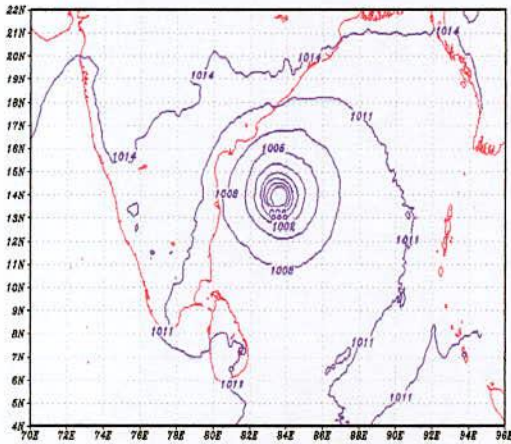


d

Figure 4.3 (a-d): Observed SLP of Thane

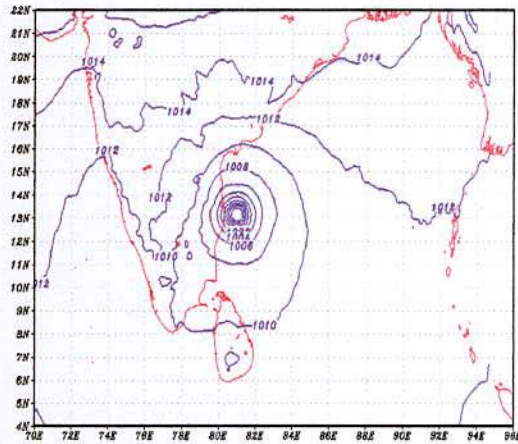
- (a) 0 hrs simulated SLP at 0000 UTC of 23 Dec. 2011(used as model initial field)
- (b) 24 hrs simulated SLP of Thane at 0000 UTC of 24 December
- (c) 72 hrs simulated SLP of Thane at 0000 UTC of 25 December
- (d) 90 hrs simulated SLP of Thane 1800 UTC of 26 December.

Simulated Sea Level Pressure, WRF_TC_Thane
 DAY FCST VALID FOR 18Z28DEC2011
 Atmospheric Physics Laboratory, KUET



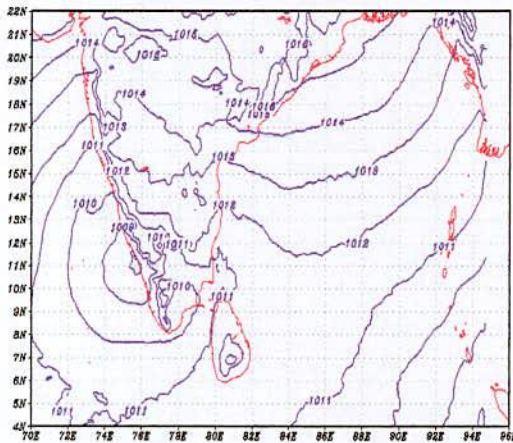
e

Simulated Sea Level Pressure, WRF_TC_Thane
 DAY FCST VALID FOR 18Z29DEC2011
 Atmospheric Physics Laboratory, KUET



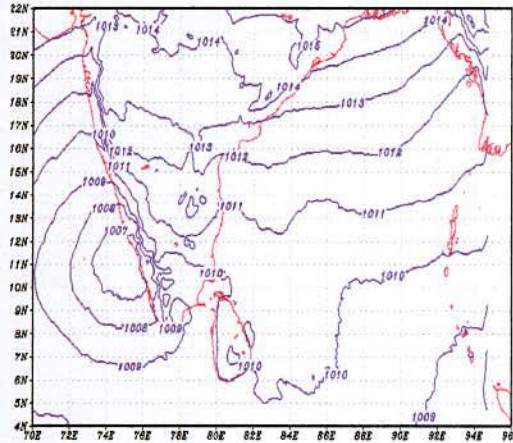
f

Simulated Sea Level Pressure, WRF_TC_Thane
 DAY FCST VALID FOR 18Z30DEC2011
 Atmospheric Physics Laboratory, KUET



g

Simulated Sea Level Pressure, WRF_TC_Thane
 DAY FCST VALID FOR 00Z31DEC2011
 Atmospheric Physics Laboratory, KUET



h

Figure 4.4 (e-h): Observed SLP of Thane (used at 0000 UTC of 23 Dec. 2011, as model initial field) (e) 138 hrs simulated SLP of Thane at 1800 UTC of 28 December (f) 162 hrs simulated SLP of Thane at 1800 UTC of 29 December (g) 186 hrs simulated SLP of Thane at 1800 UTC of 30 December (h) 190 hrs simulated SLP of Thane at 0000 UTC of 31 December.

4.1.3 Cyclonic Storm Mahasen (2013)

A cyclonic storm, Mahasen crossed Bangladesh coast near lat.22.8°N and long.91.4°E, about 30km south of Feni around 1330 hrs IST of 16th May 2013 with a sustained maximum wind speed of about 85-95 kmph. It weakened into a well marked low pressure area over Nagaland in the early morning and moved away towards Myanmar as a low pressure area in the morning of 17th May. The cyclonic storm moved very fast (about 40-50km per hour on the day of landfall, i.e. on 16th May 2013. Such type of fast movement of the cyclonic storm is very rare. Due to the faster movement, the adverse weather due to the cyclonic storm was relatively less. A depression formed over southeast Bay of Bengal at 1430 hrs IST of 10th May 2013 near latitude 5.0°N and longitude 92.0°E. It moved northwestwards and intensified into a deep depression in the evening of the same day. The prediction was performed with initial field of 0000 UTC of 08 May 2011 to catch the formation of the system continuing its northwestward movement, it further intensified into a cyclonic storm, Mahasen in the morning of 11th May 2013. Under the influence of the anticyclonic circulation lying to the east, the cyclonic storm changed its direction of movement initially from northwesterly to northerly and then to north-northeasterly on 13th and 14th May respectively. On 15th May, it further came under the influence of the mid-latitude westerly trough running roughly along 77°E, which further helped in enhancing the north-northeastward soeed of the cyclonic storm significantly increased, becoming about 40-50 kmph. The cyclonic storm crossed Bangladesh coast near lat.22.8°N and long. 91.4°E, about 30 km south of Feni around 1330 hrs IST of 16th May 2013 with a sustained maximum surface wind speed of about 85-95 kmph. After the landfall, it continued to move north-northeastwards and weakened gradually due to interaction with land surface. It weakened into a deep depression over Mizoram in the evening and into a depression over Manipur around mid-night of 16th. It further weakened into a well marked low pressure area over Nagaland in the early morning and moved away towards Myanmar as a low pressure area in the morning of 17th May. These are shown in figure [4.5(a-d) to 4.6(e-h)].

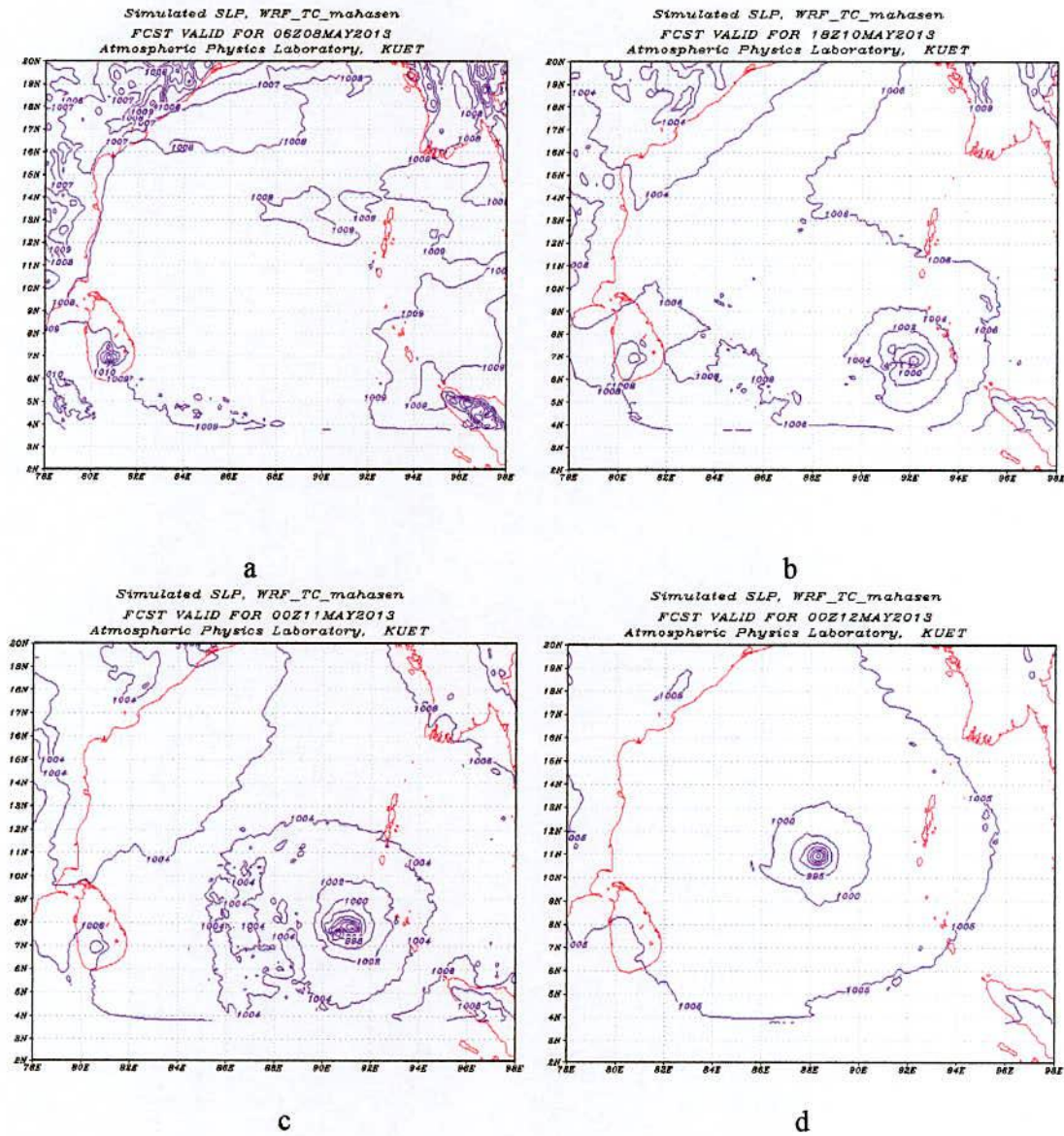


Figure 4.5 (a-d): Observed SLP of Mahasen

- (a) at 0600 UTC of 08 May, 2013 (used 0000 UTC as model initial field)
- (b) 66 hrs simulated SLP of Thane at 1800 UTC of 10 May
- (c) 72 hrs simulated SLP of Mahasen at 0000 UTC of 11 May
- (d) 96 hrs simulated SLP of Mahasen 0000 UTC of 12 May.

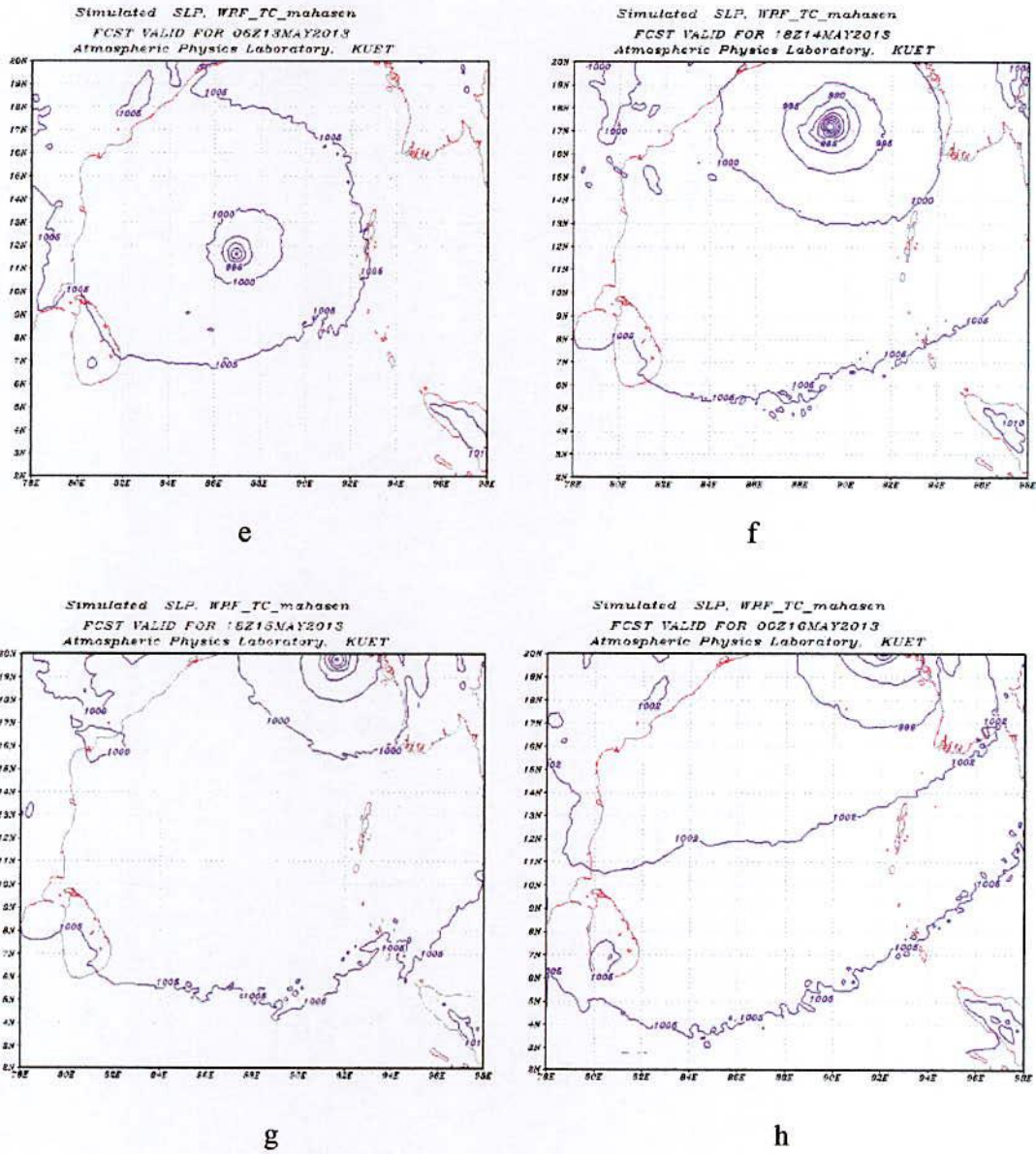


Figure 4.6 (e-h): Observed SLP of Mahasen (used at 0000 UTC of 08 May 2013, as model initial field) (e) 126 hrs simulated SLP of Mahasen at 0600 UTC of 13, May (f) 162 hrs simulated SLP of Mahasen at 1800 UTC of 14, May (g) 186 hrs simulated SLP of Mahasen at 1800 UTC of 15, May (h) 192 hrs simulated SLP of Mahasen at 0000 UTC of 16, May.

4.2 Evolution of Tropical Cyclones

This section is mainly on the evolution of selected tropical cyclones in terms of different parameters viz. Minimum Sea Level Pressure (MSLP), Pressure Drop (Δp), Maximum Wind Speed (MWS), Radius of Maximum Wind (RMW) and Relative Vorticity (ξ). These parameters are directly related to the intensity of tropical cyclone. To study the evolution of tropical cyclones the model was run for 24hrs, 48hrs, 72hrs, 96hrs, 120hrs, 144hrs, for Nargis (2008) using initial field condition, run for 24hrs, 48hrs, 72hrs, 96hrs for Thane (2011) using initial field condition and run for 24hrs, 48hrs, 72hrs, 96hrs, 120hrs, for cyclone Mahasen (2013) using initial field condition before the approximate landfall time. Model simulated variables and the derived parameters are compared with JTWC best track data except the relative vorticity (ξ) and Radius of Maximum Wind (RMW) due to unavailability of observed data. The model outputs have been taken at every 06 hrs interval.

4.2.1 Evolution of Minimum Sea level Pressure (MSLP)

Minimum sea level pressure (MSLP) of a tropical cyclone is of great importance as it helps to measure the intensity of a cyclone. Since tropical cyclones develop over the vast oceanic areas, where observations are sparse or not available, it is of great difficulty to make any validation of model simulated MSLP with sea truth data before the landfall. With the advent of satellite technology meteorologists are now able to estimate MSLP and maximum sustained wind (MSW) using interpretations of satellite products [84]. Figure 4.7(a, b, c) shows the comparative evolution of observed and model simulated MSLP of tropical cyclones Nargis (2008), Thane (2011) and Mahasen (2013). It appears from figure 4.7(a, b, c) that model simulated and observed MSLP gradually drops with time for all cases and attains peak intensity just before the landfall time and thereafter its MSLP increases. But for all the cases and at all the time points' model simulated MSLPs are more or less systematically higher and lower than the observed values except for severe cyclonic storm Mahasen (Figure 4.7c) which shows that the model simulated MSLP are lower than observed values.

The simulated values obtained using initial field condition, among all simulated values the 29 April's values is better agreement with observed values for very severe cyclonic storm Nargis

(2008), the 27 December's values is better agreement with observed values for very severe cyclonic storm Thane (2011) and 16 May's values is better agreement with observed values for severe cyclonic storm Mahasen (2013).

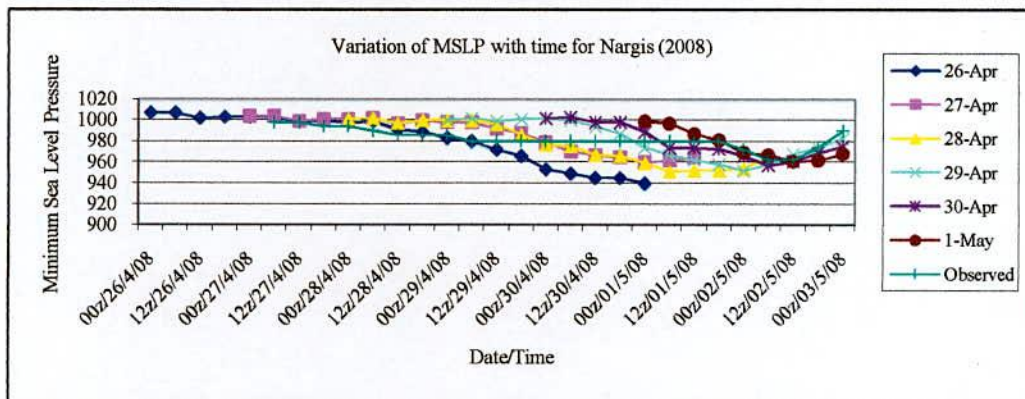
Also in figure 4.7 (a, b, c) shows that the model simulated MSLPs are higher and lower for Nargis (2008), lower and higher for Thane(2011), and lower for Mahasen (2013) with the compression of observed values. The variation of MSLPs with time for the cyclones Nargis, Thane and Mahasen shows better agreement with observed variations compared with simulated MSLPs.

However, the model simulates more or less realistic temporal variation of MSLP. Figure [4.8(a-d)-4.22(a-d)] shows the horizontal distribution of sea level pressure (SLP) of cyclones Nargis, Thane and Mahasen at different stages. The figures demonstrate that the intensity of the respective cyclones increases as the MSLP drops with time up to its peak intensity and after the landfall the intensity decreases rapidly. The table 4.1 summarizes the modeled and observed MSLP of all selected cyclones at the stage of their highest intensity. It is noted that for Nargis 144 hrs prediction simulated the lowest MSLP and 120 & 72 hrs prediction simulates the higher MSLP. But for 96, 48, 24 hrs prediction it is decreases with time. On the other hand for Thane, for 96 hrs prediction simulates the lowest MSLP, 24 hrs predictions simulates the highest MSLP and 96, 48 hrs it is same. And for Mahasen 48 hrs predictions simulates the highest MSLP.

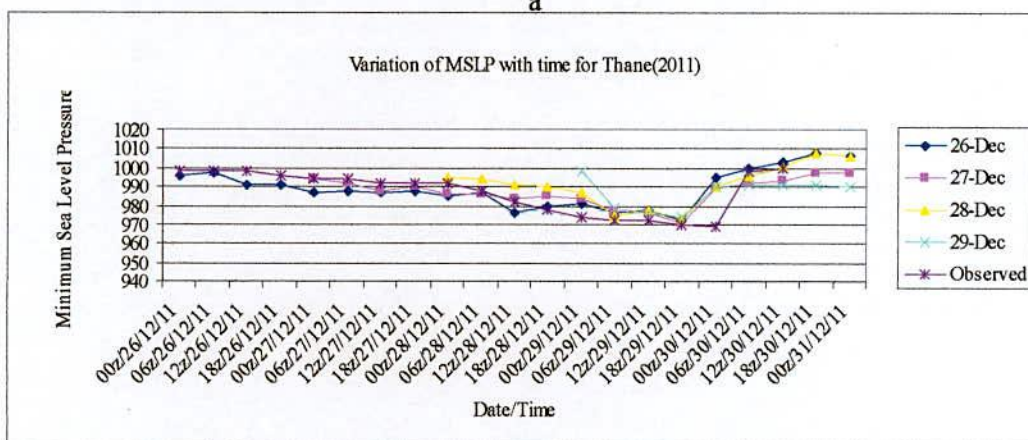
However, with respect to observed lowest MSLP 72 hrs simulation gives better estimation of MSLP for both cyclones Nargis, Thane and Mahasen. So it is also seen that the model underestimates the intensity in terms of MSLP for all the tropical cyclones under consideration. Though this could be due to weak representation of the system in the initial field of FNL. It is further to note that the resolution of FNL fields which also affects the intensification process due to weak representation of spatial distribution.

Table 4.1: Minimum sea level pressure (MSLP) of selected tropical cyclone at the stage of highest intensity.

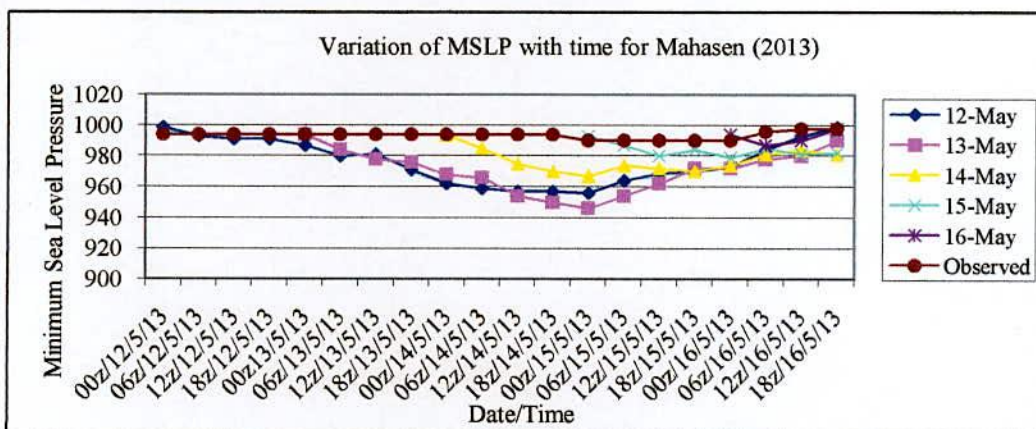
Name of cyclones	Initial Date/Time (UTC)	Forecasting hours	Simulated MSLP(hPa) [Date/Time]	Observed MSLP(hPa) [Date/Time]	Observed Min. MSLP(hPa) [Date/Time]
Nargis (2008)	26 April/0000	144	955 [02 May/1800]	974 [02 May/1800]	962 [02 May/0600]
	27 April/0000	120	965 [02 May/0900]	962 [02 May/0900]	962 [02 May/0600]
	28 April/0000	96	960 [02 May/0300]	972 [02 May/0300]	962 [02 May/0600]
	29 April/0000	72	965 [02 May/0600]	962 [02 May/0600]	962 [02 May/0600]
	30 April/0000	48	958 [02 May/1500]	964 [02 May/1500]	962 [02 May/0600]
	01 May/0000	24	962 [02 May/1800]	974[02 May/1800]	962 [02 May/0600]
Thane (2011)	26 December/0000	96	990 [30 December/1200]	1000 [30 December/1200]	969 [30 December/0000]
	27 December/0000	72	986 [30 December/0600]	998 [30 December/0600]	969 [30 December/0000]
	28 December/0000	48	989 [30 December/0600]	998 [30 December/0600]	969 [30 December/0000]
	29 December/0000	24	991 [30 December/0300]	986 [30 December/0300]	969 [30 December/0000]
Mahasen (2013)	12 May/0000	120	993 [16 May/0000]	990 [16 May/0000]	992 [15 May/0300]
	13 May/0000	96	997 [16 May/0600]	990 [16 May/0600]	992 [15 May/0300]
	14 May/0000	72	993 [16 May/0900]	994 [16 May/0900]	992 [15 May/0300]
	15 May/0000	48	991 [16 May/1200]	996 [16 May/1200]	992 [15 May/0300]
	16 May/0000	24	998 [16 May/0600]	990 [16 May/0600]	992 [15 May/0300]



a



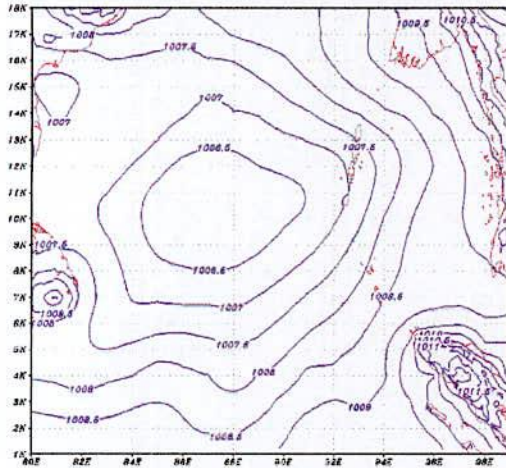
b



c

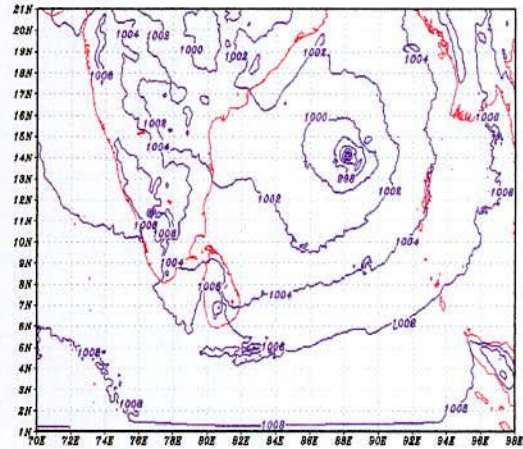
Figure 4.7:(a,b,c): Evolution of model simulated and observed MSLP with time of selected cyclones (a) Nargis (2008), (b) Thane (2011) and (c) Mahasen (2013)

Simulated SLP, WRF_TC_Nargis
 FCST VALID FOR 00Z26APR2008
 Atmospheric Physics Laboratory, KUET



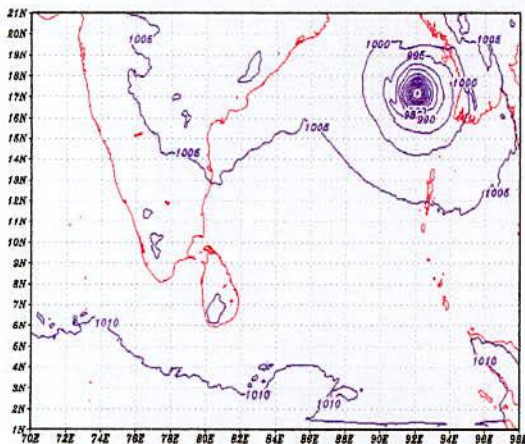
a

Simulated SLP, WRF_TC_Nargis
 FCST VALID FOR 18Z28APR2008
 Atmospheric Physics Laboratory, KUET



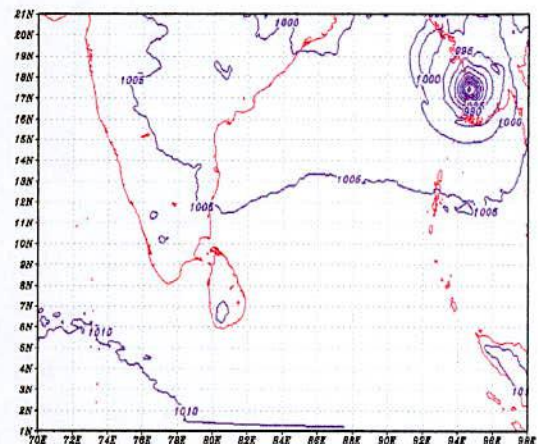
b

Simulated SLP, WRF_TC_Nargis
 FCST VALID FOR 18Z30APR2008
 Atmospheric Physics Laboratory, KUET



c

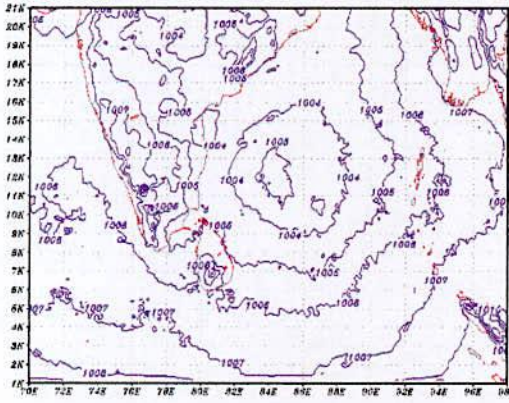
Simulated SLP, WRF_TC_Nargis
 FCST VALID FOR 18Z01MAY2008
 Atmospheric Physics Laboratory, KUET



d

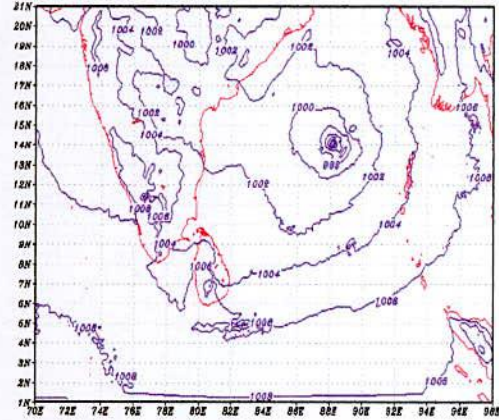
Figure 4.8 (a-d): Model simulated SLP (hPa) of cyclone Nargis (2008) at different stages:
 (a) at 0000UTC of 26 April (used as initial field) (b) at 1800UTC of 28 April
 (c) at 1800UTC of 30 April (d) at 1800UTC of 01 May.

Simulated SLP, WRF_TC_Nargis
 FCST VALID FOR 00Z27APR2008
 Atmospheric Physics Laboratory, KUET



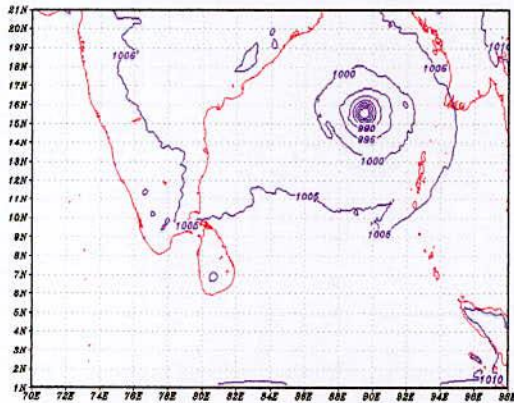
a

Simulated SLP, WRF_TC_Nargis
 FCST VALID FOR 18Z28APR2008
 Atmospheric Physics Laboratory, KUET



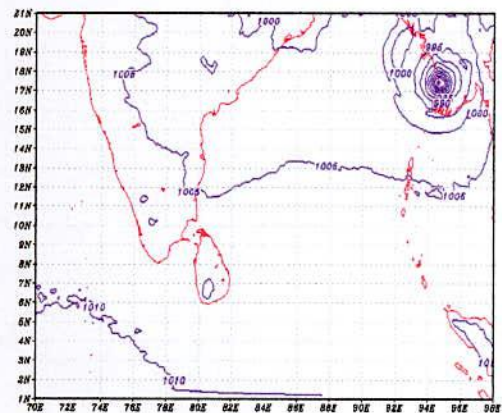
b

Simulated SLP, WRF_TC_Nargis
 FCST VALID FOR 18Z29APR2008
 Atmospheric Physics Laboratory, KUET



c

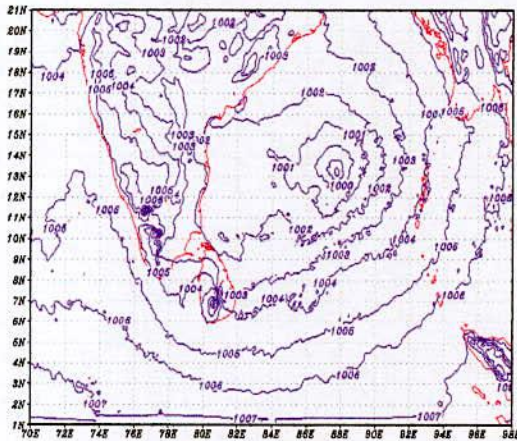
Simulated SLP, WRF_TC_Nargis
 FCST VALID FOR 18Z01MAY2008
 Atmospheric Physics Laboratory, KUET



d

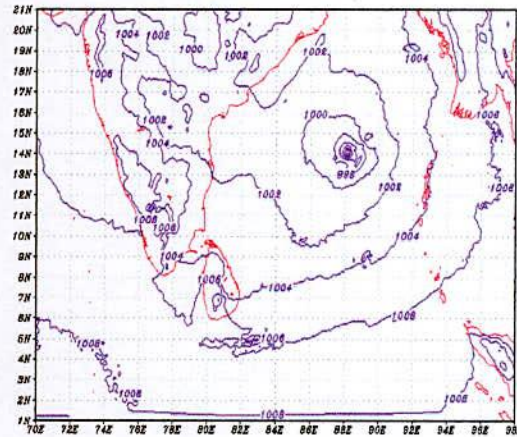
Figure 4.9 (a-d): Model simulated SLP (hpa) of cyclone Nargis (2008) at different stages:
 (a) at 0000UTC of 27 April (used as initial field) (b) at 1800UTC of 28 April
 (c) at 1800UTC of 29 April (d) at 1800UTC of 01 May..

Simulated SLP, WRF_TC_Nargis
 FCST VALID FOR 00Z28APR2008
 Atmospheric Physics Laboratory, KUET



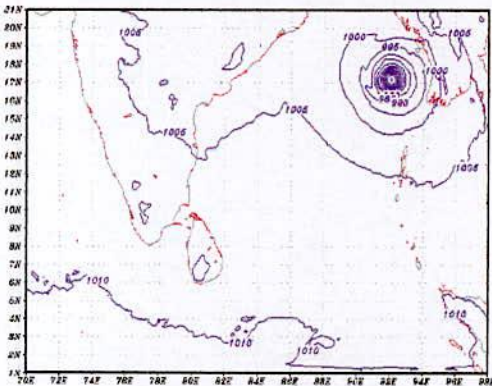
a

Simulated SLP, WRF_TC_Nargis
 FCST VALID FOR 18Z28APR2008
 Atmospheric Physics Laboratory, KUET



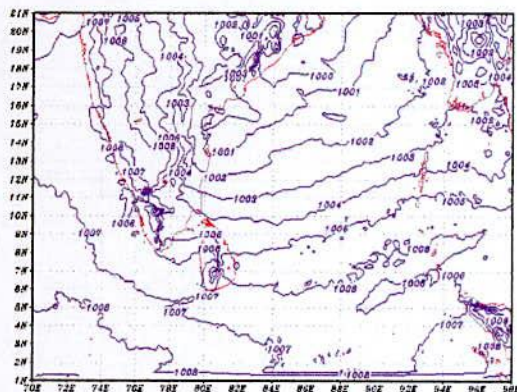
b

Simulated SLP, WRF_TC_Nargis
 FCST VALID FOR 18Z30APR2008
 Atmospheric Physics Laboratory, KUET



c

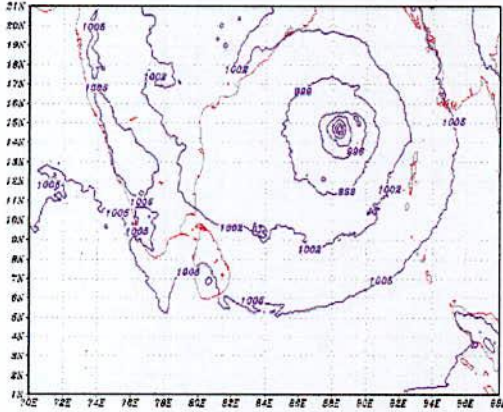
Simulated SLP, WRF_TC_Nargis
 FCST VALID FOR 00Z03MAY2008
 Atmospheric Physics Laboratory, KUET



d

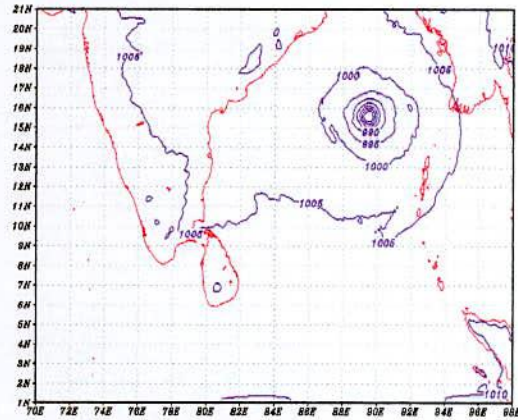
Figure 4.10 (a-d): Model simulated SLP (hpa) of cyclone Nargis (2008) at different stages:
 (a) at 0000UTC of 28 April (used as initial field) (b) at 1800UTC of 28 April
 (c) at 1800UTC of 30 April (d) at 0000UTC of 03 May.

Simulated SLP, WRF_TC_Nargis
 FCST VALID FOR 00Z29APR2008
 Atmospheric Physics Laboratory, KUET



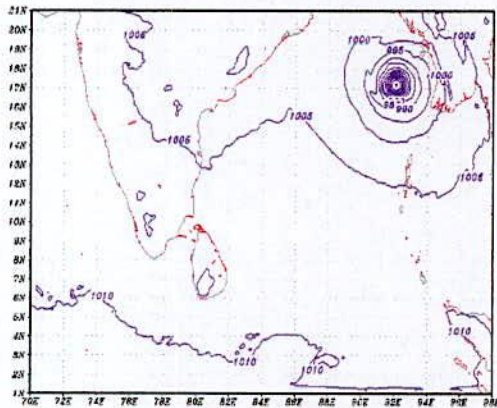
a

Simulated SLP, WRF_TC_Nargis
 FCST VALID FOR 18Z29APR2008
 Atmospheric Physics Laboratory, KUET



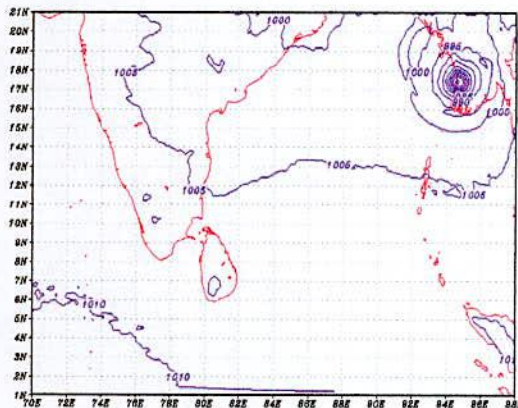
b

Simulated SLP, WRF_TC_Nargis
 FCST VALID FOR 18Z30APR2008
 Atmospheric Physics Laboratory, KUET



c

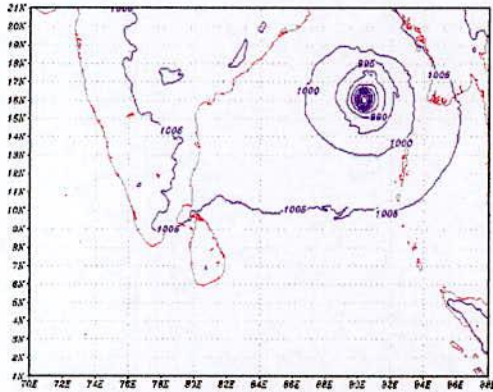
Simulated SLP, WRF_TC_Nargis
 FCST VALID FOR 18Z01MAY2008
 Atmospheric Physics Laboratory, KUET



d

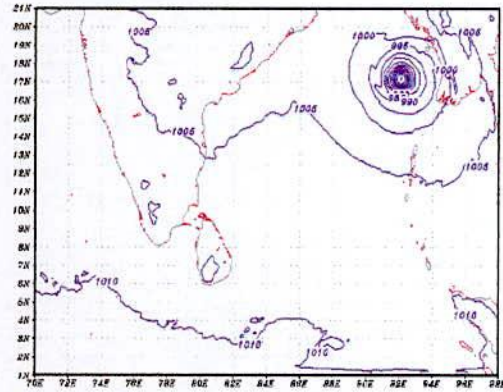
Figure 4.11 (a-d): Model simulated SLP (hpa) of cyclone Nargis (2008) at different stages:
 (a) at 0000UTC of 29 April (used as initial field) (b) at 1800UTC of 29 April
 (c) at 1800UTC of 30 April (d) at 1800UTC of 01 May.

Simulated SLP, WRF_TC_Nargis
 FCST VALID FOR 00Z30APR2008
 Atmospheric Physics Laboratory, KUET



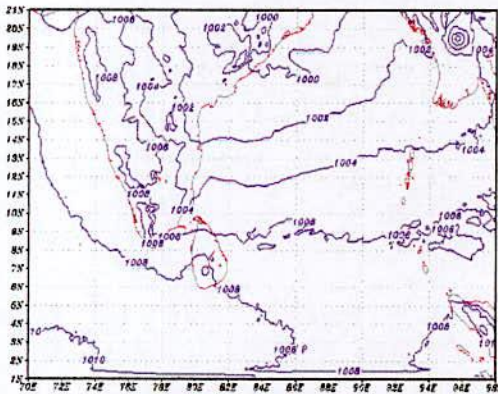
a

Simulated SLP, WRF_TC_Nargis
 FCST VALID FOR 18Z30APR2008
 Atmospheric Physics Laboratory, KUET



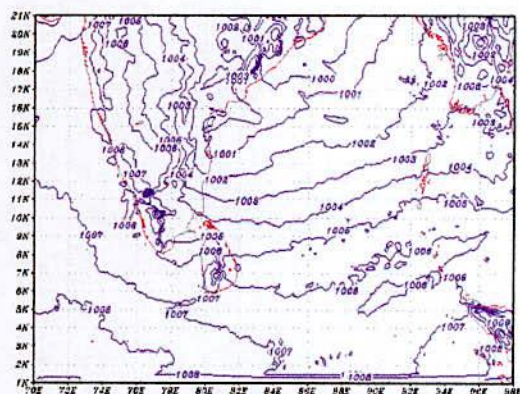
b

Simulated SLP, WRF_TC_Nargis
 FCST VALID FOR 18Z02MAY2008
 Atmospheric Physics Laboratory, KUET



c

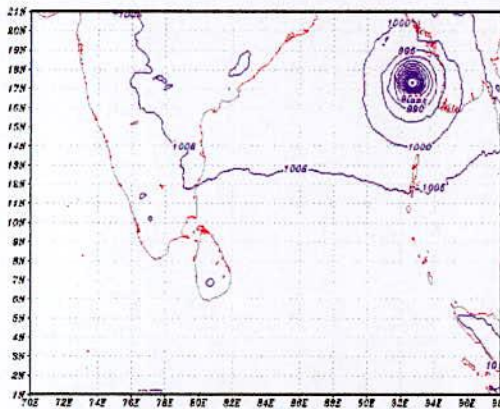
Simulated SLP, WRF_TC_Nargis
 FCST VALID FOR 00Z03MAY2008
 Atmospheric Physics Laboratory, KUET



d

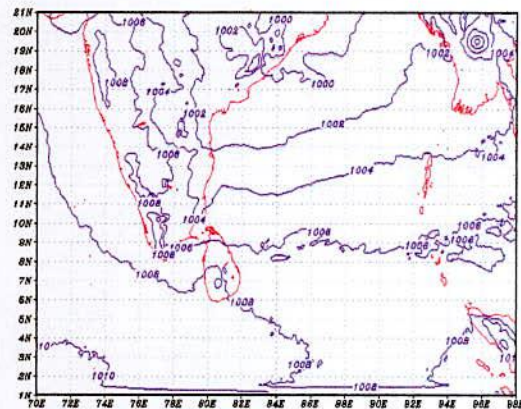
Figure 4.12 (a-d): Model simulated SLP (hpa) of cyclone Nargis (2008) at different stages:
 (a) at 0000UTC of 30 April (used as initial field) (b) at 1800UTC of 30 April
 (c) at 1800UTC of 02 May (d) at 0000UTC of 03 May.

Simulated SLP, WRF_TC_Nargis
 FCST VALID FOR 00Z01MAY2008
 Atmospheric Physics Laboratory, KUET



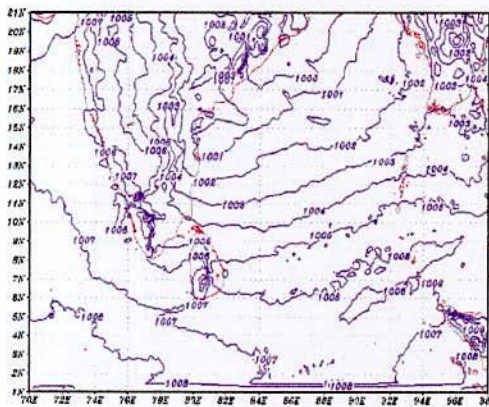
a

Simulated SLP, WRF_TC_Nargis
 FCST VALID FOR 18Z02MAY2008
 Atmospheric Physics Laboratory, KUET



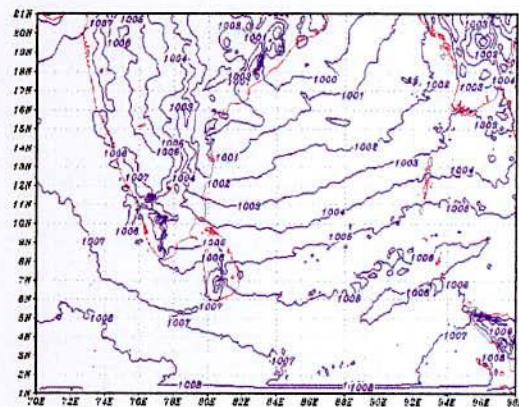
b

Simulated SLP, WRF_TC_Nargis
 FCST VALID FOR 00Z03MAY2008
 Atmospheric Physics Laboratory, KUET



c

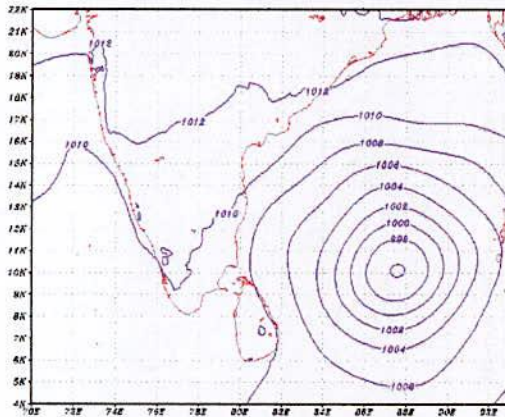
Simulated SLP, WRF_TC_Nargis
 FCST VALID FOR 00Z03MAY2008
 Atmospheric Physics Laboratory, KUET



d

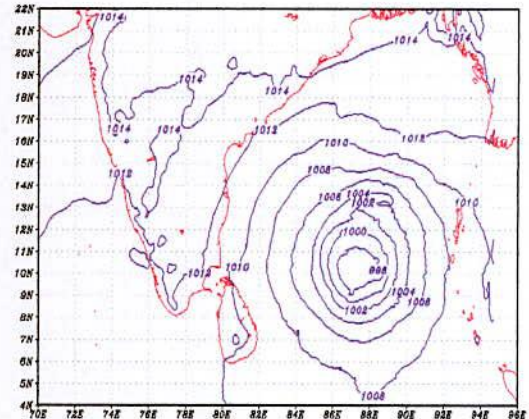
Figure 4.13 (a-d): Model simulated SLP (hpa) of cyclone Nargis (2008) at different stages:
 (a) at 0000UTC of 01 May (used as initial field) (b) at 1800UTC of 02 May
 (c) at 0000UTC of 03 May (d) at 0000UTC of 03 May

Simulated SLP, WRF_TC_Thane
 DAY FCST VALID FOR 00Z26DEC2011
 Atmospheric Physics Laboratory, KUET



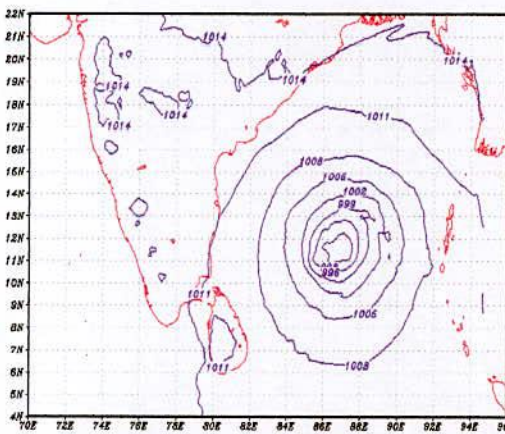
a

Simulated Sea Level Pressure, WRF_TC_Thane
 DAY FCST VALID FOR 06Z26DEC2011
 Atmospheric Physics Laboratory, KUET



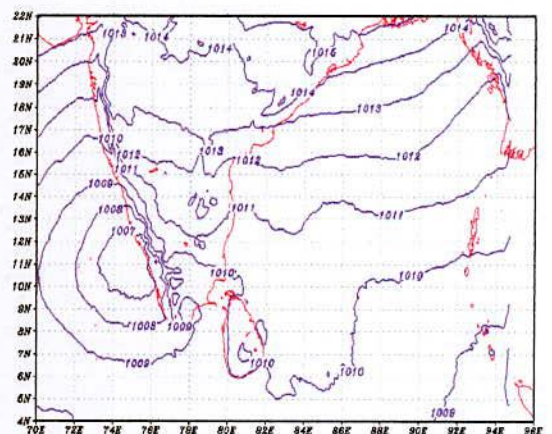
b

Simulated Sea Level Pressure, WRF_TC_Thane
 DAY FCST VALID FOR 18Z26DEC2011
 Atmospheric Physics Laboratory, KUET



c

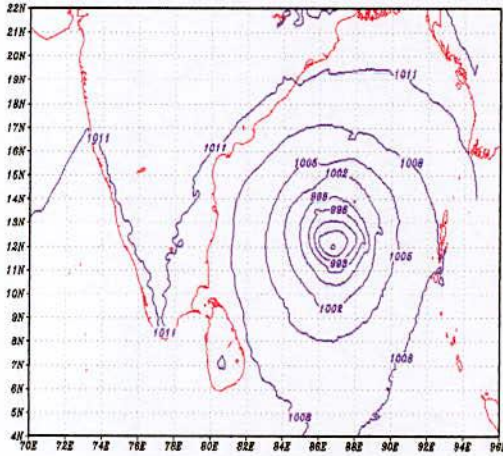
Simulated Sea Level Pressure, WRF_TC_Thane
 DAY FCST VALID FOR 00Z31DEC2011
 Atmospheric Physics Laboratory, KUET



d

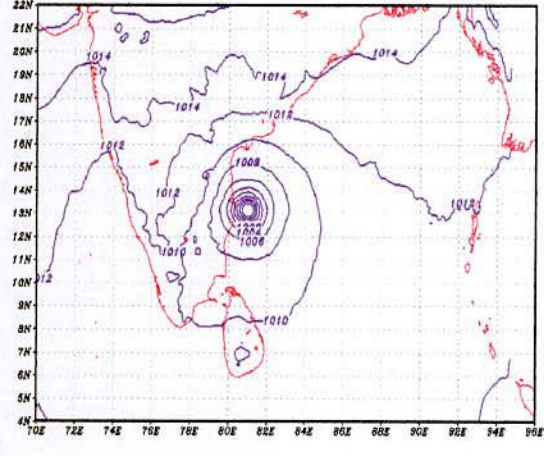
Figure 4.14 (a-d): Model simulated SLP (hpa) of cyclone Thane (2011) at different stages:
 (a) at 0000UTC of 26 December (used as initial field)
 (b) at 0060UTC of 26 December (c) at 1800UTC of 27 December
 (d) at 0000UTC of 31 December.

Simulated Sea Level Pressure, WRF_TC_Thane
 DAY FCST VALID FOR 00Z27DEC2011
 Atmospheric Physics Laboratory, KUET



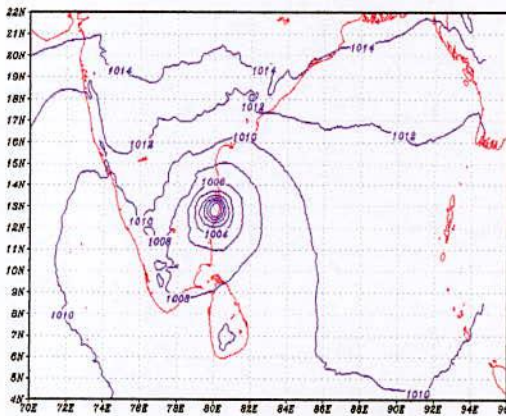
a

Simulated Sea Level Pressure, WRF_TC_Thane
 DAY FCST VALID FOR 18Z29DEC2011
 Atmospheric Physics Laboratory, KUET



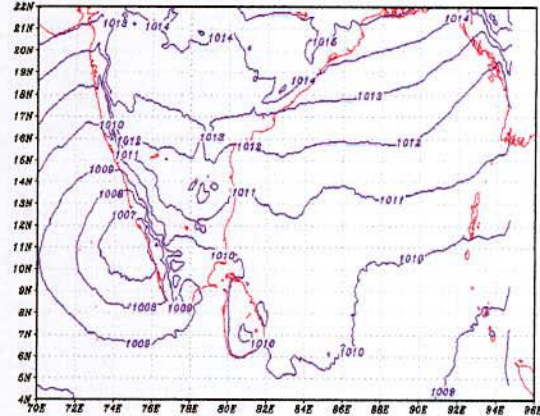
b

Simulated Sea Level Pressure, WRF_TC_Thane
 DAY FCST VALID FOR 00Z30DEC2011
 Atmospheric Physics Laboratory, KUET



c

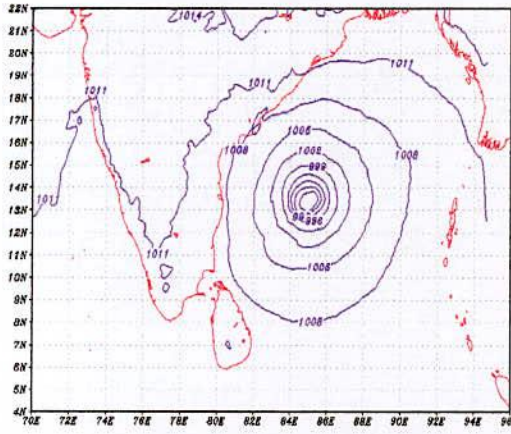
Simulated Sea Level Pressure, WRF_TC_Thane
 DAY FCST VALID FOR 00Z31DEC2011
 Atmospheric Physics Laboratory, KUET



d

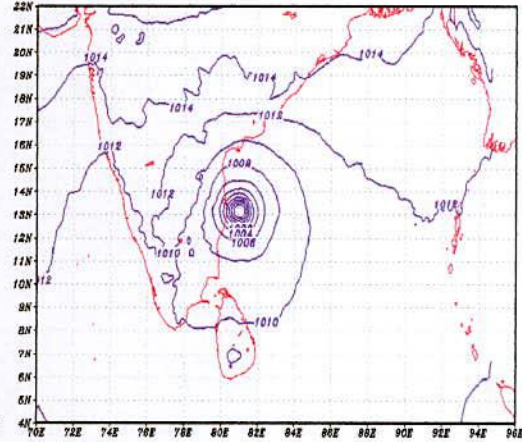
Figure 4.15 (a-d): Model simulated SLP (hpa) of cyclone Thane (2011) at different stages:
 (a) at 0000UTC of 27 December (used as initial field)
 (b) at 1800UTC of 29 December (c) at 0000UTC of 30 December
 (d) at 0000UTC of 31 December.

Simulated Sea Level Pressure, WRF_TC_Thane
 DAY FCST VALID FOR 00Z28DEC2011
 Atmospheric Physics Laboratory, KUET



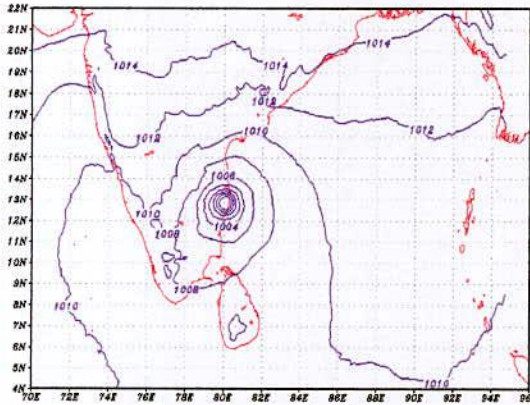
a

Simulated Sea Level Pressure, WRF_TC_Thane
 DAY FCST VALID FOR 18Z29DEC2011
 Atmospheric Physics Laboratory, KUET



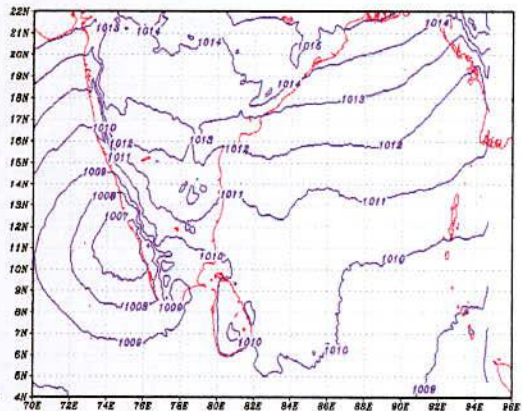
b

Simulated Sea Level Pressure, WRF_TC_Thane
 DAY FCST VALID FOR 00Z30DEC2011
 Atmospheric Physics Laboratory, KUET



c

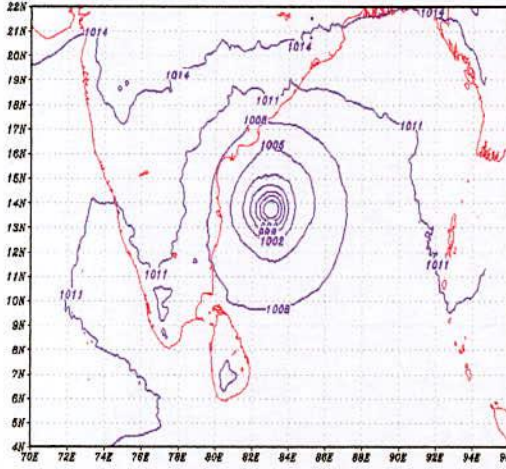
Simulated Sea Level Pressure, WRF_TC_Thane
 DAY FCST VALID FOR 00Z31DEC2011
 Atmospheric Physics Laboratory, KUET



d

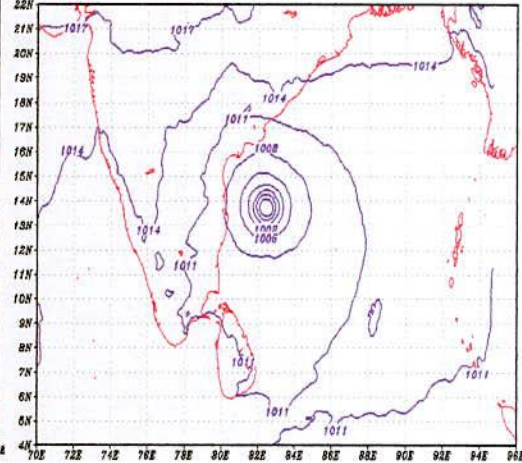
Figure 4.16 (a-d): Model simulated SLP (hpa) of cyclone Thane (2011) at different stages:
 (a) at 0000UTC of 28 December (used as initial field)
 (b) at 1800UTC of 29 December (c) at 0000UTC of 30 December
 (d) at 0000UTC of 31 December.

Simulated Sea Level Pressure, WRF_TC_Thane
 DAY FCST VALID FOR 00Z29DEC2011
 Atmospheric Physics Laboratory, KUET



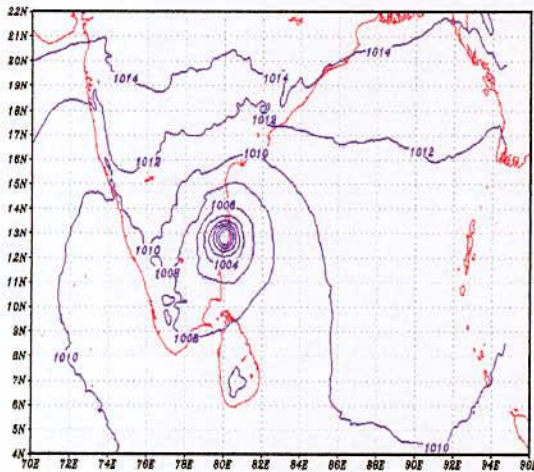
a

Simulated Sea Level Pressure, WRF_TC_Thane
 DAY FCST VALID FOR 06Z29DEC2011
 Atmospheric Physics Laboratory, KUET



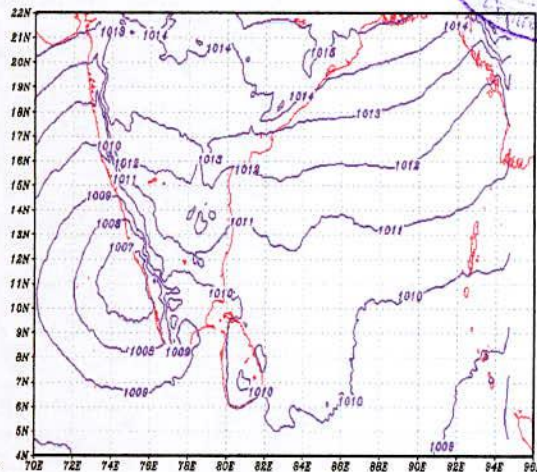
b

Simulated Sea Level Pressure, WRF_TC_Thane
 DAY FCST VALID FOR 00Z30DEC2011
 Atmospheric Physics Laboratory, KUET



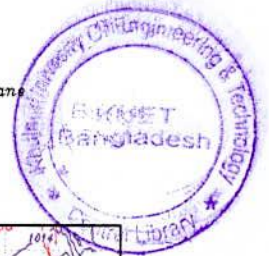
c

Simulated Sea Level Pressure, WRF_TC_Thane
 DAY FCST VALID FOR 00Z31DEC2011
 Atmospheric Physics Laboratory, KUET



d

Figure 4.17 (a-d): Model simulated SLP (hpa) of cyclone Thane (2011) at different stages (used at 0000UTC of 29 December as initial field):
 (a) at 0060UTC of 29 December (b) at 0000UTC of 30 December
 (c) at 0000UTC of 30 December (d) at 0000UTC of 31 December.



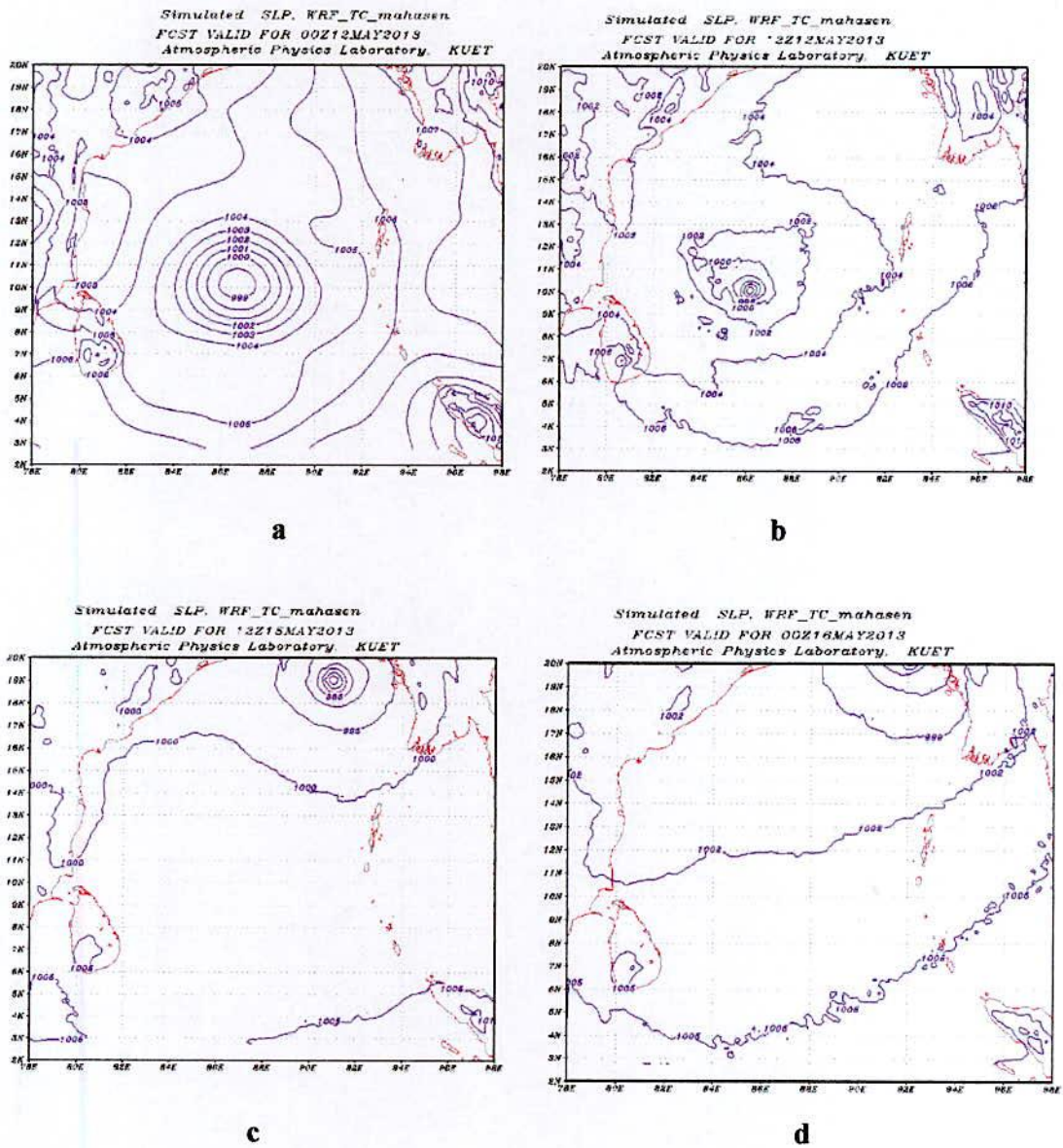


Figure 4.18 (a-d): Model simulated SLP (hpa) of cyclone Mahasen (2013) at different stages: (a) at 0000UTC of 12 May (used as initial field) (b) at 0012UTC of 12 May (c) at 1200UTC of 15 May (d) at 0000UTC of 16 May.

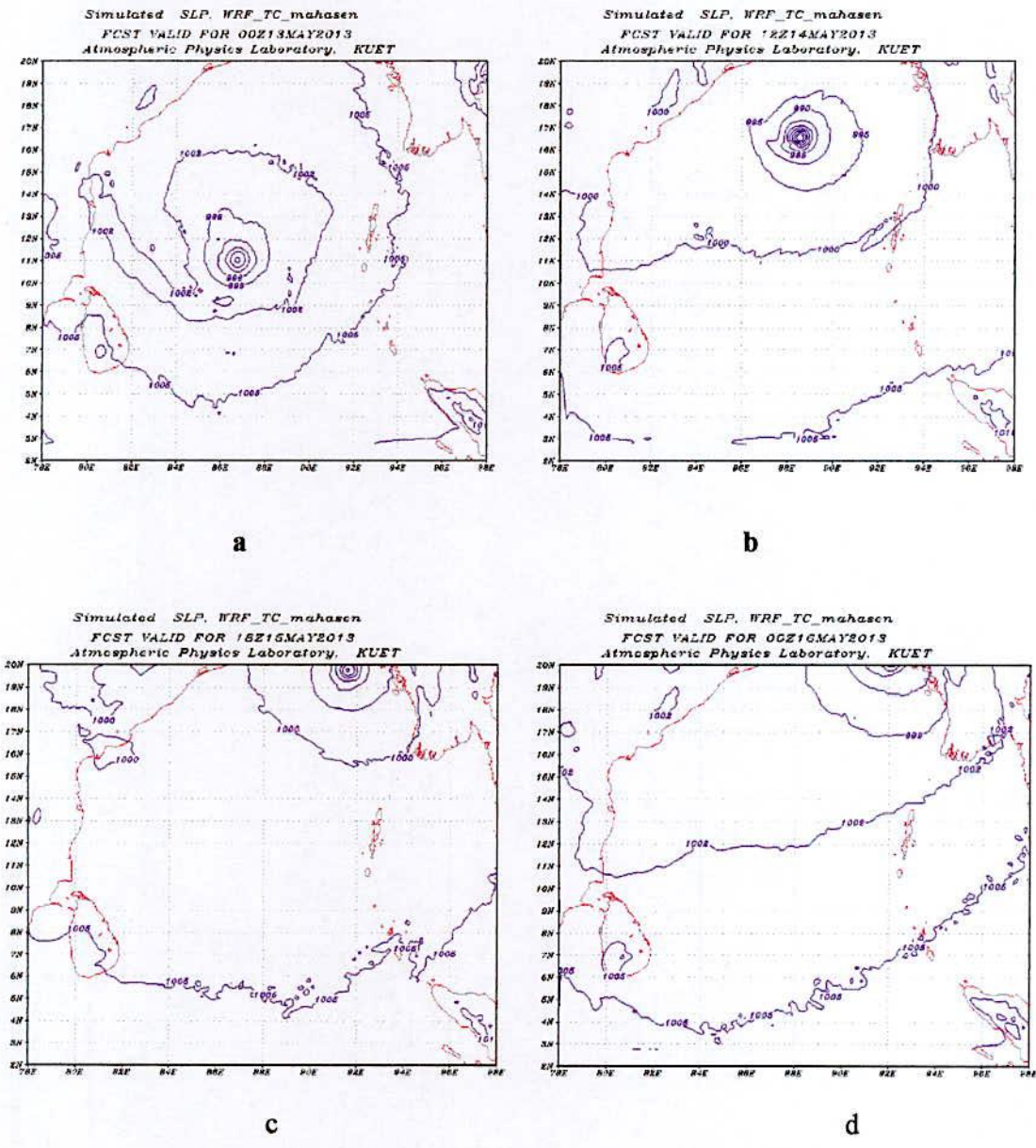


Figure 4.19 (a-d): Model simulated SLP (hpa) of cyclone Mahasen (2013) at different stages: (a) at 0000UTC of 13 May (used as initial field) (b) at 1200UTC of 14 May (c) at 1800UTC of 15 May (d) at 0000UTC of 16 May.

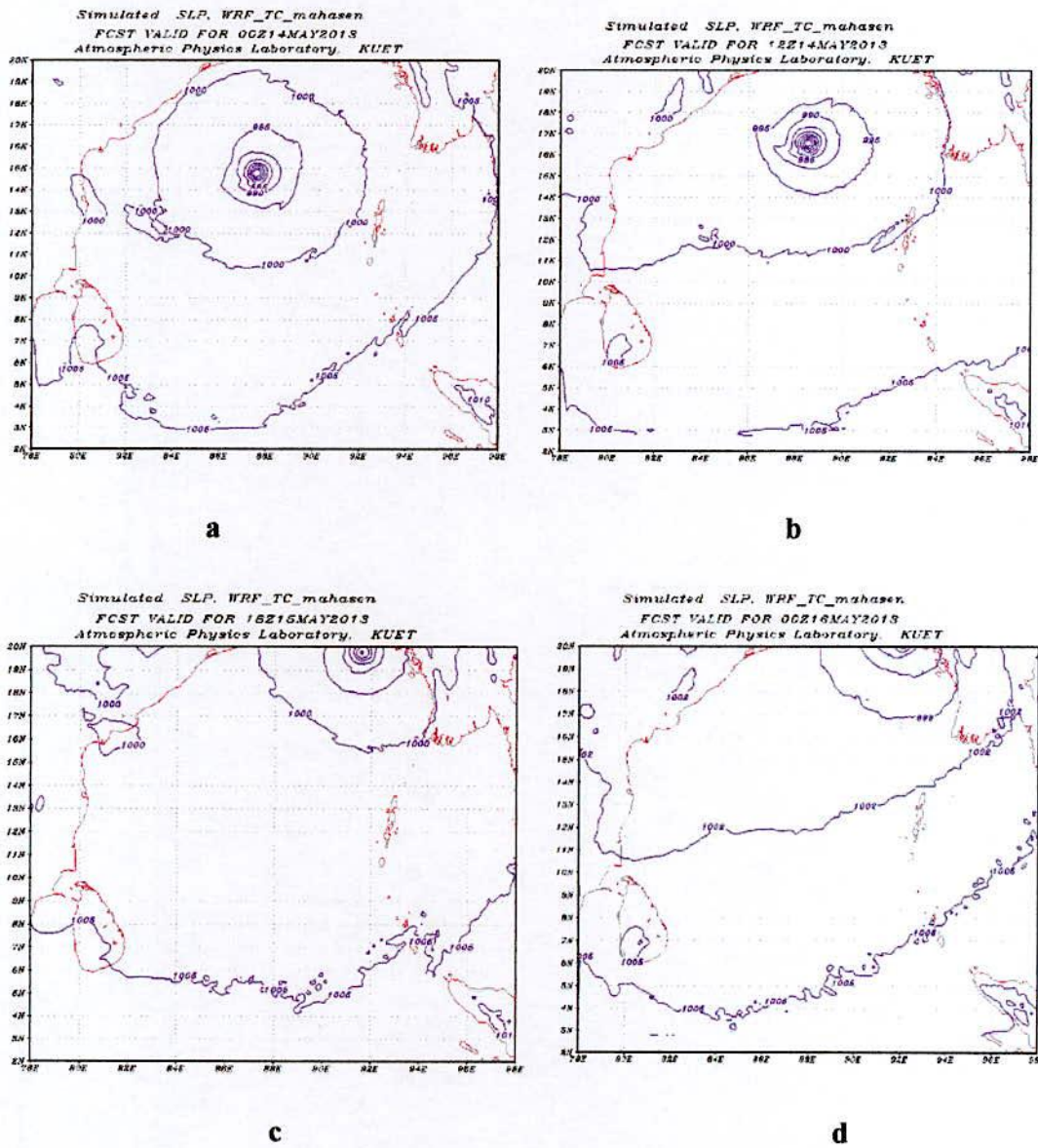


Figure 4.20 (a-d): Model simulated SLP (hpa) of cyclone Mahasen (2013) at different stages: (a) at 0000UTC of 14 May (used as initial field) (b) at 0012UTC of 14 May (c) at 1800UTC of 15 May (d) at 0000UTC of 16 May.

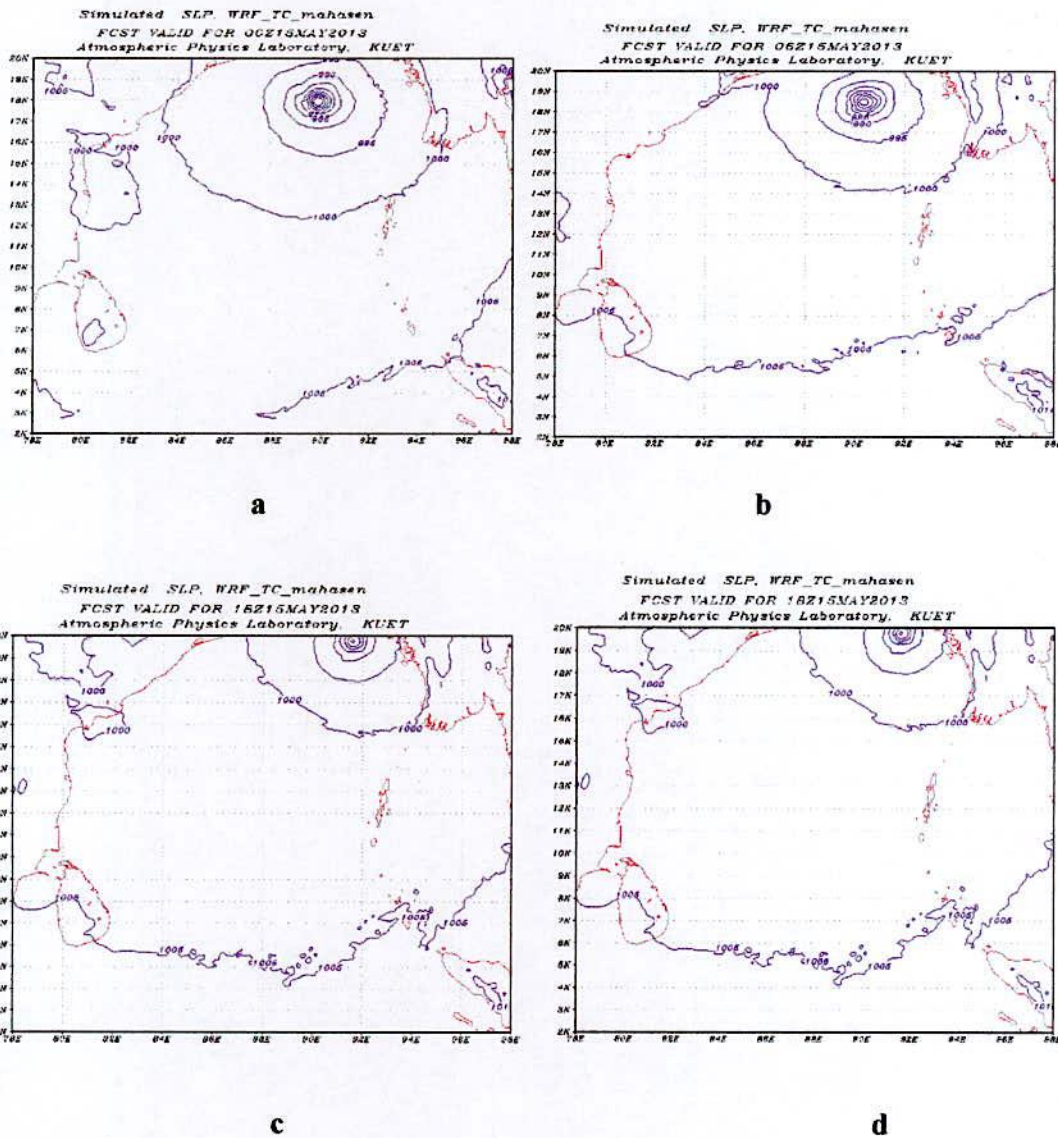
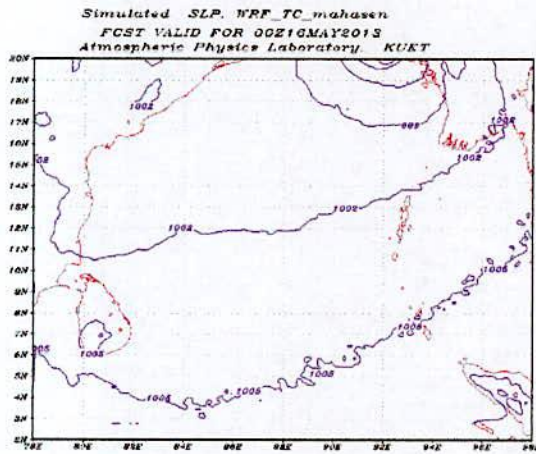
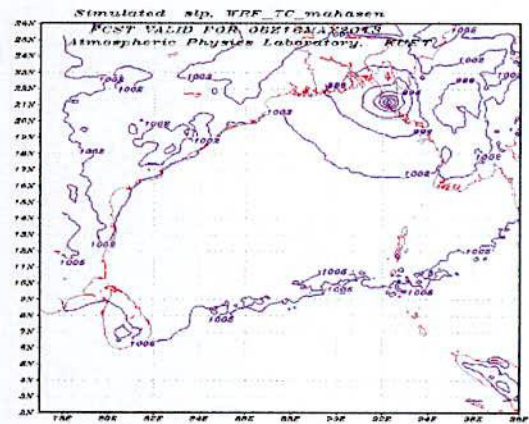


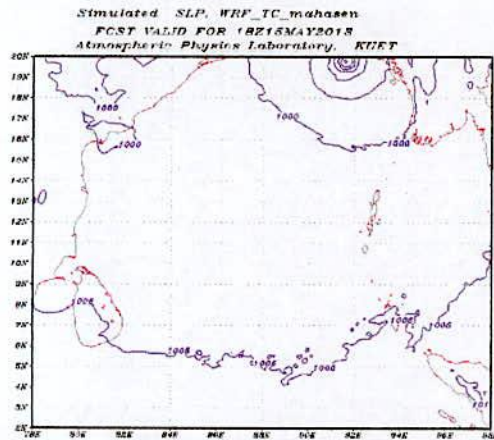
Figure 4.21 (a-d): Model simulated SLP (hpa) of cyclone Mahasen (2013) at different stages:
 (a) at 0000UTC of 15 May (used as initial field) (b) at 0060UTC of 15 May
 (c) at 1800UTC of 15 May (d) at 1800UTC of 16 May.



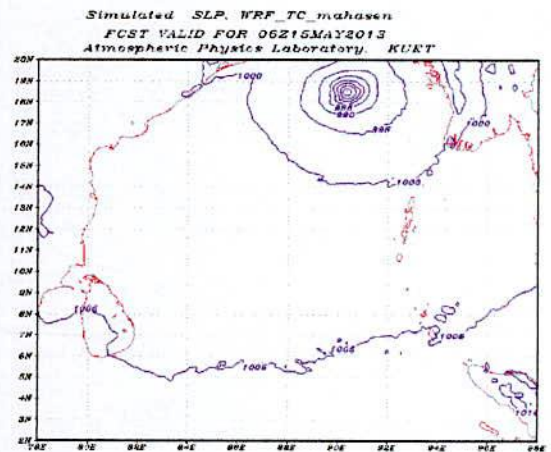
a



b



c



d

Figure 4.22 (a-d): Model simulated SLP (hpa) of cyclone Mahasen (2013) at different stages (used at 0000UTC of 16 May as initial field):
(a) at 0000UTC of 16 May (b) at 0060UTC of 16 May
(c) at 1800UTC of 16 May (d) at 0060UTC of 17 May.

4.2.2 Evolution of Pressure Drop (Δp)

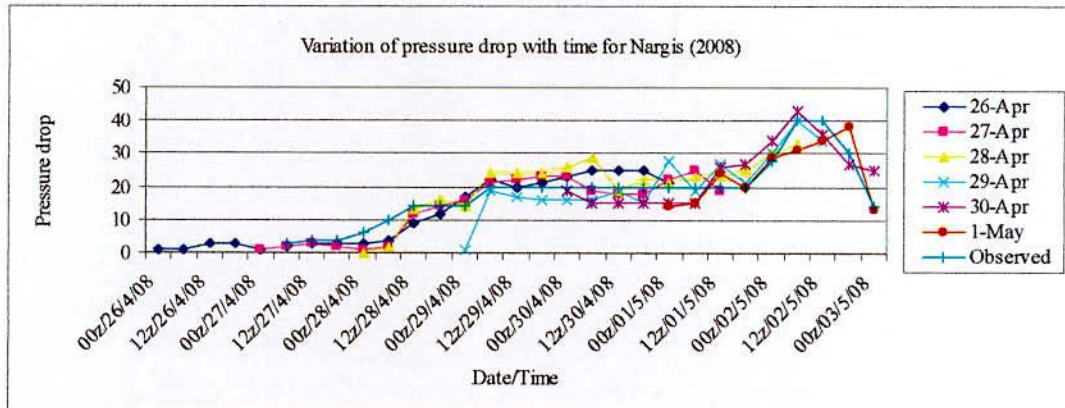
Pressure drop (Δp) is another important parameter of tropical cyclone in measuring its intensity. Pressure drop of the tropical cyclone is determined as the difference between pressure of the outer most closed isobar and MSLP. Figure 4.23 (a, b, c) shows the time variations of model simulated and observed pressure drop. Time variations of simulated pressure drop show similar pattern as MSLP. For all cases it increases with time up to the highest maturity stage of the respective cyclones and then it decreases [also seen from Figure {4.8(a-d) to 4.22(a-d)}], which are more or less in good agreement with the observed variations.

The simulated values obtained using initial field condition, among all simulated values the 29 April's values is better agreement with observed values for very severe cyclonic storm Nargis (2008), the 27 December's values is better agreement with observed values for very severe cyclonic storm Thane (2011) and 16 May's values is better agreement with observed values for severe cyclonic storm Mahasen (2013). But the values of simulated pressure drop recorded at 6 hourly intervals are initially lower than the observed values, at the middle it is higher than the observed values and lastly it is same for cyclone Nargis(2008). Where as pressure drop initially higher than the observed values, at middle it is lower and lastly it is same like cyclone Thane (2011). And for Mahasen(2013) all cases simulated values are higher than observed values.

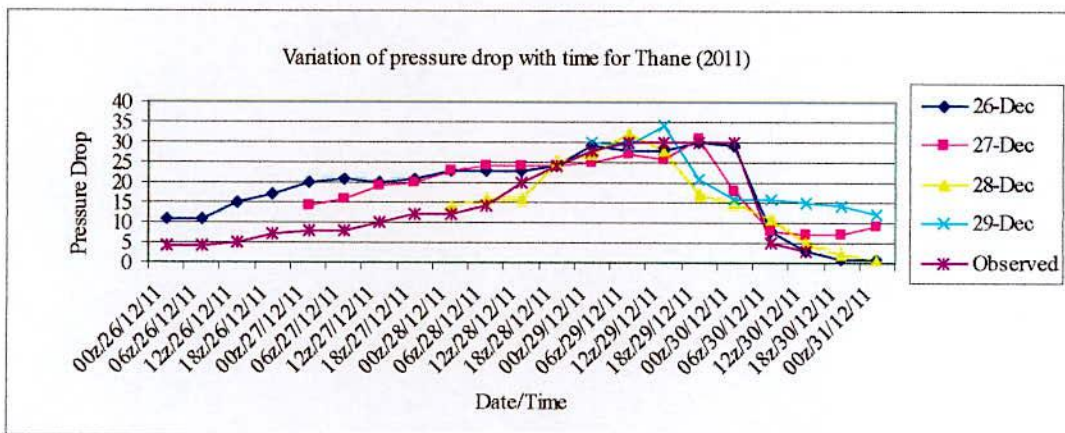
Table 4.2 summarizes highest pressure drop of all selected cyclones. The table shows that the 120 & 96 hrs predictions shows high pressure drop and 120, 72, 48 hrs it is same, but for all cases the observed values are higher than the simulated values for Nargis. On the other hand for Thane 96 hrs predictions shows high pressure drop, 72 & 48 hrs it is same, but for all cases the simulated pressure drop are lower than the observed values. And for Mahasen all cases simulated pressure drop are higher except 24 hrs of that.

Table 4.2: Maximum pressure drop of selected tropical cyclone

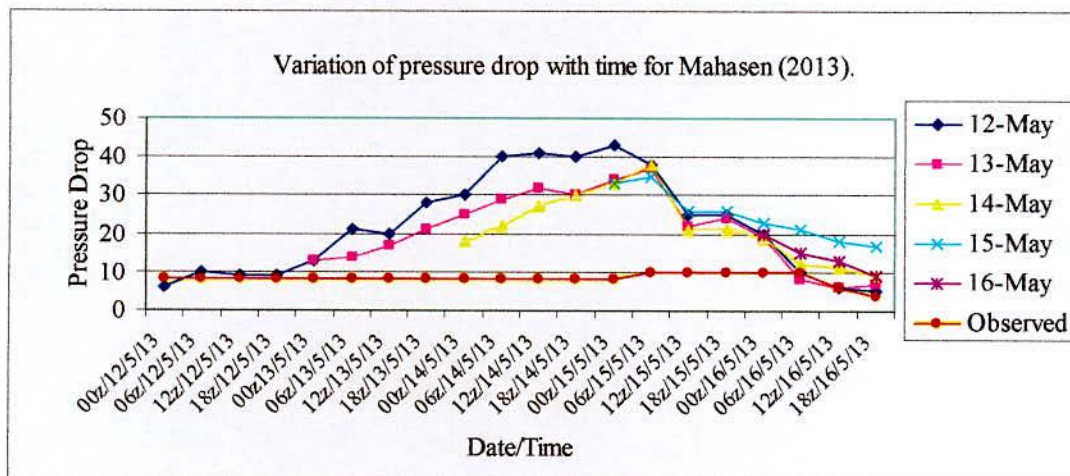
Name of cyclones	Initial Date/Time (UTC)	Forecasting heures	Simulated pressure drop (hPa) [Date/Time]	Observed pressure drop (hPa) [Date/Time]	Observed Max. pressure drop (hPa)
Nargis (2008)	26 April/0000	168	38 [02 May/1800]	38 [02 May/1800]	40 [02 May/0600]
	27 April/0000	144	36 [02 May/0900]	36 [02 May/0900]	40 [02 May/0600]
	28 April/0000	120	38 [02 May/0300]	38 [02 May/0300]	40 [02 May/0600]
	29 April/0000	96	36 [02 May/0600]	37 [02 May/0600]	40 [02 May/0600]
	30 April/0000	72	36 [02 May/1500]	40 [02 May/1500]	40 [02 May/0600]
	01 May/0000	48	37 [02 May/1800]	37 [02 May/1800]	40 [02 May/0600]
Thane (2011)	26 December/0000	120	25 [30 Dec/1200]	30 [30 Dec/1200]	30 [30 Dec/0600]
	27 December/0000	96	23 [30 Dec/0600]	23 [30 Dec/0600]	30 [30 Dec/0600]
	28 December/0000	72	23 [30 Dec/0600]	30 [30 Dec/0600]	30 [30 Dec/0600]
	29 December/0000	48	24 [30 Dec/0300]	24 [30 Dec/0300]	30 [30 Dec/0600]
Mahasen (2013)	12 May/0000	144	12 [16 May/0000]	13 [16 May/0000]	10 [16 May/0000]
	13 May/0000	120	11 [16 May/0600]	12 [16 May/0600]	10 [16 May/0000]
	14 May/0000	96	14 [16 May/0900]	11 [16 May/0900]	10 [16 May/0000]
	15 May/0000	72	19 [16 May/1200]	17 [16 May/1200]	10 [16 May/0000]
	16 May/0000	48	14 [16 May/0600]	13 [16 May/0600]	10 [16 May/0000]



a



b



c

Figure 4.23: (a, b, c): Evolution of model simulated and observed pressure drop with time of selected Cyclones (a) Nargis, (b) Thane (2011) (c) Mahasen (2013).

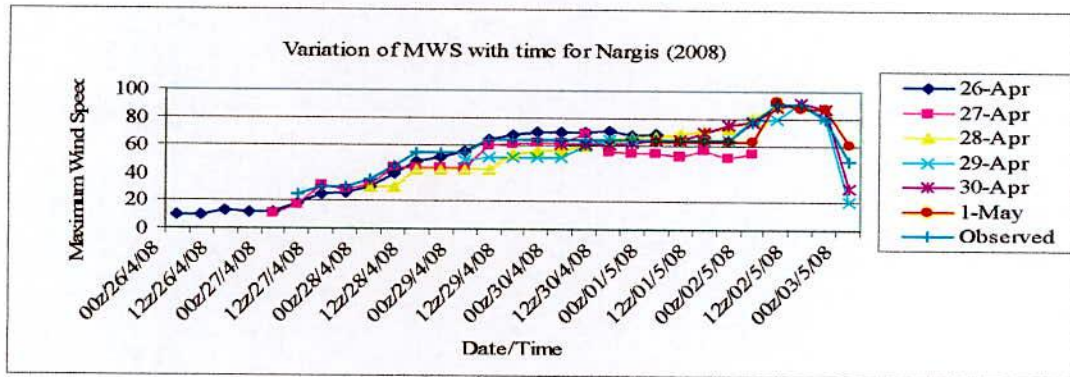
4.2.3 Evolution of Maximum Wind Speed (MWS)

Maximum wind speed (MWS) is another important parameter of tropical cyclones for measuring its intensity. It is of importance as it directly devastates the affected area at the time of landfall, it is the most active driving force of generating storm surge over the area of landfall. As it is mentioned in the previous section, the in-situ observations are not widely available over the ocean to determine or to estimate the intensity of the system, which would certainly help the disaster management institutions for taking proactive measures to mitigate the anticipated damages. Space based satellite technology is doing a great job in filling this gap and now-a-days it estimates MWS and other important parameters quite accurately. Figure 4.24 (a, b, c) shows the time variations of JTWC observed winds and model simulated MWS and that estimated from simulated pressure drop using modified Fletcher's (1995) [42] formula. Table 5.5 summarizes modeled, estimated and observed MWS of selected cyclone. These surface winds are taken at the standard meteorological height of 10m in an unobstructed exposure. MWS has been estimated by modified Fletcher's formula [42], $V_{\max}=13.6\sqrt{\Delta p}$, [43] using modeled pressure drop (Δp). Here Δp is in hPa and V_{\max} is in knots. From figure 4.24 (a, b, c) it appears that MWS shows similar pattern of variation as of pressure drop because MWS is proportional to the square root of the pressure drop (Δp). Here for cyclone the time variations of model simulated and estimated MWS increases up to the stage of its highest intensity and then decreases after the landfall which is similar to observed variation. The simulated values obtained using initial field condition, among all simulated values the 29 April's values is better agreement with observed values for very severe cyclonic storm Nargis (2008), the 27 December's values is better agreement with observed values for very severe cyclonic storm Thane (2011), the 16 May's values is better agreement with observed values for severe cyclonic storm Mahasen (2013). It is noted that the simulated and estimated MWS are lower than that observed for cyclones Nargis (2008), Thane (2011) and Mahasen (2013). Figure [4.25(a-d), 4.26(e-h), 4.27(a-d), 4.28(e-h), 4.29(a-d), & 4.30(e-h)] shows the distribution of surface wind (10m-wind) at different stages (with 24 hrs interval) of cyclones Nargis, Thane and Mahasen. The figures demonstrate that the surface wind speed (in m/s) of respective cyclone increases up to its maximum maturity. The wind speed decreases with the landfall. The figures also exhibit that for strong systems the distribution is more organized in bands with asymmetries in the circular distribution. Further the wind is much lower in the landside for a land falling cyclone. Table 4.3 shows that the MWS estimated by modified Fletcher's formula using the model simulated pressure drop are much closer to the observed. The results indicate that MWS is high for 144 hrs and low for 48 hrs for Nargis. Whereas 72hrs

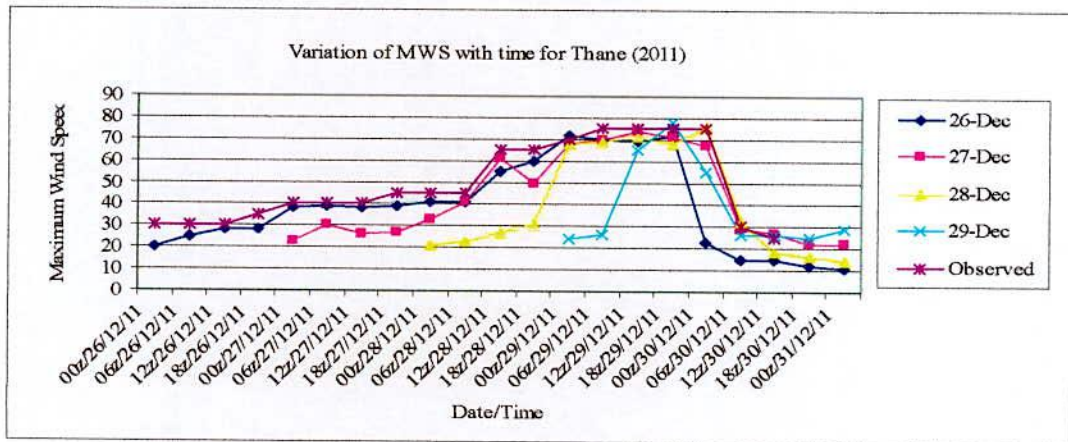
prediction it is high and 48 hrs it is low compared with others for Thane and for Mahasen 48 hrs simulated values coincide with observed value. It is because of the fact that since the model starts running with low resolution (100km) initial fields, it takes some more time of integration to attain the realistic pressure drop and winds in higher resolution setup.

Table 4.3: maximum wind speed (MWS) of selected tropical cyclone at the stage of highest intensity.

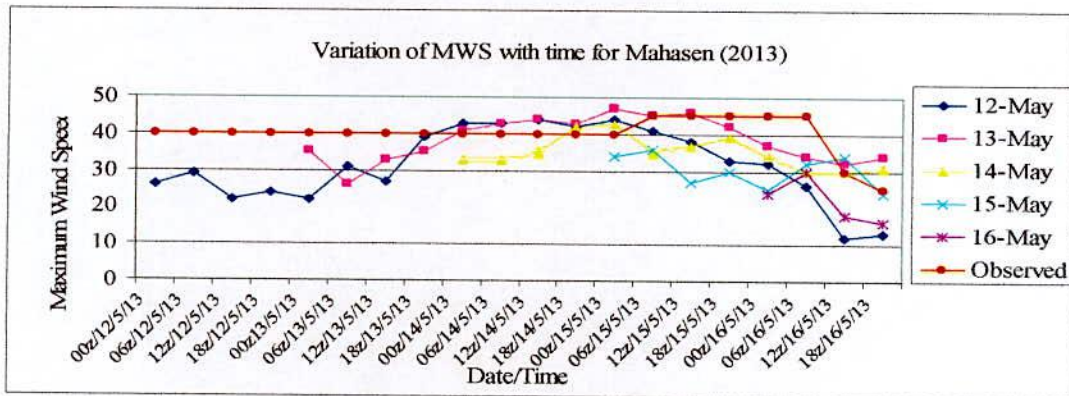
Name of cyclones	Initial Date/Time (UTC)	Forecasting hours	Simulated MWS(m/s) [Date/Time]	Estimated MWS(m/s) [Date/Time]	observed Max. MWS(m/s) [Date/Time]
Nargis (2008)	26 April/0000	144	42 [02 May/1800]	43 [02 May/1800]	46 [02 May/0600]
	27 April/0000	120	39 [02 May/0900]	44 [02 May/0900]	46 [02 May/0600]
	28 April/0000	96	41 [02 May/0300]	43 [02 May/0300]	46 [02 May/0600]
	29 April/0000	72	40 [02 May/0600]	43 [02 May/0600]	46 [02 May/0600]
	30 April/0000	48	36 [02 May/1500]	43 [02 May/1500]	46 [02 May/0600]
	01 May/0000	24	38 [02 May/1800]	43 [02 May/1800]	46 [02 May/0600]
Thane (2011)	26 December/0000	96	28 [30 December/1200]	35 [30 December/1200]	39 [30 December/0600]
	27 December/0000	72	30 [30December/0600]	34 [30 December/0600]	39 [30 December/0600]
	28 December/0000	48	26 [30 December/0600]	34 [30 December/0600]	39 [30 December/0600]
	29 December/0000	24	29 [30 December/0300]	35 [30 December/0300]	39 [30 December/0600]
Mahasen (2013)	12 May/0000	120	22 [16 May/0000]	24 [16 May/0000]	23 [16 May/0000]
	13 May/0000	96	25 [16 May/0600]	23 [16 May/0600]	23 [16 May/0000]
	14 May/0000	72	27 [16 May/0900]	26 [16 May/0900]	23 [16 May/0000]
	15 May/0000	48	30 [16 May/1200]	30 [16 May/1200]	23 [16 May/0000]
	16 May/0000	24	24 [16 May/0600]	26 [16 May/0600]	23 [16 May/0000]



a



b



c

Figure 4.24 (a, b, c): Evolution of model simulated, estimated from model pressure drop and observed MWS with time of selected cyclones (a) Nargis, (b) Thane (2011) and (c) Mahasen (2013)

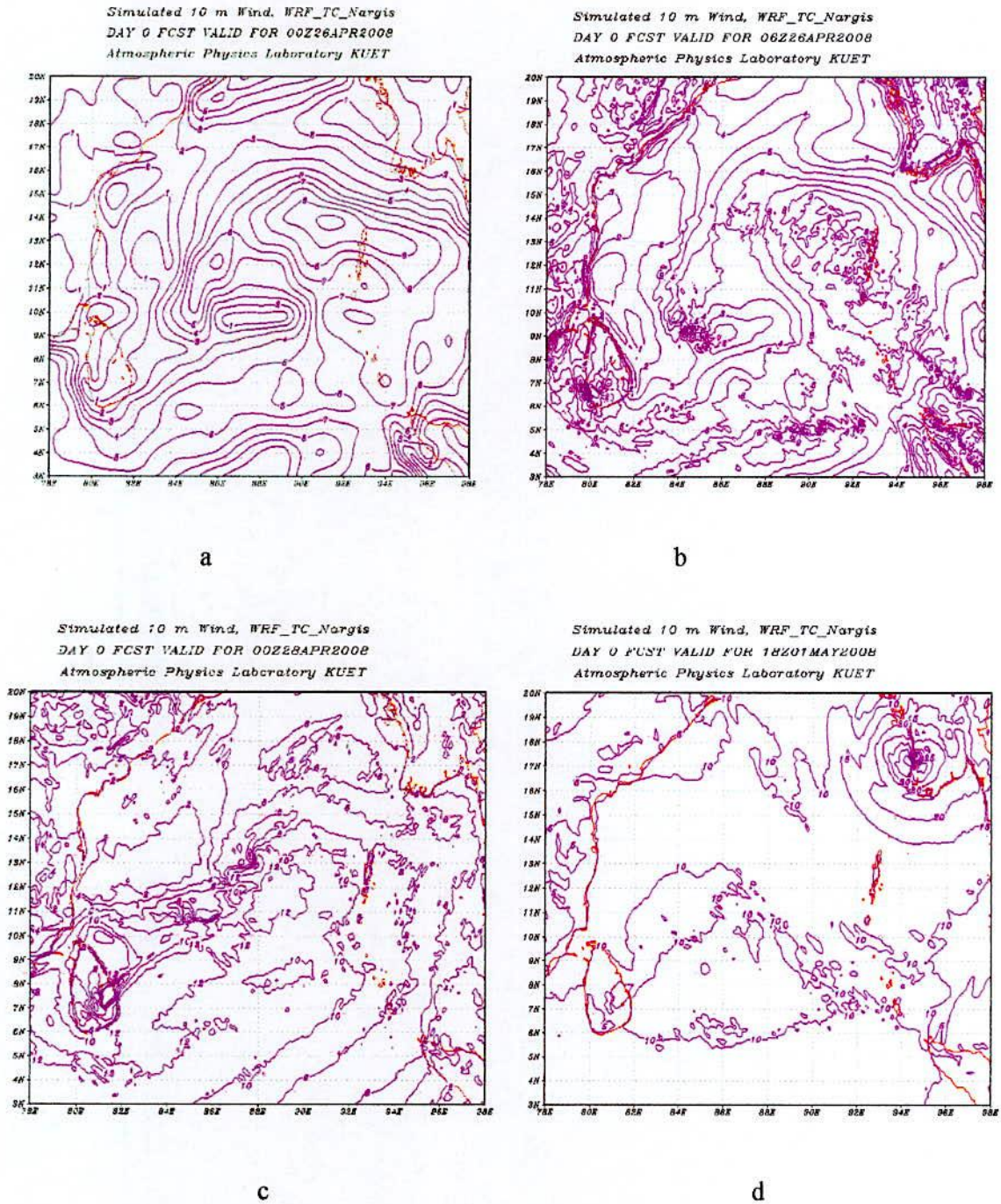


Figure 4.25 (a-d): Model simulated surface wind (speed in m/s) of cyclone Nargis (2008) at different stages: (a) at 0000UTC of 26 April (used as initial field) (b) at 0060UTC of 26 April (c) at 0000UTC of 28 April (d) at 1800UTC of 01 May.

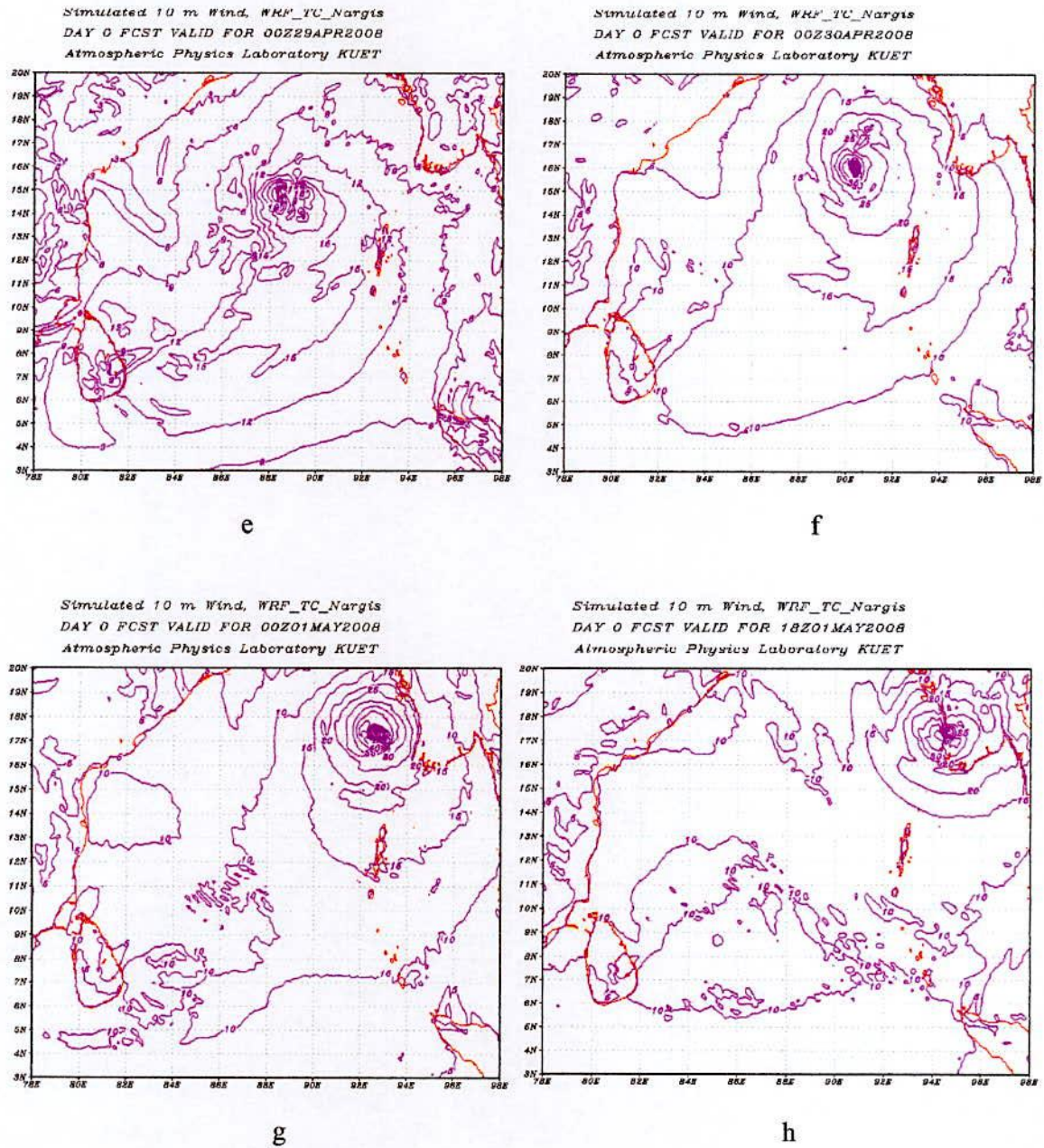
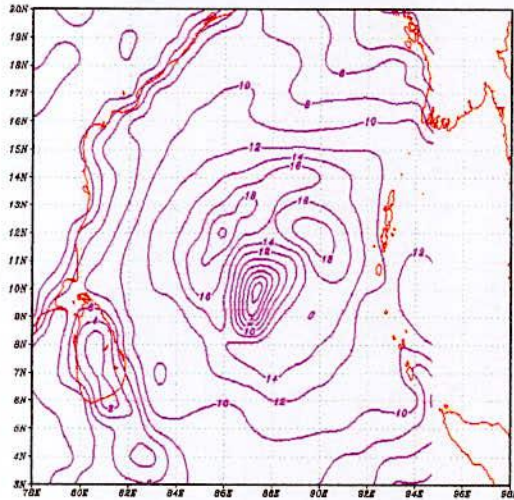


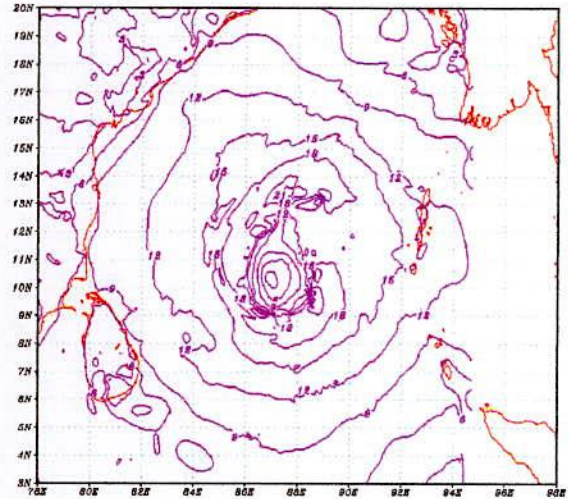
Figure 4.26 (e-h): Model simulated surface wind (speed in m/s) of cyclone Nargis (2008) at different stages (used at 0000UTC of 26 April as initial field):
 (e) at 0000UTC of 29 April (f) at 0000UTC of 30 April
 (g) at 0000UTC of 01 May (h) at 1800UTC of 01 May

Simulated 10 m Wind, WRF_TC_Thane
 DAY 0 FCST VALID FOR 00Z26DEC2011
 Atmospheric Physics Laboratory KUET



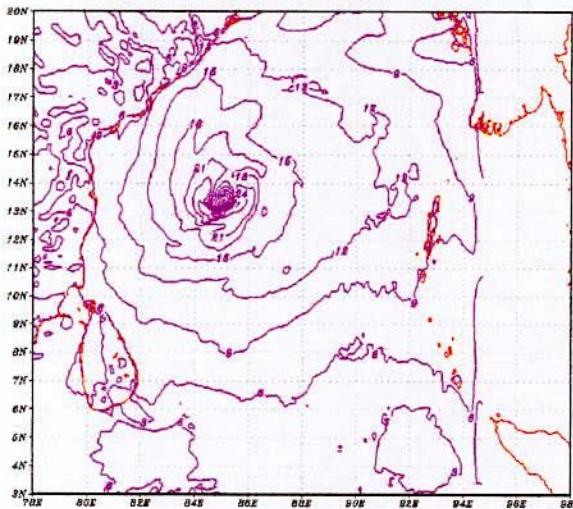
a

Simulated 10 m Wind, WRF_TC_Thane
 DAY 0 FCST VALID FOR 06Z26DEC2011
 Atmospheric Physics Laboratory KUET



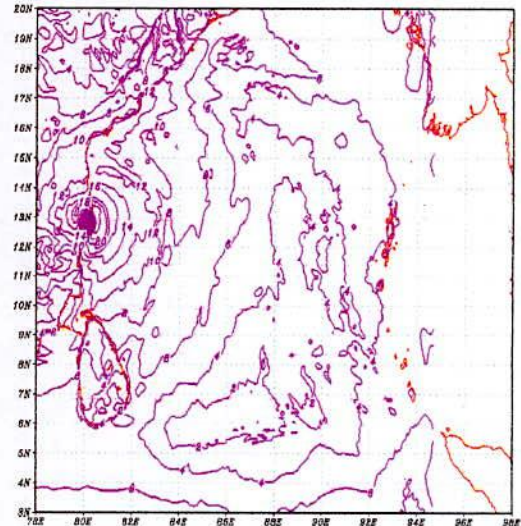
b

Simulated 10 m Wind, WRF_TC_Thane
 DAY 0 FCST VALID FOR 00Z28DEC2011
 Atmospheric Physics Laboratory KUET



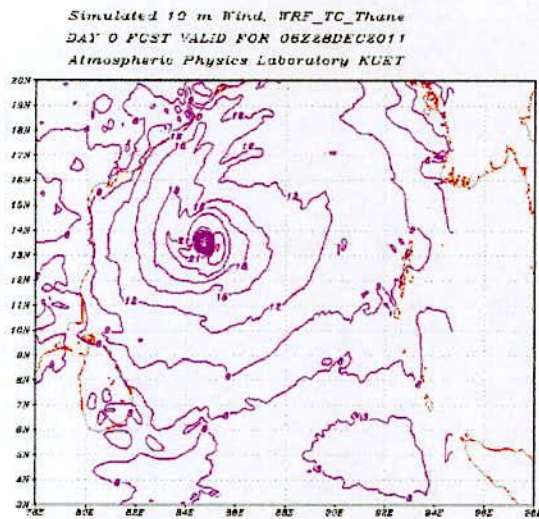
c

Simulated 10 m Wind, WRF_TC_Thane
 DAY 0 FCST VALID FOR 00Z30DEC2011
 Atmospheric Physics Laboratory KUET

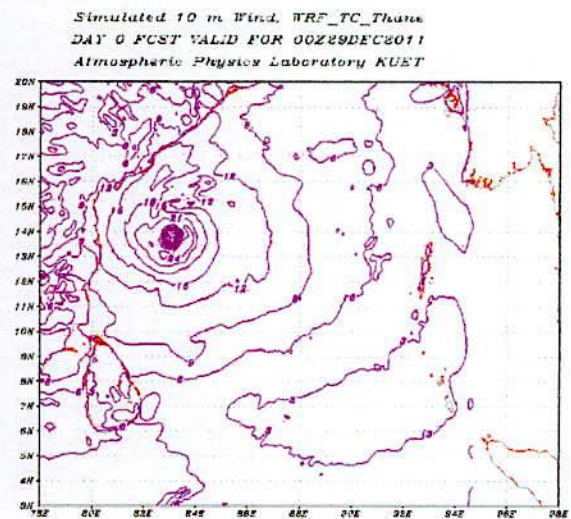


d

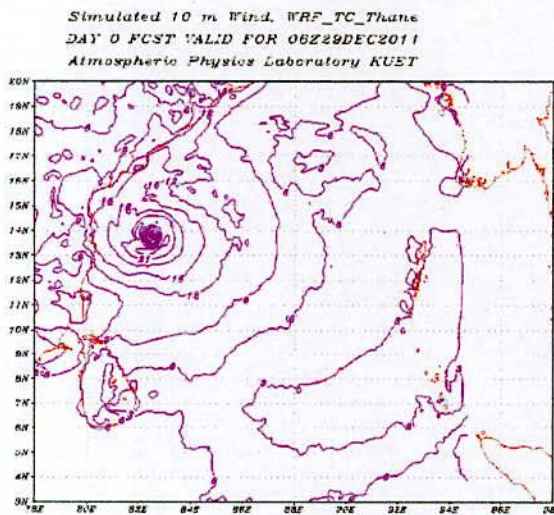
Figure 4.27 (a-d): Model simulated surface wind (speed in m/s) of cyclone Thane (2011) at different stages: (a) at 0000UTC of 26 December (used as initial field) (b) at 0060UTC of 26 December (c) at 0000UTC of 28 December (d) at 0000UTC of 30 December.



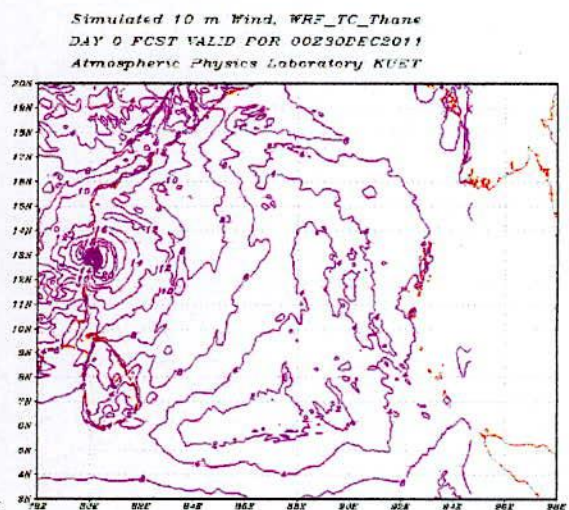
e



f

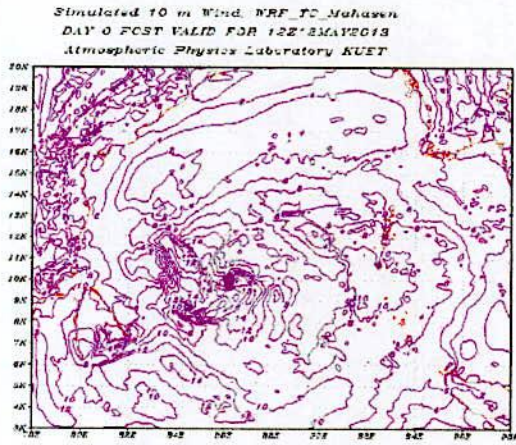


g

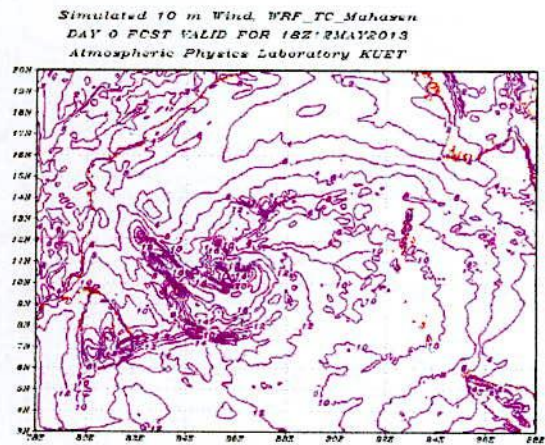


h

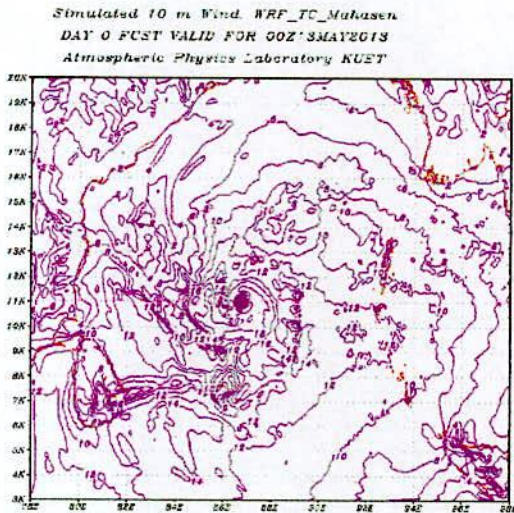
Figure 4.28 (e-h): Model simulated surface wind (speed in m/s) of cyclone Thane (2011) at different stages (used at 0000UTC of 26 December as initial field):
 (e) at 0600UTC of 28 December (f) at 0000UTC of 29 December
 (g) at 0600UTC of 29 December (h) at 0000UTC of 30 December.



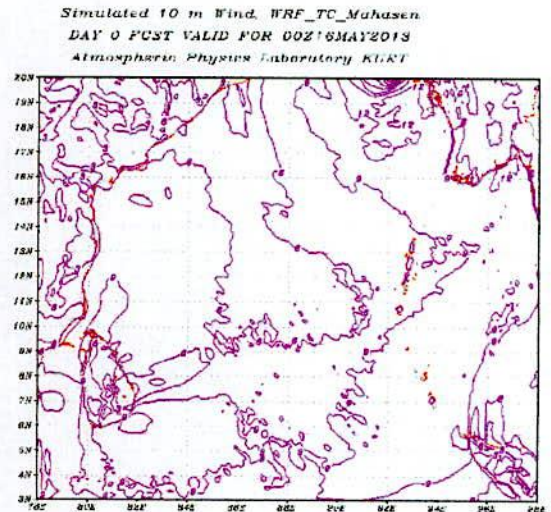
a



b



c



d

Figure 4.29 (a-d): Model simulated surface wind (speed in m/s) of cyclone Mahasen (2013) at different stages: (a) at 1200UTC of 12 May (used as initial field) (b) at 1800UTC of 12 May (c) at 0000UTC of 13 May (d) at 0000UTC of 16 May.

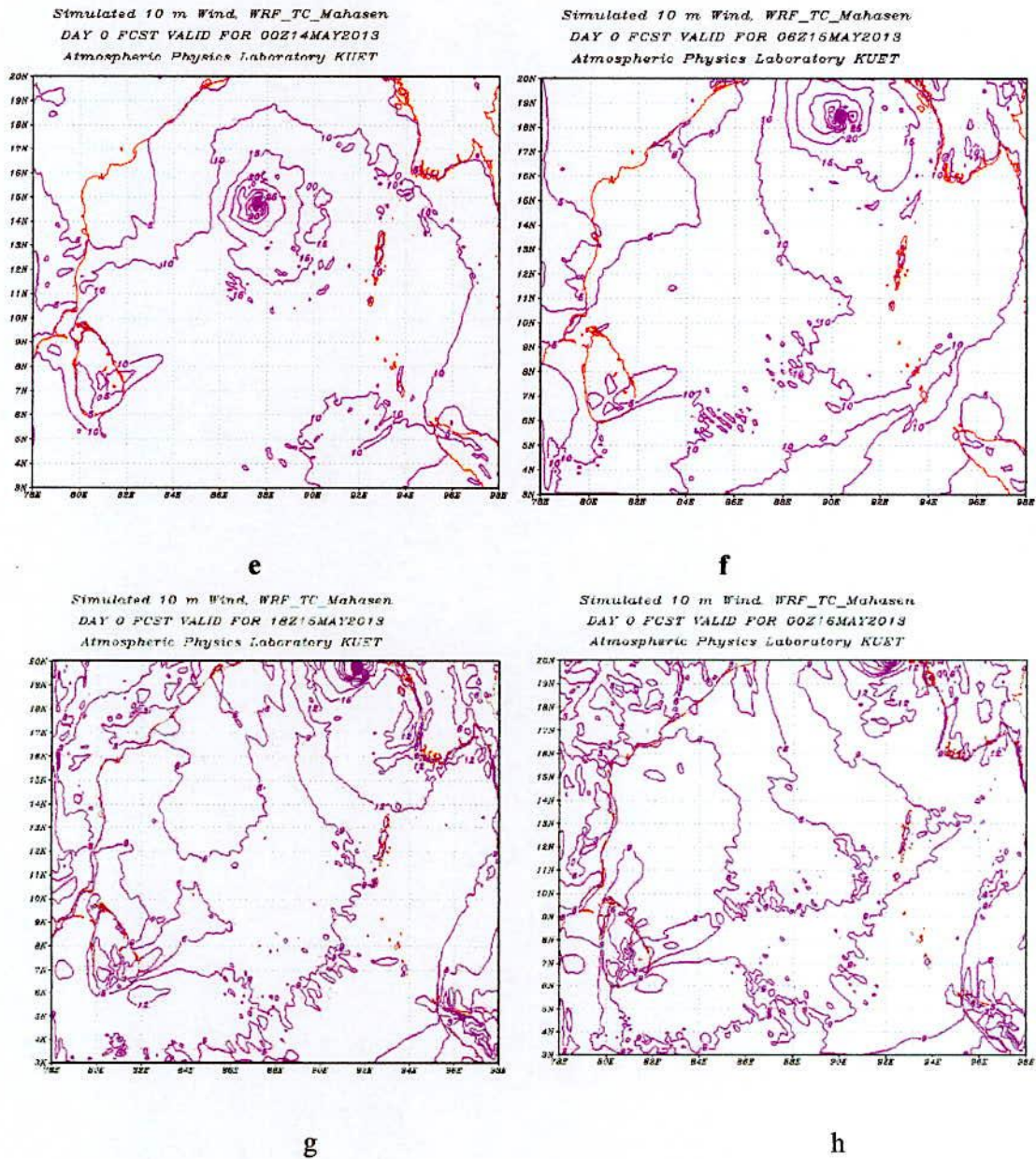


Figure 4.30 (e-h): Model simulated surface wind (speed in m/s) of cyclone Mahasen (2013) at different stages (used at 0000UTC of 12 May as initial field):
 (e) at 0000UTC of 14 May (f) at 0060UTC of 15 May
 (g) at 1800UTC of 15 May (h) at 0000UTC of 16 May.

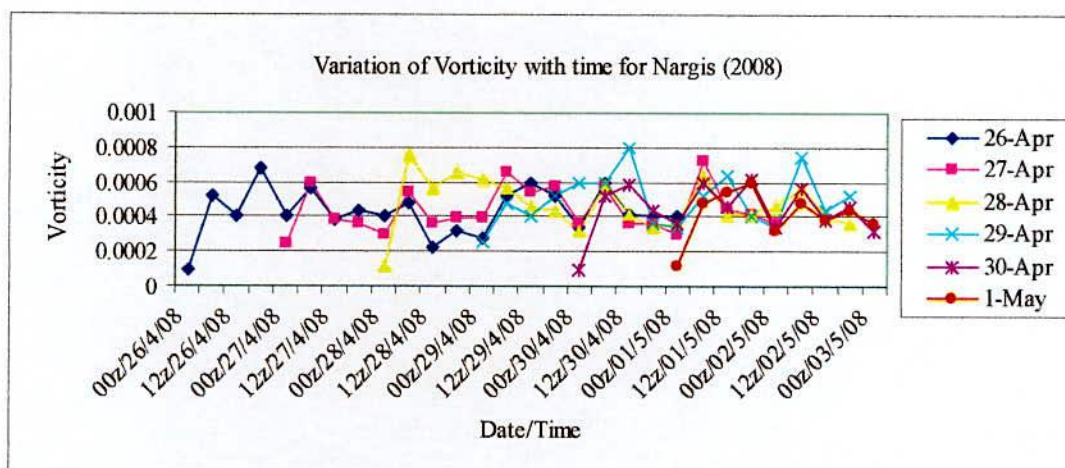
4.2.4 Evolution of Relative Vorticity (ξ)

The plots of the evolution of model simulated low level relative vorticity maxima at 850 hpa are shown as function of time [Figure 4.31 (a, b, c) for cyclones Nargis (2008), Thane (2011) and Mahasen (2013)]. The analysis reveals that there is a sharp rise in the vorticity value in the first 48 hrs of integration of the model with little fluctuations for very severe cyclonic storm Nargis (2008), very severe cyclonic storm Thane (2011) and severe cyclonic storm Mahasen (2013). The decline in the vorticity curve after peaking of forecast, even when the storm is actually intensifying, may be due to several factors, such as lower resolution of the FNL field and inadequacy of the modeling of the physical processes of ARW itself which need to be further investigated. The simulated values obtained using initial field condition, among all simulated values the 29 April's values is better agreement with observed values for very severe cyclonic storm Nargis (2008), the 27 December's values is better agreement with observed values for very severe cyclonic storm Thane (2011), and the 16 May's values is better agreement among all values for severe cyclonic storm Mahasen (2013). Figure [4.32 (a-d) to 4.46(a-d)] shows the spatial distribution of 850 hPa relative vorticity at different stages of cyclone Nargis, Thane & Mahasen. It is observed that the relative vorticity of respective cyclone increases and decreases with the increases of forecast hours up to its peak value and then it decreases. Figure exhibit that the distribution of relative vorticity show asymmetric feature in the horizontal. The distribution of positive vorticity is concentrated in or near the centre at its mature stage compared to the distribution at the stages before maturity and after landfall when the maximum vorticity is found to concentrate away from the centre for most of the cases. It is also seen that for strong system the vorticity distribution is more organized compared to the weak system.

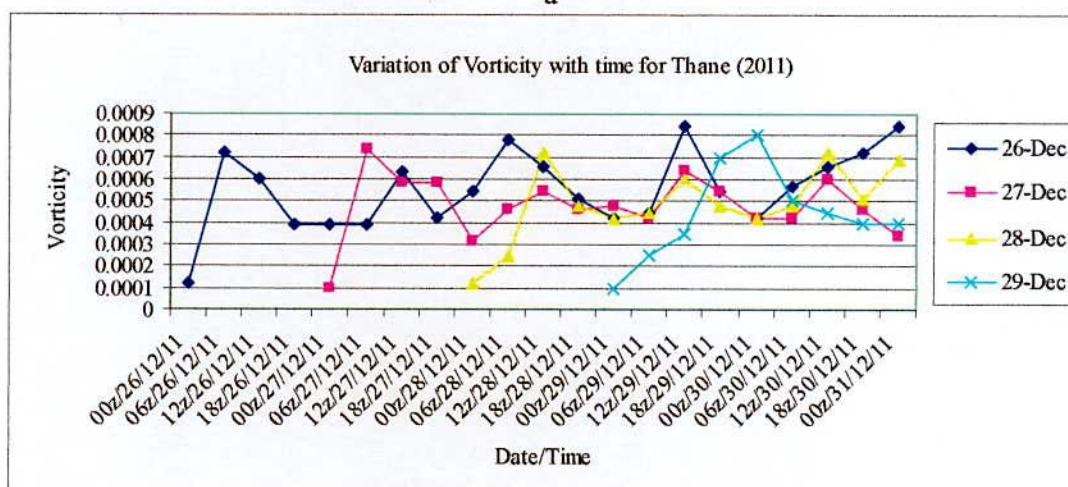
Table 5.6 shows the model simulated maximum vorticity at 850 hPa of selected tropical cyclones. From table it is noted that the 120 hrs & 24 hrs simulated vorticity of Nargis, 72 hrs & 24 hrs simulated vorticity of Thane are coincide and 120 hrs simulated vorticity of Mahasen coincide with 96 hrssimulated vorticity of Thane.

Table 4.4: Maximum relative vorticity (ξ) at 850 hPa of selected tropical cyclones

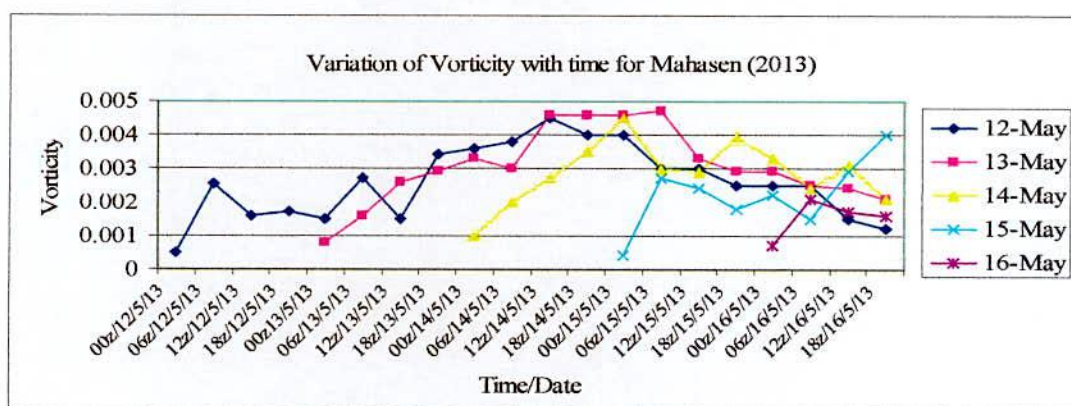
Name of cyclones	Initial Date/Time (UTC)	Forecasting hours	Simulated vorticity (s^{-1}) [Date/Time]	Maximum Vorticity(s^{-1})
Nargis (2008)	26 April/0000	144	0.00068 [02 May/1800]	0.00084
	27 April/0000	120	0.00072 [02 May/0900]	
	28 April/0000	96	0.00076 [02 May/0300]	
	29 April/0000	72	0.00080 [02 May/0600]	
	30 April/0000	48	0.00082 [02 May/1500]	
	01 May/0000	24	0.00084 [02 May/1800]	
Thane (2011)	26 December/0000	96	0.00070 [30 December/1200]	0.00076
	27 December/0000	72	0.00072 [30 December/0600]	
	28 December/0000	48	0.00074 [30 December/0600]	
	29 December/0000	24	0.00076 [30 December/0300]	
Mahasen (2013)	12 May/0000	120	0.00070 [16 May/0000]	0.00070
	13 May/0000	96	0.00021 [16 May/0600]	
	14 May/0000	72	0.00030 [16 May/0900]	
	15 May/0000	48	0.00017 [16 May/1200]	
	16 May/0000	24	0.00021 [16 May/0600]	



a



b



c

Figure 4.31 (a, b, c): Evolution of vorticity at 850 hPa with forecasting hour of selected cyclones (a) Nargis(2008) (b) Thane (2011) and (c) Mahasen (2013)

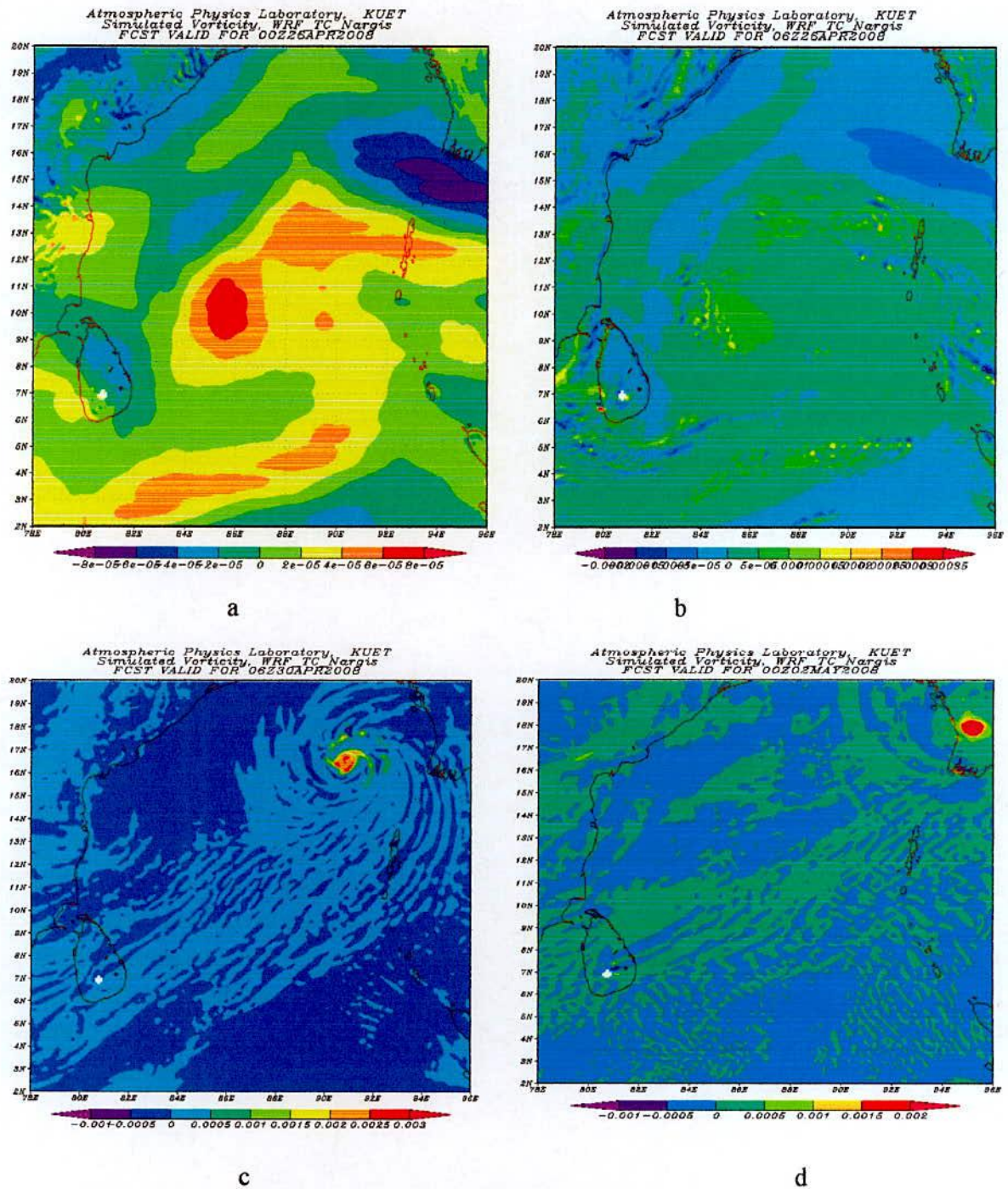


Figure 4.32 (a-d): Model simulated 850 hPa relative vorticity ($\times 10^{-5} \text{ s}^{-1}$) of cyclone Nargis (2008) at different stages: (a) at 0000UTC of 26 April (used as initial field) (b) at 0600UTC of 26 April (c) at 0600UTC of 30 April (d) at 0000UTC of 02 May.

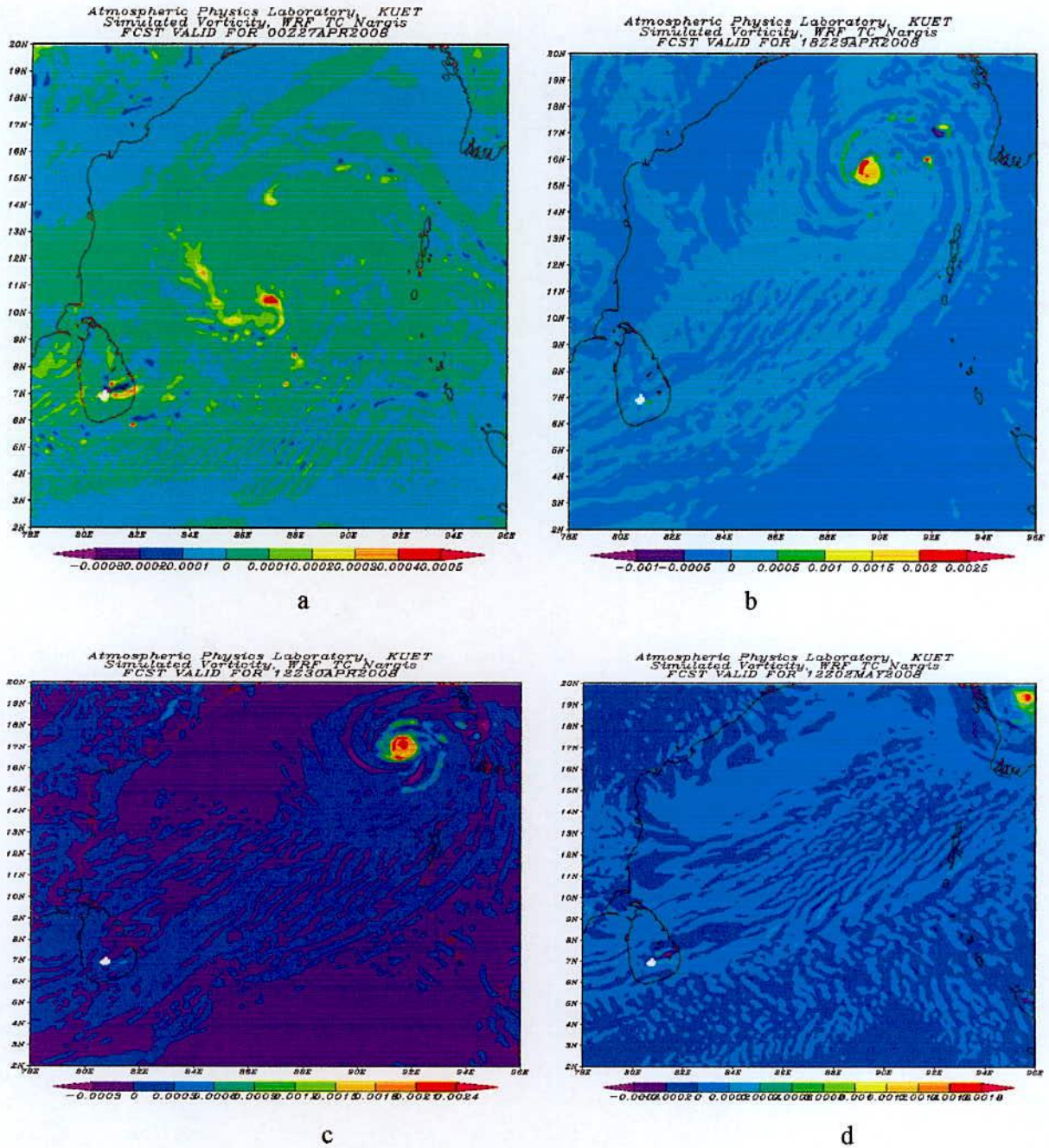
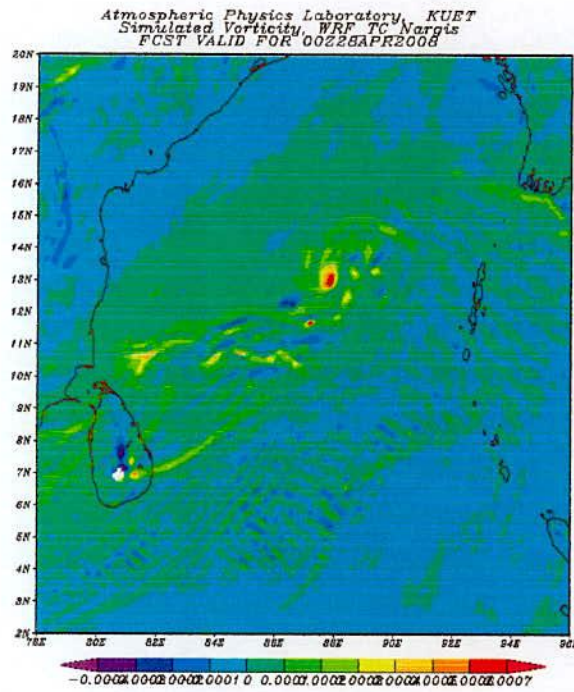
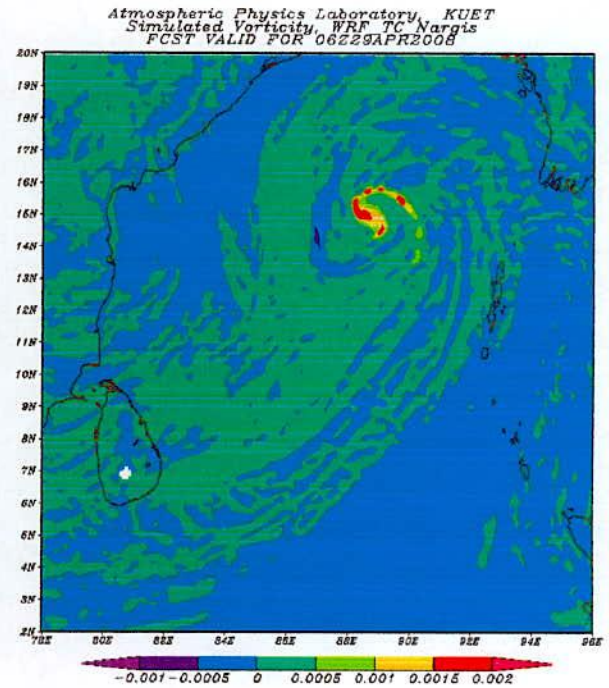


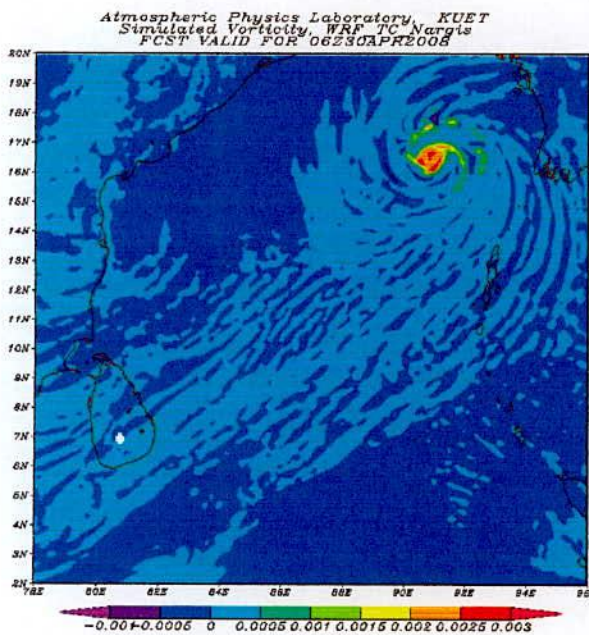
Figure 4.33 (a-d): Model simulated 850 hpa relative vorticity ($\times 10^{-5} \text{s}^{-1}$) of cyclone Nargis (2008) at different stages: (a) at 0000UTC of 27 April (used as initial field) (b) at 1800UTC of 29 April (c) at 1200UTC of 30 April (d) at 1200UTC of 02 May.



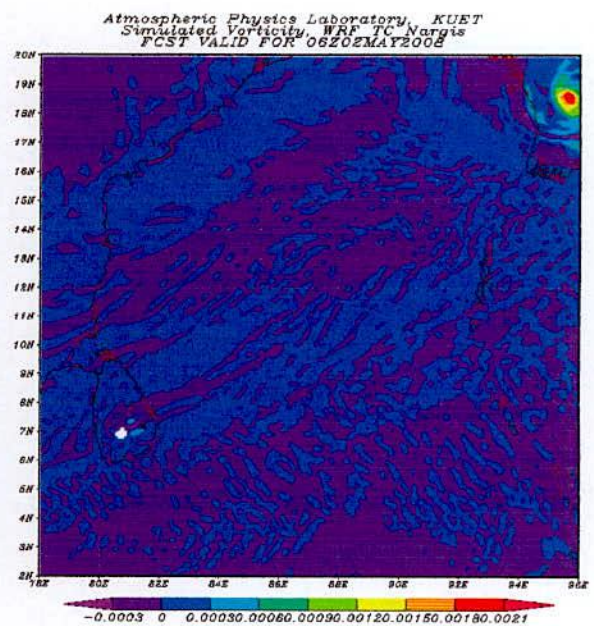
a



b



c



d

Figure 4.34 (a-d): Model simulated 850 hpa relative vorticity ($\times 10^{-5} \text{s}^{-1}$) of cyclone Nargis (2008) at different stages: (a) at 0000UTC of 28 April (used as initial field) (b) at 0600UTC of 29 April (c) at 0600UTC of 30 April (d) at 0600UTC of 02 May.



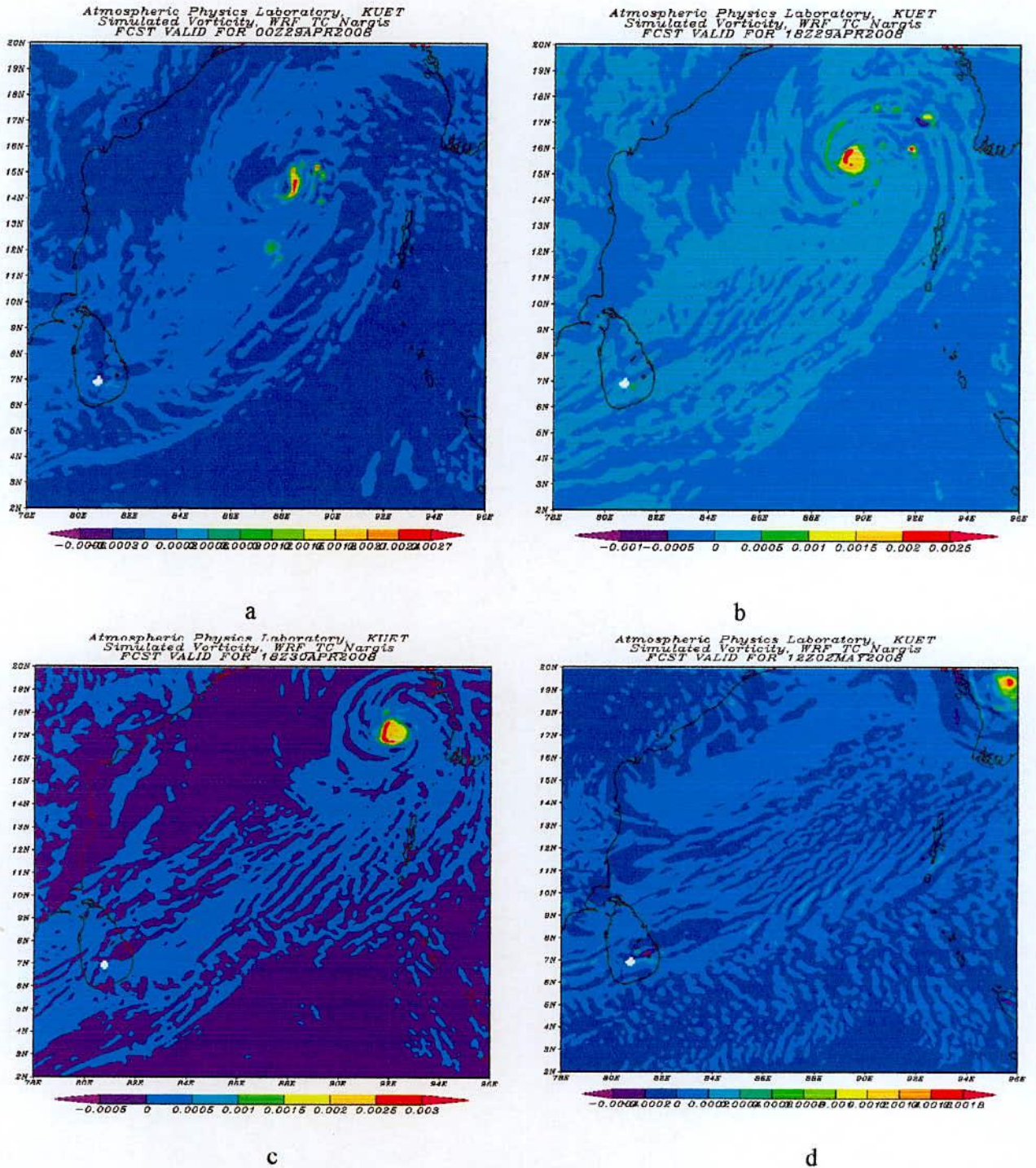


Figure 4.35 (a-d): Model simulated 850 hpa relative vorticity ($\times 10^{-5} \text{s}^{-1}$) of cyclone Nargis (2008) at different stages: (a) at 0000UTC of 29 April (used as initial field) (b) at 1800UTC of 29 April (c) at 1800UTC of 30 April (d) at 1200UTC of 02 May.

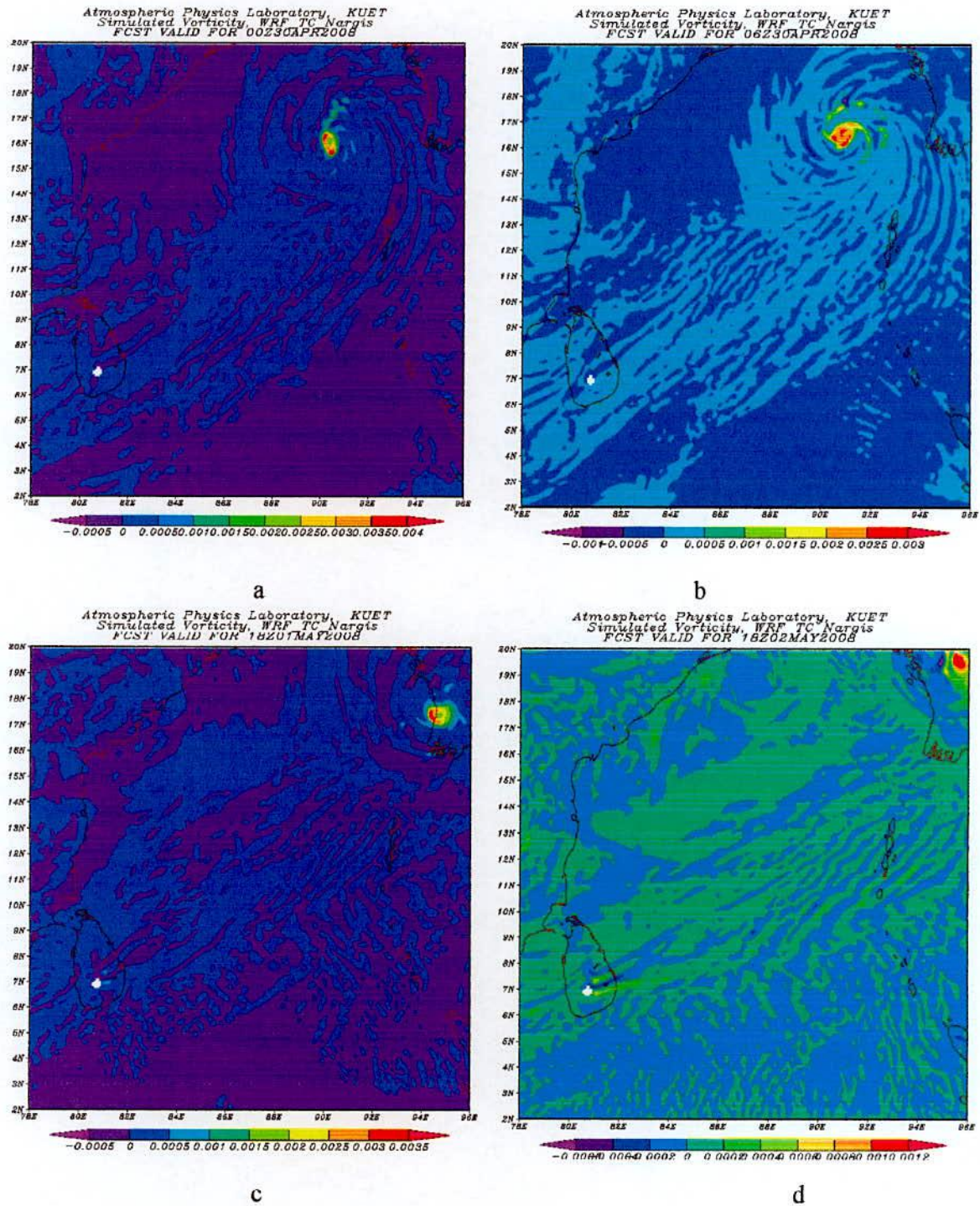


Figure 4.36 (a-d): Model simulated 850 hpa relative vorticity ($\times 10^{-5} \text{s}^{-1}$) of cyclone Nargis (2008) at different stages: (a) at 0000UTC of 30 April (used as initial field) (b) at 0600UTC of 30 April (c) at 1800UTC of 01 May (d) at 1800UTC of 02 May.

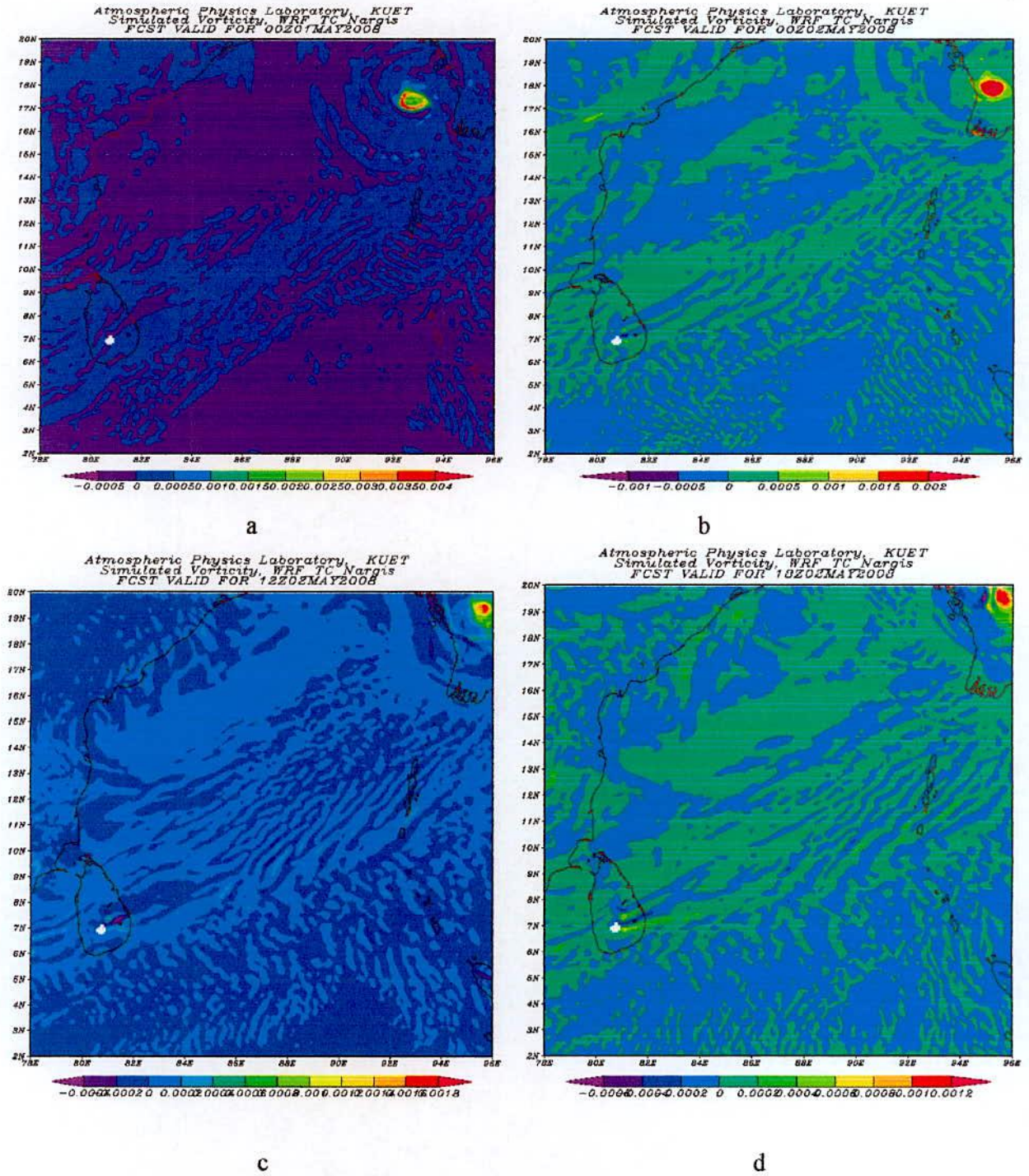


Figure 4.37 (a-d): Model simulated 850 hpa relative vorticity ($\times 10^{-5} \text{s}^{-1}$) of cyclone Nargis (2008) at different stages (used at 0000UTC of 26 April as initial field):
 (a) at 0000UTC of 01 May (b) at 0000UTC of 02 May.
 (c) at 1200UTC of 02 May (d) at 1800UTC of 02 May

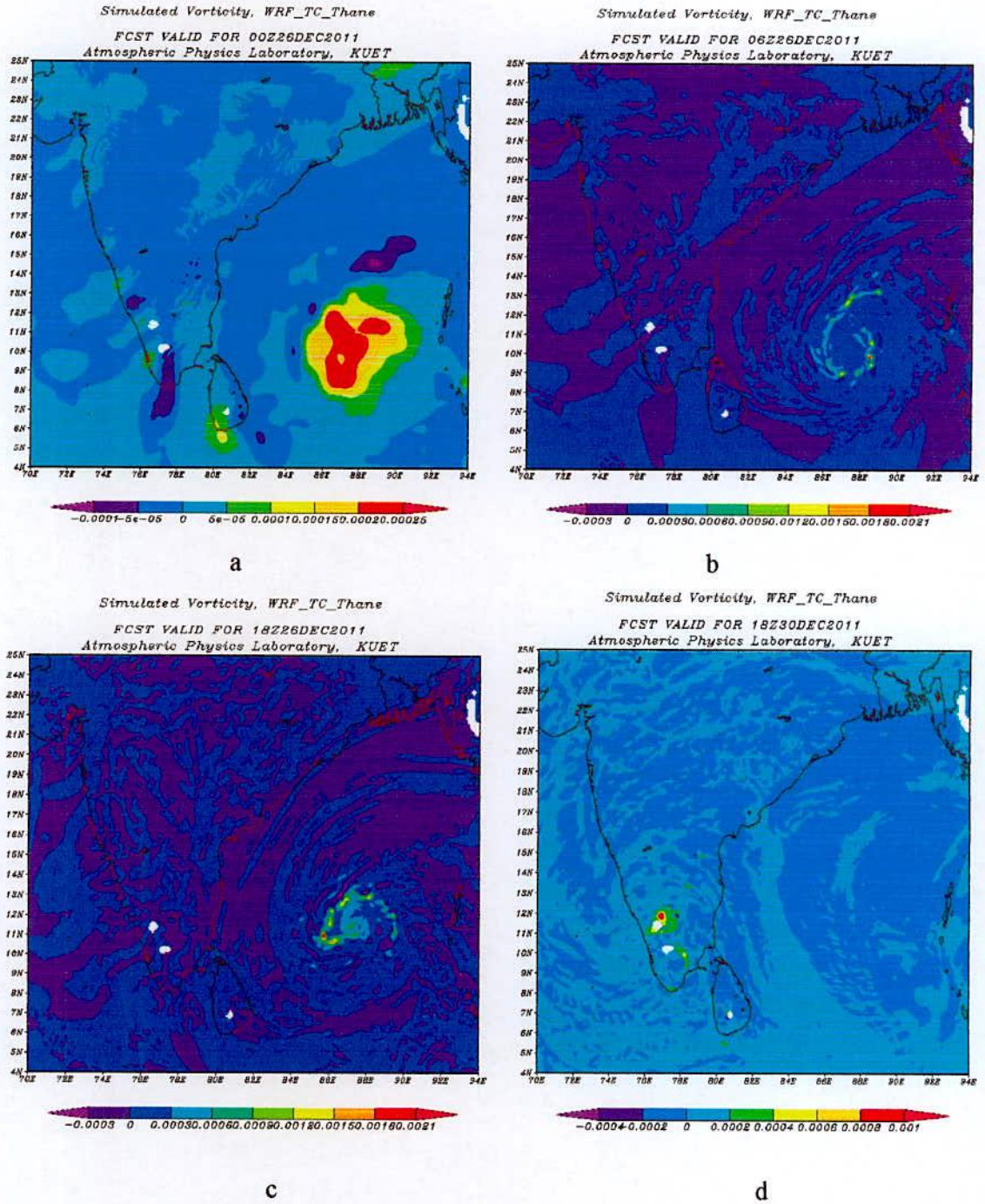


Figure 4.38 (a-d): Model simulated 850 hpa relative vorticity ($\times 10^{-5} \text{s}^{-1}$) of cyclone Thane (2011) at different stages: (a) at 0000UTC of 26 Dec. (used as initial field) (b) at 0600UTC of 26 December (c) at 1800UTC of 26 December (d) at 1800UTC of 30 December

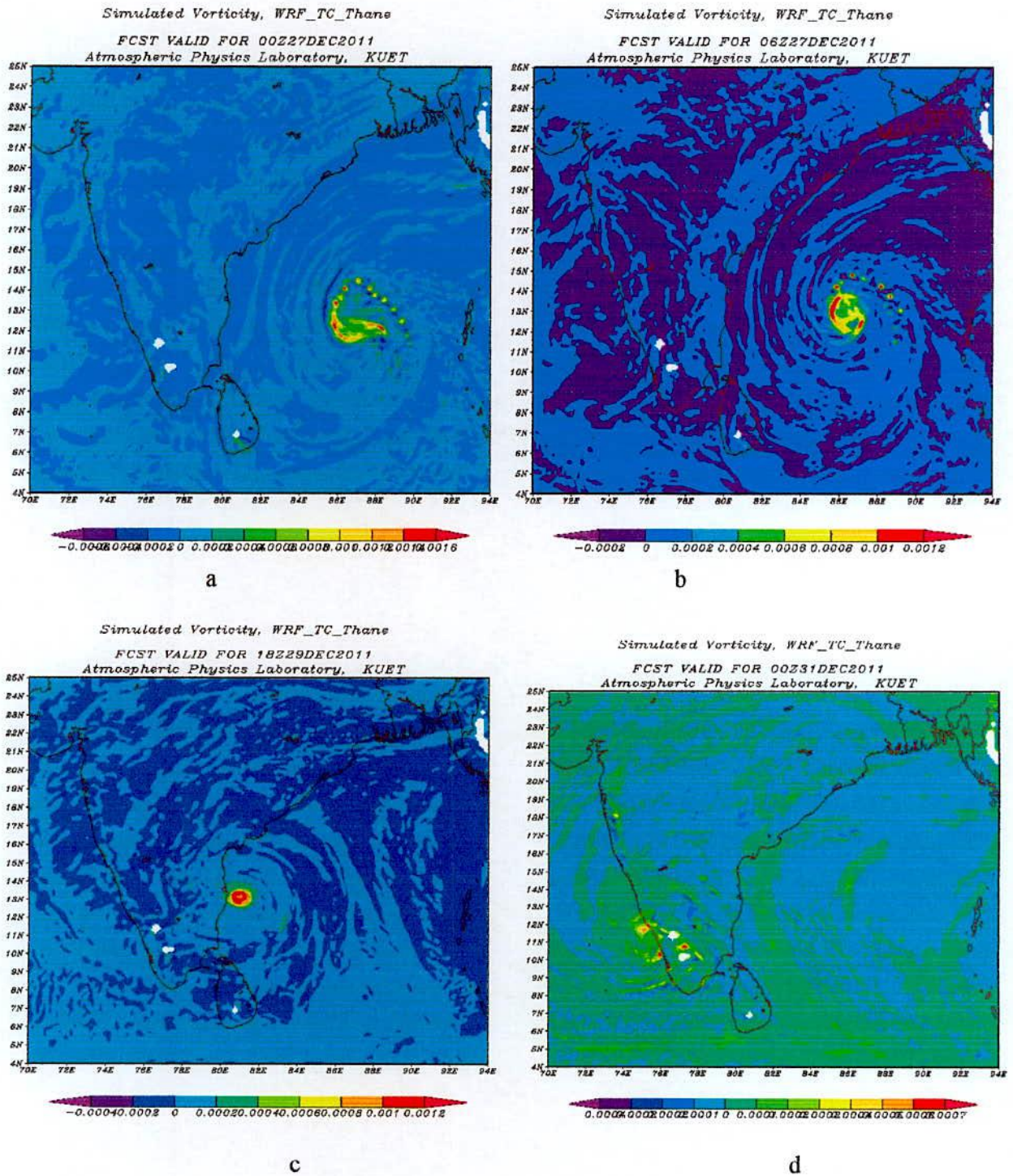


Figure 4.39 (a-d): Model simulated 850 hpa relative vorticity ($\times 10^{-5} \text{s}^{-1}$) of cyclone Thane (2011) at different stages: (a) at 0000UTC of 27 Dec. (used as initial field) (b) at 0600UTC of 27 Dec. (c) at 1800UTC of 29 December (d) at 0000UTC of 31 December

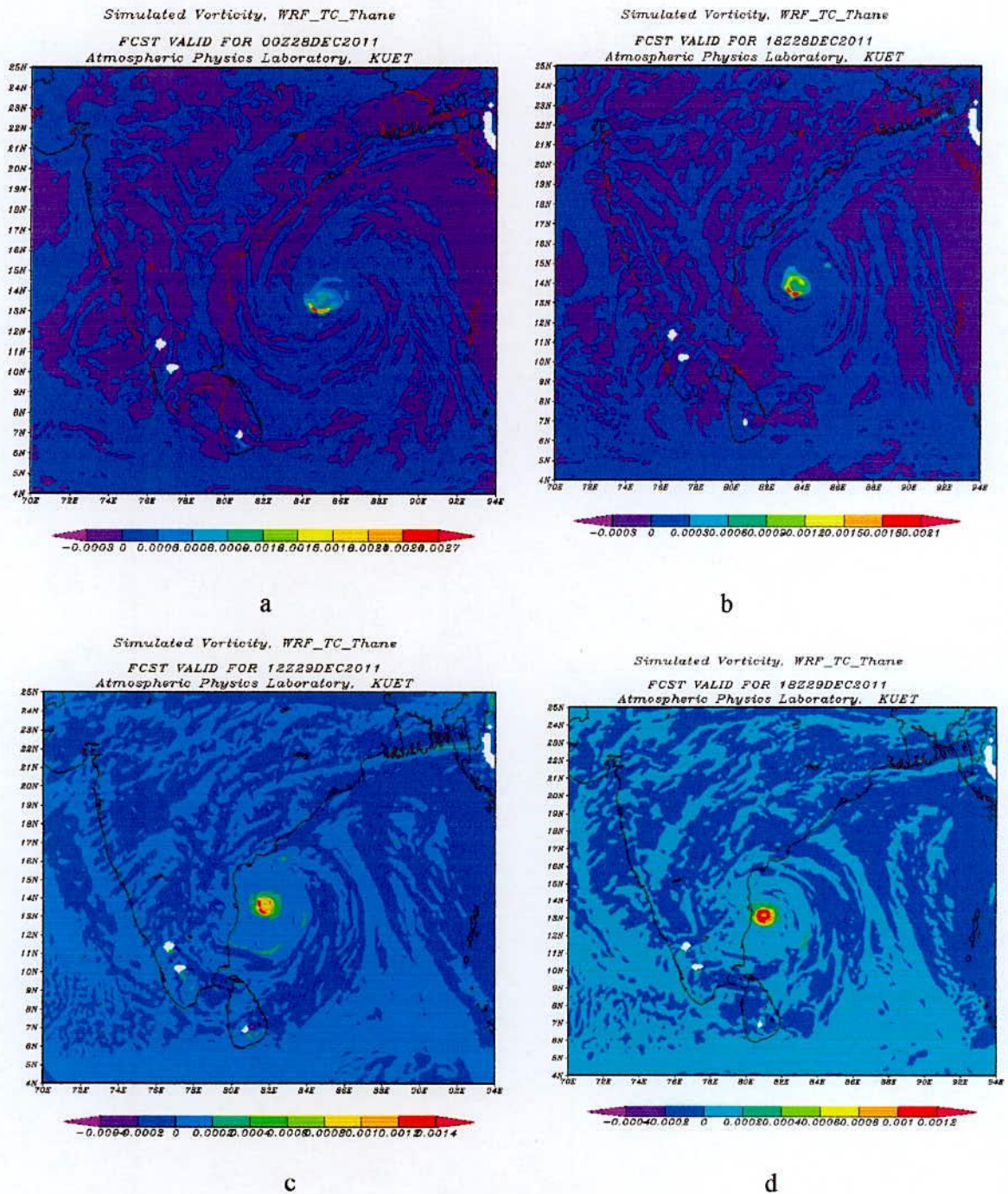
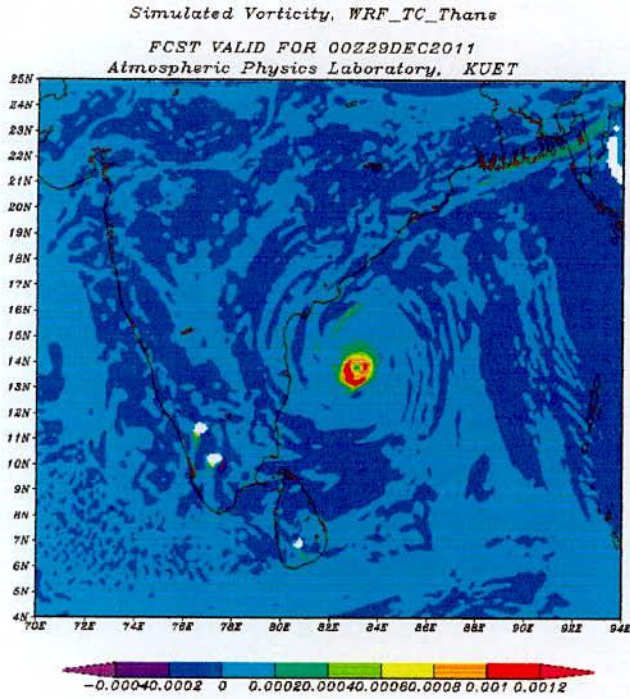
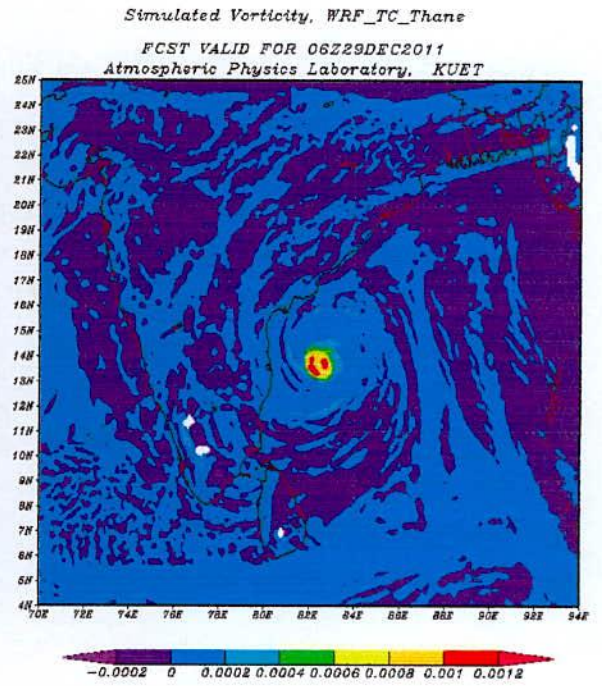


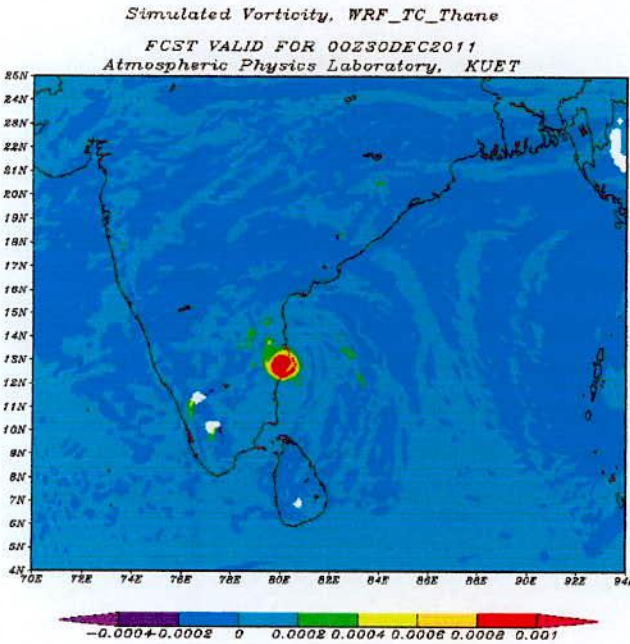
Figure 4.40 (a-d): Model simulated 850 hpa relative vorticity ($\times 10^{-5} \text{s}^{-1}$) of cyclone Thane (2011) at different stages: (a) at 0000UTC of 28 Dec. (used as initial field) (b) at 1800UTC of 28 Dec. (c) at 1200UTC of 29 December (d) at 1800UTC of 30 December.



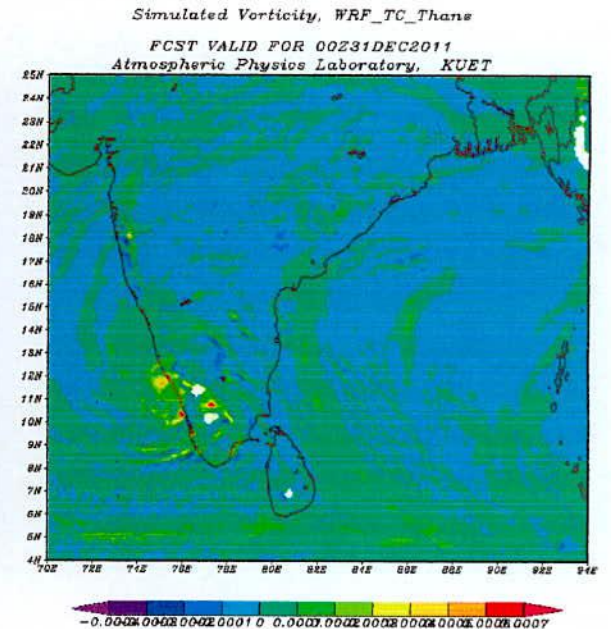
a



b



c



d

Figure 4.41 (a-d): Model simulated 850 hpa relative vorticity ($\times 10^{-5} \text{s}^{-1}$) of cyclone Thane (2011) at different stages: (a) at 0000UTC of 29 Dec. (used as initial field) (b) at 0600UTC of 29 Dec. (c) at 0000UTC of 30 Dec. (d) at 0000UTC of 31 Dec.

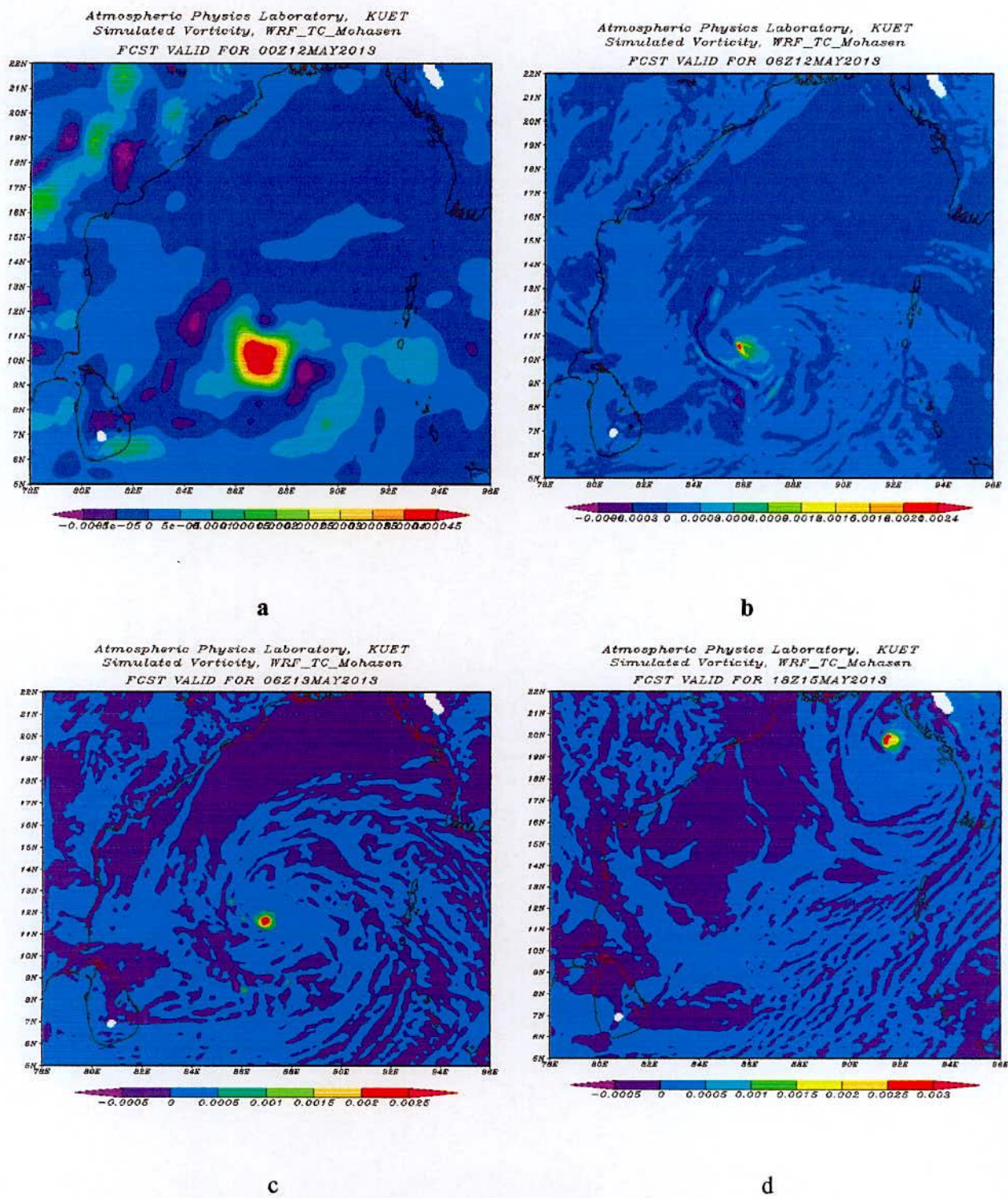


Figure 4.42 (a-d): Model simulated 850 hpa relative vorticity ($\times 10^{-5} \text{s}^{-1}$) of cyclone Mahasen (2013) at different stages: (a) at 0000UTC of 12 May (used as initial field) (b) at 0600UTC of 12 May (c) at 0600UTC of 13 May (d) at 1800UTC of 15 May.

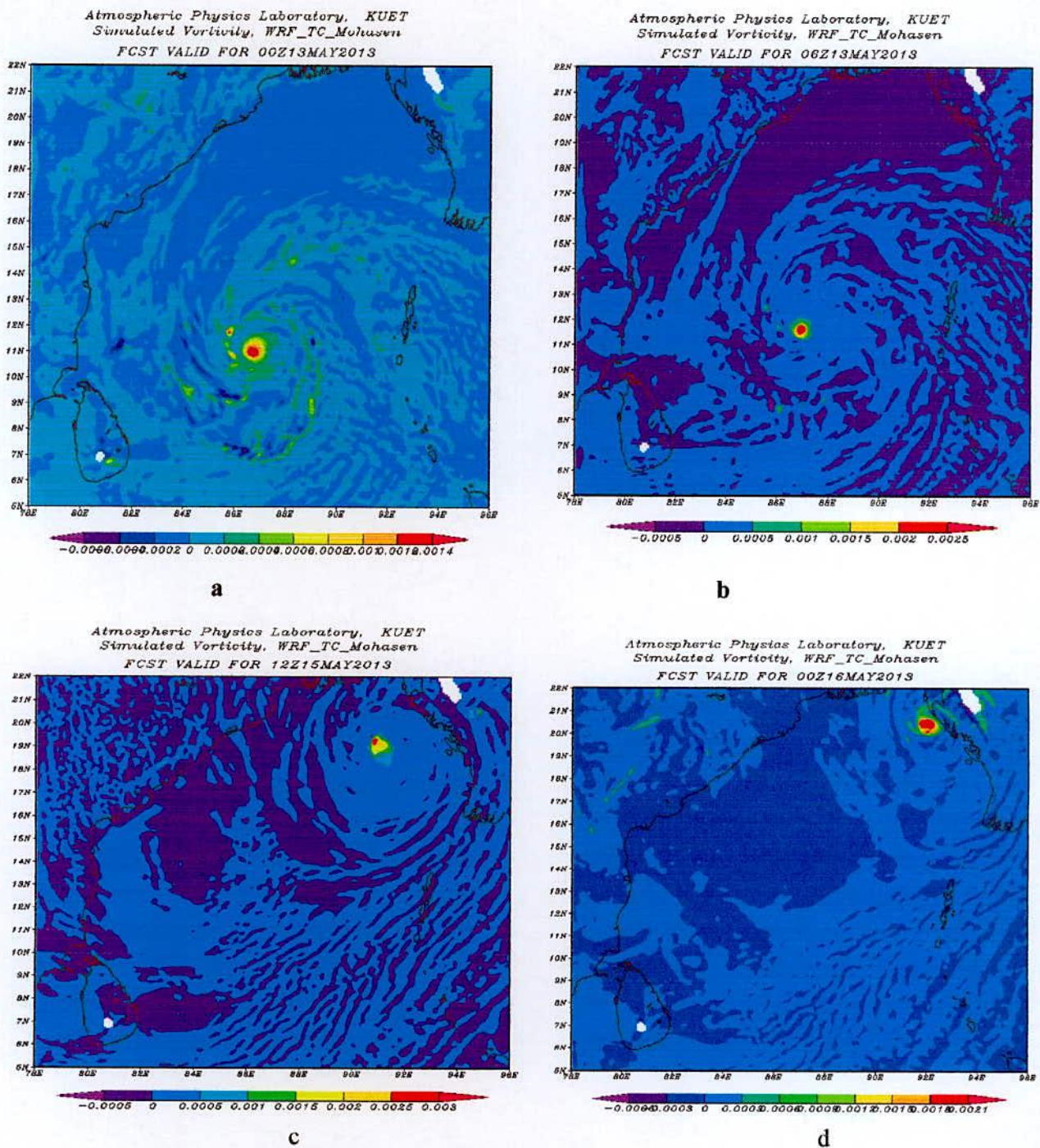


Figure 4.43 (a-d): Model simulated 850 hpa relative vorticity ($\times 10^{-5} \text{s}^{-1}$) of cyclone Mahasen (2013) at different stages: (a) at 0000UTC of 13 May (used as initial field) (b) at 0600UTC of 13 May (c) at 1200UTC of 15 May (d) at 0000UTC of 16 May.

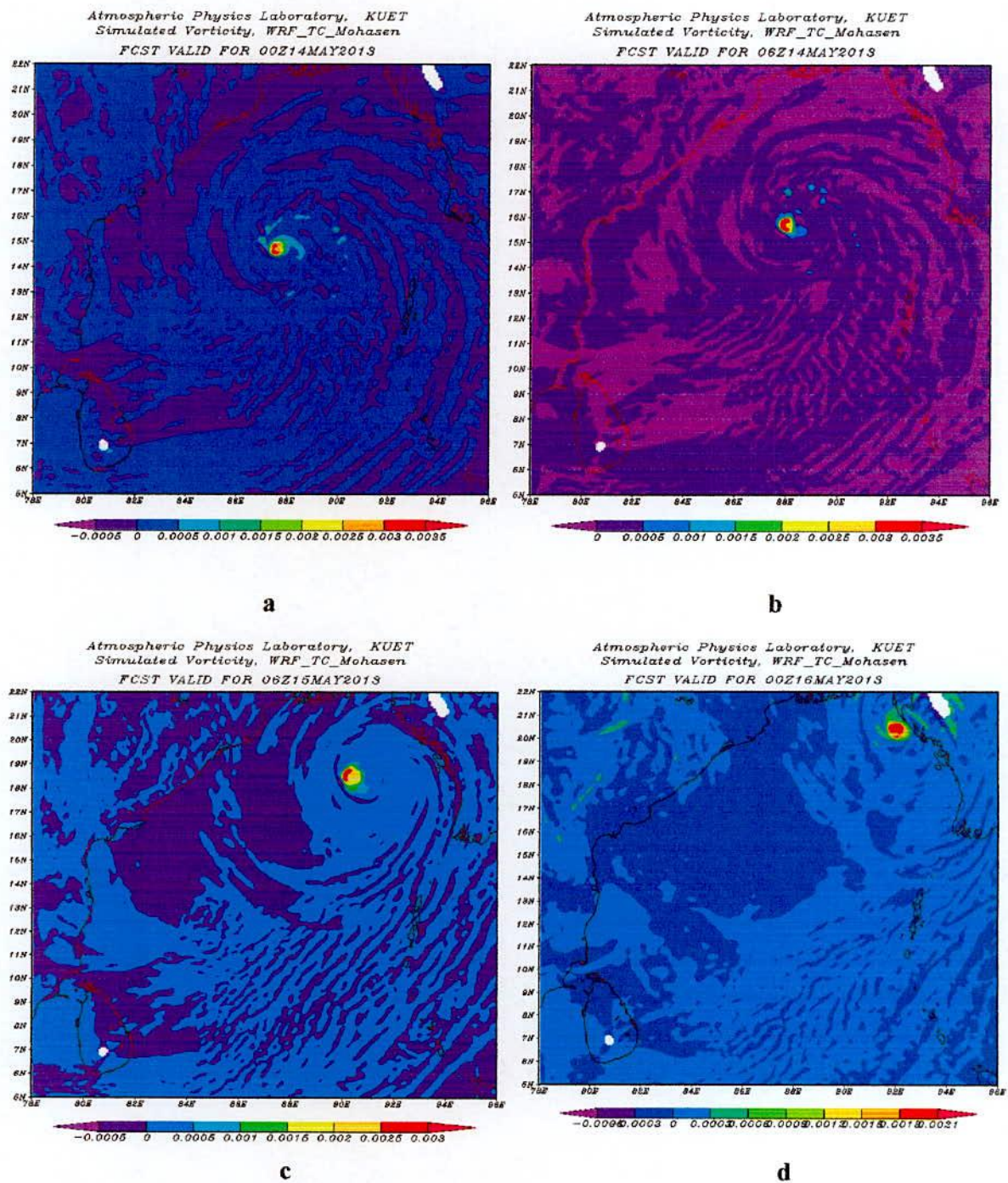


Figure 4.44 (a-d): Model simulated 850 hpa relative vorticity ($\times 10^{-5} \text{s}^{-1}$) of cyclone Mahasen (2013) at different stages: (a) at 0000UTC of 14 May (used as initial field) (b) at 0600UTC of 14 May (c) at 0600UTC of 15 May (d) at 0000UTC of 16 May.

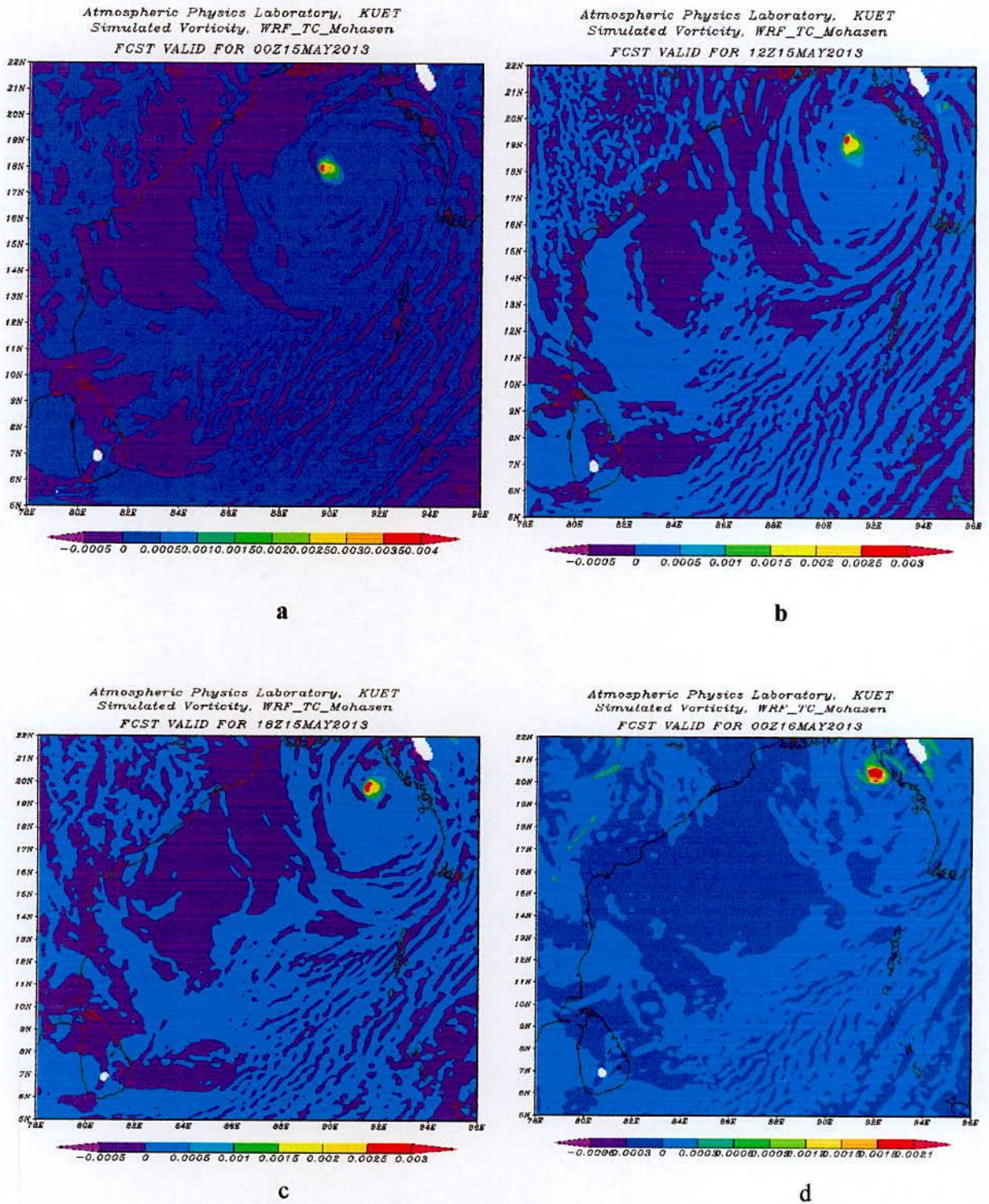


Figure 4.45 (a-d): Model simulated 850 hpa relative vorticity ($\times 10^{-5} \text{s}^{-1}$) of cyclone Mahasen (2013) at different stages: (a) at 0000UTC of 15 May (b) at 1200UTC of 15 May (c) at 1800UTC of 15 May (d) at 0000UTC of 16 May.

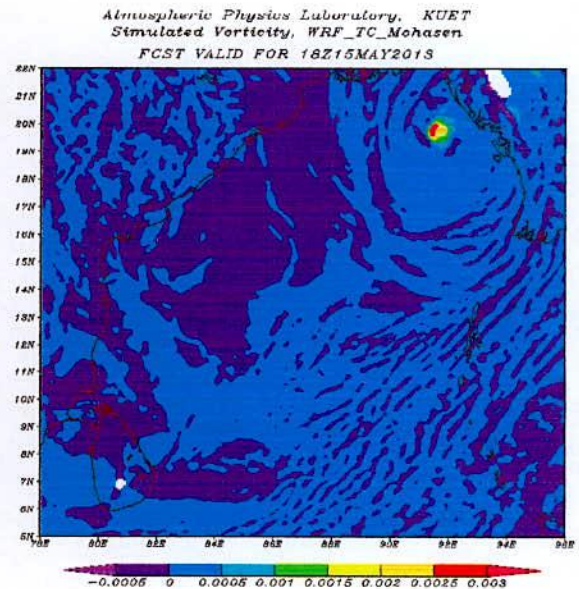
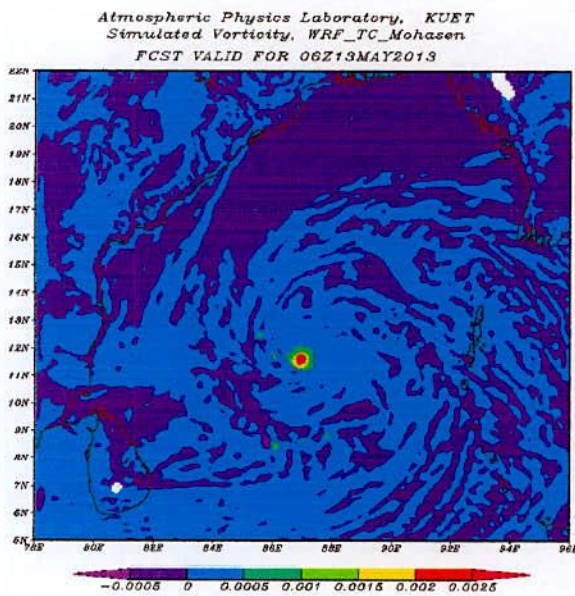
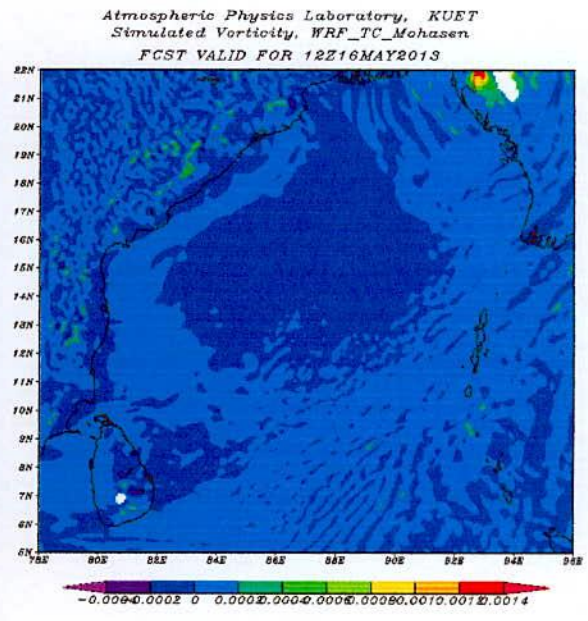
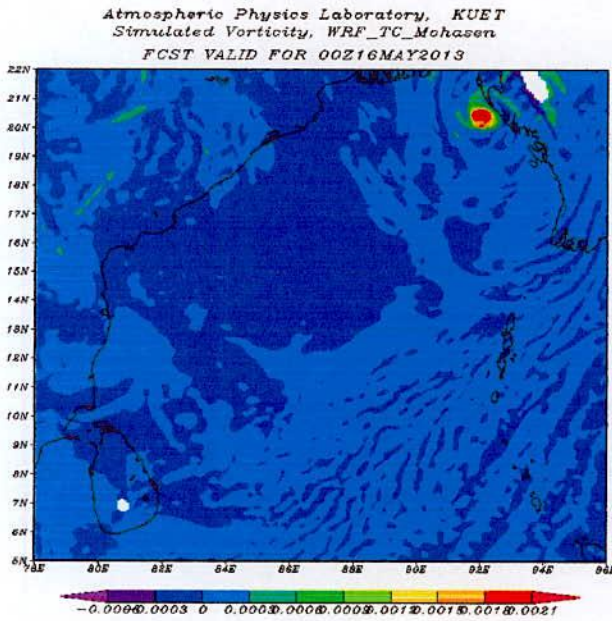


Figure 4.46 (a-d): Model simulated 850 hpa relative vorticity ($\times 10^{-5} \text{s}^{-1}$) of cyclone Mahasen (2013) at different stages: (a) at 0000UTC of 16 May (used as initial field) (b) at 1200UTC of 16 May (c) at 0600UTC of 13 May (d) at 1800UTC of 15 May.

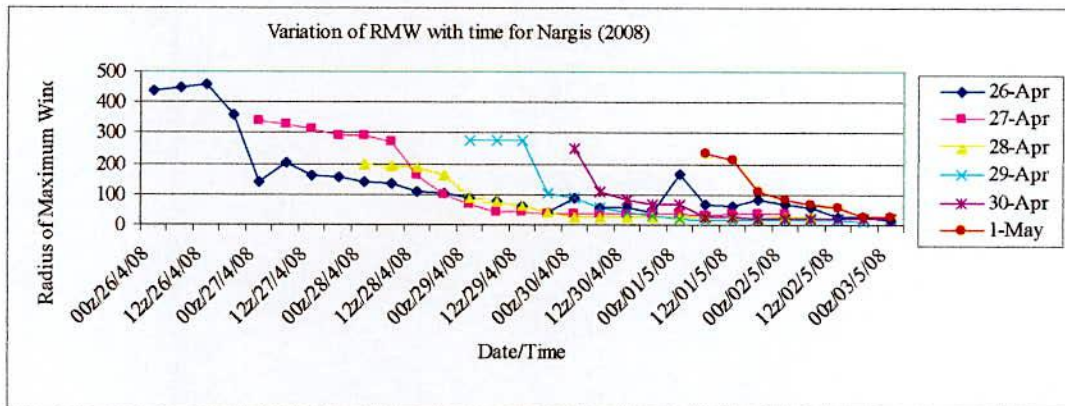
4.2.5 Radius of Maximum Wind (RMW)

Radius of maximum wind (RMW) is considered as an important parameter of tropical cyclone structure which is defined to be the distance between the center of the cyclone and its band of strongest winds. The highest storm surge is normally coincident with the radius of maximum wind. When the cyclone reaches peak intensity it attains the lowest RMW.

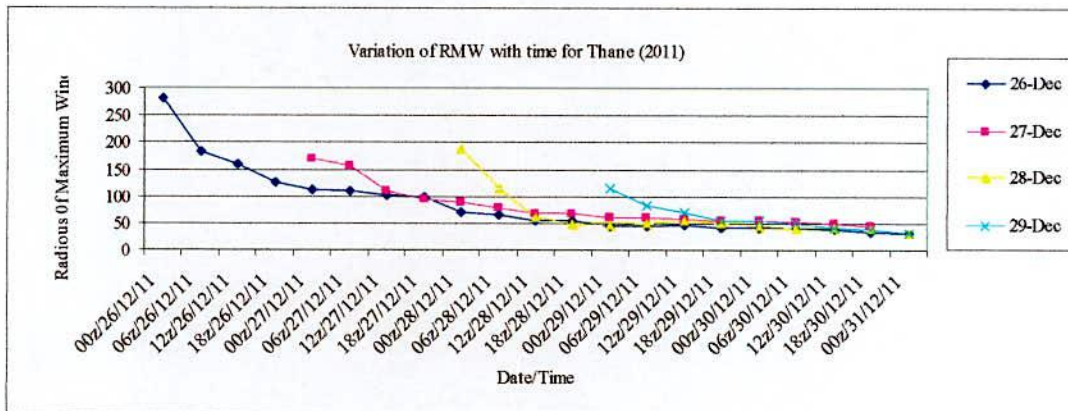
The simulated values obtained using initial field condition, among all simulated values the 29 April's values is better agreement with observed values for very severe cyclonic storm Nargis (2008), the 27 December's values is better agreement with observed values for very severe cyclonic storm Thane (2011), and the 16 May's values is better agreement among all values for severe cyclonic storm Mahasen (2013). The evolution of simulated RMW of selected cyclone is shown in figure 4.47 (a, b, c). From the figure, it appears that the model simulated RMW gradually decreases with the intensification of the cyclonic system which reflects real situation. Table 4.7 shows the simulated RMW of cyclone Nargis, Thane, and Mahasen. It is noted that the 72hrs simulated RMW of Nargis, 96 hrs simulated RMW of Thane and 120 hrs simulated RMW of Mahasen are closer.

Table 4.5: Radius of Maximum Wind (RMW) of Selected Tropical Cyclone

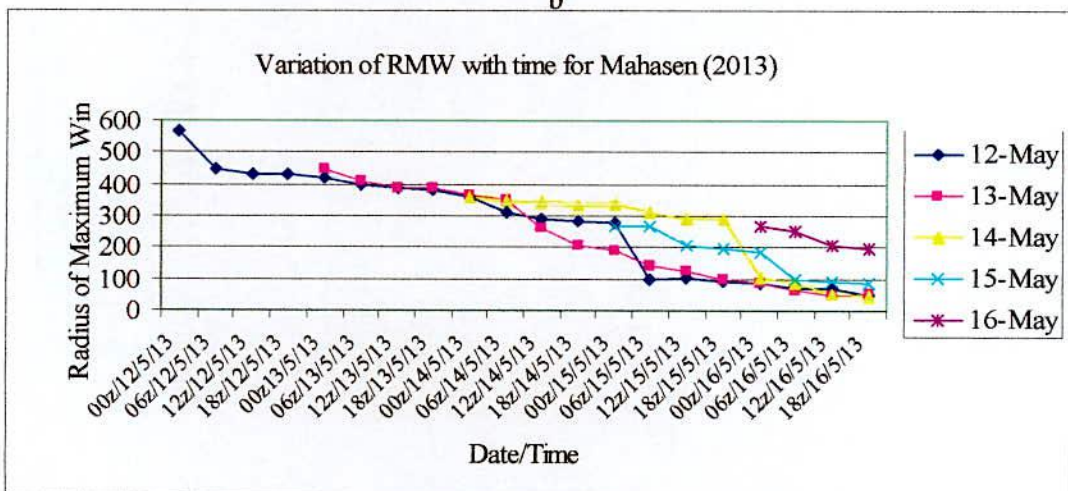
Name of cyclones	Initial Date/Time (UTC)	Forecasting hours	Simulated RMW (km) [Date/Time]	Highest RMW (km)
Nargis (2008)	26 April/0000	144	457 [02 May/1800]	457
	27 April/0000	120	341 [02 May/0900]	
	28 April/0000	96	298 [02 May/0300]	
	29 April/0000	72	275 [02 May/0600]	
	30 April/0000	48	247 [02 May/1500]	
	01 May/0000	24	236 [02 May/1800]	
Thane (2011)	26 December/0000	96	281 [30 December/1200]	281
	27 December/0000	72	171 [30 December/0600]	
	28 December/0000	48	134 [30 December/0600]	
	29 December/0000	24	116 [30 December/0300]	
Mahasen (2013)	12 May/0000	120	270 [16 May/0000]	270
	13 May/0000	96	250 [16 May/0600]	
	14 May/0000	72	230 [16 May/0900]	
	15 May/0000	48	210 [16 May/1200]	
	16 May/0000	24	250 [16 May/0600]	



a



b



c

Figure 4.47 (a, b, c): Evolution of model simulated RMW of selected cyclones (a) Naggis (2008), (b) Thane (2011) and (c) Mahasen (2013).

4.2.6 Relations among Different Parameters of Tropical Cyclones derived from Model Results

In this sub-section the relations of maximum wind speed (MWS) with other intensity related parameters such as central pressure drop (Δp), relative vorticity (ξ), and radius of maximum wind (RMW) have been discussed. The variables were picked from the model simulated field at the stage highest intensity level for all the three selected cyclones which are shown in Table 4.6. Thus there are four set of observation for each of the relations.

The 4 scatter diagrams figure [(4.48(a-d), 4.49(a-d) & 4.50(a-d)] have been plotted with MWS or V_{\max} as y-axis and the variables (Δp) and its square root $\sqrt{\Delta p}$, 850 hpa vorticity as x-axis. The Figure (a) shows the linear relations between the MWS and central pressure drop where MWS increases with the increases of Δp . The equation of the relationship is given below.

$$\text{MWS} = 1.41\Delta p + 22 \text{ for Nargis (2008),}$$

$$\text{MWS} = 1.50\Delta p + 72 \text{ for Thane (2011) and}$$

$$\text{MWS} = 0.61\Delta p + 18 \text{ for Mahasen, where MWS is in m/s and } \Delta p \text{ is in hpa.}$$

The figure (b) has been drawn with special purpose to demonstrate that the model results are consistent with modified Fletcher's formula developed [43] which can be seen in section 4.2.3. The regression analysis using the model simulated parameters for the selected cyclones shows the linear relation between the V_{\max} with $\sqrt{\Delta p}$ of the form.

$$V_{\max} = 12\sqrt{\Delta p} \text{ for Nargis (2008),}$$

$$V_{\max} = 12\sqrt{\Delta p} \text{ for Thane (2011) and}$$

$$V_{\max} = 12\sqrt{\Delta p} \text{ for Mahasen (2013); where, } V_{\max} \text{ is in knots.}$$

The scatter diagram between models simulated MWS and 850 hpa. Level relative vorticity of selected tropical cyclones at the stage of their highest intensity is shown in figure (c). It is seen from the figure MWS increases linearly with the increase of relative vorticity (ξ). The relation is found to be as:

$$\text{MWS} = 10000(\xi) + 15 \text{ for Nargis (2008),}$$

$$\text{MWS} = 14285(\xi) + 50 \text{ for Thane (2011) and}$$

$$\text{MWS} = 4444(\xi) + 30 \text{ for Mahasen (2013)}$$

Figure (d) shows the relationship between the model simulated MWS and RMW of the selected cyclones at their highest maturity stage. It is seen that the RMW decreases with the increase of MWS

Table 4.6: The model simulated different parameters of selected tropical cyclones at the stage of highest intensity.

Tropical cyclones	Different date	MWS (m/s)	V_{max} (knots)	Central pressure drop (hPa)	RMW (km)	850 hPa Vorticity
Nargis(2008)	26 April	50	97	21	457	0.00056
	27 April	60	116	25	341	0.00065
	28 April	71	138	33	298	0.00076
	29 April	85	157	42	270	0.00085
	30 April	93	171	51	247	0.00092
	01 May	95	178	53	246	0.00098
Thane (2011)	26 December	72	140	30	281	0.00021
	27 December	74	144	31	171	0.00052
	28 December	76	147	32	134	0.00065
	29 December	78	151	34	116	0.00084
Mahasen (2013)	12 May	44	84	43	565	0.0025
	13 May	42	80	40	374	0.0039
	14 May	41	78	38	321	0.0045
	15 May	39	75	35	296	0.0047
	16 May	30	57	20	285	0.0054

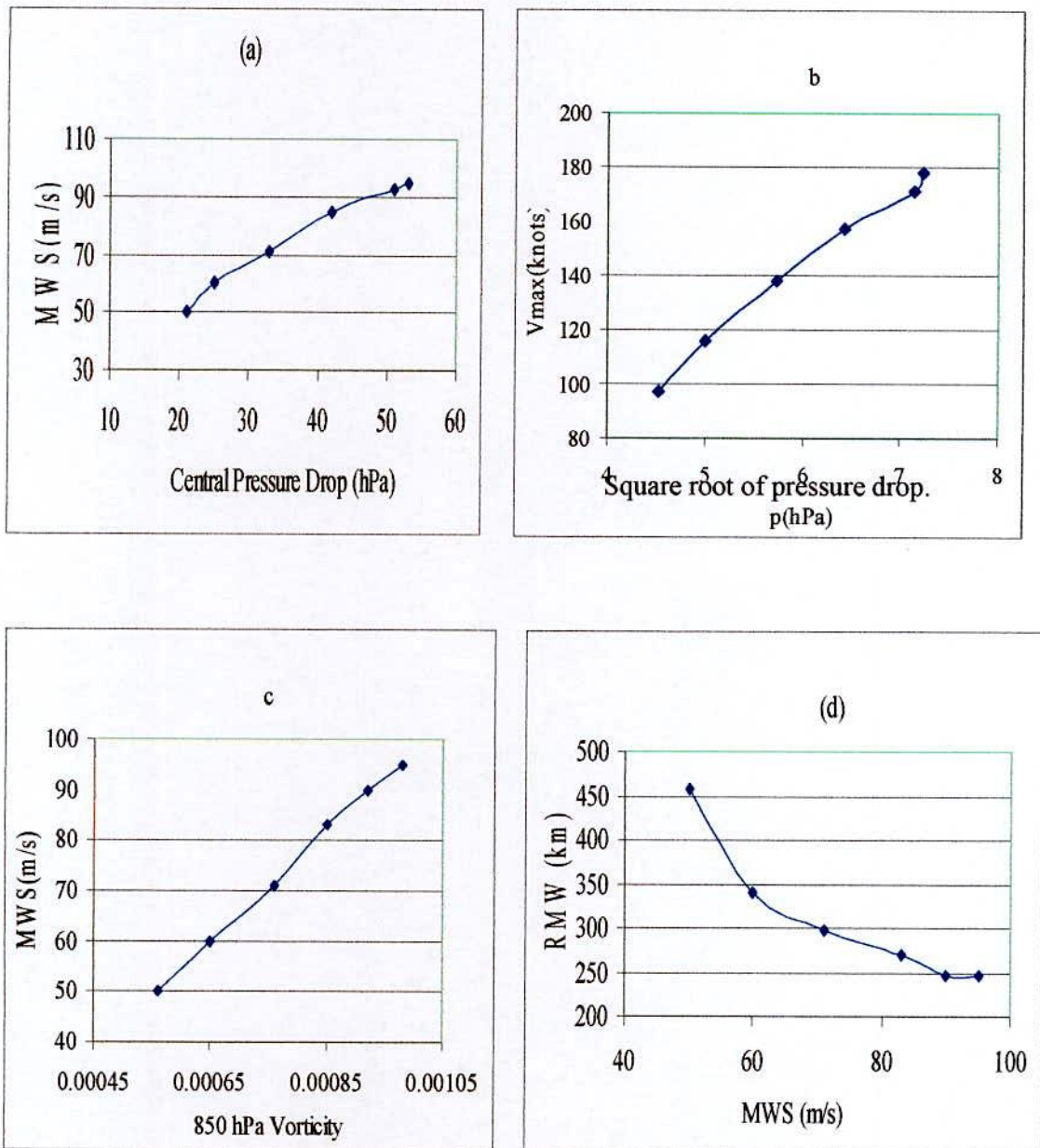


Figure 4.48(a, b, c, d): Relationship of simulated maximum wind speed (MWS)

V_{\max} and simulated (a) central pressure drop (Δp),

(b) square root of pressure drop ($\sqrt{\Delta p}$), (c) 850 hpa vorticity and

(d) radius of maximum wind (RMW) of selected tropical cyclone Nargis (2008) at the stage of highest intensity.

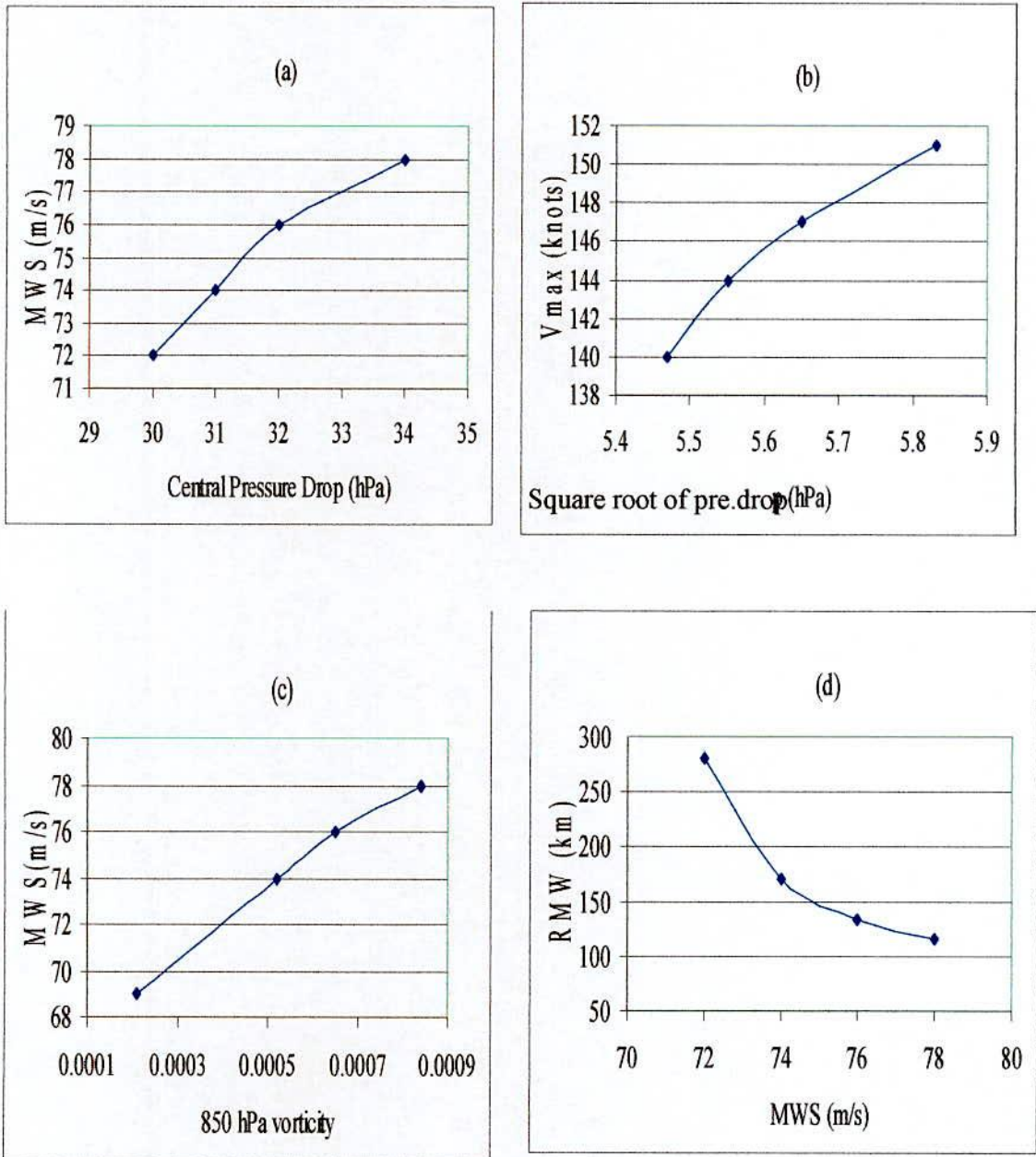


Figure 4.49(a, b, c, d): Relationship of simulated maximum wind speed (MWS) i.e., V_{max} and simulated (a) central pressure drop (Δp), (b) square root of pressure drop ($\sqrt{\Delta p}$), (c) 850 hPa vorticity and (d) radius of maximum wind (RMW) of selected tropical cyclone Thane (2011) at the stage of highest intensity.

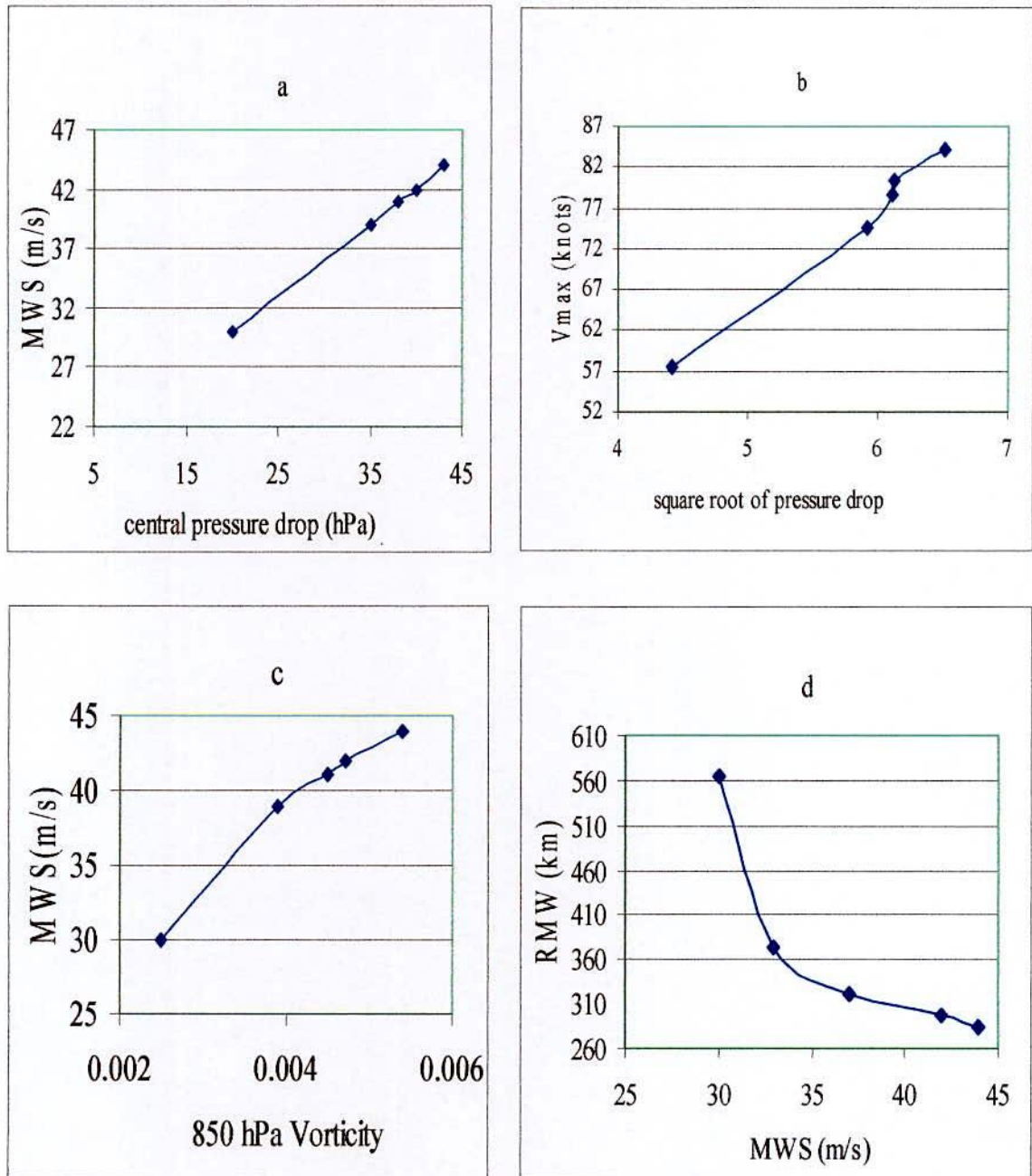


Figure 4.50 (a, b, c, d): Relationship of simulated maximum wind speed (MWS) i.e., V_{max} and simulated (a) central pressure drop (Δp), (b) square root of pressure drop ($\sqrt{\Delta p}$), (c) 850 hpa. vorticity and (d) radius of maximum wind (RMW) of selected tropical cyclone Mahasen(2013) at the stage of highest intensity.

From these discussions of the sub-section 4.2.2, it may be summarized that the ARW model used in the present study generates more or less realistic intensification of tropical cyclones. The model successfully simulates the evolution of minimum sea level pressure (MSLP), Pressure drop (Δp), maximum wind speed (MWS), relative vorticity and radius of maximum wind (RMW) at different stages. The model results indicate realistic relations of MWS with different intensity related parameters of the selected tropical cyclones. However, for some cases, especially for very severe cyclonic storm Nargis(2008) and very severe cyclonic storm Thane (2011), the intensity is under estimated. This could be due to weak representation of the system in the initial field of FNL. Prasad [107] showed that incorporation of an idealized vortex in the initial field improves the QLM model's ability to maintain the intensity of the cyclonic system and give a forecast to a satisfactory degree of accuracy. In view of this, it is important to do some experiments on bogusing technique with WRF model in order to improve the model performance for cyclone prediction. Other reason could be due to parameterization schemes used in the present study (Kain-Fritch cumulus parameterization scheme, Yonsei University PBLand WSM 3-class simple ice. These improvements were made with proper combination of Kain-Fritsch scheme, Mellor-Yamada PBL scheme and Mixed Phase explicit moisture scheme. Therefore, sensitivity experiments with proper combination of parameterization schemes need to be carried out for better simulations. In this study, horizontal grid resolution is used as 24km with 27 eta levels in the vertical. Horizontal and vertical grid resolutions are other important model features to be tested to improve the simulations.

4.2.7 Evolution of Track's Movement of Tropical Cyclones

Track forecasting has been a challenging task for meteorologists over the last few decades in spite of the rapid development of numerical weather prediction techniques. There had been numerous studies on track forecasting using several models such as QLM, MM5, FSU GSM & NRSM, GFDL, BMRC, etc. over the Bay of Bengal and other basins as well. Accurate track forecasting is also of great importance for disaster management for taking proactive measures to mitigate the damages to life and property.

4.2.7.1 Very Severe Cyclonic Storm Nargis (2008)

To study the tracks of cyclone Nargis the model was run for 24, 48, 72, 96, 120, and 144 hrs. Figure 4.51, Shows the predicted tracks of cyclone Nargis (2008) beginning from 0000UTC of 26 April, 0000UTC of 27 April, 0000UTC of 28 April, 0000UTC of 29 April, 0000UTC of 30 April, 0000UTC of 01 May. This experiment is carried out with the initial field of 0000UTC of 26 April for capturing recurvature of the track. The prediction experiments captured well the direction of motion, recurvature and probable areas of landfall. The tracks of Nargis show that the prediction experiments captured well the direction of motion and probable areas of landfall within the accuracy of 17-120 km. The 24, 48, 72 and 120 hrs forecast tracks agreed well with the observed track and indicated landfall at Myanmar coast fairly close to the actual. The 96, and 144 hrs predicted tracks (Fig. a, c) finally deviated to northeast from the observed track and landfall points departed by about 120 km. It is noted from observed information that the very severe cyclonic storm Nargis remained stationary near 13°N/85.3°E for some time on 28 April 2008 and abruptly changed its direction and started to move towards the north-east direction. Fig. 4.51(a, b, c, d, e,) shows that the model forecast also captured well this recurvature towards northeast after the initial northwest movement and the stationary feature of the track which indicating the remarkable success of ARW model. But in Fig. 4.51(f) shows dissimilarity between simulated values and observed values because the shortage simulated data range.

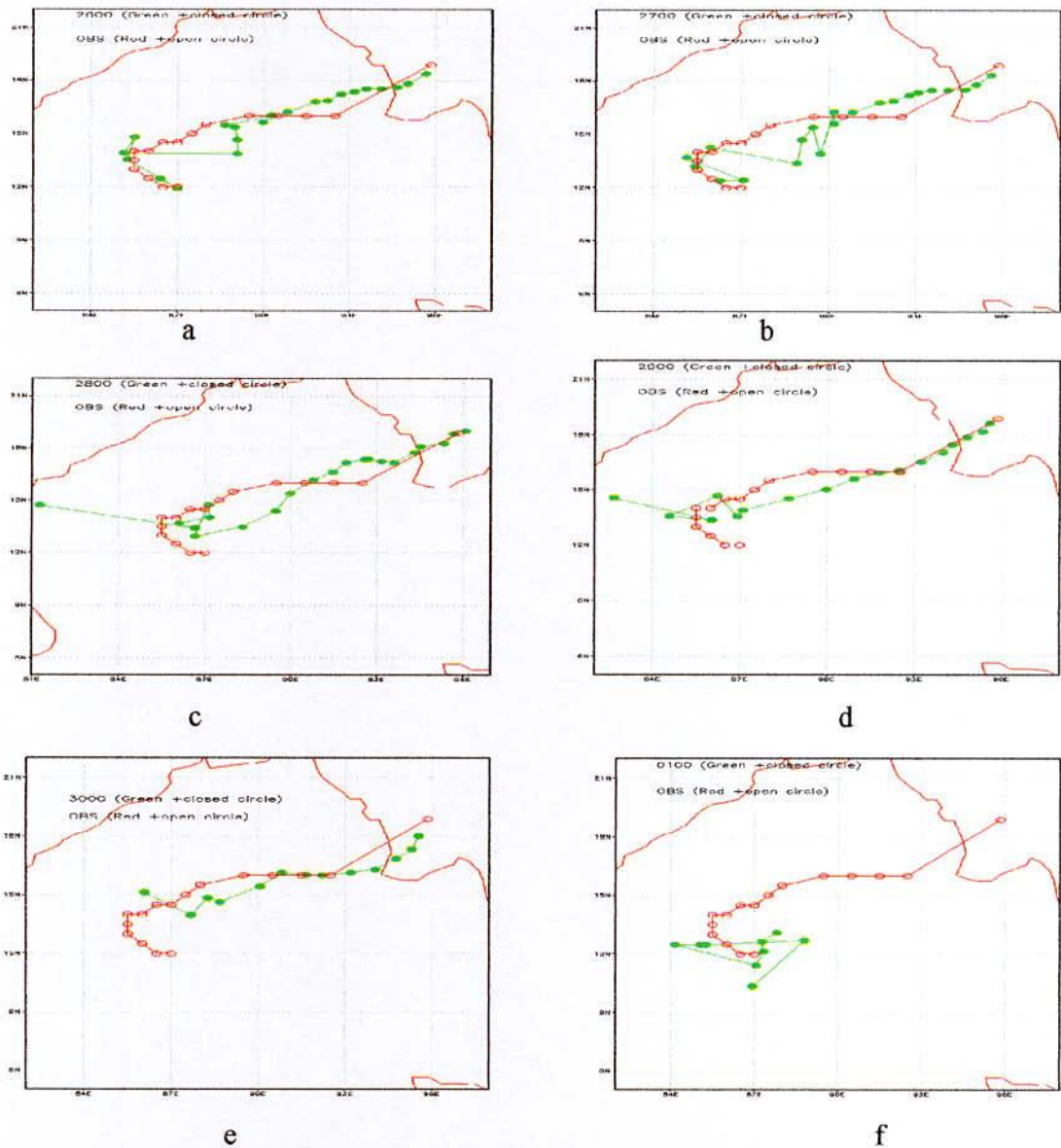


Figure 4.51(a, b, c, d, e, f): Model simulated and observed track of very severe cyclonic storm Nargis (2008) (a) 144 hrs forecast beginning 0000UTC of 26 April, (b) 120 hrs forecast beginning 0000UTC of 27 April, (c) 96 hrs forecast beginning 0000UTC of 28 April, (d) 72 hrs forecast beginning 0000UTC of 29 April, (e) 48 hrs forecast beginning 0000UTC of 30 April, (f) 24 hrs forecast beginning 0000UTC of 01 May.

4.2.7.2 Very Severe Cyclonic Storm Thane (2011)

To study the tracks of cyclone Thane the model was run for 24, 48, 72, and 96 hrs. Figure 4.52 Shows the predicted tracks of cyclone Thane (2011) beginning from 0000UTC of 26 December, 0000UTC of 27December, 0000UTC of 28 December, 0000UTC of 29December. This experiment is carried out with the initial field of 0000UTC of 26 December for capturing

recurvature of the track. The prediction experiments captured well the direction of motion, recurvature and probable areas of landfall. It reveals that model was capable to capture westward movement in this case. The 96 hrs forecast track shows some erratic movement in early stages of simulation, when the system is far away from the India coast, mainly due to less representation of the system in the initial field and after making a circular loop in 48 hrs it followed the observed track. The 72 hrs predicted track closely follow observed track up to 60 hrs forecast then it defects to northwestward. It is found that the simulated landfall point of Thane seems quite accurate with 48 hrs forecast based on 0000 UTC of 26 December. The model results produce an overall view that for weak system the predictions generate the direction of the motion very efficiently indicating the probable areas of the coast to be hit. However, the 24 and 48 hrs predictions show the better representation of the tracks and landfall within 50 km accuracy. But in these cases the model landfall was delayed by about 12 hrs.

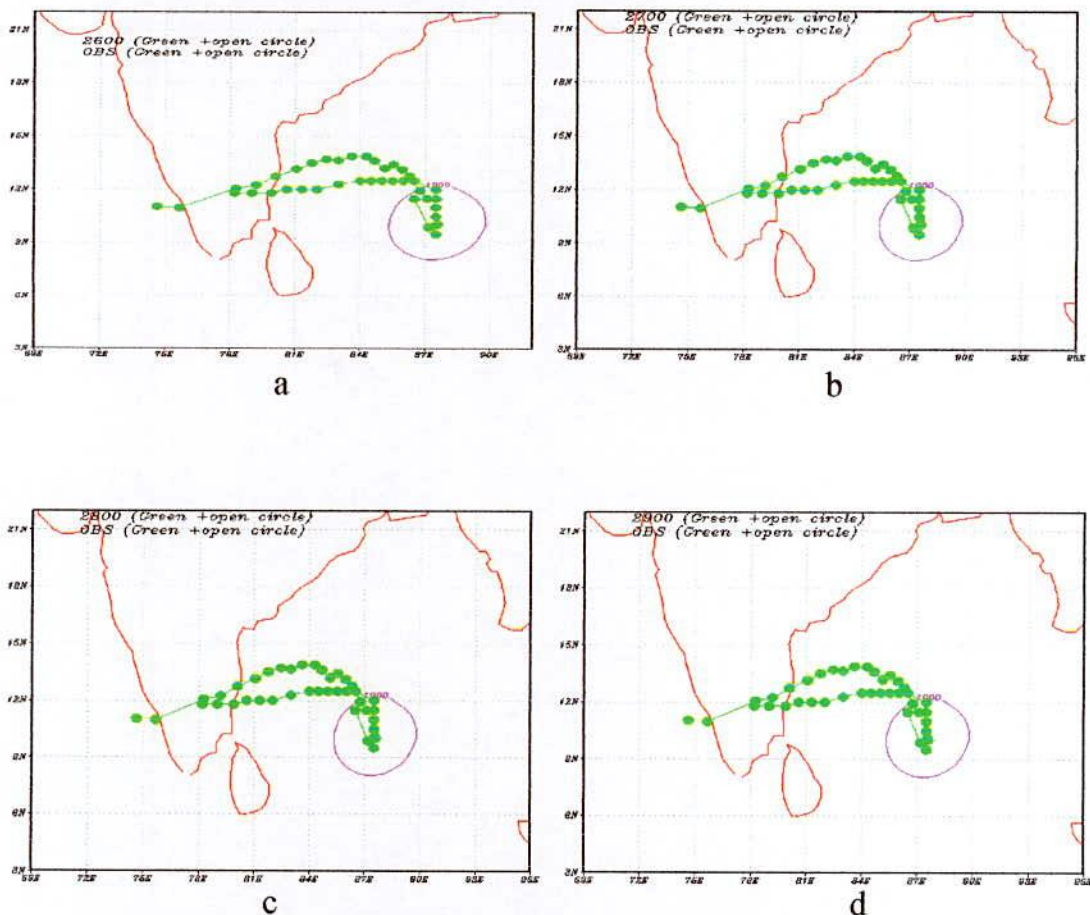


Figure 4.52 (a, b, c, d): Model simulated and observed track of very severe cyclonic storm Thane (2011) (a) 96 hrs forecast beginning 0000UTC of 26 December, (b) 72 hrs forecast beginning 0000UTC of 27 December, (c) 48 hrs forecast beginning 0000UTC of 28 December, (d) 24 hrs forecast beginning 0000UTC of 29 December.

4.2.7.3 Cyclonic Storm Mahasen (2013)

To study the tracks of cyclone Mahasen the model was run for 24, 48, 72, 96, and 120 hrs. Figure 4.53 Shows the predicted tracks of cyclone Mahasen (2013) beginning from 0000UTC of 12 May, 0000UTC of 13 May, 0000UTC of 14 May, 0000UTC of 15 May, 0000UTC of 16 May.. This experiment is carried out with the initial field of 0000UTC of 12 May for capturing recurvature of the track. The prediction experiments captured well the direction of motion, recurvature and probable areas of landfall. The tropical cyclone Mahasen is a system of medium strength. It is found that model captures northward movement very well. The 48, 72, 96 and 120 hrs prediction experiments captured well the direction of motion and probable areas of landfall within the accuracy of 120-160 km but the forecast track shows some erratic movement in the early stage of simulation. The 24 and 48 hrs predictions produce much better matching of the tracks and landfall with the observed with accuracy of about 40 km.

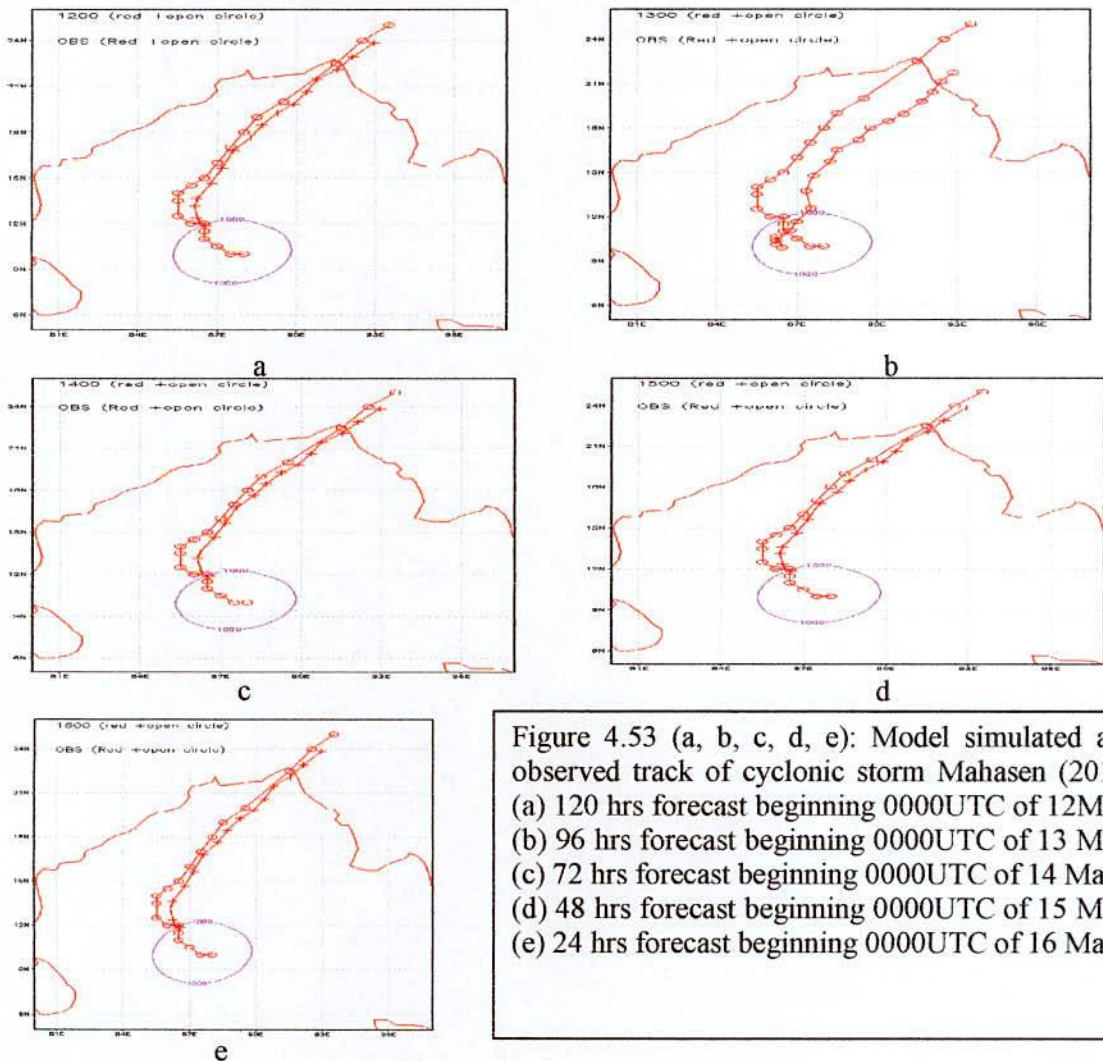


Figure 4.53 (a, b, c, d, e): Model simulated and observed track of cyclonic storm Mahasen (2013) (a) 120 hrs forecast beginning 0000UTC of 12May, (b) 96 hrs forecast beginning 0000UTC of 13 May, (c) 72 hrs forecast beginning 0000UTC of 14 May, (d) 48 hrs forecast beginning 0000UTC of 15 May, (e) 24 hrs forecast beginning 0000UTC of 16 May.

4.2.7.4 Errors in Track Forecasting

Table 4.7: shows mean position errors in track prediction of some previous studies. Mathur and Ruess (1993)[92], in an evaluation of the QLM's forecast track guidance in NMC Washington during the period 1998-90 reported mean forecast errors in the range of 180-190 km for 24 hrs, 300-370 km for 48 hrs, and 400-540 km for 72 hrs forecasts. Rao and Prasad (2005) [108] have reported mean position errors of around 167 km for 24 hrs, 367 km for 48 hrs and 433 km for 72 hrs forecasts in respect of the QLM experiments carried out earlier. Goerss (2000) [183] has reported mean position errors in track prediction with GFDL of about 142 km for 24 hrs, 246 km for 48 hrs and 364 km for 72 hrs predictions. After making cyclone track prediction experiments with QLM at 40 km horizontal resolution for nine cyclonic storms developing during the period 1997-2000, Prasad (2004) [107] have reported the mean position errors of about 122 km for 24 hrs, 256 km for 48 hrs and 286 km for 72 hrs predictions. Though this level of forecast errors is quite large, particularly in the higher forecast range, from the point of view of dependability of NWP guidance for operational cyclone track prediction, this aspect should be viewed in light of the fact that uncertainties of forecasts based on purely subjective methods using synoptic data and satellite observations are much larger and could still be minimized with the help of numerical guidance.

Table 4.7: Mean position errors in the track forecasting of some previous studies

Author/Reference	Used NWP	Mean Position Error (km)		
	Model	24 hrs period	48 hrs period	72 hrs period
Mathur and Ruess (1993)[92]	QLM	180-190	300-370	400-540
Goerss (2000) [183]	GFDL	142	246	364
Goerss (2000) [183]	NOGAPS	152	255	383
Goerss (2000) [183]	NOGAPS	152	244	348
Goerss (2000) [183]	GLIPER	187	389	607
After Hossain (2003) [18]	FSUNRSM	144	150	150
Prasad (2004)[107]	QLM	122	256	286
Rao and Prasad (2005)[108]	QLM	167	367	433

Forecast verification has been carried out in the present study by computing the position error—the geographical distance between the predicted location of the storm and the verifying position at the valid hour. The position error of a tropical cyclone is an essential indicator for researchers to understand the model performance. It helps them to properly tune the model by conducting sensitivity experiments before applying for real time prediction. It is worth noting that the mean position errors is calculated considering all the forecasted points for the period ranging from 24 to 96 hrs throughout the passage of cyclone till the landfall. The mean position errors for 24, 48, 72 and 96 hrs predictions are shown in Table 4.8. It is seen that the mean position errors are in the range of 48-152 km for 24 hrs, 100-205 km for 48 hrs, 133-268 km for 72 hrs and 135-306 km for 96 km hrs predictions. The combined mean errors (i.e. the average forecast errors of the four selected cyclones) for 24, 48, 72 and 96 hrs forecasts are 92, 155, 194 and 233 km respectively. This clearly demonstrates that the track prediction error increases as the forecast hours increases (also seen from Figure 4.54). It is of interest to note that the mean position errors of the cyclone Nargis are lower than other two selected tropical cyclones and that of Mahasen are higher than other two selected tropical cyclones. But for Thane it is coincide with CMF values. Though the forecasted landfall points of cyclones Thane and Mahasen seems quite close to the actual landfall point, the mean position errors are comparatively lower in all 24, 48, 72 and 96 hrs forecasts. This is because of the fact that the simulated translational speed of Thane and Mahasen was lower than that observed.

Therefore, the mean position errors of present study are much lower than the forecast errors of other models as shown in Table 4.7. ARW model not only provides improved track forecast with relatively lower position error but it has provided highly encouraging results in 96 hrs prediction, while the earlier works did not go for such a longer range prediction (see Table 4.7). This shows the advantage of using ARW model with high

Resolution (24 km horizontal resolution is used for this study) for Bay of Bengal cyclone predictions. However, use of higher model resolution may provide even better results. Due to time constraints, the higher resolution options were not applied in this work.

Table 4.8: Mean position errors in track of the selected tropical cyclones of the present study.

Forecast Hours	Nargis (2008) (km)	Thane (2011) (km)	Mahasen (2013) (km)	Combined Mean Error
24 hrs	158	77	152	129
48 hrs	255	160	205	207
72 hrs	235	181	268	228
96 hrs	152	250	308	237

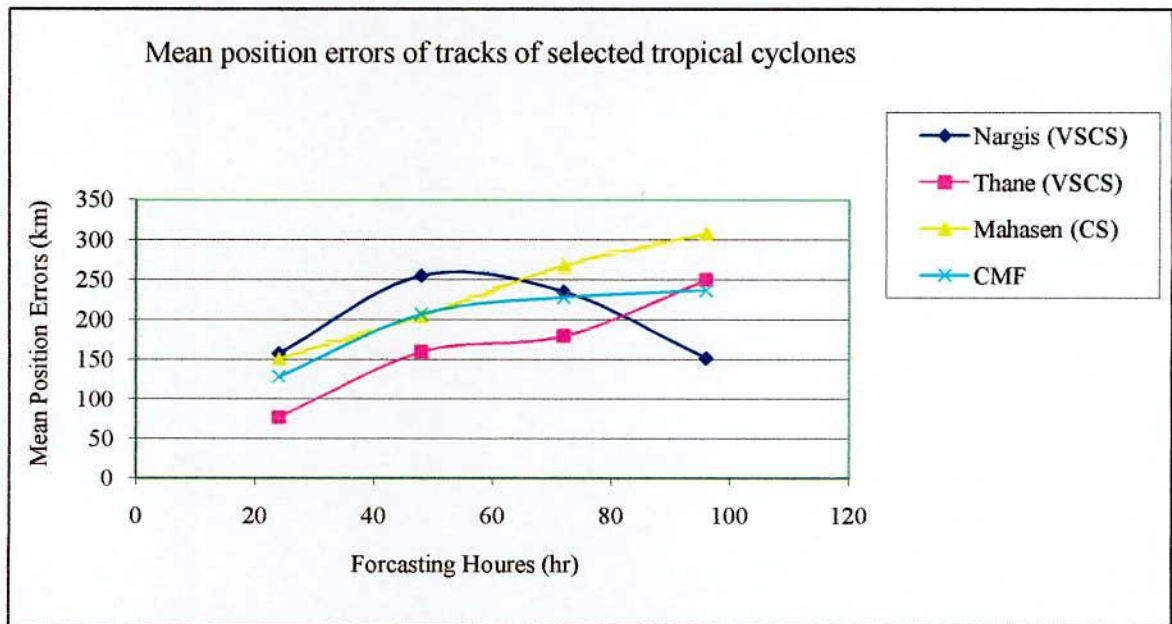


Figure 4.54: Comparison of mean position error in track forecasting against the range of the forecasting hours (Note: CME means combined mean error in track forecasts of three selected cyclones, VSCS mean very severe cyclonic storm, CS mean cyclonic storm).

Chapter- V

Conclusions

A study has been conducted for the prediction of tropical cyclones of the Bay of Bengal using Numerical Weather Prediction (NWP) model. The study has been performed for the following three land falling tropical cyclones of different intensities-formed in the Bay of Bengal to the coast of Bangladesh, Myanmar and east coast of India. Severe cyclonic storm with a core of hurricane wind (very severe cyclonic storm following RSMC classification) Nargis (27 April-03 May 2008), Very Severe cyclonic storm (following RSMC classification) Thane (25-31 December 2011) and cyclonic storm (following RSMC classification) Mahasen (12-17 May, 2013). The Advanced Research WRF (ARW) version 3, a state-of-the-art NWP model, has been used for the present study of prediction of tropical cyclones. ARW is a new generation high resolution mesoscale numerical weather prediction model, which has the potential to simulate broad spectrum of meteorological phenomena ranging from meters to thousands of kilometers with high spatial details. This model like any other NWP model runs with an initial field. In the present modeling experiments the NCEP FNL data of $1^{\circ} \times 1^{\circ}$ resolution were used as initial fields and lateral boundary conditions which are updated at six hourly intervals. The model was initialized with 0000, 0600, 1200 and 1800 UTC initial fields of corresponding dates.

To simulate the above selected cyclones the regional model has been set for a domain of dimension 3° - 23° N and 65° - 98° E to cover the Bay of Bengal basin at 24 km horizontal resolution having 127×127 grid points with 27 vertical η levels. Mercator map projection has been chosen. In the present modeling exercise Kain-Fritsch (KF) cumulus parameterization scheme, WRF-single moment (WSM) 3-class microphysics scheme and Yonsei University PBL scheme have been chosen for simulating all the events. The ARW model with above domain setup and parameterization options was used to study the formation and evolution of the above 3 tropical cyclones. The model results were compared with JTWC best track data for validation of the model performance. The results of the study are summarized below:

1. To predict the formation of selected tropical cyclones the prediction experiments were performed up to 144 hrs for Nargis (2008) and 96 hrs for Thane (2011) and 120 hrs for Mahasen, using the initial fields 24 hrs before the formation of the first low pressure system. The predictions have been updated every 6 hrs using the corresponding initial fields of respective dates until the model could produce the low pressure system. The predicted fields were analyzed to study the formation of cyclones using sea level pressure (SLP). The model captured well north-west movement of the systems at the stage of formation.

2. To study the evolution of tropical cyclones the model was run for 24, 48, 72, 96, 120, and 144 hrs. The model outputs have been taken at every 6 hrs interval. It is seen from simulated results that the model generated more or less realistic intensification of tropical cyclones. It successfully simulated the evolution of minimum sea level pressure (MSLP), central pressure drop (Δp), maximum wind speed (MWS), 850 hPa level relative vorticity and radius of maximum wind (RMW) at different stages. The model results show that in general the 96 hrs predicted intensity of the cyclones was much better compared with that of 24, 48, 72, hrs prediction. The spatial distribution of wind and vorticity fields at different stages showed that it was more organized for the strong systems at the stage of the higher maturity. The simulated low level (850hpa) relative vorticity was found to be high for the strong systems compared to the weak system. The model results showed that the RMW of the strong systems was lower than that of weak systems and the lowest RMW was found at the stage of highest intensity of respective cyclones. The model simulated MWS was found to exhibit realistic relations with other intensity related parameters of selected tropical cyclones. The simulated V_{\max} and $\sqrt{\Delta p}$ were found to have liner relations among them. The relationship has close matching with the modified Fletcher's formula which is valid for Bay of Bengal.

3. The distribution of model simulated surface pressure, winds, relative vorticity and rainfall were investigated for understanding the horizontal and vertical structure of the selected cyclones at their highest maturity stage. The simulated results showed that the model was able to simulate realistic structure of tropical cyclones. Sharp pressure gradients in the vicinity of the centre of the cyclones were observed in the simulated pressure field at surface level. Well organized circulation patterns were simulated in all selected two cyclones at 850 hPa level confirming that maximum winds are confined to the right of the cyclone movement. Anticyclone circulation patterns at 100 hPa level were visible in most of the simulated cyclones. Low level convergence and upper level divergence were simulated well. The model successfully simulated the strong relative vorticity at lower level spreading over the strong convective regions of each cyclone. For the very strong systems the positive vorticity was found to extend up to 100 hPa level.

From the above, the following conclusions are drawn:

1. The ARW model is capable of forecasting the formation of the first low pressure system 24-36 hrs ahead from its actual genesis without incorporation of an artificial vortex. It is also able to forecast the intensification of the system and is capable to predict the well-marked low before the formation. This indicates the high and unique predictive power of ARW model for predicting the tropical cyclone formation.
2. The model successfully simulates the realistic evolution process and more or less realistic intensification of tropical cyclones. For some cases the model underestimated the intensity of the cyclonic system. The model results indicate that the longer range prediction provides better intensity forecasting.
3. The model generates a realistic structure of the tropical cyclones with high spatial details without use of any idealized vortex in the initial. This has been possible due to the higher spatial resolution of the regional model.
4. One of the outstanding finding of the study is that the model has successfully predicted the probable areas and time of landfall of the selected tropical cyclones with high accuracy predictions.
5. It may finally be concluded that the ARW model used in the present study with high resolution has high potential to predict the formation and evolution of the tropical cyclones of the Bay of Bengal. Thus, the model may be used for operational prediction of cyclones of Bay of Bengal. However, there are scopes for further studies on sensitivity experiments with proper combination of physical and dynamical options along with appropriate sub-grid scale parameterization schemes for proper tuning of the model to improve the prediction and reduce the forecast errors.
6. In order to further improve the model performance for cyclone predictions it is important to do some experiments on bogussing technique with ARW model. Horizontal and vertical grid resolutions preferably with nesting options are other important model features to be tested to improve the model performance.

7. The Bay of Bengal is a data sparse region, improvement of the meteorological network through deployment of fixed and floating data collection buoys over the Bay of Bengal will improve the initial field and thus the performance of the model will also improve.

REFERENCES

1. Anthes, R.A., 1982: Tropical Cyclones: Their Evolution, Structure and Effects. Meteor. Monogr. No. 41, Amer. Meteor. Soc.
2. Gray, W.M., and C.W. Landsea 1992: African rainfall as a precursor of hurricane-related destruction on the U.S. East Coast. Bull. Amer. Meteor. Soc., 73, 1352-1364.
3. Gray, W.M., C.W. Landsea, P.W. Jr. Mielke, and K. J. Berry, 1993: Predicting Atlantic seasonal tropical cyclone activity by 1 August. Wea. Forecasting, 8, 73-86.
4. Gray, W.M., C.W. Landsea, P.W. Jr. Mielke, and K. J. Berry, 1994: Predicting Atlantic seasonal tropical cyclone activity by 1 August. Wea. Forecasting, 9, 103-115.
5. Tonkin, H., C. Landsea, G.J. Holland, and S. Li, 1997: Tropical cyclones and climate change: A preliminary assessment. Assessment Climate change: Results from the Model evaluation consortium for climate assessment, W. Howe and A. Henderson-Sellers, Eds., Gordon and Breach, Sydney, Australia, 327-360.
6. Emanuel, K., 1994: Tropical Cyclones, Nikos Drakos, Computer Based Learning Unit, University of Leeds.
7. Choudhury, M.A., 2009: Protecting Bangladesh from Natural Disasters, Academic Press and publishers Library, Dhaka.
8. Emanuel, K. A., 1987: The dependence of hurricane intensity on climate. Nature, 326, 483.
9. Evans, J.L., 1992: Comment on "Can existing climate models be used to study anthropogenic changes in tropical cyclone climate?" Geophys. Res. Lett., 19, 1523-1524
10. Lighthill, J., G. J. Holland, W.M. Gray, C. Landsea, K. Emanuel, G. Craig, J. Evans, Y. Kurihara, and C. P. Guard, 1994: Global climate change and tropical cyclones. Bull. Amer. Meteor. Soc., 75, 2147-2157
11. Henderson-Sellers, A., H. Zhang, G. Berz, K. Emanuel, W. Gray, C. Landsea, G. Holland, J. Lighthill, S.-L. Shieh, P. Webster, and K. McGuffie, 1998: Tropical Cyclones and Global climate change: A Post-IPCC Assessment. Bull. Amer. Meteor. Soc., 79, 19.

12. Ali, A.,1999a: Ghurnijhar, BanglaAcademy, Dhaka.
13. NASA, 2008:<http://earthobservator.nasa.gov>
14. Abbott, P.L.,2004: Natural disasters (4thed.), McGraw-Hill, New York, pp.302-333.
15. Quadir,D.A., and M.A. Iqbal, 2008: Investigation of the variability of tropical cyclones impacting on the livelihood of coastal inhabitants of Bangladesh, report of IUCN, Bangladesh.
16. Sadhuram, Y., B. P. Rao, D.P. Rao, P.N.M. Shastri, and M.V.Subrahmanyam2004: Seasonal Variability of Cyclone Heat Potential in the Bay of Bengal, Natural Hazards: 32 (2):191-209.
17. McBride, J.L.,1995: Tropical cyclone formation. Global Perspectives on Tropical Cyclones, R.L. Ed. Elsberry: WMO/TD-NO. 693 No. TCP-38, World MeteorologicalOrganization, Geneva, 63-105.
18. Hossain, M.A.,2003: Prediction of Cyclonic Events over Bay of Bengal UsingNumerical Weather Prediction Model with High Resolution, Ph. D. Thesis, Department of Mathematics, University of Rajshahi, Bangladesh.
19. WMO, 2009: Tropical Cyclone Operational Plan for Bay of Bengal and the Arabian Sea. World Meteorological Organization Technical Document, WMO/TD No. 84.Tropical Cyclone Program Report Not. TCP21, Geneva, Switzerland.
20. IMD, 1979: Traks of Storms and Depressions in the Bay of BengalandArabianSea (14877-1970). Cyclone Atlas, Indian Meteorological Department, Regional Meteorological Centre, Chennai, India.
21. Karmaker, S. (M.L. Shrestha edited), 1998: The impact of tropical cyclones on the coastal regions of the SAARC countries and their influence in the region, Report No. I, SAARC MeteorologicalResearchCenter (SMRC).
22. Ali, A.,1999b: Climate change impacts and adaptation assessment in Bangladesh. Climate Research, 12, 109-116.
23. Dube, S. K.,P. Chittibabu, P.C. Sinha, and A.D. Rao, 2004: Numerical modelling of storm surges in the Head Bay of Bengal using location specific model, Natural Hazards, 31, 437-453.

24. Neumann,C.J.,1993: Global Overview. Global Guide to Tropical Cyclone Forecasting, WMO/TC-No. 560, Report No. TCP-31, World Meteorological Organization, Geneva, 1-1-1-43.
25. JTWC, 2010: Joint Typhoon Warnig Center (JTWC) best track data available on: http://www.unso.navy.mil/NOOC/nmfc-ph/RSS/jtwc/best_tracks/ioindex.html.
26. P. Webster, 2008:Myanmar's deadly daffodil, Nature Geosci. 1, 488-490.
27. Skamarock,W.C.,J.B. Klemp, J. Dudhia, D.O. Barker, M.G. Duda, X-Y. Huang, W. Wang and J.G. Powers, 2008: A description of the Advanced Research WRF Version 3 . NCAR Technical Notes, NCAR/TN-475+STR, Boulder, Colorado,USA.
28. World Atlas, 2009: <http://www.worldatlas.com/aatlas/infopage/baybengal.htm>.
29. Banglapedia,2006:http://www.banglapedia.org/httpdocs/HT/C_03_97.HTM.
30. Encyclopedia Britannica, 2010:
<http://www.britannica.com/EBchecked/topic/60740/Bay-of-Bengal>
31. UCAR, 2006: Cyclone Glossary, University Corporation for Atmospheric Research (UCAR) (<http://meted.ucar.edu/>)
32. Holland, G.J. (ed.), 1993: The Global Guide to Tropical Cyclone Forecasting. WMO/TD-560, World Meteorological Organization, Geneva, 337pp.
33. Oliver, J. E. and J.J. Hidore, 2003: Climatology, An Atmospheric Science (2nd ed.), Pearson Education (Singapore) Pte. Ltd. P. 159-164.
34. Wikipedia, 2007: http://en.wikipedia.Org/wiki/1991_Bangladesh_cyclone.
35. NOAA, 2009: http://www.srh.noaa.gov/jetstream/tropics/tropics_intro.htm.
36. ESA,2010:EarthScienceAustralia,Originsofbadweather,
<http://earthscience.org.flooding/unit1>
37. IMD, 2009: Best track data, available on www.imd.gov.in
38. Ahrens, C.D.,2005: Essentials of Meteorology: An Invitation to the Atmosphere (3rd ed.), Thomson Brooks/Cole.



39. Quadir,D.A., M. Nessa, H. Rahman and A.M. Choudhury, 1999: On the relationship of rainfall and satellite base cloud top temperature, *Journal of Remote Sensing and Environment*, 3, 55-67.
40. Holland, G.,1997: The Maximum potential intensity of tropical cyclones. *J. Atmos. Sci.*, 54,2519-2541.
41. Emanuel, K.A.,1986: An air-sea interaction theory for tropical cyclones. Part I.*J. Atmos. Sci.*, 42, 1062-1071.
42. Fletcher, R.D.,1955: Computation of maximum surface winds in hurricane. *Bull.Amer. Meteo. Soc.*, 36, 247-250.
43. Nessa, M. and A.M. Choudhury, 1981: Estimation of maximum wind speed in tropical cyclones of Bay of Bengal from observed pressure drop. *Geophysics*, 1, 63-66.
44. HKO, 2007: Hong Kong Observatory website: <http://www.hko.gov.hk>.
45. Gray, W.M.,1979: Hurricanes: Their formation, structure and likely role in the general circulation. *Meteorology Over the Tropical Oceans*, D.B. Shaw, Ed., Royal Meteorological Society, James Glaisher House, Grenville Place, Bracknell, Berks, RG 121BX, 155-218.
46. Frank, W.M.,1987: Tropical cyclone formation. A Global View of Trepanation R.L. Elsberry, Ed., U.S. Office of Naval Research, Marine Meteorology Program, Washington, DC, 53-90.
47. Gray, W.M.,1968: Global view of the origin of tropical disturbances and storms. *Mon. Wea. Rev.*, 96,669-700.
48. Gray, W.M.,1975: Tropical cyclone genesis. Dept. of Atmos.Sci.PaperNo.234.ColoradoStateUniversity, Ft.Collins. Co.121 pp.
49. Gray, W.M.,1981: Recent advances in tropical cyclone research from rawinsonde composite analysis. *World Meteorological Organisation*, 407 pp.
50. Neumann, C.J.,G.W. Cry, F.L. Caso, and B.R. Jarvinen, 1985: Tropical cyclones of the North Atlantic Ocean, 1871-1980. NOAA Special Publication, National Hurricane Center, 174 pp.

51. Holland, G.J.,1984a: On the climatology and structure of tropical cyclones in the Australian/Southwest Pacific region. I: Data and tropical storms. *Aust. Met. Mag.*, 32, 1-16.
52. Holland, G.J.,1984b: On the climatology and structure of tropical cyclones in the Australian/Southwest Pacific region, I: Hurricanes. *Aust. Met. Mag.*, 32,17-32.
53. Holland, G.J., J.L. McBride, and N.N. Nicholls, 1988: Australian tropical cyclones and the Greenhouse effect. *Greenhouse: Planning for Climate Change*, G.I. Pearman, Ed., CSIRO, Melbourne, 438-455.
54. Evans, J.L.,1990: Envisaged impacts of enhanced greenhouse warming of tropical cyclones in the Australian region. CSIRO Division of Atmospheric Research Tech. Paper, No. 20, 31pp.
55. Prasad, O.,2005: Storm Surge Prediction in North Indian Ocean, In proceedings of the Seminar on 'Tropical Cyclones and Storm Surges in South Asian Region' held in Dhaka, 20-22 December 2003, Published by SMRC, Dhaka.
56. Frank,N. L. and S.A. Husain, 1971: The Deadliest Tropical Cyclone in History, *Bulletin of the American Meteorological Society*, 52 (6) 438-445.
57. Knabb, R.D.,J.R. Rhome and D.P. Brown, 2005. Tropical Cyclone Report.Hurricane Katrina: 23-30 August 2005, NationalHurricaneCenter.
58. Dunnavan, G.M.and J.W. Dierks. 1980: An Analysis of Super Typhoon Tip (October 1979), Joint Typhoon Warning Center (JTWC).
59. Haque, M.S., D.A. Quadir, M.A.M. Chowdhury, M.N. Ahasan and S.S. Sultana, 2009: Study of Vulnerability of the Coastal Zone of Bay of Bengal due to tropical cyclones, *Jahangirnagar University Journal of Science*, 32(2), 69-81.
60. Ali,A.1996: Vulnerability of Bangladesh to climate change and sea level rise through tropical cyclones and storm surges. *Water, Air and Soil Pollution*, 92:171-179.
61. Dvorak,V.F., 1984: Tropical Cyclone Intensity Analysis using satellite data. NOAA Tech. Rep NESDIS 11, US Dept. Commerce, Washington DC, 20233, 47pp
62. Mishra, D. K., and G.R Gupta, 1976: Estimation of maximum wind speed in tropical cyclones occurring in India Sea. *Indian J. Hydr. And Geohys.* 27,3,285-290.

63. Dunn, G.E., 1940: Aerology in the hurricane warning service. *Mon. Wea. Rev.*, 68,303-315.
64. Riehl, H., 1948: On the formation of West Atlantic Hurricanes, Part I. *Miscellaneous Report 24, Dept. of Met., University of Chicago*, 1-64.
65. Malkus, J., and H. Riehl, 1960: On the dynamics and energy transformations in steady state hurricanes. *Tellus*, 12,-1-20.
66. Simpson, R.H., N.L. Frank, D. Shideler and H.M. Johnson, 1969: Atlantic Tropical Disturbances of 1968. *Mon. Wea. Rev*, 240-255.
67. Ooyama, K., 1964: A dynamical model for the study of tropical cyclone development. *Geophysica International*, 4-187-198.
68. Kuo, H.L., 1965: On formation and intensification of tropical cyclones through latent heat release by cumulus convection. *J. Atmos. Sci.*, 22,40-63.
69. S.L., Rosenthal, 1970: A circularly symmetric primitive equation model of tropical cyclone development containing an explicit water vapor cyclone. *Mon. Wea. Rev.*, 98, 643
70. Riehl, H., 1954: *Tropical Meteorology*. McGraw-Hill Book Company
71. Charny, J.G., 1973a: Moveable CISK. *J. Atmos. sci.*, 30,50-52.
72. Charny, J.G., 1973b: Planetary fluid dynamice. *Dynamic Meteorology*, P. Morel (ed.), Reidel Publ., 331-344.
73. Yamasaki, M., 1969: Large-Scale disturbances in a conditionally unstable atmosphere in low latitudes. *Papers in Meteorl. Geophysics*, 20,289-336.
74. Hayashi, Y., 1970: A theory of large-Scale equatorial waves generated by condensation heat and accelerating the zonal wind. *J. Meteor. Soc. Jap.*, 48,140-160.
75. Lindgen, R.S., 1974: Wave-CISK in the topics. *J. Atmos. Sci.*, 31, 1232-1240.
76. Emanuel, K.A., 1989: The finite-amplitude nature of tropical cyclogenesis. *J. Atoms.Sci.*, 46, 3431-3456.
77. Emanuel, K.A., 1993: The Physics of tropical cyclogenesis over the Estern Pacific. *Tropical ICyclone Disturbances*, J. Lighthill, Z. Zhemin, G.J. Holland, K.A. Emanuel (eds.), Peking University Press, Beijing, 136-142.

78. Yano, J-L., and K.A. Emanuel, 1991: An improved model of the equatorial tropopause in low latitudes. *Papers in Meteorol. Geophysics*, 20,289-336.
79. Emanuel, K.A., J.D. Neelin and C.S. Bretherton, 1994: On Large-scale circulations in convecting atmosphere. *Q.J. Roy. Meteo. Soc.*, 120, 1111-1143.
80. Alam, M.M.,M.A. Hossain, and S. Shafee. 2002: Statistical analysis of cyclones and depressions in the Bay of Bengal during 1974-1999. *J. Bang. Ac. Sci.*, 26, 207-218.
81. Alam, M.M.,M.A. Hossain, and S. Shafee. 2003: Frequency of Bay o Begnalcyclonic storms and depressions crossing different coastal zones. *Int. J. Climatol.*, 23, 1119-1125.
82. Choudhurey, A.M., and A. Ali, 1974a: Prediction of Maximum wind speed in cyclones in the Bay of Bengal: a preliminary investigation. *Nuc. Sci. and App.*, 7 (B).
83. Choudhury, A.M.,and A. Ali, 1974b: Prediction of maximum surge height associated with cyclones affecting Bangladesh. *Nuc. Sci. and App.*, 7 (B).
84. Choudhury. A.M., D.A Quadir and M. Nessa, 1998: Monitoring of TropicalCyclone of May 1979 that Hit Bangladesh Using Data from GMS-5 Satellite,*Journal of Remote Sensing and Environment*. 2,51-69.
85. Choudhury, A.M., 1978: Rose Petal for tropical cyclones. *Nuc. Sci. and App.*, 11(B).
86. Hossain,M.A.,and M.M. Alam, 1999: Approximation of Bay of Bengal cyclone tracks using polynomial regression. *Fluid Mechanics and Heat Transfer*, D.K. Das,M.Q Islam, A.K.M.S Islam (eds.) Bangladesh University of Engineering and Technology, Dhaka, 141-145.
87. Mohanty,U.C.,and A. Gupta, 1997: Deterministic Methods for prediction oftropical cyclone tracks. *Mausam*, 48, 257-272.
88. Prasad, K.,1997: Prediction of tropical cyclones by numerical models-A review. *Mausam*, 48, 225-238.
89. Prasad,K., Y.V.R. Rao, and S. Sen, 1997: Tropical cyclone track prediction by a high resolution limited area model using synthetic observation. *Mausam*, 48, 351-366.

90. Krisnamurti, T.N.,A. Kamar, K.S Yap, A.P. Dastoor, N. Devidson, and J.Shyeng,1990: Performance of a high resolution mesoscale tropical prediction model. *Adv geo. Phys.*, 32,132-286
91. Mathur, M.B.,1991: The National Meteorological Centre's quasi-Lagrangian model for hurricane prediction, *Mon. Wea. Rev.*, 119-1447.
92. Mathur, M.B.,and J. Ruess, 1993: Further evaluation of the quasi-Lagrangion model's forecast track guidance, *Mon. Wea. Rev.*, 121, 1514-1530.
93. Prasad, K.and Rama Rao, Y.V., 2003: Cyclone track prediction by a quasi-Lagrangian model, *Meteorol, and Atoms. Phys.*, 83, 173-185.
94. Dhudia J., 1993: A non-Hydrostatic version of the penn state NCAR mesoscale model validation, test and simulation of Atlantic cyclone and cold front, *Mon. wea. ReV.* 121, 1493-1531.
95. Nagata, M.,et. al, 2001: A Mesoscale Model Intercomparison: A case of Explosive development of a Tropical Cyclone (COMPARE III), *Journal of Meteorological Society of Japan*, Vol. 79, No 5, 999-1033.
96. Debsarma, S.K.,1994: Storm Track Prediction (STP) Model. Presented at the be WARES Workshop at the University of Victoria, Canada (1994) and at the International Symposium on Natural Disasters and their Mitigation: Bangladesh Perspective, Dhaka, Bangladesh, 27-29 March, 1995.
97. Debsarma,S.K.,1995: Steering and Persistence (STEEPER) Model for the Storm Track Prediction. Presented at the workshop on ``Global Change and Tropical Cyclones" START, SASCOM, Bangladesh Academy of Sciences, Dhaka 18-20 December, 1995. Report: Ministry of Disaster Management & Disaster Management Bureau, Aug. 1998 pp. 55-60.
98. Krishnamurti, T. N., and B. Jha, 1998: Cyclone track prediction. *Sadhana*, 23,563-684.
99. Liu, Y.,D.-L. Zhang and M.K. Yau, 1997: A multiscale numerical Study of Hurricane Andrew (1992). Part I: Explicit simulation and verification, *Mon. Wea. Rev.*, 125, 3073-3093.

100. Davis, C.A., and L.F. Bosart, 2001: Numerical simulations of the genesis of Hurricane Diana (1984), Part I: Control simulation, *Mon. Wea. Rev.*, 129, 1859-1881.
101. Barun, S.A., 2002: A cloud-resolving simulation of Hurricane Bob (1991): Storm Structure and eyewall buoyancy, *Mon. Wea. Rev.*, 130, 1573-1592.
102. Trivedi, D.K., J. Sanjay and S.S. Singh, 2002: Numerical Simulation of a super cyclonic storm, Orissa (1999): Impact of initial conditions. *Meteorol. Appl.*, 9, 367-376
103. Rao, G.V., and D.V.B. Rao, 2003: A review of some observed mesoscale characteristics of tropical cyclones and some preliminary numerical simulation of their kinematic features, *proc. of Ind. Nat. Sci. Acad.*, 69A, 5, 523-541.
104. Mohanty, U.C., M. Mandal and S. Raman. 2004: Simulation of Orissa super cyclone (1999) using PSU/NCAR Mesoscale model. *Natural Hazards*, 31, 373-390.
105. Yang, M.-J., and L. Ching, 2005: A Modeling study of typhoon Toraji (2001): Physical Parameterization sensitivity and topographic effect. *Terrestrial, Atmospheric and Oceanic Sciences*, 16(1), 177-213.
106. Debsarma, S.K., 2003: Cyclone Forecasting and its Constraint for the Bay of Bengal. *Journal of BAKP The Atmosphere* 2, 40-52.
107. Prasad, K., (Quadir, D.A. ed.), 2004: Cyclone track prediction experiments with a Quasi-Lagrangian model. SAARC Meteorological Research Centre (SMRC) Report No. 9, Dhaka, Bangladesh.
108. Rao, Y.V.R., and K. Prasad, 2005: Further evaluation of the quasi-Lagrangian model for cyclone track prediction in the North Indian Ocean, SAARC Meteorological Research Centre Publication No. 12, Dhaka, Bangladesh.
109. Goswami, P., A. Mandal, H.C. Upadhyaya and F. Hourdin, 2006: Advance forecasting of cyclone track over north Indian Ocean using global circulation model. *Mausam*, 57(1), 111-118.
110. Prasad, K., and Y.V.R. Rao, 2006: Simulation studies on cyclone track prediction by Quasi-Lagrangian Model (QLM) in some historical and recent cases in the Bay Bengal, Using Global Re-analysis and forecast Grid Point datasets, SAARC Meteorological Research Centre Publication No. 15, Dhaka, Bangladesh.

111. Rao, D. V. B., and D. H. Prasad, 2006: Numerical prediction of the Orissa super cyclone (1999): Sensitivity to the parameterization of convection, boundary layer and explicit moisture processes, *Mausam*, 57(1), 61-78.
112. Lin, I.-I., C. H. Chen, I. F. Pun, W. T. Liu and C. C. Wu., 2008: Warm ocean anomaly, air sea fluxes, and the rapid intensification of tropical cyclone I, c&u (2008), *Geophysical Research Letter*, 36, L03817, doi: 10.1029/2008GL035815, 2009.
113. Debsarma, S. K., M. M. Rahman and F. F. Nessa, 2010: Simulation of cyclone Aila-2009 by using WRF-ARW Model and Numerical Storm Surge Model, Presented in the International Conference on Recent Advance in Physics (RAP-2010) Held on 27-29 March 2010, Organized by Department of Physics, University of Dhaka.
114. Simpson, R. H., and R. A. Pielke, 1976: Hurricane development and movement, *App. Mech. Rev.*, (May, 1976), 601-609.
115. Norton, G., 1949: A soliloquy on hurricane forecasting, National Hurricane Centre, Miami.
116. Riehl, H., W. H. Haggard and R. W. Sanborn, 1956: On the prediction of 24-Hour Hurricane Motion. *J. Meteorol.*, 13, 415-430
117. Miller, B. I. and P. Moore, 1960: A comparison of Hurricane steering levels, *Bull. Amer. Met. Soc.*, 41, 59-63.
118. Miller B. I. and P. Chase, 1966: Prediction of Hurricane motion by statistical Methods. *Mon. Wea. Rev.*, 94, 399-405
119. Kivgnov. A. F., and U. C. Mohanty, 197: On the Physical statistical method for forecasting the movement of tropical storms in the Bay of Bengal, *Meteor. Hydrol.*, 5 19-25.
120. Kivgnov. A. F., and U. C. Mohanty, 1979: On the application of nonlinear regression analysis to forecast the movement of tropical cyclones in the Bay of Bengal, *Tr. Hydrometrol. Centre, USSR*, 125, 47-58.
121. Sikka, D. R. and R. Suryanarayan, 1972: Forecasting the movement of tropical storms/ depressions in the Indian region by a computer oriented technique using climatology and persistence, *Indian, J. Meteor. Geophys.*, 23, 35-40.

122. Renard, R.J., S.G. Golgan, M.J. Daley and S.K. Rinard, 1973: Forecasting the motion of North Atlantic tropical cyclones by the Objective MOHATT Scheme, *Mon. Wea. Rev.*, 101, 206-214.
123. Hope, J.R. and C.J. Neumann, 1970: An operational technique for relating the movement of existing tropical cyclones to past track, *Mon Wea. Rev.*, 98, 925-933.
124. Neumann, C.J., 1972: An Alternative to HURRAN tropical cyclone forecast system, *Tech. Memo. NWS SR-52*.
125. Neumann, C.J. and M. Lawrence, 1975: An experiment in the statistical- dynamical prediction of tropical cyclone motion, *Mon*
126. Sanders, R. and R. burpee, 1968: Experiments in barotropic hurricane track forecasting, *J. App. Meteorl.*, 6, 313-323
127. Anthes, R.A., 1972: The development of Asymmetries in a Three-Dimensional Numerical Model of Tropical Cyclone, *Mon. Wea. Rev.*, 100, 461-476.
128. Miller, B.I., P.O. Chase and B.R. Jarvinen, 1972: Numerical prediction of tropical weather system, *Mon. Wea. Rev.*, 100, 825-835.
129. Ceselski, B.F., 1974: Cumulus convection in weak and strong tropical disturbances, *J. Atmos. Sci.*, 31, 1241-1255.
130. Leg, G.W. and R.L. Elsbery, 1976: Forecast of typhoon Irma using a Nested Grid Model, *Mon. Wea. Rev.*, 104, 1154-1163.
131. Ooyama K.V., 1990: A thermodynamic foundation for modeling the moist atmosphere, *J. Atmos. Sci.*, 47, 2580-2593.
132. Laprise R., 1992: The Euler Equations of Motion with hydrostatic pressure as a Independent variable, *Mon Wea. Rev.*, 120, 197-207.
133. Haltiner and G. J. and R. T. Williams. 1980: Numerical Prediction and dynamic meteorology. John Wiley & Sons. Inc., 477pp.
134. Klemp, J.B., W.C. Skamarock, and J. Dudhia, 2007: Conservative Split-explicit time integration methods for the compressible nonhydrostatic equations. *Mon. Wea. Rev.*, 135, 2897-2913.

135. Wicker, L.J. and W.C. Skamarock, 2002: Time splitting methods for elastic models using forward time schemes, *Mon. Wea. Rev.*, 130, 2088-2097.
136. Lyncey, P. and X-Y. Huang, 1994: Diabatic initialization using recursive filters. *Tellus*, 46A, 583-597.
137. Huang, X.-Y. and P. Lynch. 1993: Diabatic Digital-Filtering Initialization: Application to the HIRLAM Mode. *Mon. Wea. Rev.*, 121, 589-603.
138. Klemp, J.B., and D.K. Lilly, 1978: Numerical simulation of hydrostatic mountain waves, *J. Atmos. Sci.*, 35, 78-107.
139. Klemp, J.B., and R. Wilhelmson, 1978: The simulation of three-dimensional convective storm dynamics, *J. Atmos. Sci.*, 35, 1070-1096.
140. Davies, H. C., and R.E Turner, 1977: Updating Prediction models by dynamical relaxation: An Examination of the technique. *Quart. J. Roy. Meteor. Soc.*, 103, 225-245.
141. Michalakes, J., J. Dudhia, D. Gill, T. Henderson, J. Klemp, W. Skamarock, and W. Wang, 2004: The Weather Research and Forecast Model: Software Architecture and Performance. To appear in proceeding of the Eleventh ECMWF Workshop on the Use of High Performance Computing in Meteorology. 25-29 October 2004 Reading U.K., Ed. George Mozdzynski.
142. Kessler, E., 1969: On the distribution and continuity of water substance in atmospheric circulation, *Meteor. Monogr.*, 32, Amer. Meteor. 84 pp.
143. Lin, Y. -L., R.D. Farley, and H.D. Orville, 1983: Bulk parameterization of the snow field in a cloud model. *J. Climate Appl. Meteor.*, 22, 1065-1092.
144. Rutledge, S.A., and P.V. Hobbs. 1984: The Mesoscale and microscale structure and organization of clouds and precipitation in multistage cyclones. II: A diagnostic Modeling study of precipitation development in narrow cloud-frontal trainbands. *J. Atmos. Sci.*, 20, 2949-2972.
145. Hong, S.-Y., J. Dudhia, and S.-H. Chen, 2004: Revised Approach to Ice Microphysical processes for the bulk Parameterization of Clouds and Precipitation. *Mon. Wea. Rev.*, 132, 103-120.

146. Hong, S.-Y., and J.-o.j.Lim, 2006: The WRF Single-Moment 6-Class Microphysics Scheme (WSM6). *J. Korean Meteor. Soc.*, 42, 129-151.
147. TPB,2001:TechnicalProceduresBulletin(TPB)at <http://www.emc.ncep.noaa.gov/mmb/mmbpll/etal2tpb/> and on the COMET page at <http://meted.Ucar.edu/nwp/pcu2/etapcp1.htm>
148. Dudhia, J.,S-y Hong, and K.-S. Lim, 2008: A new method for representing mixed phase particle fall speeds in bulk microphysics parameterizations. *J. Met. Soc. Japan*, in press.
149. Tao, W.-K., and J. Simpson, 1993: The Goddard Cumulus Ensemble model. Part I: Model description. *Terr. Atmos. Oceanic. Sci.*, 4, 35-72.
150. Thompson, G., R. M Rasmussen, and K. Manning, 2004: Explicit forecastsofwinterprecipitation using an improved bulk microphysics scheme. Part I: Description and sensitivity analysis. *mon. Wea. Rev* 132, 519-542.
151. Micrison, H.,G. Thompson, and V. Tatarskii, 2008 Ingter of Micrpohysics on the development of trailing stratiform precipitation in simulted Squall line: Comparison of one-and two-moment schemes. Submitted *wea. Rev.*
152. Kain, J.S., 2004: The kain-Fritsch convective Paramettion : An update. *J. Appl.Meteor.*, 43. 170-181.
153. Kain,J.S.,and J.M. Fritsch, 1990: A one-dimensional entraining/detraining plume model and its application in convective parameterization. *J. Atmos. Sci.* 47, 2784- 2802.
154. Kain,J. S.,and J. M. Fritsch, 1993: Convective parameterization for mesoscale models: The Kain-Fritsch scheme, The representation of cumulus convection in numerical models, K.A. Emanuel and D.J. Raymond, Eds. *Amer. Meteor. Soc.*, 246 pp.
155. Janjic, Z.I.,1994: The step mountain eta coordinate model: Further developments of the convection, Viscous sublayer and turbulence closure schemes, *Mon, Wea. Rev.*, 122,927-945.
156. Janjic,Z.I., 2000: Comments on "Development and Evaluation of a convection Scheme for use in Climate Models" *J. Atmos. Sci.*, 57,mp. 3686.
157. Grell, G. A., and D. Devenyi, 2002: A generalizd approach to Parameterizing Convection combining ensemble and data assimilation teachniques. *Geophysa. Res. Lett.*, 29 (14), Article 1963.

158. A.S Monin, and A.M. Obukhov, 1954: Basic laws of turbulent mixing in the Surface layer of the atmosphere coontrib. Geophys. Last. Acad sci, USSR, (151), 163-187 (in Russian)
159. Janjic, Z. I.,1996: The surface layer in the NCEP Eta Mode, Eleventh Cpmference on Numerical Weather Predicton, Norfolk, VA, and 19-23 August: Amer Meteor. Soc. Boston, Ma, 354-355.
160. Janjic, Z. I., 2002: Nonsingular Implementation of the Mellor-Yamada Level 2.5 Scheme in the NCEP Meso model, NCEP Office Note, No 437, 61 pp.
161. Zilitinkevich, S.S., 1995: Non-Local turbulent transport: Pollution dispersion Aspects of coherent structure of convective flows, Air pollution III- Volume I, Air Pollution Theory and simulation, Eds. H. Power, N. Moussiopoulos and C.A Brebbia.Computational Mechanics Publications. Southampton Boston, 53-60.
162. Pleim,J.E., 2006: ASimple efficient solutionof flux-profile relationshipsinthe atmospheric surface layer. J. Appl. Metreor and Clim. 45,341-347.
163. Chen, F., and J. Dudhia, 2001: Coupling an advanced land-surface/hydrology modelwith the penn state/NCAR MM5 modeling system. Part 1: Model ldescription and Implementation. Mon. Wea. Rev. 129,569-585.
164. Smirnova, T.G., J.M Brown, and S.G. Benjamin, 1997: Performance of different soil model configurations in simulating ground surface temperature and swurface fluxes. Mon. WEa. Rev., 125, 1870-1884.
165. Smirnova,T.G., J.M. Brown, S.G. Benjamin, and D. Kim, 2000: Parameterizationof coldseason Processes in the MAPS land-surface scheme. J. Geophys. Res., Res.,105 (D3)/ 4077-4086.
166. Pleim,J.E.,and A. Xiu, 1995: Development and testing of a surface flux and planetaryboundary layer model for application nmesoscale models. J. Appl. Meteor., 34, 16-32.
167. Xiu, A. and J. E. Pleim, 2001: Development of a land surface model part 1: Application in a mesoscale meteorology mode. J. Appl. Meteor., 40 192-209.

168. Hong, S.-Y., and H.-L. Pan, 1996, Nonlocal boundary layer vertical diffusion in a medium-range forecast model, *Mon. Wea. Rev.*, 124, 2322-2339.
169. Hong, S.-Y., Y. Noh, and J. Dudhia, 2006: A new vertical diffusion package with an explicit treatment of entrainment processes. *Mon. Wea. Rev.*, 134, 2318-2341.
170. Janjic, Z. I., 1990: The step-mountain coordinates: Physical package, *Mon. Wea. Rev.*, 118, 1429-1443.
171. Pleim, J.E., 2007: A combined local and non-local closure model for the atmospheric boundary layer, Part 1: Model description and testing, *J. Appl. Meteor. and Clim.*, 46, 1383-1395
172. Mlawer, E. J., S.J. Taubman, P.D. Brown, M.J. Iacono, and S.A. Clough, 1997: Radiative transfer for inhomogeneous atmosphere: RRTM, a validated correlated-K model for the longwave. *J. Geophys. Res.*, 102 (D14), 16663-16682.
173. Collins, W.D. et al., 2004: Description of the NCAR Community Atmosphere Model (CAM 3.0) NCAR Technical Note, NCAR/TN-464+STR, 226pp.
174. Dudhia, J., 1989: Numerical Study of convection observed during the winter Monsoon experiment using a mesoscale two-dimensional model, *J. Atmos. Sci.*, 46, 3077-3107.
175. Chou, M.-D., and M. J. Suarez, 1994: An efficient thermal infrared radiation parameterization for use in general circulation models. NASA Tech. Memo. 104606, 3,85 pp.
176. Lacis, A. A., and J.E. Hansen, 1974: A Parameterization for the absorption of solar radiation in the earth's atmosphere. *J. Atmos. Sci.*, 31, 118-133.
177. IMD, 2010: Report on cyclonic disturbances over North Indian Ocean during 2009, RSMC-Tropical Cyclones. New Delhi.
178. O' Hara, J.F. and R.J. Falvey, 2007: Annual Tropical Cyclone Report-2007, U.S., Naval Maritime Forecast Center/Joint Typhoon Warning Center (JTWC), Pearl Harbor. Hawaii.
179. Dundee, 2009: Dundee Satellite Receiving Station (www.sat.dundee.ac.uk)
180. Cooper, G.A. and R.J. Falvey, 2008: Annual Tropical Cyclone Report-2008, U.S. Naval Maritime Forecast Center/Joint Typhoon Warning Center (JTWC) Pearl Harbor, Hawaii.

181. Cooper, G.A. and R.J. Falvey, 2009: Annual Tropical Cyclone Report-2009, U.S. Naval Maritime Forecast Center/Joint Typhoon Warning Center (JTWC), Pearl Harbor, Hawaii.
182. Ashrit, R., M.D. Gupta and A.K. Bohra, 2006: MM5 simulation of the 1999 Orissa super cyclone: impact of bogus vortex on track and intensity prediction, *Mausam*, 57(1), 129-134.
183. Goerss, J.S., 2000: Tropical Cyclone Track Forecasts Using an Ensemble Dynamical Models, *Mon. Wea. Rev.*, 128, 1187-1193.

Appendices

Physical Constants

The following is a list of physical constants used in the model.

$\pi = 3.1415926$	Pi
$k = 0.4$	Von Karman constant
$re = 6.370 \times 10^6 \text{ m}$	Radius of earth
$g = 9.81 \text{ m s}^{-2}$	Acceleration due to gravity
$\Omega_e = 7.2921 \times 10^{-5} \text{ s}^{-1}$	Angular rotation rate of the earth
$\sigma_b = 5.67051 \times 10^{-8}$	$\text{W m}^{-2} \text{ K}^{-4}$ Stefan - Boltzmann constant
$Rd = 287 \text{ J kg}^{-1} \text{ K}^{-1}$	Gas constant for dry air
$Rv = 461.6 \text{ J kg}^{-1} \text{ K}^{-1}$	Gas constant for water vapor
$cp = 7 \times Rd/2 \text{ J kg}^{-1} \text{ K}^{-1}$	Specific heat of dry air at constant pressure
$cv = cp - Rd \text{ J kg}^{-1} \text{ K}^{-1}$	Specific heat of dry air at constant volume
$cpv = 4 \times Rv \text{ J kg}^{-1} \text{ K}^{-1}$	Specific heat of water vapor at constant pressure
$cvv = cpv - Rv \text{ J kg}^{-1} \text{ K}^{-1}$	Specific heat of water vapor at constant volume
$cliq = 4190 \text{ J kg}^{-1} \text{ K}^{-1}$	Specific heat capacity of water
$cice = 2106 \text{ J kg}^{-1} \text{ K}^{-1}$	Specific heat capacity of ice
$Lv = 2.5 \times 10^6 \text{ J kg}^{-1}$	Latent heat of vaporization
$Ls = 2.85 \times 10^6 \text{ J kg}^{-1}$	Latent heat of sublimation
$Lf = 3.50 \times 10^5 \text{ J kg}^{-1}$	Latent heat of fusion
$\rho_w = 1.0 \times 10^3 \text{ kg m}^{-3}$	Density of liquid water

Appendices

Physical Constants

The following is a list of physical constants used in the model.

$\pi = 3.1415926$	Pi
$k = 0.4$	Von Karman constant
$r_e = 6.370 \times 10^6 \text{ m}$	Radius of earth
$g = 9.81 \text{ m s}^{-2}$	Acceleration due to gravity
$\Omega_e = 7.2921 \times 10^{-5} \text{ s}^{-1}$	Angular rotation rate of the earth
$\sigma_b = 5.67051 \times 10^{-8}$	$\text{W m}^{-2} \text{ K}^{-4}$ Stefan - Boltzmann constant
$R_d = 287 \text{ J kg}^{-1} \text{ K}^{-1}$	Gas constant for dry air
$R_v = 461.6 \text{ J kg}^{-1} \text{ K}^{-1}$	Gas constant for water vapor
$c_p = 7 \times R_d / 2 \text{ J kg}^{-1} \text{ K}^{-1}$	Specific heat of dry air at constant pressure
$c_v = c_p - R_d \text{ J kg}^{-1} \text{ K}^{-1}$	Specific heat of dry air at constant volume
$c_{pv} = 4 \times R_v \text{ J kg}^{-1} \text{ K}^{-1}$	Specific heat of water vapor at constant pressure
$c_{vv} = c_{pv} - R_v \text{ J kg}^{-1} \text{ K}^{-1}$	Specific heat of water vapor at constant volume
$c_{liq} = 4190 \text{ J kg}^{-1} \text{ K}^{-1}$	Specific heat capacity of water
$c_{ice} = 2106 \text{ J kg}^{-1} \text{ K}^{-1}$	Specific heat capacity of ice
$L_v = 2.5 \times 10^6 \text{ J kg}^{-1}$	Latent heat of vaporization
$L_s = 2.85 \times 10^6 \text{ J kg}^{-1}$	Latent heat of sublimation
$L_f = 3.50 \times 10^5 \text{ J kg}^{-1}$	Latent heat of fusion
$\rho_w = 1.0 \times 10^3 \text{ kg m}^{-3}$	Density of liquid water